TECHNISCHE UNIVERSITÄT MÜNCHEN

Lehrstuhl für Technische Chemie II

Investigation of hydrocarbon transport phenomena on surface modified H-ZSM5 zeolites

Stephan Johannes Reitmeier

Vollständiger Abdruck der von der Fakultät für Chemie
der Technischen Universität München zur Erlangung des akademischen Grades eines

Doktors der Naturwissenschaften (Dr. rer. nat.)

genehmigten Dissertation.

Vorsitzender: Univ.-Prof. Dr. K.-O. Hinrichsen
Prüfer der Dissertation:

1. Univ.-Prof. Dr. J. A. Lercher
2. Univ.-Prof. Dr. U. K. Heiz
3. Univ.-Prof. Dr. K. Köhler

Die Dissertation wurde am 29.06.2009 bei der Technischen Universität München
eingereicht und durch die Fakultät für Chemie am 23.07.2009 angenommen.

For my parents, grandparents
and for Gabi

"In Gedenken an meinen
Großvater Karl Egidi"

„ What we know is just a droplet compared
to an ocean of what we do not know, yet! "

Sir Isaac Newton
(1643 − 1727)

Acknowledgements

Working on a dissertation project not only includes complex scientific challenges and goals but also means being part of an international research group and sharing (non-)scientific discussions and experiences. Having finished my dissertation thesis, I would like to thank all who have contributed to the success of this work within the last years.

First of all I want to thank Prof. Dr. Johannes A. Lercher for the opportunity to become part of his international working group at the Chair of Technical Chemistry 2 (TC-2) which I enjoyed very much. Thank you for providing me the research topic and all technical equipment necessary for achieving my research goals. I am grateful for your guidance, support and the scientific freedom you granted me throughout my dissertation. I also enjoyed very much the possibility you gave me, to attending international scientific conferences to present and discuss my research results among the scientific community.

I am very grateful to my personal supervisor, PD Dr. Andreas Jentys for his support. Thank you for always considering my questions and comments, for giving me the possibility to directly discuss scientific results and upcoming problems and for introducing me into new techniques and methodologies. I was always enlightened to hear your point of view, be it on the deeper insights of chemical engineering, on the spectroscopic side of the work or all other matters not included in the above.

Moreover, I am grateful to my co-worker O. Gobin for our, sometimes even controversial, discussions and for sharing his thoughts, scientific knowledge and chemical engineering background. Thanks a lot for the help with the Matlab scientific software. Without your programming skills, fast and reliable evaluation of the multitude of frequency response experiments would not have been possible.

I want to thank the "Studienstiftung des Deutschen Volkes" for the financial support of throughout my dissertation and studies in Chemistry. I am really proud for having been part of this exceptional and illustrious community. I especially thank H. Kohrs, K. Windisch, M. Frenz and A. König for their support and all our personal discussions and talks, either in Bonn, Munich, elsewhere or via telephone. The DFG is

Nomenclature

1. Arabic letters

Letter	Description [Unit]
$*$	Catalytically active center
A	Infrared absorbance [Absorbance units]
A_e	Amplitude of the excitation function in FR experiment [a.u.]
A_r	Amplitude of the response function in FR experiment [a.u.]
a, c	Frequency response parameter
B, B_i	Characteristic rotation constant [cm^{-1}]
B	Magnetic field strength [T]
B_{local}	Local magnetic field near NMR-active nucleus [T]
B_{CSA}	Local magnetic field caused by chemical shift anisotropy (NMR) [T]
c_i	Concentration [mmol g^{-1}], [molecules (u.c.)$^{-1}$]
c	Speed of light [$3 \cdot 10^8$ m s^{-1}]
Δc_{OH}	Coverage change of hydroxyl group [mmol g^{-1}], [molecules (u.c.)$^{-1}$]
$\Delta c_{eq,OH}$	Saturation coverage change [mmol g^{-1}], [molecules (u.c.)$^{-1}$]
-CH$_2$-, -CH$_3$	Methylene and methyl fragment
d_p	Micropore diameter [nm]
d	Sample, wafer thickness, lattice plane distance [m], [nm]
d_m	Overlayer pore diameter [nm]
D_p	Particle diameter [μm]
D_0	Transport diffusion coefficient [m^2 s^{-1}]
D	Diffusion coefficient [m^2 s^{-1}]

E	Energy [J], [kJ mol^{-1}]
E_{tot}	Total energy of a system, Sum of microstates energies [J], [kJ mol^{-1}]
$E(i,J)$	Energy of rotational vibrational states [cm^{-1}], [J]
E_i	Energy of a microstate of a system [cm^{-1}], [J]
e	Euler constant 2.718
$F(t)$	Square wave excitation function (FR experiment) [a.u.]
f	Frequency [s^{-1}], [Hz]
G	Gibbs free enthalpy [kJ mol^{-1}]
h	Planck constant $6.626 \cdot 10^{-34}$ $[Js]$
$\hbar$	Reduced Planck constant ($h/2\pi$)
H	Enthalpy [kJ mol^{-1}]
H_{ads}	Enthalpy of adsorption [kJ mol^{-1}]
I	Moment of inertia [kg m^2]
I, I_0	Transmitted and incident light intensity [a.u.]
I	Integrated absorbance [cm^{-1}]
i	Vibrational quantum number [0, 1, … n]
J	Rotational quantum number [0, 1, ... n]
K_{ads}	Equilibrium constant of sorption [-]
K_i	Frequency response equilibrium uptake constant [-]
k	Force constant [kg s^{-2}]
k	Order of reflexion (XRD) [-]
k_B	Boltzmann constant [$1.38 \cdot 10^{-23}$ J K^{-1}]
l	Overlayer thickness [nm]
L	Angular momentum [kg m^2 s^{-1}]

L	Length dimension [m]
L	Half-thickness of a planar sheet [m]
L^2 / D	Frequency response time constant [s]
M	Molar mass [g mol^{-1}]
m	Mass [kg], atomic mass [amu]
Δm	Mass resolution [g]
m_z	Magnetic quantum number (z-component) of the magnetic momentum
N_A	Avogadros' constant [$6.022 \cdot 10^{23}$ mol^{-1}]
N	Number of particles
n	Infinite summation term [-]
n	Harmonic order of a periodic wave function
n_i, n_1, n_0	Population numbers of energetic microstates
n_{tot}	Total number of microstates
P_i	Boltzmann probability [%]
P_B	Pressure amplitude (FR experiment, blank) [mbar]
P_Z	Pressure amplitude (FR experiment, sample) [mbar]
p	Pressure, partial pressure [mbar], [kPa]
q	Molecular partition function [-]
q_{rot}, q_{vib}	Rotational, vibrational single particle partition function [-]
q_{trans}, q_{el}	Translational, electronic single particle partition function [-]
$q^{\#}$, q^{gas}	Gas phase partition function, Partition function in the adsorbed state [-]
q_i	Coverage [mmol g^{-1}], [molecules (u.c.)$^{-1}$]
q_{sat}	Saturation coverage [mmol g^{-1}], [molecules (u.c.)$^{-1}$]
$q_{sat,i}$	Saturation coverage [mmol g^{-1}], [molecules (u.c.)$^{-1}$]
Q	Heat [kJ mol^{-1}]

Nomenclature

Q	Total partition function of a system
Q_{iso}	Isosteric heat [kJ mol^{-1}]
R	General gas constant [8.314 J mol^{-1} K^{-1}]
$R(t)$	Square wave response function (FR-experiment) [a.u.]
S	Entropy [J mol^{-1} K^{-1}]
S_A	Surface area [m^2 g^{-1}]
S_{BET}	BET surface area [m^2 g^{-1}]
S_{rot}	Rotational entropy [J mol^{-1} K^{-1}]
Δs	Pathlenght [nm]
t	Time [s]
t	t-plot parameter [-]
t_p	Cycle time [s]
T	Temperature [K]
T	IR-transmittance [-]
T_1, T_2	Longitudinal and transversal relaxation time [s]
u	Velocity [m s^{-1}]
$\langle u \rangle$	Mean gas velocity [m s^{-1}]
V	Volume [m^3]
V_m	Monolayer volume [m^3]
V_{micro}	Micropore volume [cm^3 g^{-1}]
V_{meso}	Mesopore volume [cm^3 g^{-1}]
V_{total}	Total pore volume [cm^3 g^{-1}]
$V_{standard}^{ads}(p)$	Adsorbed volume of N$_2$ under standard conditions [cm^3 g^{-1}]
x,y,z	Cartesian Coordinates [m]

2. Greek letters

Letter	Description [Unit]
α	Experimental sticking probability [-]
$\alpha^{\#}$	Theoretical sticking probability [-]
α_S	Comparative plot analysis formalism
$a\kappa$	Surface barrier parameter [s^{-1}]
γ_N	Nuclear gyromagnetic ratio
δ_C, δ_S	Characteristic in- and out-phase frequency response functions [-]
δ_s, δ_{as}	Symmetric and asymmetric deformation vibration [-]
σ	Symmetry number [-]
σ_{tot}	Total symmetry number [-]
η	Frequency response transport parameter [-]
ε_t	Energy of single energetic state i [J], [kJ mol^{-1}]
ε	(Molar) extinction coefficient for infrared bands [g mmol^{-1} cm^{-1}]
φ_B, φ_Z	Frequency response phase lag (blank, zeolite sample) [rad]
λ	Wavelength of light [m]
Λ	Thermal wavelength [m]
μ	Reduced mass [kg]
μ	Nuclear magnetic moment [J T^{-1}]
ν	Frequency [s^{-1}]
ν_s, ν_{as}	Symmetric and asymmetric stretching vibration
ν_L	Lamor frequency [s^{-1}]
$\bar{\nu}$	Wavenumber [cm^{-1}]
θ	Coverage [%]

θ	Angle between magnetic field and molecular axis [°]
2θ	Braggs' angle (XRD) [°]
Θ_{rot}	Rotational, vibrational temperature [K]
Θ_{vib}	Vibrational temperature [K]
ρ	Volume density [g m^{-3}]
τ	FR Time constant [s]
τ_{ad}	Time constant of the adsorption process [s]
τ_{de}	Time constant of the desorption process [s]
χ	Trapping coefficient [-]
ω	Radial frequency [s^{-1}], [rad s^{-1}]
$\omega_{x,y,z}$	Radial frequency along the Cartesian coordinates [s^{-1}]

Abbreviations

Acronym	Description
°C	Degree Celsius
AAS	Atomic Absorption Spectroscopy
ATR	Attenuated Reflectance Spectroscopy
a.u.	Arbitrary Units
BAS	Brønsted Acid Sites
BET	Brunnauer, Emmet, Teller
BEA	Zeolite Beta
BJH	Barrett, Joyner and Halenda Method
CHA	Chabazite
CVD	Chemical Vapor Deposition
CLD	Chemical Liquid Deposition
CLO	Chloverite Zeolite
CO	Carbonmonoxide
DLS	Dynamic Light Scattering
DTGS	Deutero-Triglycylsulfate Detector
DSC	Differential Scaning Calorimetry
DTA	Differential Thermoanalysis
DRIFTS	Diffuse Reflectance Spectroscopy
EFAL	Extra Framework Aluminium
FAU	Faujasite
FCC	Fluidized Catalytic Cracking
FT	Fourier Transformation

FTIR	Fourrier Transformation Infrared
FR	Frequency Response
FRM-II	Forschungsreaktor München II
GC	Gas Chromatography
H-ZSM5	H-form of Zeolite Socony Mobile 5
H-ZSM5-p, -1m, -3m	Parent (p), modified (m), three-fold modified (3m) sample
IR-IFM	Infrared Interference Microscopy
IRM	Infrared Microscopy
IZA	International Zeolite Association
K	Kelvin, SI-Temperature Unit
KBr	Potassium Bromide
LAS	Lewis Acid Sites
LTA	Linde Type A Zeolite
MAS	Magic Angle Spinning
MCT	Mercury-Cadmium-Telluride Detector
MEC	Molar Extinction Cofficient
MFI	Mobil Five
MEL	Mobil Eleven
MIR	Mid-Infrared radiation
mL	Milliliter
MOR	Mordenite
MTC	Molecular Traffic Control
MS	Mass Spectrometry, Mass Spectrometer
MTG	Methanol to gasoline

NIR	Near-Infrared Radiation
NMR	Nuclear Magnetic Resonance
PFG	Pulsed Field Gradient
PSS	Product Shape Selectivity
QENS	Quasi-Elastic Neutron Scattering
RSS	Reactant Shape Selectivity
RS-IR	Rapid Scan Infrared Spectroscopy
SBU	Secondary Building Unit
SEM	Scanning Electron Microscopy
SiC	Siliciumcarbide
S/N	Signal-to-noise ratio
SPODI	Strcutural Powder Diffractometer
STP	Standard Temperature and Pressure
TSS	Transition State Selectivity
TEM	Transmision Electron Microscopy
T-atom	Tetrahedrally coordinated Si or Al atom
TG	Thermogravimetry
TGA	Thermogravimetric Analysis
TPD	Temperature Programmed Desorption
UHV	Ultra High Vacuum
VPI-5	VFI Zeolite
XRD	X-ray Diffraction
XPS	X-ray Photoelectron Spectroscopy
ZSM5, ZSM11	Zeolite Socony Mobil 5, 11
ZLC	Zero Length Column Method

Table of Contents

Chapter 1

Chapter 2

Chapter 3

3.   Theoretical methods – Statistical thermodynamics and collision theory........ 69

Chapter 4

4.   Experimental and theoretical investigation of the sticking probability of aromatic hydrocarbons on H-ZSM5 and SiO₂

Appendix C

Chapter 1

1. Introduction section

1.1 General Introduction

1.1.1 Porous solids – properties and applications

Micro- and mesoporous materials with well-defined structure play an important role as catalyst, catalyst support or sorbent for a variety of catalytic processes in the refining and petrochemical industry.[1-3] Zeolites, which are the most widespread used group of such materials are crystalline tectosilicates with silicon and aluminium atoms tetrahedrally coordinated (T-atoms) to oxygen atoms that bridge between these tetrahedra.[4]
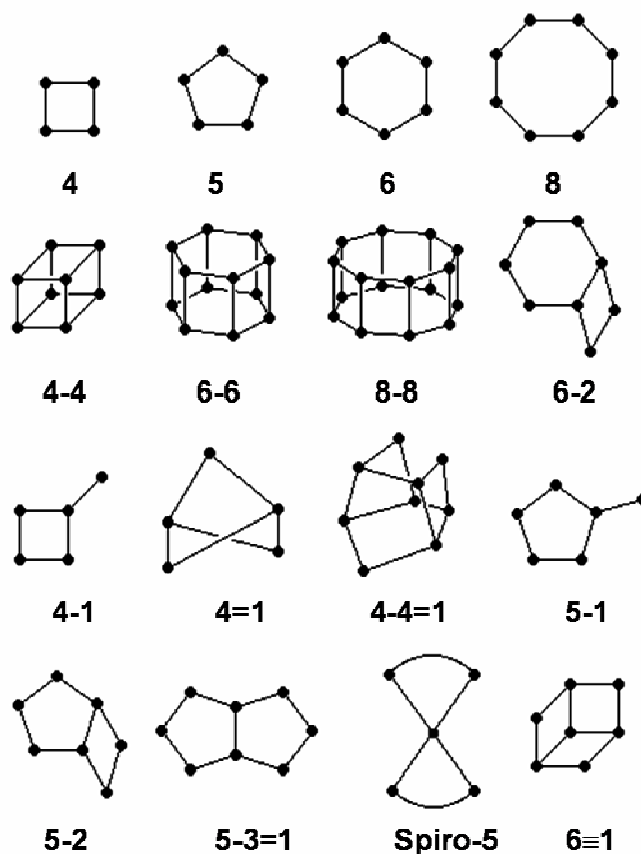
Figure 1.1 **Selection of secondary building units (SBUs) in the framework of zeolites. The vertices of the polyhedra indicate the T atoms, the lines the oxygen bridges. (Adopted from C. Baerlocher *et al.* Atlas of zeolite framework types, 5th ed., Elsevier, Amsterdam, 2001 [4])**

The primary tetrahedral SiO_4^{4-} and AlO_4^{5-} units can be further structurally arranged within up to 20 topological subunits in a well-defined way. A selection of

these, so are called secondary building units (SBU), is illustrated in figure 1.1.[4, 5] In order to balance the resulting negative charge of the framework structure, originating from the isomorphous substitution of Si^{4+} by Al^{3+} atoms, counter ions such as protons, alkaline or alkaline earth metal ions (i.e., sodium, calcium and magnesium) are required. These naturally present ions can furthermore be easily exchanged by desirable transition metal ions such as copper, iron or lanthanum via conventional ion exchange procedures.[6, 7]

Table 1.1   **Selection of some most commonly used zeolites and zeolite-related materials with characteristic channel systems and pore dimensions**

Zeolite	Code	Number of T-atoms		Channel type	d_P [nm]
VPI-5	VFI	18	1D	1 straight channel	1.27×1.27
CIT-5	CFI	14	1D	1 straight channel	0.72×0.75
Mordenite	MOR	12	1D	2 straight channels	0.70×0.65
		8			0.57×0.26
ZSM11	MEL	10	2D	2 straight channels	0.54×0.53
Zeolite A	LTA	8	3D	Cage structure, cubic array	0.41x0.41
ZSM5	MFI	10	3D	1 straight and 1 sinusoidal channel	0.56×0.54
		10			0.58×0.54
Beta	BEA	12	3D	2 straight and 1 sinusoidal channel	0.77×0.66
		12			0.56×0.56
Cloverite	-CLO[1]	20	3D	2 straight channels	0.40×1.32
		8			0.38×0.38

Owing to the unique structural connectivity between the silica and alumina tetrahedral units, a huge scaffold of structures with variable void spaces, ranging from channel segments to cages, super-cages and also side pockets, in which guest

---

[1] The hyphen within the three-letter code indicates partially open zeolite-like frameworks.

molecules such as e.g., CO, ammonia, pyridine and in particular aliphatic and aromatic hydrocarbon molecules can adsorb and react.[8-10] The resulting three-dimensional, periodic lattice structure is terminated at the outer surface by strained oxygen bridges and terminal hydroxyls groups.
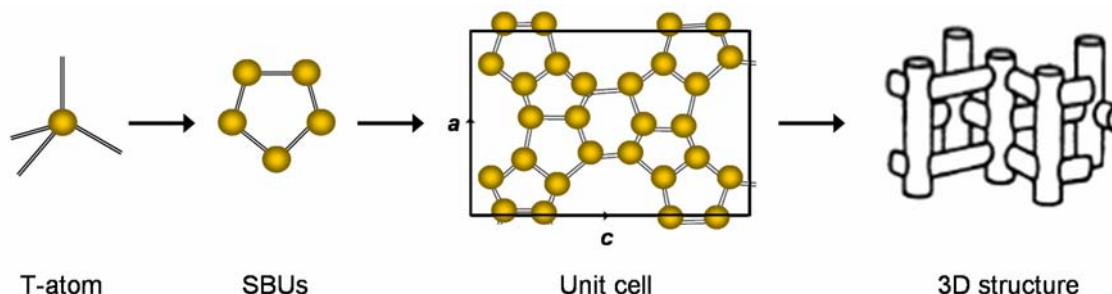
Figure 1.2   **Scheme showing the stepwise formation of porous aluminosilicates exemplified for MFI-zeolites.[11]**
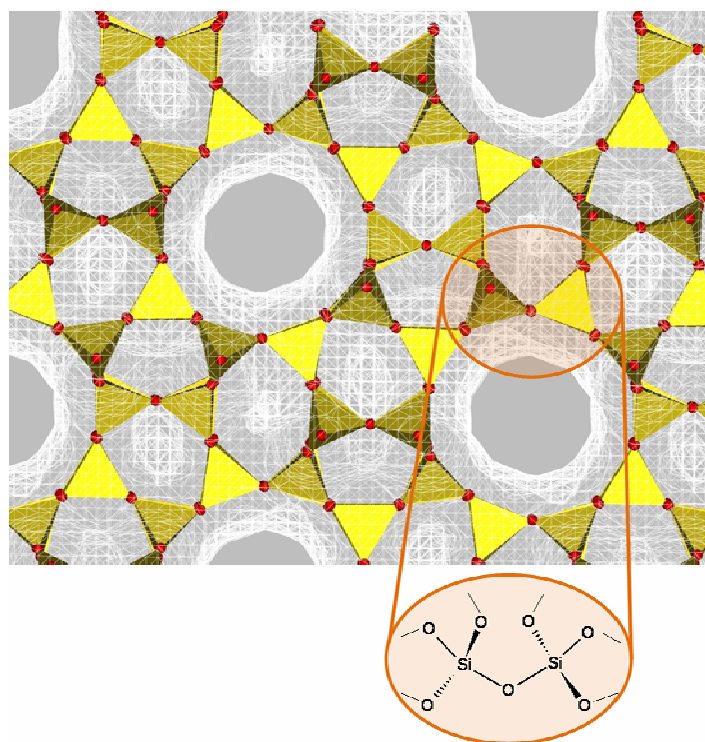
Figure 1.3   **Sketch of the framework structure of a ZSM5 is shown in cross section in direction of the straight and perpendicular to the sinusoidal channel segments. The tetrahedral building units are highlighted in yellow with the bridging oxygen atoms in red. The wired mesh indicates the respective van-der-Waals surface accessible for sorbate molecules.**

The size of the channels, channel intersections and cages generated depends on the numbers of T-atoms forming the pores, which are typically between four and fourteen (so called 4 to 14 membered rings) with some zeolite-related structures having, up to 20 membered rings. In Table 1.1, a selection of most frequently used zeolite types together with a short description of their channel networks is given to emphasize on the structural variability and the industrial relevance of zeolite materials. A typical sketch of a framework structure is exemplified in Figure 1.3 for an MFI-type zeolite with the tetrahedral coordinated atoms (T-atoms) highlighted in yellow and oxygen atoms in red.

The first natural zeolite material was identified and reported by the Swedish mineralogist Cronstedt[10, 12] in 1757. Nevertheless, because of the high amount of impurities, the distinct variations in the chemical composition and their rather low natural abundance, the natural forms of zeolites have only attracted minor interest for chemical and catalytic applications. Almost 200 years later, following the first successful synthesis of stable zeolite structures described by Barrer[13, 14], first applications of novel synthetic zeolites were reported subsequently. The usage of zeolites for purification and industrial separation of air, as performed by the Union Carbide Corporation based on the work of Milton *et al.*[12, 15] in the middle of the 1950s, is among the first industrial applications of synthetic zeolites, reported.[12, 16] In the following years, the zeolites X and Y, belonging to the class of faujasite materials (FAU)[4], were rapidly recognized by the petrochemical industry as beneficial catalysts in the fluidized catalytic cracking (FCC) reaction for the production of high octane gasoline out of heavy petroleum distillates.[16-21] This development has opened up a new, broad field of applications within petroleum refining[9, 22-25] and thus novel synthetic porous solids rapidly gained technical importance for petrochemical industry in general.[23, 26]

Nowadays, more than 180 different zeolite structures - 40 natural and over 140 synthetic ones - are known and distinctly classified using a three-letter code classification system endorsed by the International Union of Pure and Applied Chemistry (IUPAC)[5] and the structure commission of the International Zeolite Association (IZA).[4, 27] In addition, more and more zeolite-related materials were synthesized i.e., by isomorphous substitution of a certain fraction of the T-atoms[28] by

other trivalent elements such as e.g., gallium[29] atoms. Another approach is the total replacement of the silicate structure by aluminophosphates, resulting in a novel the class of AlPO materials.[30-34]

Due to the remarkable structural and chemical features in terms of high crystallinity, thermal stability, well-defined multi-dimensional pore systems and cavities with large pore volumes, very high internal surface areas and especially their non-toxicity[35], molecular sieves and zeolite materials in particular have found entrance into various, not only technical fields of applications today. Besides medicine, agriculture and environmental protection, especially petrochemistry and the whole industrial heterogeneous catalysis have to be named hereby. A short selected overview is compiled within Figure 1.4.
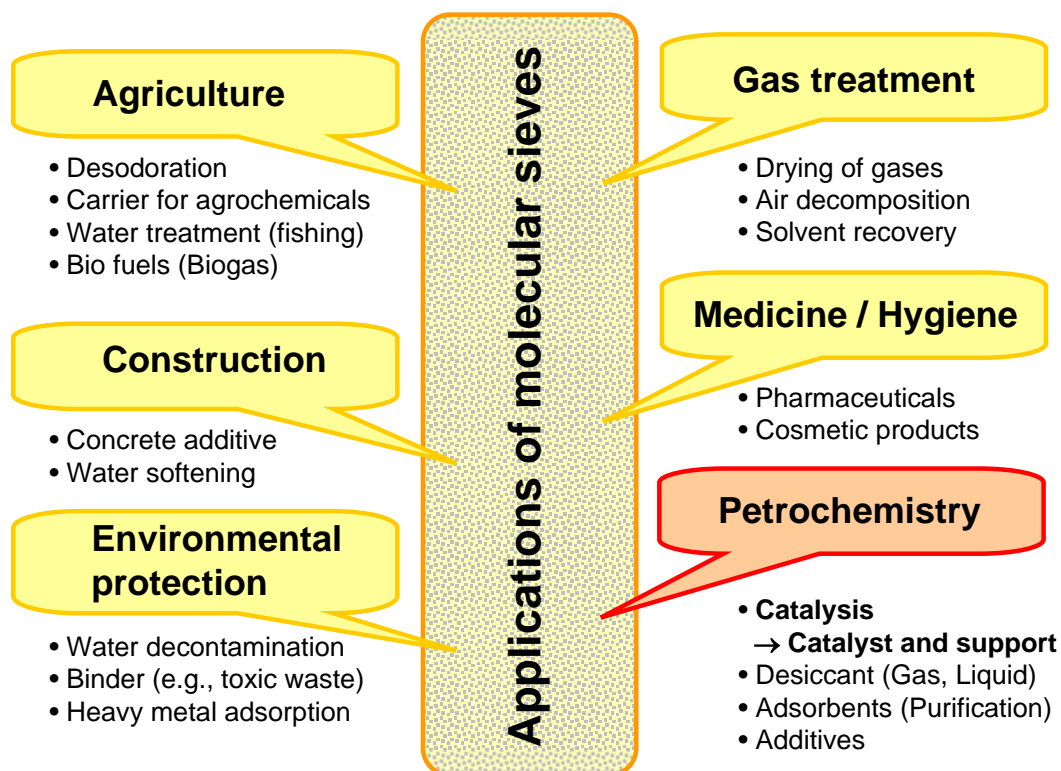
Figure 1.4 **Compilation of currently established e.g., technical applications of molecular sieve materials.[10]**

The replacement of formerly used acid catalyzed processes on large scale, utilizing strongly corrosive acids such as hydrofluoric, hydrochloric, sulphuric or supported phosphoric acid or less efficient silica-alumina gels[12], by solid acid

catalysts was not only accompanied by increased environmental welfare but has brought in the same way significant economic benefits for the petrochemical industry. The incentive of zeolite materials can accordingly be seen in their unique potential to be utilized either for highly specialized and also large scale industrial processes or as well for all-day life applications such as detergents[35-38], waste water treatment or cosmetic products.[39, 40] This is underlined by the fact that the patent activity in a variety of areas utilizing zeolite materials is strongly enormously growing.[12]

1.1.2 Zeolites and shape selective catalysis

1.1.2.1 Nature of catalytically active sites

Modern hydrocarbon catalysis mainly benefits from the unique acidic properties of zeolites[11, 41], which can be best described as solid polyacids materials.[42] Brønsted acidic hydroxyl groups (SiOHAl) are generated when the net charge within the framework, resulting from the substitution of Si^{4+} by Al^{3+} atoms in tetrahedral position, is neutralized by protons, covalently bound to the bridging oxygen atoms of the Si-O-Al linkage.[43] Lewis acid sites are formed by exchanged metal cations, extra-lattice aluminium (EFAl) species and defect sites within the framework. In an ideal case, the total number of cations divided by their valence or of protons corresponds to the number of AlO_4 tetrahedral units.
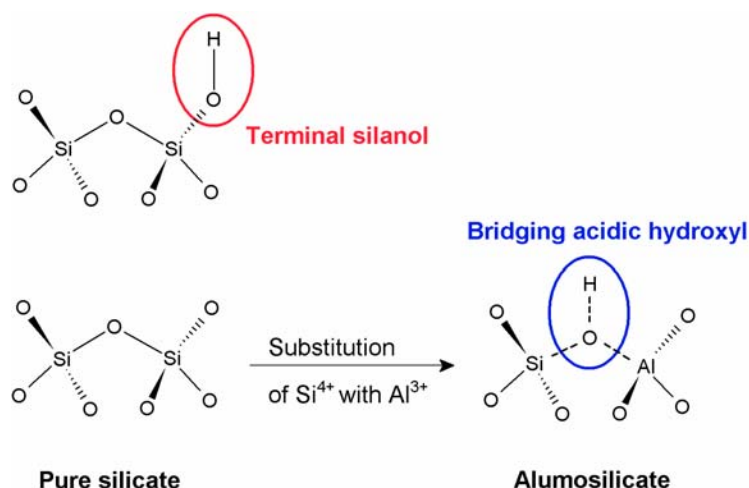
Figure 1.5 **Schematic representations of the characteristic terminal and bridging acidic hydroxyl sites of zeolites and silicates[43]**

High temperature treatment of zeolites may induce the removal of fractions of aluminium sites from the zeolite structure leading to extra-lattice alumina species residing in the micropores and crucially affecting the catalytic activity.[44-48] The strength of the Brønsted acid sites depends on the chemical composition and on the structure of the molecular sieve[49-51], however, it manifests itself only against the specific sorbate. The concentration of aluminium atoms influences the acid strength via the formation of Si-O-Al-O-Si-O-Al groups of tetrahedra which lead to unusually weaker Brønsted acid sites than for the case of isolated SiOHAl sites, described in the work of D. Barthomeuf.[51, 52] A more detailed discussion can be found in several reviews.[11, 29, 53] For illustration, a characteristic section of the zeolite framework and the corresponding acidic and terminal hydroxyl groups are shown in Figure 1.5.

The above discussed well-defined, acid-base properties of zeolite materials are complemented in importance by the regularity of their pore structure. While being flexible within limits, the uniform pore dimensions similar to the size of small organic molecules induce steric confinements and partially dramatic entropic effects that are only beginning to be currently explored.[54-56] The effects range from the classic shape selectivity[57-63] over the concept of molecular traffic control[64, 65] to the effects of entropy of the adsorbed molecules in the pores on the overall pathways of catalyzed reactions.[10, 66, 67]

1.1.2.2 MFI-type zeolites and shape selectivity

Within the following chapters of this thesis, the investigation of the elementary hydrocarbon transport processes in zeolite catalysts is focussed on medium pore zeolites with a strong emphasis on the MFI structure (ZSM5, Zeolite Socony Mobil-5) highlighted in Figure 1.3. ZSM5 zeolite was developed by the Mobil Oil Corporation[12] in the early 1970s and first synthesized by Argauer *et al.*[68] Structurally, the orthorhombic unit cell of ZSM5 crystals is formed by 196 T-atoms and Si/Al ratios between 10 and ∞ can be synthesized with the purely siliceous material denoted Silicalite-1.[69] The pore structure is composed of ten-membered ring, straight and sinusoidal intersecting channels, generating intersections of 0.89 nm in diameter. Thereby, the sinusoidal channels[4, 70] show almost circular cross section with

0.54 to 0.56 nm and are oriented perpendicular to the straight channels having slightly elliptical cross sections of 0.54 to 0.58 nm (see Figure 1.6).
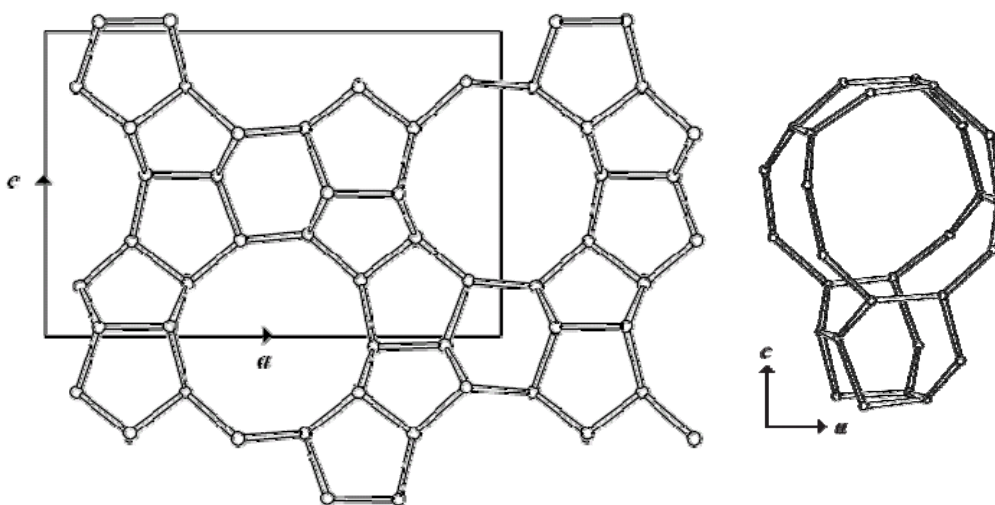
Figure 1.6   Building scheme of MFI zeolites with (left) the parallel projection of the MFI unit cell along *b* and (right) typical cavity (intersection) viewed along *b*. (Adopted from C. Baerlocher *et al*. Atlas of zeolite framework types, 5th edition, Elsevier, Amsterdam, 2001[4])

Originally, ZSM5 was envisaged for the selective production of synthetic gasoline[71] and has rapidly achieved numerous applications for shape-selective reactions involving aromatic hydrocarbons molecules such as the xylene isomerization and toluene disproportionation processes in the following years.[72-76] The desirably high selectivity of H-ZSM5 to *para*-products in these reactions was demonstrated by Olson and Haag.[77] ZSM5 has been found to exhibit the property to differentiating between hydrocarbon molecules of slightly different minimum kinetic dimensions with a strict cut-off, which is commonly known as shape selectivity.[78]

Originating from the analysis of enzyme-catalyzed processes, the genuine concept of shape selectivity was transferred to the material class of molecular sieves by Weisz *et al.*[78-82] in the 1970s and further developed by Csicsery[58-61], Derouane[64] and Chen *et al.*[83] In short, shape selectivity manifests in different ways[22]: (1) the exclusion of larger reactants from the catalytically active sites (reactant shape selectivity, RSS), (2) retention of larger molecules formed inside a catalysts by a slower diffusion rate (product shape selectivity, PSS) and (3) the hindrance of achieving a transition state because severe steric constraints in the confined pore

environment do not allow its formation (transition state selectivity, TSS).[84] A related conceptual idea, molecular traffic control (MTC), was introduced by Derouane and Gabilica[59, 64] based on independently diffusing streams of reactants that react at the intersections of the channel systems.

As a direct consequence of the broad industrial application of H-ZSM5 in many large scale petrochemical processes such as, the production[61], trans-alkylation[85], disproportionation[27, 75, 86] and isomerization of aromatic molecules[22, 27, 87] as well as the separation of hydrocarbon molecules (e.g., the Parex© process[88] for the xylene isomer separation), the concept of shape selectivity has been subject of various theoretical and experimental studies[30, 55, 56, 89, 90] in the past. Moreover, it has become one of the central concepts in zeolite catalysis. The reader further interested in this topic is also pointed to the excellent reviews on shape selectivity published by Smit[91], Degnan[25, 63] and Marcilly.[22]

Several novel and alternative reactions, allowing the optimization and the development of novel generations of molecular sieves, including inverse and secondary shape selectivity are currently explored.[54, 55, 90] The exploitation of intrinsic shape selective properties in a predicted way represents a demanding challenge for modern material research. In this context, hierarchically structured, porous materials with precisely tailored network topologies have accounted special interest[92] and designer-made materials with pre-defined activities and selectivities would be highly desirable.

1.1.3 Investigation of hydrocarbon transport in zeolites

While the experimental and theoretical efforts have led to an impressive advancement of understanding and utilizing shape selectivity in the past, the *de-novo* design of processes based on shape selectivity is still far from being practicably realizable. The best chances for this are at present related to processes involving the differentiation between molecules via transport, either into or out of the porous system. This section of the thesis aims, therefore, to shortly summarize the current view on molecular transport processes and elementary steps during diffusion and adsorption of

hydrocarbons in zeolites from the perspective of the recent experiments reported in literature.

Numerous *in-situ* or *ex-situ* experimental studies have already addressed sorption[93-95], transport and diffusion phenomena in zeolites involving aromatic and aliphatic hydrocarbons.[65, 96-100] Either equilibrium or non-equilibrium characterization techniques (see Figure 1.7) have been developed within the past decades and were successfully applied to explore the underlying fundamental principles.[101, 102] Among those, the FTIR and Raman spectroscopy[103-107], NMR spectroscopy (Pulsed-field gradient (PFG) and exchange NMR)[108-111], infrared microscopy IFM[112-114], neutron diffraction (QENS, INS)[115-117], uptake experiments such as ZLC[118, 119] and also the frequency response (FR) technique[87, 120, 121] have to be mentioned. Within this thesis, the experimental focus will be exclusively laid on the FTIR spectroscopy accompanied by the FR method, which are introduced in detail in chapter two.
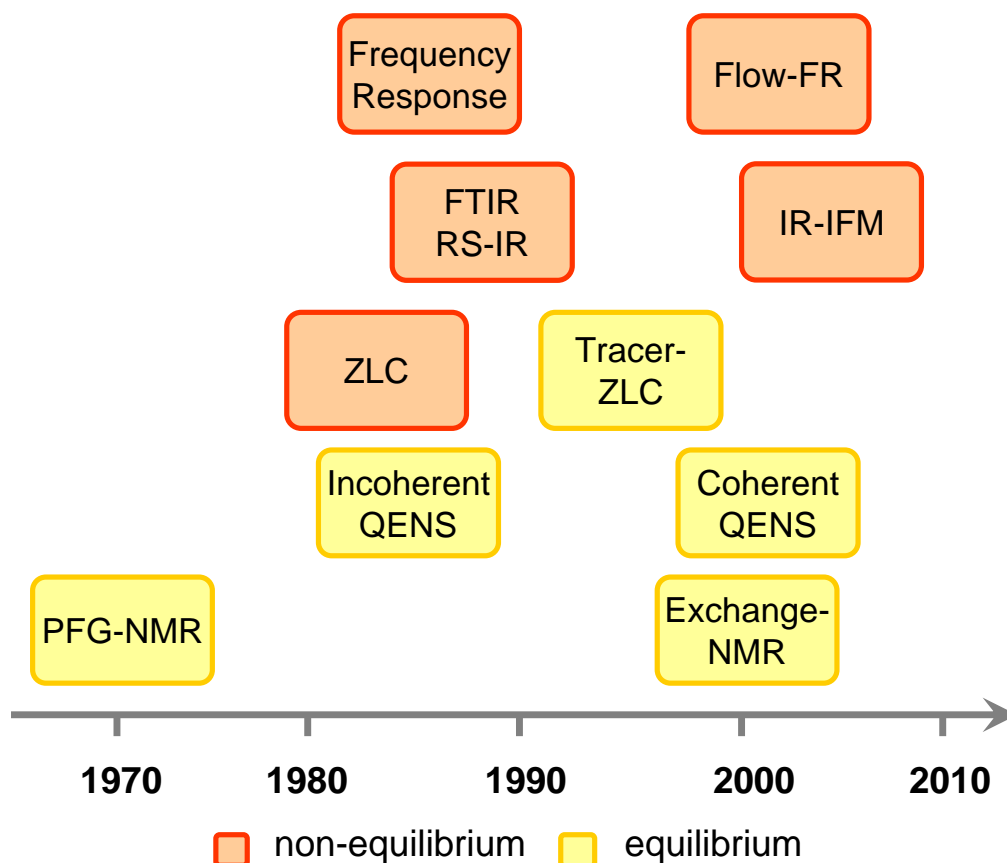
Figure 1.7   **Overview of different experimental techniques developed in the past decades to study transport phenomena of hydrocarbon reactants on molecular sieves.**

Mass transfer to the active sites inside the pores of a molecular sieve under equilibrium conditions is described by the self-diffusivity of the molecules which has to be distinguished from the transport diffusivity related to the motion of the molecules, under non-equilibrium conditions e.g., when pressure gradients are applied. When comparing the results obtained by different transport experiments, thermodynamic corrections (i.e., the Darken correction[100]) become necessary.[89]

The adsorption of hydrocarbon molecules such as e.g., benzene, toluene and *p*-xylene inside the zeolite pores was shown not only to be influenced by the strength and the concentration of the acid/base sites, but also by the respective geometry of the intra-zeolite void spaces.[104, 122, 123] The detailed sorption studies by Mukti *et al.*[124] using (thermo)-gravimetry and infrared spectroscopy have described the entropic and enthalpic contributions during sorption of the alkyl-substituted aromatic molecules in the pores of MFI zeolites. It was shown that, depending on the size of the sorbate molecule, sterically constrained sorption at the bridging hydroxyl groups inside the pores and at the pore openings occurs. By comparing gravimetry and infrared spectroscopy, it is concluded that at low sorbate coverages (< 1 molecule per unit cell), preferential sorption at the acid sites dominates the sorption process.[124] Reaching higher sorbate coverages, sorption sites without acid hydroxyl group i.e., the channel segments, are populated.

For the case of intra-crystalline transport of aromatic hydrocarbon molecules in MFI-type zeolites, it could be recently shown that the diffusion processes strongly depend on the ability of the molecules to reorient themselves inside the channel intersections without steric restrictions. If the space requirements do not allow the reorientation and the exchange between the channel segments (such as for *p*-xylene), anisotropic diffusion with two slightly different rates can be observed, while for smaller molecules such as benzene an isotropic diffusion process is observed.[125] The molecular transport of hydrocarbons from the gas phase to the active sites inside a zeolite proceeds via a series of interconnected steps, which are highlighted in chapter four. The steps of sticking and trapping of the sorbate on the zeolite surface and of the subsequent entering into the pore network were probably controversially discussed. Simon *et al.* reported estimated sticking probabilities of approximately one[126, 127] for *n*-butane on Silicalite-1 and Kärger *et al.*[128] found values of around 10^{-4} for benzene

in Silicalite-1, using pulse-field-gradient (PFG)-NMR spectroscopy.[128, 129] In contrast the results of our studies, based on time-resolved infrared spectroscopy with ZSM5 [130], showed much smaller values of around 10^{-7} for benzene, toluene and the xylene molecules.[131, 132] These findings unambiguously underline the necessity for more profound investigations in this field and are subjected in the following chapters.

It can furthermore be stated, that the whole process of entering the zeolite pores originated from the gas phase involves either external or internal diffusion barriers[65, 133-135], the intrinsic size exclusion during the pore entry itself[126, 136], and the subtle interplay between the entropic and enthalpic effects occurring during sorption within the confined spaces.[106] The clear differentiation between these, presumably simultaneously occurring effects is challenging. Post-synthetically surface modified zeolite materials have turned out to be the ideal target to study these effects. In an innovative experimental approach Chmelik *et al.*[137, 138] studied *iso*-butane ad-/ and desorption on surface treated Silicalite-1 crystals using infrared interference microscopy. Their results indicate that the surface barriers are related to direct to the entrance into the pores and that the extent of surface modification can induce discretely enhanced barriers, if larger organic modifying agents are used. While this may be the best defined example, a plethora of methods is reported in the literature.[139-145] Besides advanced pre-coking techniques[146], NaOH treatment[147] and impregnation methods using e.g., bulky amines to block surface sites[148], the post-synthetic modification of the external crystallite surface by chemical vapour or liquid deposition (CVD, CLD)[149, 150] of precursors of amorphous silica were the most frequently applied techniques to adjust catalytic properties of a large variety of different zeolite materials.[72, 151, 152]

Summarizing, the attempts mentioned above clearly indicate that an exact control of the effective pore dimensions of the porous catalyst, of the surface morphology as well as of the distribution of the acidic sites[153, 154] inside as well as outside the zeolite pores will in the future allow for rational design of catalyst and highly selective sorbent materials.[42, 57, 67]

1.2 Scope of this thesis

This dissertation thesis deals with the detailed investigation of the fundamental principles of sorption and transport phenomena occurring on catalytically relevant zeolite materials, involving different hydrocarbon reactants. In particular, a series of zeolite H-ZSM5 samples which have been gradually surface modified via post-synthetic, chemical liquid deposition technique (CLD) with tetraethyl orthosilicate (TEOS) represented the subject of interest within these studies.

The general characterization of the zeolite materials used together with a short description of each of the applied characterization techniques including nitrogen physisorption, infrared spectroscopy, electron microscopy, atomic absorption spectroscopy and solid state magic angle spinning nuclear magnetic resonance spectroscopy (MAS-NMR) is added to chapter two, section 2.1. Experimentally, for the determination of the characteristic transport parameters for the series of aromatic hydrocarbon molecules studied, a combination of advanced time-resolved infrared spectroscopy (FTIR) and the frequency response (FR) method was applied. A short introduction to the theoretical background, the data recording and a concise evaluation for both techniques is included within chapter two.

In order to understand the macroscopically observed transport processes and the influences of the surface post-treatment, it is mandatory to primarily identify the underlying elementary kinetic steps on the unmodified zeolite samples. Therefore the experimental focus is set on the identification of the interplay of interrelated individual kinetic steps within the complex transport network for a series of rather rigid alkyl-substituted aromatic sorbate molecules (benzene, toluene, p-xylene and o-xylene) in chapter four. In every heterogeneously catalyzed reaction, the gas phase molecules have to be primarily captured by the external zeolite surface before they can react at the active sites. This essential transport step can be described for H-ZSM5 crystals by the sticking probability (defined in chapter three) of the molecules on the outer surface which was experimentally derived from the time-resolved infrared spectroscopic measurements described within chapter four. In order to gain a complete understanding of the trends in the sticking probabilities on ZSM-5 surfaces with respect to the differences in the sorbate molecules, theoretical estimations of the well-balanced

enthalpic and entropic factors involved in the sticking process are required. To account for this, a short introduction into the general formalisms and the terminology of statistical thermodynamics is given in chapter three. Focus is thereby set on the description of the molecular partition functions.

Based on the variety of interconnected elementary steps included in the overall transport model on unmodified H-ZSM5, the influences of external surface modifications could be addressed. The results of the time-resolved infrared spectroscopic approach provided the profound kinetic basis to explain on a molecular level the influences of altered external surface morphologies on the sorption and transport properties of benzene unravelled on the surface silylated materials. This topic is subjected within the chapters five and six. Furthermore, instead of differentiating benzene, toluene and the three xylene isomers as conventionally described according to their minimum kinetic diameters, the surface modified materials exhibit hydrocarbon transport properties differentiated with respect to the radius of gyration of the molecules. A detailed explanation for this phenomenon which was observed for the first time on this kind of MFI-type zeolite materials is given in chapter six. The presented findings open up totally novel ways to, in the future allow tailor-made catalyst properties and rational de-novo catalyst design by overcoming current empirically driven experimental approaches, especially in the field of kinetic sorptive separation technology.

1.3 References

[1]   D. W. Breck, W. G. Eversole, R. M. Milton, *J. Am. Chem. Soc.* **1956**, *78*, 2338.

[2]   D. W. Breck, W. G. Eversole, R. M. Milton, T. B. Reed, T. L. Thomas, *J. Am. Chem. Soc.* **1956**, *78*, 5963.

[3]   P. B. Weisz, V. J. Frilette, *J. Phys. Chem.* **1960**, *64*, 382.

[4]   C. Baerlocher, W. M. Meier, D. Olson, *Atlas of Zeolite Framework Types*, 5 ed., Elsevier, Amsterdam, **2001**.

[5]   *Compendium of Chemical Terminology IUPAC Research Triangle Park NC*, **1997**.

[6]   R. Carvajal, P.-J. Chu, J. H. Lunsford, *J. Catal.* **1990**, *125*, 123.

[7]   R. Kumar, W. C. Cheng, K. Rajagopalan, A. W. Peters, P. Basu, *J. Catal.* **1993**, *143*, 594.

[8]   M. E. Davis, *Nature* **2002**, *417*, 813.

[9]   P. R. Pujado, J. A. Rabo, G. J. Antos, S. A. Gembicki, *Catal. Today* **1992**, *13*, 113.

[10]   I. Chorkendorff, J. W. Niemantsverdriet, *Concepts of Modern Catalysis and Kinetics*, 2nd ed., Wiley VCH GmbH, Weinheim, **2007**.

[11]   J. Weitkamp, *Solid State Ionics* **2000**, *131*, 175.

[12]   J. A. Rabo, M. W. Schoonover, *App. Catal. A-Gen.* **2001**, *222*, 261.

[13]   R. M. Barrer, D. J. Marshall, *American Mineralogist* **1965**, *50*, 484.

[14]   R. M. Barrer, *Nature* **1949**, *164*, 112.

[15]   J. A. Rabo, *Catal. Rev.-Sci. Eng.* **1981**, *23*, 293.

[16]   J. D. Sherman, *Proc. Natl. Acad. Sci. U. S. A.* **1999**, *96*, 3471.

[17]   U. Navarro, C. A. Trujillo, A. Oviedo, R. Lobo, *J. Catal.* **2002**, *211*, 64.

[18]   M. Guisnet, S. Mignard, *Actualite Chimique* **2000**, 14.

[19]   W. S. Letzsch, J. S. Magee, L. L. Upson, F. Valeri, *Oil and Gas Journal* **1988**, *86*, 57.

[20]   C. Marcilly, *Arab. J. Sci. Eng.* **1996**, *21*, 297.

[21]   J. Scherzer, *Appl. Catal.* **1991**, *75*, 1.

[22]   C. R. Marcilly, *Top. Catal.* **2000**, *13*, 357.

[23]   N. Y. Chen, T. F. Degnan, *Chem. Eng. Prog.* **1988**, *84*, 32.

[24]   M. W. Schoonover, M. J. Cohn, *Top. Catal.* **2000**, *13*, 367.

[25]   T. F. Degnan, *Top. Catal.* **2000**, *13*, 349.

[26]   K. Tanabe, W. F. Holderich, *App. Catal. A-Gen.* **1999**, *181*, 399.

[27]   T. C. Tsai, S. B. Liu, I. K. Wang, *App. Catal. A-Gen.* **1999**, *181*, 355.

[28]   R. Fricke, H. Kosslick, G. Lischke, M. Richter, *Chem. Rev.* **2000**, *100*, 2303.

[29]   D. Barthomeuf, *J. Phys. Chem.* **1993**, *97*, 10092.

[30]   C. B. Khouw, M. E. Davis, *ACS Symposium Series* **1993**, *517*, 206.

[31]   G. Muller, E. Bodis, J. Kornatowski, J. A. Lercher, *Phys. Chem. Chem. Phys.* **1999**, *1*, 571.

[32]   T. Kimura, *Microp. Mesop. Mat.* **2005**, *77*, 97.

[33]   H. O. Pastore, S. Coluccia, L. Marchese, *Ann. Rew. Mater. Res.* **2005**, *35*, 351.

[34]   D. B. Akolekar, *Journal of Molecular Catalysis A* **1995**, *104*, 95.

[35]   C. Fruijtier-Polloth, *Arch. Tox.* **2009**, *83*, 23.

[36]   K. H. Bergk, K. Pilchowski, F. Wolf, *Zeitschrift für Chemie* **1980**, *20*, 191.

[37]   K. Pilchowski, K. H. Bergk, H. J. Mallon, F. Wolf, *Zeitschrift für Chemie* **1980**, *20*, 191.

[38]   M. Ettlinger, H. Ferch, *Manufacturing Chemist and Aerosol News* **1978**, *49*, 51.

[39]   A. C. Savitsky, *Soap Cosmet. Chem. Spec.* **1977**, *53*, 29.

[40]   A. R. Elmore, F. A. Andersen, *Int. J. Toxicol.* **2003**, *22*, 37.

[41]   J. M. Thomas, R. G. Bell, C. R. A. Catlow, in *Handbook of heterogeneous catalysis, Vol. 1* (Eds.: G. Ertl, H. Knözinger, J. Weitkamp), Wiley-VCH, Weinheim, **1997**, pp. 286.

[42]   A. Corma, *Current Opinion in Solid State and Materials Science* **1997**, *2*, 63.

[43]   W. J. Mortier, J. Sauer, J. A. Lercher, H. Noller, *J. Phys. Chem.* **1984**, *88*, 905.

[44]   V. L. Zholobenko, L. M. Kustov, V. B. Kazansky, E. Löffler, U. Lohse, G. Oehlmann, *Zeolites* **1991**, *11*, 132.

[45]   A. Corma, H. Garcia, *Chem. Rev.* **2003**, *103*, 4307.

[46]   G. Lischke, E. Schreier, B. Parlitz, I. Pitsch, U. Lohse, M. Wöttke, *App. Catal. A-Gen.* **1995**, *129*, 57.

[47]   V. L. Zholobenko, L. M. Kustov, V. Y. Borovkov, V. B. Kazanskii, *Kin. Catal.* **1987**, *28*, 847.

[48]   P. L. Benito, A. G. Gayubo, A. T. Aguayo, M. Olazar, J. Bilbao, *J. Chem. Technol. Biot.* **1996**, *66*, 183.

[49]   G. T. Kokotailo, S. L. Lawton, D. H. Olson, W. M. Meier, *Nature* **1978**, *272*, 437

[50]   P. A. Jacobs, *Catal. Rev.-Sci. Eng.* **1982**, *24*, 415.

[51]   D. Barthomeuf, *Mater. Chem. Phys.* **1987**, *17*, 49.

[52]   B. Hunger, M. Heuchel, L. A. Clark, R. Q. Snurr, *J. Phys. Chem. B* **2002**, *106*, 3882.

[53]   H. A. Benesi, B. H. C. Winquist, *Advances in Catalysis* **1978**, *27*, 97.

[54]   B. Smit, *Chem. Rev.* **2008**, *108*, 4125.

[55]   M. Schenk, S. Calero, T. L. M. Maesen, T. J. H. Vlugt, L. L. van Benthem, M. G. Verbeek, B. Schnell, B. Smit, *J. Catal.* **2003**, *214*, 88.

[56]   T. L. M. Maesen, E. Beerdsen, S. Calero, D. Dubbeldam, B. Smit, *J. Catal.* **2006**, *237*, 278.

[57]   A. Corma, in *Studies In Surface Science And Catalysis, Recent Advances in the Science and Technology of Zeolites and Related Materials, Vol. 154* (Eds.: E. van Steen, L. H. Callanan, M. M. Claeys), Elsevier B.V., Amsterdam, **2004**, pp. 25.

[58]   S. M. Csicsery, *Abstr. Paper Am. Chem. Soc.* **1983**, *185*, 44.

[59]   S. M. Csicsery, *Zeolites* **1984**, *4*, 202.

[60]   S. M. Csicsery, *Chemistry in Britain* **1985**, *21*, 473.

[61]   S. M. Csicsery, *Pure Appl. Chem.* **1986**, *58*, 841

[62]   S. M. Csicsery, *Catalysis by Microporous Materials* **1995**, *94*, 1.

[63]   T. F. Degnan, *J. Catal.* **2003**, *216*, 32.

[64]   E. G. Derouane, Z. Gabelica, *J. Catal.* **1980**, *65*, 486.

[65]   J. Kärger, *Adsorption* **2003**, *9*, 29.

[66]   A. Corma, *Chem. Rev.* **1995**, *95*, 559

[67]   A. Corma, *J. Catal.* **2003**, *216*, 298.

[68] R. J. Argauer, M. Kensington, G. R. Landolt, in *U.S. Patent, Vol. 3.702.886*, **1972**.

[69] E. M. Flanigen, J. M. Bennett, R. W. Grose, J. P. Cohen, R. L. Patton, R. M. Kirchner, J. V. Smith, *Nature* **1978**, *271*, 512.

[70] D. H. Olson, G. T. Kokotailo, S. L. Lawton, W. M. Meier, *J. Phys. Chem.* **1981**, *85*, 2238.

[71] S. A. Tabak, F. J. Krambeck, W. E. Garwood, *Aiche Journal* **1986**, *32*, 1526.

[72] L. B. Young, S. B. Butter, W. W. Kaeding, *J. Catal.* **1982**, *76*, 418.

[73] N. Y. Chen, *J. Catal.* **1988**, *114*, 17.

[74] A. E. Palomares, G. EderMirth, J. A. Lercher, *J. Catal.* **1997**, *168*, 442.

[75] N. R. Meshram, *J. Chem. Technol. Biot.* **1987**, *37*, 111.

[76] G. Eder-Mirth, H. D. Wanzenböck, J. A. Lercher, *Stud. Surf. Sci. Catal.* **1995**, *94*, 449.

[77] W. O. Haag, D. H. Olson, in *U.S. Patent, Vol. 4.117.026*, **1978**.

[78] P. B. Weisz, J. V. Frilette, *J. Phys. Chem.* **1960**, *64*, 382.

[79] P. B. Weisz, *Pure Appl. Chem.* **1980**, *52*, 2091.

[80] P. B. Weisz, *Chemtech* **1973**, 498.

[81] P. B. Weisz, *Chimia* **1979**, *33*, 154.

[82] P. B. Weisz, *Science* **1973**, *179*, 433.

[83] N. Y. Chen, W. E. Garwood, *Catal. Rev.-Sci. Eng.* **1986**, *28*, 185.

[84] M. Seitz, E. Klemm, G. Emig, in *Catalyst Deactivation 1999, Vol. 126*, Elsevier Science Publication, Amsterdam, **1999**, pp. 221.

[85] F. J. Llopis, G. Sastre, A. Corma, *J. Catal.* **2004**, *227*, 227.

[86] N. Arsenova, W. Haag, H. Karge, *Stud. Surf. Sci. Catal.* **1995**, *94*, 441.

[87] S. R. Zheng, H. Tanaka, A. Jentys, J. A. Lercher, *J. Phys. Chem. B* **2004**, *108*, 1337.

[88] K. Vener, Y. Velker, G. Zaidel, *Petrol. Chem.* **1971**, *11*, 50.

[89] A. Jentys, H. Tanaka, J. A. Lercher, in *Studies in Surface Science and Catalysis, Recent Advances in the Science and Technology of Zeolites and Related Materials, Vol. 154* (Eds.: E. van Steen, L. H. Callanan, M. Claeys), Elsevier B.V., Amsterdam, **2004**, pp. 2041.

[90]   T. L. M. Maesen, R. Krishna, J. M. van Baten, B. Smit, S. Calero, J. M. C. Sanchez, *J. Catal.* **2008**, *256*, 95.

[91]   B. Smit, T. L. M. Maesen, *Nature* **2008**, *451*, 671.

[92]   J. Perez-Ramirez, C. H. Christensen, K. Egeblad, C. H. Christensen, J. C. Groen, *Chem. Soc. Rev.* **2008**, *37*, 2530.

[93]   C. G. Pope, *J. Phys. Chem.* **1984**, *88*, 6312.

[94]   C. G. Pope, *J. Phys. Chem.* **1986**, *90*, 835.

[95]   A. Corma, V. Fornes, L. Forni, F. Marquez, J. Martinez-Triguero, D. Moscotti, *J. Catal.* **1998**, *179*, 451.

[96]   S. Brandani, D. M. Ruthven, J. Kärger, *Microporous Mater.* **1997**, *8*, 193.

[97]   D. M. Ruthven, in *Studies in Surface Science and Catalysis, Zeolites: A Refined Tool for Designing Catalytic Sites, Vol. 97* (Eds.: L. Bonneviot, S. Kaliaguine), Elsevier B.V., Amsterdam, **1995**, pp. 223.

[98]   D. M. Ruthven, *Adsorption* **2007**, *13*, 225.

[99]   D. M. Ruthven, M. Eic, *Abstr. Paper Am. Chem. Soc.* **1988**, *195*, 201.

[100]   J. Kärger, D. M. Ruthven, in *Studies in Surface Science and Catalysis, Progress in Zeolite and Microporous Materials, Vol. 105* (Eds.: H. Chon , S.-K. K. Ihm, Y. S. Uh), Elsevier B.V., Amsterdam, **1997**, pp. 1843.

[101]   T. Kunieda, J. H. Kim, M. Niwa, *J. Catal.* **1999**, *188*, 431.

[102]   R. Cartarius, H. Vogel, J. Dembowski, *Phys. Chem. Chem. Phys.* **1997**, *101*, 193.

[103]   S. Zheng, H. R. Heydenrych, A. Jentys, J. A. Lercher, *J. Phys. Chem. B* **2002**, *106*, 9552.

[104]   M. Trombetta, G. Busca, L. Storaro, M. Lenarda, M. Casagrande, A. Zambon, *Phys. Chem. Chem. Phys.* **2000**, *2*, 3529.

[105]   A. K. Tripathi, A. Sahasrabudhe, S. Mitra, R. Mukhopadhyay, N. M. Gupta, V. B. Kartha, *Phys. Chem. Chem. Phys.* **2001**, *3*, 4449.

[106]   S. J. Reitmeier, O. C. Gobin, A. Jentys, J. A. Lercher, *Angew. Chem. Int. Ed.* **2009**, *48*, 533.

[107]   A. Jentys, H. Tanaka, J. A. Lercher, *J. Phys. Chem. B* **2005**, *109*, 2254.

[108] U. Hong, J. Kärger, H. Pfeifer, U. Muller, K. K. Unger, *Z. Phys. Chem.* **1991**, *173*, 225.

[109] C. Krause, S. Klein, J. Kärger, W. F. Maier, *Advanced Materials* **1996**, *8*, 912.

[110] S. Vasenkov, W. Bohlmann, P. Galvosas, O. Geier, H. Liu, J. Kärger, *J. Phys. Chem. B* **2001**, *105*, 5922.

[111] J. Kärger, H. Pfeifer, *J. Am. Chem. Soc. Faraday Trans.* **1991**, *87*, 1989.

[112] L. Heinke, C. Chmelik, P. Kortunov, D. M. Ruthven, D. B. Shah, S. Vasenkov, J. Kärger, *Chem. Eng. Technol.* **2007**, *30*, 995.

[113] L. Heinke, C. Chmelik, P. Kortunov, S. Vasenkov, D. M. Ruthven, D. B. Shah, J. Kärger, *Chemie Ingenieur Technik* **2007**, *79*, 1195.

[114] U. Schemmert, J. Kärger, J. Weitkamp, *Microp. Mesop. Mat.* **1999**, *32*, 101.

[115] H. Jobic, M. Bee, J. Kärger, C. Balzer, A. Julbe, *Adsorption* **1995**, *1*, 197.

[116] H. Jobic, M. Bee, S. Pouget, *J. Phys. Chem. B* **2000**, *104*, 7130.

[117] H. Jobic, A. N. Fitch, J. Combet, *J. Phys. Chem. B* **2000**, *104*, 8491.

[118] S. Brandani, Z. Xu, D. Ruthven, *Microporous Mater.* **1996**, *7*, 323.

[119] J. R. Hufton, S. Brandani, D. M. Ruthven, in *Studies in Surface Science and Catalysis; Zeolites and Related Microporous Materials: State of the Art 1994, Vol. 84* (Eds.: E. J. P. Feijen, J. A. Martens, P. A. Jacobs), Elsevier B.V., Amsterdam **1994**, pp. 1323.

[120] Y. Yasuda, in *Studies in Surface Science and catalysis; Zeolites and Related Microporous Materials: State of the Art 1994, Vol. 84* (Eds.: E. J. P. Feijen, J. A. Martens, P. A. Jacobs), Elsevier B.V., Amsterdam, **1994**, pp. 1331.

[121] Y. Yasuda, *Het. Chem. Rev.* **1994**, *1*, 103.

[122] F. Eder, J. A. Lercher, *J. Phys. Chem. B* **1997**, *101*, 1273.

[123] M. Trombetta, T. Armaroli, A. G. Alejandre, H. Gonzalez, J. R. Solis, G. Busca, *Catal. Today* **2001**, *65*, 285.

[124] R. R. Mukti, A. Jentys, J. A. Lercher, *J. Phys. Chem. C* **2007**, *111*, 3973.

[125] O. C. Gobin, S. J. Reitmeier, A. Jentys, J. A. Lercher, *Microp. Mesop. Mat.* **2009**, *(in press)*.

[126] J.-M. Simon, J.-P. Bellat, S. Vasenkov, J. Kärger, *J. Phys. Chem. B* **2005**, *109*, 13523.

[127] J. M. Simon, A. Decrette, J. B. Bellat, J. M. Salazar, *Mol. Sim.* **2004**, *30*, 621.

[128] J. Kärger, S. Vasenkov, *J. Phys. Chem. B* **2006**, *110*, 17694.

[129] J. A. Z. Pieterse, S. Veefkind-Reyes, K. Seshan, J. A. Lercher, *J. Phys. Chem. B* **2000**, *104*, 5715.

[130] A. Jentys, R. R. Mukti, J. A. Lercher, *J. Phys. Chem. B* **2006**, *110*, 17691.

[131] S. J. Reitmeier, R. R. Mukti, A. Jentys, J. A. Lercher, *J. Phys. Chem. C* **2008**, *112*, 2538.

[132] S. J. Reitmeier, R. R. Mukti, A. Jentys, J. A. Lercher, *J. Phys. Chem. C* **2009**, *113*, 1640.

[133] J. Kärger, J. Caro, *J. Am. Chem. Soc. Faraday Trans.* **1977**, *73*, 1363.

[134] P. Kortunov, S. Vasenkov, C. Chmelik, J. Kärger, D. M. Ruthven, J. Wloch, *Chem. Mater.* **2004**, *16*, 3552.

[135] J. Kärger, D. M. Ruthven, in *Handbook of Porous Solids, Vol. 4* (Eds.: F. Schüth, K. S. Sing, J. Weitkamp), Wiley-VCH, Weinheim, **2002**, p. 2089.

[136] A. Schüring, *J. Phys. Chem. C* **2007**, *111*, 11285.

[137] C. Chmelik, A. Varma, L. Heinke, D. B. Shah, J. K. Kärger, F., U. Wilzok, W. Schmidt, *Chem. Mater.* **2007**, *19*, 6012.

[138] C. Chmelik, P. Kortunov, S. Vasenkov, J. Kärger, *Adsorption* **2005**, *11*, 455.

[139] X. X. Wang, X. Chen, H. B. Xu, X. Z. Fu, *Chin. J. Inorg. Chem.* **2002**, *18*, 541.

[140] A. Gupta, R. Q. Snurr, *J. Phys. Chem. B* **2005**, *109*, 1822.

[141] R. W. Weber, K. P. Moller, C. T. O'Connor, *Microp. Mesop. Mat.* **2000**, *35-6*, 533.

[142] J. Wloch, *Microp. Mesop. Mat.* **2003**, *62*, 81.

[143] J. H. Kim, A. Ishida, M. Okajima, M. Niwa, *J. Catal.* **1996**, *161*, 387.

[144] S. Zheng, H. R. Heydenrych, H. P. Roger, A. Jentys, J. A. Lercher, *Top. Catal.* **2003**, *22*, 101.

[145] J. H. Kim, M. Okajima, M. Niwa, *Prog. Zeol. Microp. Mat.* **1997**, *105*, 1965.

[146] F. Bauer, W. H. Chen, E. Bilz, A. Freyer, V. Sauerland, S. B. Liu, *J. Catal.* **2007**, *251*, 258.

[147] G. Lietz, K. H. Schnabel, C. Peuker, T. Gross, W. Storek, J. Volter, *J. Catal.* **1994**, *148*, 562.

[148]   W. W. Kaeding, L. B. Young, C. Chu, *J. Catal.* **1984**, *89*, 267.

[149]   Z. Zhu, Z. Xie, Q. Chen, K. Dejin, W. Li, W. Yang, C. Li, *Microp. Mesop. Mat.* **2007**, *101*, 169.

[150]   F. Dong, G. R. Wang, X. S. Wang, *Chin. J. Chem. Eng.* **1995**, *3*, 208.

[151]   C. D. Chudasama, J. Sebastian, R. V. Jasra, *Ind. Eng. Chem. Res.* **2005**, *44*, 1780.

[152]   S. Zheng, PhD thesis, TU München (München), **2002**.

[153]   A. H. de Vries, P. Sherwood, S. J. Collins, A. M. Rigby, M. Rigutto, G. J. Kramer, *J. Phys. Chem. B* **1999**, *103*, 6133.

[154]   M. Brandle, J. Sauer, *J. Am. Chem. Soc.* **1998**, *120*, 1556.

Chapter 2

2. Experimental methods and materials

2.1   Materials and Characterization

Dealing with investigation of the relations between the kinetics of sorption and transport on molecular sieves, a complete chemical and structural characterization[1] of the target materials including sorption capacity, hydroxyl site density and strength, as well as particle size and morphology is mandatory.
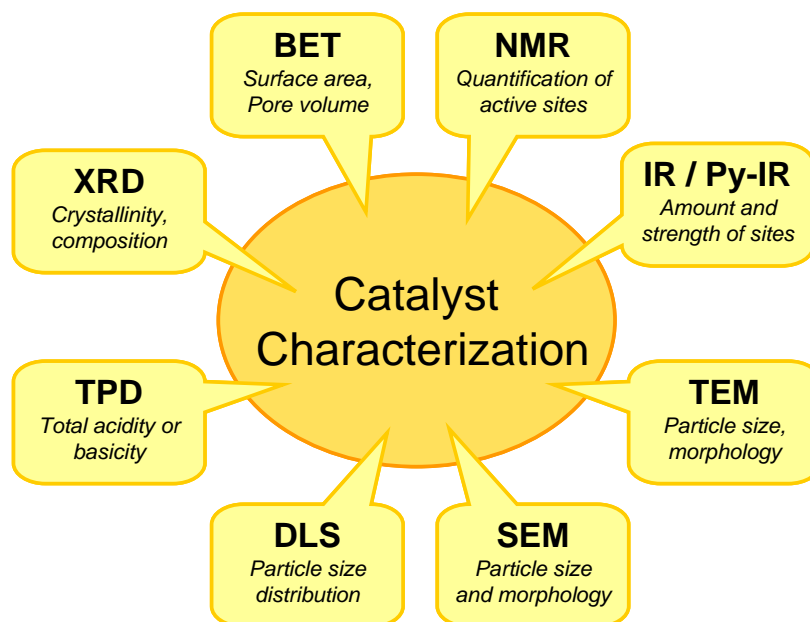
Figure 2.1   **Summary of relevant techniques to characterize porous, solid catalyst materials.**

A variety of experimental techniques is available within modern catalyst characterization and material research, probing specific properties via the direct interaction of the catalyst material with incident radiation, ions or electron beams. For the purpose of this thesis, the following methods have been applied to characterize the zeolite samples prior to the transport experiments: (1) X-ray powder diffraction (XRD) to determine the structure, (2) atomic absorption spectroscopy (AAS) for composition analysis, (3) nitrogen physisorption and BET to analyze surface area and pore volume and (4) scanning or (5) transmission electron microscopy (SEM and TEM) to determine particle size and morphology. In addition, (6) solid state nuclear magnetic resonance (NMR) spectroscopy was used to confirm the concentrations of surface and

intra-pore hydroxyl groups. Infrared spectroscopy (7) yielded information about the presence, amount and strength of the hydroxyls in views to hydrocarbon sorption.

2.1.1 Target materials

Due to their unique structural properties, medium pore sized zeolites represent an ideal target material for studying the influence of the external surface properties on pore entering, surface and intra-pore transport processes of aromatic $C_6 - C_8$ hydrocarbon reactant molecules. For the transport experiments, described within the following chapters of this thesis, MFI-type zeolites with pore apertures similar to the minimum kinetic diameters of the hydrocarbon molecules of interest have been chosen. The parent material (unmodified material), commercial ZSM5 zeolite was provided in proton form by the Süd-Chemie AG with a nominal silica to alumina ratio of 90 (Si/Al-ratio = 45) and will be denoted H-ZSM5-p in the following. To provide a comparison of the surface transport processes in absence of micropores, amorphous, non-porous silica (Aerosil200) was used.

Aiming to directly unravel the influences of the surface composition, surface morphology and the effective pore apertures on hydrocarbon transport, surface modified samples were used. The post-synthetic silylation of the commercial zeolite sample by chemical liquid deposition (CLD) of tetraethyl orthosilicate (TEOS) was experimentally performed by S. Zheng et al. [2-4] following a hydrothermal synthesis procedure. For completeness, a short description is given herein. The zeolite samples in powder form were grinded, suspended in *n*-hexane and heated under stirring to reflux. Subsequently, TEOS as silica source was added with an amount equal to 4 wt-% of SiO_2 per modification cycle to the solution and the molecules attached to the hydroxyl groups of the zeolite via condensation reaction. After removal of the organic solvent and water, the TEOS was converted to SiO_2 during calcinations at 773 K in synthetic air for several hours. The procedure was repeated up to three times and the resulting samples were denoted H-ZSM5-m and H-ZSM5-3m according to the degree of silylation. Due to the fact, that the minimum kinetic diameter of the TEOS molecule with 1.0 nm exceeds the pore dimensions of the zeolite, only terminal hydroxyl groups on the external surface and acidic hydroxyl groups in the pore mouth regions can react. The effect of the external surface modification on the distribution of the active sites, in

particular in the pore mouth regions is described elsewhere.[3, 4] In the following, focus is set on the structural and chemical characterization of the parent zeolite material. A detailed description of the structure and the properties of the amorphous silica formed on the surface during post-treatment is subject of investigation in chapter four and five.

2.1.2 Nitrogen physisorption measurements and the BET model

Porous solid materials are characterized by means of their specific surface area S_A, the micro- and mespore volume V_{mi} and V_{me} as well as the pore dimensions and size distributions of the channel network d_p. Following the classification of the International Union of Pure and Applied Chemistry (IUPAC), pore diameters below 2.0 nm are called micropores, pore diameters larger than 50 nm macropores and in between mesopores. Typically, pore diameters vary from sub-nanometer range for the case of zeolite micropores up to several nanometers for mesoporous silica materials. Conventional porous solids, e.g., charcoal show even pores in the macropore range (see Figure 2.3).[5]
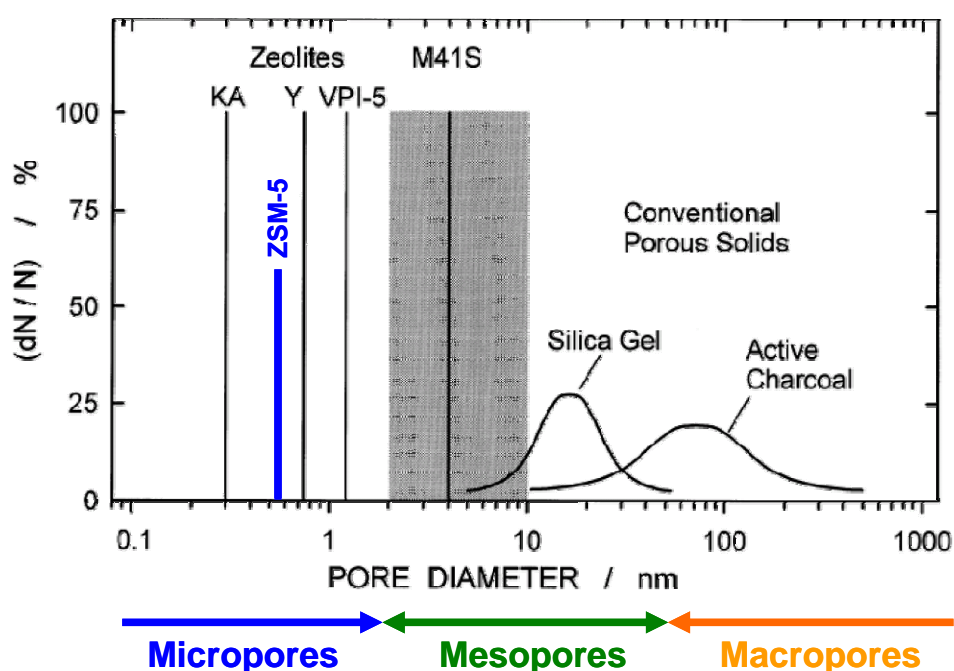

Figure 2.2 **Pore dimensions of porous solid catalyst materials and IUPAC pore system classification (Adopted from ref. [4])**

A commonly used technique to precisely determine the surface area and pore volume of solid catalysts is the non-specific sorption (physisorption) of nitrogen at

liquid nitrogen temperature. Following the ad- and desorption branches with increasing partial pressure, characteristic sorption isotherms are obtained. The so called BET isotherm (Brunauer, Emmet and Teller)[6-8] conceptually accounts for multi-layer adsorption effects and represents an extended description of the Langmuir sorption model. Mathematically, the BET isotherm in linear form[9] can be expressed as follows as a function of the sorbate partial pressure.

$$\frac{p}{V_{ads} \cdot (p_0 - p)} = \frac{1}{C \cdot V_0} + \frac{(C-1)}{C \cdot V_0} \frac{p}{p_0} \quad with \quad C = \exp\left(\frac{\Delta H_{ad,1} - \Delta H_{ad,2}}{R \cdot T}\right) \qquad (2.1)$$

Herein, p denotes the nitrogen partial pressure; p_0 is given by the equilibrium pressure of the condensed nitrogen gas at 77 K, V_0 is the volume of an adsorbed nitrogen monolayer. C expresses the change in the enthalpy of adsorption between the first and the second sorbate layer.[10] Linearization of the BET equation[8] and graphical evaluation of $p \cdot (V_{ads} \cdot (p_0 - p))$ plotted against p / p_0 yields a straight line. Slope and intercept directly result C and V_0. Knowing that one molecule of nitrogen occupies an area equal to 0.162 nm^2 $molecule^{-1}$ the BET specific surface area[9], representing the overall surface area of the material is directly calculated from V_0. Note, that due to the boundary conditions, the BET equation does not fit to the complete range of the sorption isotherm. Therefore additional evaluation methods have been developed.

Most commonly used are the so called comparative plot methods.[11] They comprise e.g., the de Boer's t-plot equation and the standard reduced adsorption (α_S) method introduced by K. Sing. For the α_S formalism, the experimentally determined sorption isotherms under study are compared with the sorption isotherms of a non-porous or macroporous reference solids such as e.g., LiChrospher Si-1000[12, 13], chosen specifically according to its chemical similarity to the investigated adsorbent material. Both methods allow satisfactorily to quantitatively distinguishing between the individual contributions of micropores, mesopores or macropores to the total pore volume present within the material.[14] Practically, the amount adsorbed on the porous solid is plotted as function of the amount adsorbed on a reference solid, expressed by either the statistical film thickness t [nm] or the dimensionless standard reduced adsorption α_S at standard temperature and pressure conditions (STP). The adsorption

process observed in a certain region is presumably described by a straight line with the intercept defining the maximum adsorption in e.g., the micropores.[15]

$$t(nm) = 0.1 \cdot \left(\frac{13.99}{0.034 + \log \dfrac{p}{p_0}} \right)^{0.5} \tag{2.2}$$

$$\alpha_S(p') = \frac{V_{standard}^{ads}(p')}{V_{standard}^{ads}(p'=0.4)} \quad \text{with} \quad p' = \frac{p}{p_0} \tag{2.3}$$

Consequently, the shape of the t- or α_S-plot reveals characteristic differences for non-porous, micro- or mesoporous materials. For a more detailed description of the theoretical and practical issues of comparative plot analyses and the choice of the reference standard, it is referred to literature.[11-13] A convenient way to determine pore size distributions is given by the BJH (Barrett, Joyner and Halenda)[8, 16, 17] method.
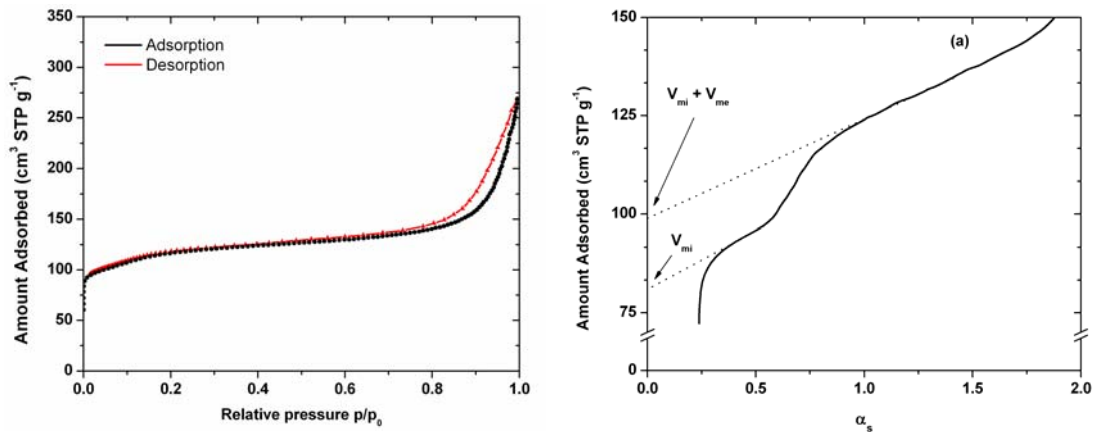

Figure 2.3 **(left) Nitrogen physisorption isotherm for H-ZSM5-p with adsorption and desorption branch and (right) exemplified α_S-plot indicating micro- and mesopore volume fractions.[18]**

Experimentally, all nitrogen physisorption measurements were performed on a PMI automated Sorptomatic 1990 instrument operating at liquid nitrogen temperature (77 K). Before the adsorption of nitrogen, 100 mg of the zeolite samples were outgassed and activated under vacuum (10^{-4} mbar) at 473 K for at least 6 h. After activation the samples were weighted to obtain the reference weight and subsequently cooled to 77 K. Specific surface areas were calculated by applying the BET-formalism the adsorption branch of the isotherms over the relative pressure range p/p_0 from 0.03

to 0.15. Pore volumes were evaluated from the α_s comparative plot with nonporous hydroxylated silica as the reference adsorbent.[11, 12]

2.1.3 Atomic absorption spectroscopy (AAS)

Atomic absorption spectroscopy (AAS) represents a powerful analysis technique to investigate and quantify the elementary composition of inorganic sample materials. ZSM5 samples were analyzed concerning the silicon and aluminium content and to ensure the absence of transition metals i.e., iron as impurities. AAS measurements were performed on an UNICAM 939 spectrometer. Prior to the measurements, an amount of 10 to 50 mg of sample was dissolved in a boiling mixture of hydrofluoric acid (HF, 0.5 ml) and nitro-hydrochloric acid (0.1 ml) to ensure complete dissolution of the sample. For H-ZSM5-p the nominal Si/Al-ratio of 45 could be verified (see Table 1). Accounting for the amount of amorphous silica deposited during post-synthesis modification with TEOS, this ratio remained unchanged.[2]

Table 2.1   Elementary composition of the zeolites derived from AAS analysis.

Sample	Si [wt-%]	Al [wt-%]	Fe [wt-%]	Na [wt-%]	Si/Al-ratio
H-ZSM5-p	38.5	0.86	< 0.02	< 0.01	44.8
H-ZSM5-1m	38.7	0.82	< 0.02	0.01	45.1
H-ZSM5-3m	40.6	0.83	< 0.02	< 0.01	44.0

2.1.4 X-ray powder diffraction (XRD)

The XRD method belongs to the most frequently applied characterization techniques, applied to determine the three-dimensional structure of crystalline solid catalyst materials and to identify different crystalline phases present in the material. The samples are irradiated with coherent, monochromatic X-ray radiation, in our case from the Cu-Kα1 transition. When the crystalline material interacts with the incident X-ray photons, elastic scattering occurs at the atoms in the periodic lattice of the material and the scattered X-rays show interference. It is important to note, that XRD has a clear limitation, because it requires suitable long-range ordering within the material to detect diffraction lines. Therefore, amorphous phases can not be detected.
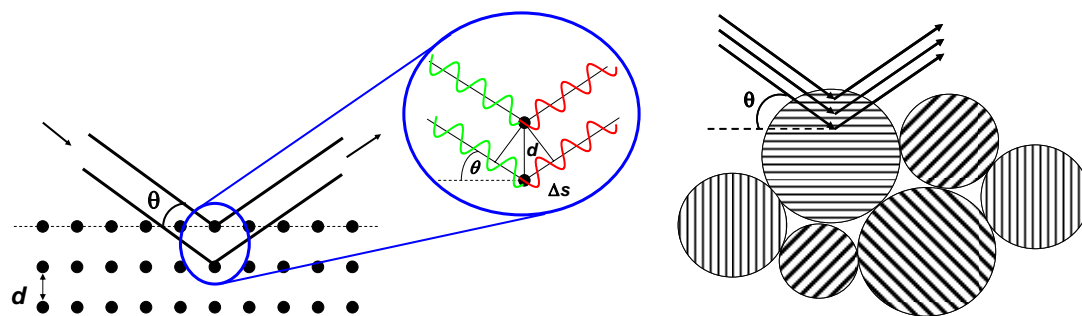
Figure 2.4 **(left) Derivation of Braggs' law of diffraction, schematically illustrated for a crystalline material with crystal plane distance *d* and pathlength difference Δs. (right) Polycrystalline powder sample subjected to X-rays (Figure adopted from ref. [19])**

The position of the reflexes in the obtained diffraction pattern depends on the distance between the lattice planes *d*, the wavelength of the radiation λ. It is a characteristic function of the incident angle of the radiation θ with respect to the reflecting lattice plane, described by the so called Braggs' relation with *k* being an integer representing the order of the reflection.

$$\Delta s = k \cdot \lambda = 2 \cdot d \cdot \sin \theta \tag{2.4}$$

When the difference in the pathlength Δ*s* between the incident X-ray beam and the scattered beam (see Figure 2.4) equals an integer times the wavelength of the radiation, constructive interference occurs, generating an observable maximum.[19, 20] For the case of powdered samples, the detection of the intensities of the diffraction lines as function of the incident angle *θ* of the X-rays results in a characteristic XRD powder pattern of the polycrystalline sample. From this, the involved crystalline phases can be identified. A distinct disadvantage of the XRD method is represented by the fact, that very small particles and also amorphous phases without long range structural ordering can not be detected.[19] Nevertheless, indirect indication for the presence of amorphous fractions within the sample can be obtained from the shape of the scattering background.

The X-ray powder diffraction patterns of the unmodified and modified zeolites H-ZSM5-p and H-ZSM5-3m as compiled in Figure 2.5 for comparison, were measured in transmission mode on a Stoe Stadi-P powder diffractometer using a germanium-

monochromated Cu-Kα1-radiation (at a wavelength of 1.540598 Å) at 40 kV. The powdered samples were placed on a plane sample carrier between two pieces of Scotch 3M® adhesive tape. A linear position-sensitive IP-PSD detector system was used. Data points were recorded between 2θ angles of 5° to 75° within 30 min for each sample. The positions of the reflexes can be attributed to crystalline H-ZSM5 zeolite for both samples, perfectly confirming that the crystallinity of the material was preserved upon surface modification. For the case of H-ZSM5-3m in addition, the presence of an amorphous fraction within the sample is evidenced from the slight increase in the background intensity at low diffraction angles. This can be explained by the amorphous silica layers deposited on the H-ZSM5 surface during surface silylation.
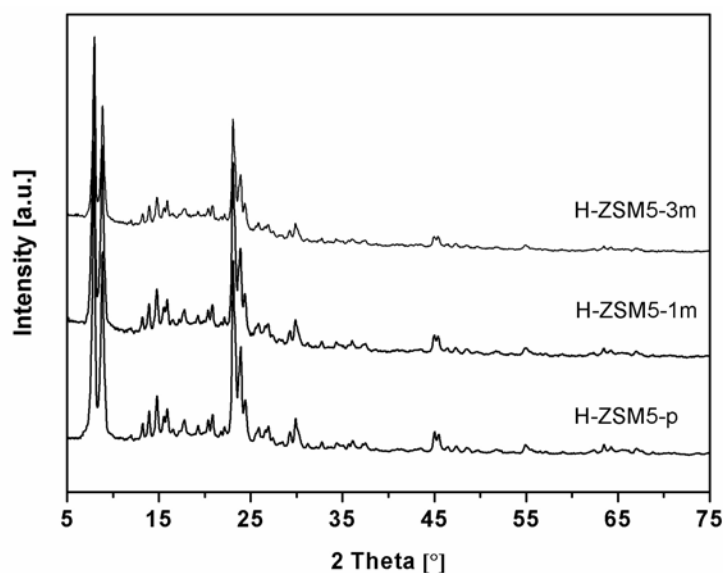

Figure 2.5   XRD pattern of H-ZSM5-p, 4 wt-% and 12 wt-% modified H-ZSM5-1m and H-ZSM5-3m.

Additional measurements in reflectance mode were carried out on a Philips X'pert Pro XRD instrument operating with Cu-Kα1-radiation and a Ni-filter to remove the Cu-Kβ-line. Data points were recorded with 2θ angles of 5° to 75° using a spinner system with an ¼ inch slit mask and a step size of 0.017° at 115 s per step.

2.1.5 Electron microscopy

The shape and the particle size of the primary zeolite particles were visualized using scanning electron microscopy. The scanning electron microscopy (SEM) measurements were performed on a REM JEOL 5900 LV microscope operated at 25

kV with a resolution of 5.0 nm and a maximum magnification of 3.0×10^6. From the micrographs shown in Figure 2.6, non-regularly shaped H-ZSM5 particles and a certain fraction of larger agglomerates can be seen. Instead of a sharp, homogenously distributed particle diameter, a broader particle size distribution was observed for the sample with some larger agglomerates and an average diameter of 0.5 μm.
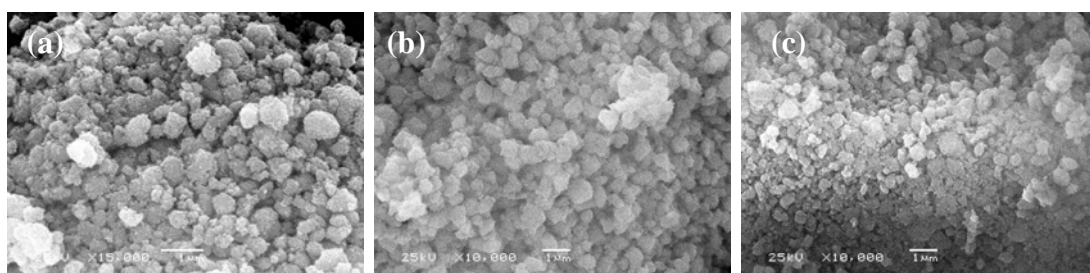

Figure 2.6 **Scanning electron micrographs of (a) unmodified H-ZSM5-p and (b) 4 wt-% and (c) 12 wt-% surface modified H-ZSM5-1m and H-ZSM5-3m, respectively, showing a distribution of particle sizes. The average particle size was determined to 0.5 mm.**

Transmission electron microscopy (TEM) was performed on a JEOL 2011 microscope with resolution of 0.2 nm. The acceleration voltage used was 200 kV. Prior to the measurements the powdered samples were dispersed in ethanol in an ultrasonic bath, deposited and dried on a carbon coated copper grid as support. The crystal lattice of the H-ZSM5 zeolite is clearly seen in the TEM images compiled in Figure 2.7 even at the edges of the crystallites.
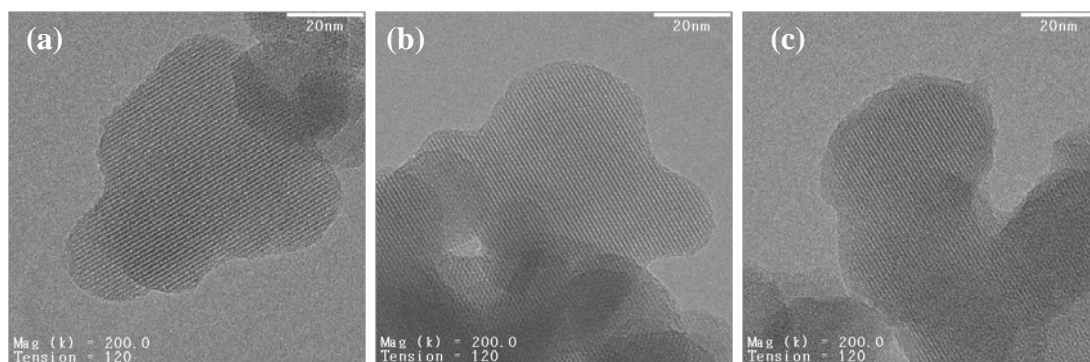

Figure 2.7 **Transmission electron micrographs of (a) unmodified H-ZSM5-p zeolite crystals and post-synthetically surface modified materials (b) H-ZSM5-1m and (c) H-ZSM5-3m, respectively, with the crystal lattices clearly visible.**

2.1.6 Solid state nuclear magnetic resonance (NMR)

2.1.6.1 General introduction and physical background

NMR spectroscopy is widely utilized to study the local chemical environment and connectivity of atoms within catalyst materials.[21] As it selectively probes chemical elements with respect to their nuclear magnetic moment, both, crystalline and amorphous samples can be studied. Physicochemically, all nuclei with a non-zero nuclear spin momentum have a constant nuclear magnetic moment $\vec{\mu}$ and are considered NMR-active, which means being detectable by NMR-spectroscopy. The component μ_z of the nuclear magnetic moment vector $\vec{\mu}$ is defined by the nuclear gyromagnetic ratio γ_N and the magnetic quantum number m_z:

$$\mu_z = -\gamma_N \cdot \hbar \cdot m_z \quad [\text{J} \cdot \text{T}^{-1}] \tag{2.5}$$

Applying a strong external field B_0 along the z-axis, the nuclear spins (spin quantum number I_N i.e., ½ for ^{1}H) align and the $(2I_N+1)$-fold degeneracy of the energy levels is broken. This interaction is called the Zeeman splitting and the corresponding energies E_Z are given by Equation 2.6.

$$E_Z(m_z) = -\mu_z B_0 = \gamma_N \cdot \hbar \cdot m_z \cdot B_0 \tag{2.6}$$

$$\Delta E = \gamma_N \cdot \hbar \cdot B_0 = h \cdot \nu_L \equiv h \cdot \nu \tag{2.7}$$
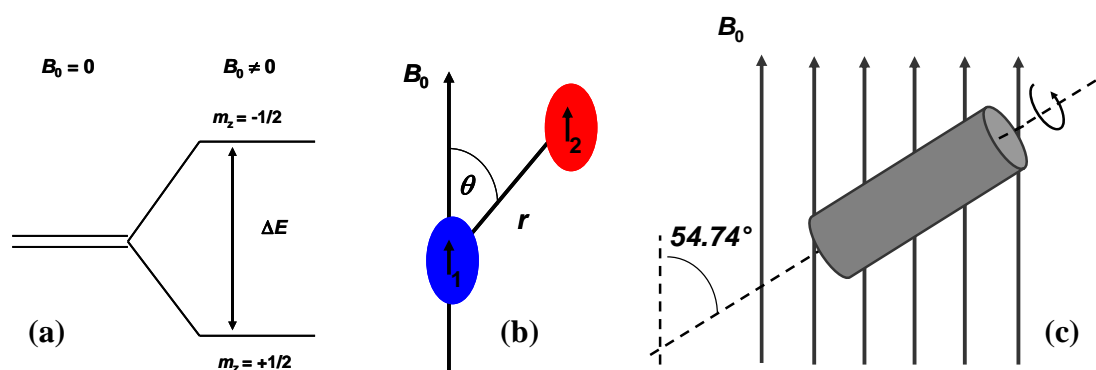

Figure 2.8   Schemes showing (a) the Zeeman-splitting, (b) the orientation dependency of the spin-spin interaction in a magnetic field B_0 and (c) the principle of the magic angle spinning MAS-NMR technique.

The excitation frequency of the electromagnetic radiation required to obtain resonance (for $\Delta m_z = \pm 1$) between two adjacent energy levels is called the nucleus-specific *Lamor*-frequency ν_L, which lies in the radio frequency range (e.g., 500 MHz for ^{1}H at 12 T magnetic field). Because each nucleus belongs to a specific chemical environment, the *Lamor* frequencies slightly differ as characteristic function of this environment. Dealing with the sorption and transport of hydrocarbon molecules at the active hydroxyls of H-ZSM5, only ^{1}H/MAS NMR will be further discussed.

2.1.6.2 Pulsed solid state MAS-NMR spectroscopy

The sample materials are placed in a strong magnetic field B_0 and subsequent excitation of the desired spin state transitions using radio frequency pulses leads to perturbation of the nuclear spin state equilibrium. This results in a well-defined temporal magnetization. Its relaxation as a function of time, the free induction decay (FID) is detected and transformed into the NMR-spectrum via direct Fourier Transformation. A reference standard is usually added to determine the differences δ within the Lamor frequencies, so called chemical shift. This shift is independent of the magnetic field strength and depends on the chemical environment of the nucleus. The local magnetic fields B_{local}, different nuclei experience is a function of the sample orientation according to the external field (chemical shift anisotropy, CSA) where θ denotes the angle between magnetic field and spin-spin axes (see Figure 2.8).

$$B_{local} \simeq B_{dipolar} \simeq B_{CSA} \sim \frac{1}{r^3} \cdot (1 - 3 \cdot \cos^2 \theta) \qquad (2.8)$$

In addition, closely located spins of the sample also influence the local magnetic field via dipolar spin-spin coupling interaction. In contrast to liquid solution where the molecules can rotate freely, these free rotations are frozen in the solid state and thus CSA and dipolar coupling do not average to zero. As consequence, significant line broadening occurs in the NMR spectra and the identification of individual NMR lines is hardly possible. To overcome this disadvantage, conventionally the magic angle spinning (MAS) technique is applied (see Figure 2.8). The cosine in equation 2.8, defining the orientation dependency of the local magnetic field B_{local}, equals unity

and thus B_{local} vanishes, when the samples are spun at an angle of 54.74 ° relative to the magnetic field vector of the external magnetic field during the NMR measurement.

2.1.6.3 Experimental details of ^{1}H/MAS-NMR

The ^{1}H/NMR spectroscopic measurements presented in the following chapters were carried out on a Bruker Avance AMX-500 NMR-spectrometer with magnetic field strength of 11.75 T. The solid zeolite samples in powder form were activated prior to the measurements in vacuum below 10^{-2} mbar at 423 K for at least 6h and subsequently stored under vacuum at 373 K for 12 h before they were packed under dry nitrogen into 4 mm ZrO_2 rotors. The rotors were spun at 15 kHz to reduce the spectral line width. For spectra recording an excitation pulse of 1.6 μs length with a power level of 6.00 dB was applied. To improve the S/N-ratio within the spectra 100 single scans were co-added for each measurement.

The obtained NMR spectra were further processed using WinNMR®, Fityk® and GramsAI®. In order to identify individual peak contributions from nuclei, peak deconvolution with Gaussian-type peaks using a fixed peak position was performed. The peak positions were assigned to the chemically different O-H species within the zeolite sample according to the literature[21-24]: chemical shifts δ of 1.4 – 2.2 ppm correspond to non-acidic terminal SiOH, of 2.0 - 2.5 ppm to defect site SiOH, of 2.6 to 3.6 ppm to extra-lattice AlOH (EFAl) or hydroxyls on aluminium clusters, of 3.8 - 4.3 ppm to bridging SiOHAl (located in large cavities) and of 4.6 - 5.6 ppm to perturbed bridging SiOHAl groups. The resulting integrated peak areas [a.u.], obtained from the deconvolution were transformed to concentrations [mmol g^{-1}] using adamantane as reference standard. A detailed discussion of the experimental quantification of the changes in the hydroxyl site concentrations for the post-treated zeolite samples H-ZSM5-p and H-ZSM5-3m is given within chapter four.

2.2   Investigation of sorption processes

The sorption behaviour of hydrocarbons (i.e., benzene, toluene and *p*-xylene) on H-ZSM5 was experimentally studied using gravimetric uptake measurements and infrared spectroscopy. The infrared sorption isotherms provide valuable information about the localized sorption of the sorbate molecules on the specific hydroxyls of the zeolite. On the contrary gravimetric sorption isotherms elucidate the total sorption capacity of the material. By correlating the results of both uptake measurements at a given temperature, molar extinction coefficients for the investigated infrared vibrational bands of the sorbates can be determined. A short introduction to both techniques is given in the following.

2.2.1   (Thermo-) gravimetry

The (thermo-)gravimetric analysis is generally carried out to analyze sorbate uptake and sorption capacities of a given material , i.e., a catalyst or catalyst support, within material science and physical chemistry. Gravimetric experiments are usually performed with a highly sensitive microbalance ($\Delta m_{\min} = 10^{-7}$ g). As basic principle the weight changes of a sample [g sorbate per g catalyst] are continuously followed with high accuracy as a function of temperature, sorbate partial pressure and gas phase composition. From the obtained mass uptake profiles during step-wise gas admission, the sorption isotherms at a given temperature can be calculated.

Conventionally, 10 to 20 mg of a solid sample being sufficient to obtain good signal to noise ratio, is filled in a quartz crucible and placed inside a heating block with adjustable temperature. In order to reduce artefacts originating from adsorption of sorbate gas to the sample holder, a non-adsorbing reference is simultaneously measured and the weight increase of the sample is determined relative to this reference. Depending on the type of the pressure gauge, a pressure range of 10^{-4} mbar up to 10^3 mbar is accessible on conventional instruments. Simultaneous recording of mass uptake and heat release within the sorption process allows determining the respective heats of adsorption released. As main prerequisite, an appropriate calibration of the detected heat signal e.g., using an iridium standard is mandatory.
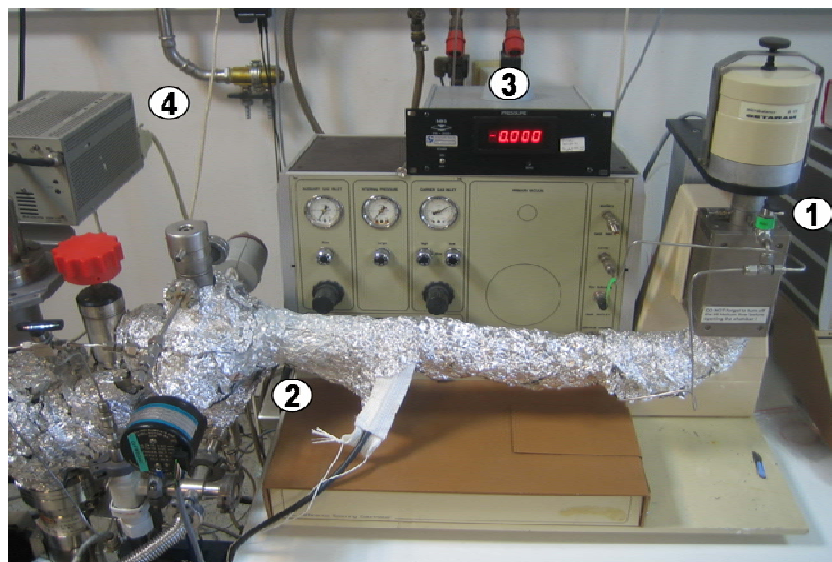
Figure 2.9 **(Thermo-)gravimetric instrument including (1) microbalance, (2) vacuum chamber and Pfeiffer UDV 040 sorbate dosing valve, (3) pressure transducer (MKS AAX122 Baratron) and (4) mass spectrometer for optional gas phase analysis.**

Gravimetric sorption isotherms were measured on a modified SETARAM TG-DSC 111 (thermo-)gravimetric instrument shown in Figure 2.9. A homebuilt high vacuum system is attached to the original TG-DSC instrument. To avoid contamination of the vacuum system by fine-dispersed powders, the zeolite samples were pressed into wafers and broken into small pellets before being placed into to the crucible. The samples were heated with a rate of 10 K min^{-1} under vacuum (below 10^{-7} mbar) and activated at 823 K for 1 h prior to the uptake measurements. Hydrocarbon sorbates were introduced to the sample chamber in small pressure steps in the range of 10^{-4} to 10 mbar using a Balzers UDV 040 dosing valve. Data recording was performed with home-built HP-Vee$^{®}$ program. A typical mass uptake profile at 373 K is exemplified in Figure 2.10 together with the extracted sorption isotherm.

Within the following chapters, gravimetric isotherms are solemnly utilized to calculate the amount of adsorbed species in [mol sorbate per g catalyst] adsorbed to the zeolite from the variations of the characteristic C-C and C-H infrared stretching vibrational bands measured. The isotherms were interpolated and correlated to the infrared isotherm data, subsequently yielding the desired molar extinction coefficient as the slope of the in the linear region of the correlation.
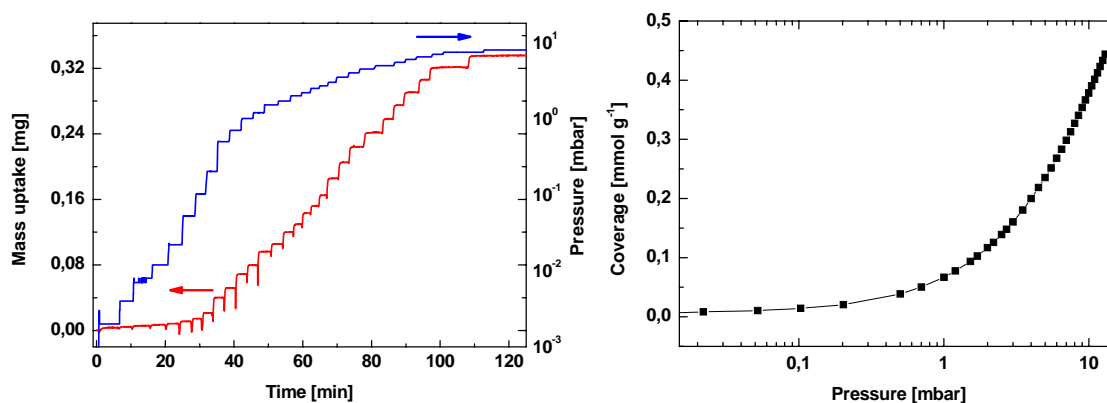
Figure 2.10   **(left) Weight increase for H-ZSM5-p during *n*-butane adsorption at 373 K and corresponding step-wise pressure change. (right) Gravimetric sorption isotherm calculated from the time profile.**

2.2.2   Fourier-transformation infrared spectroscopy (FTIR)

Optical spectroscopy, which operates in the infrared (IR) range of the electromagnetic spectrum (λ = 1 mm – 1 µm) was first introduced by W. Coblentz[25] in 1905. Infrared spectra contain a multitude of specific information about a given target system and thus infrared spectroscopy represents a highly valuable experimental technique. Different types of apparative spectrometer realizations[15, 26, 27] including transmission, emission, diffuse reflectance (DRIFTS), attenuated total reflection (ATR)[26] infrared spectroscopy and infrared microscopy (IRM)[28, 29], as well as various sample preparation methods allow for the investigation of samples either in solid, liquid or gas phase state. Fast data recording and advanced data processing allow for direct *in-situ* monitoring of kinetic processes in the millisecond to second range. For a better time resolution, rapid scan and step scan methods are available. Nevertheless, a detailed knowledge of the underlying physical principles, experimental prerequisites and limitations are of utmost importance for an optimal application within chemical research.[27] An introductory overview to transmission IR spectroscopy on solid catalysts will thus be given. For further reading, on the quantum mechanical basis of vibrational spectroscopy, the principles of data processing and evaluation as well as on the interpretation of infrared spectra in general, it is referred to the common text books and reviews dealing with infrared spectroscopy and its applications in material research.[19, 20, 25-27, 30]

2.2.2.1   General features of transmission IR spectroscopy

2.2.2.1.1   Electromagnetic radiation

Vibrating electrical charges physically cause periodically changing electromagnetic fields. These are either described as electromagnetic wave or as photon distributed through space with the speed of light following the quantum mechanical wave-particle dualism. Depending on the wavelength λ (base unit [m]), different types of radiation can be distinguished, ranging from low-energetic radio waves to highly energetic X- and γ-rays (see Figure 2.11), accessible e.g., via radioactive decay or particle accelerators. The energy of the electromagnetic radiation is proportional to its frequency (see Equation 2.11). Besides the wavelength and radiation frequency (= oscillations per unit time) ν, the wavenumber (= number of waves per unit length) $\bar{\nu}$ is conventionally chosen for spectroscopic purposes.[25]

$$\nu = \frac{c}{\lambda} \qquad [s^{-1}] \tag{2.9}$$

$$\bar{\nu} = \frac{\nu}{c} = \frac{1}{\lambda} \qquad [cm^{-1}] \tag{2.10}$$

$$E = h \cdot \nu = h \cdot \frac{c}{\lambda} \quad [J] \tag{2.11}$$

Herein h and c are two natural constants denoting the speed of light and the Planck constant, respectively. Upon interaction of radiation with matter, the radiation energy ΔE can be absorbed by the material. For the case of IR radiation, molecular vibrations and rotations are excited and the radiation energy is concerted to thermal energy. The possibility to transfer a certain amount of energy (e.g., by absorption of a photon) is, however, not continuous but strongly restricted to quantum mechanical boundary conditions.[27] As a first consequence, most materials are permeable for radiation in wide regions of the electromagnetic spectrum. Energy is only absorbed when the quantum mechanical resonance condition (given in Equation 2.12) is fulfilled. The frequency of the incident photon has to exactly match the energy difference ΔE between two energetic vibrational or vibrational-rotational states involved.
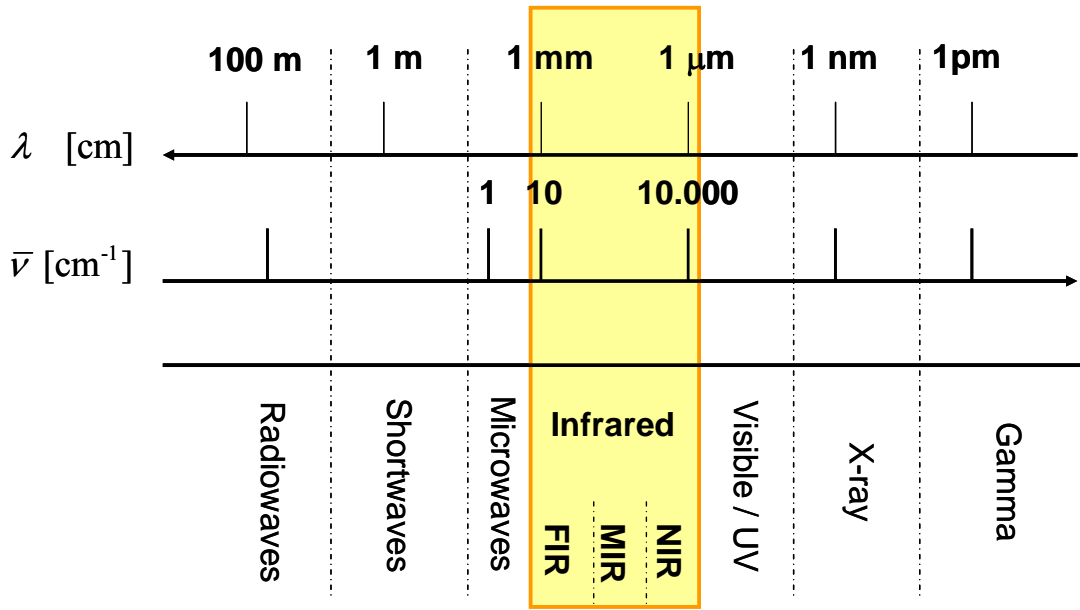
Figure 2.11   Overview to the electromagnetic spectrum with its spectral ranges.

This holds separately for the quantum mechanical selection rules $\Delta i = 0, \pm 1$ and $\Delta J = 0, \pm 1$, giving rise to characteristic infrared bands[20, 25]. The energetic states $E(i, J)$ are thus given as discrete function of these quantum numbers (see Equation 2.13).

$$\Delta E = E_2 - E_1 = h \cdot \nu_{IR} = h \cdot c \cdot \overline{\nu}_{IR} \tag{2.12}$$

$$E(i, J) = E(i) + E(J) = \left(i + \frac{1}{2}\right) h \cdot c \cdot \overline{\nu} + \frac{h^2}{8\pi^2 \cdot I} J \cdot (J + 1) \tag{2.13}$$

A detailed description of the fundamentals of vibrational and rotational states of a system according to the simplified model of a rigid rotor and the harmonic oscillator approximation and the derivation of i and J is added to chapter three.

2.2.2.1.2   Quantitative analysis of infrared data

The quantitative analysis of infrared spectra is based on the absorption law of Lambert and Beer (Equation 2.14).[31] The transmittance T of a sample is defined by the ratio between the incident intensity of the monochromatic IR radiation I_0 and of the transmitted light intensity I. For a given thickness of the sample d and concentration of irradiated species c, the transmittance can be expressed as exponential law[20, 27] as shown in Equation 2.14. A more convenient way is to take the logarithm of Equation 2.14, yielding the so called Lambert-Beer absorbance A. The Lambert-Beer formalism

assumes that (1) the absorption of radiation is additive for monochromatic light used, (2) different components present do not affect each other and that (3) ε is independent of the concentration of the component. If ε becomes a function of the concentration, additional calibrations including the whole spectral range of interest are needed. Practically, sufficiently intense and non-overlapping vibrational bands are required for a quantitative analysis.

$$T = \frac{I}{I_0} = 10^{-\varepsilon \cdot c \cdot d} \tag{2.14}$$

$$A = -\log_{10} T = \varepsilon \cdot (c \cdot d) \tag{2.15}$$

Herein, ε represents the extinction coefficient (or else called absorptivity), which is specific for the vibration mode and a specific function of the wavelength. For our purposes, the extinction coefficients were determined in the unit $[\text{g} \cdot \text{cm}^{-1} \cdot \text{mmol}^{-1}]$ when comparing infrared and thermogravimetric uptake experiments. The amount of target species i.e., adsorbed hydrocarbon molecules present in the sample can be directly expressed as the product of concentration and thickness and can be calculated when the extinction coefficient is known.

2.2.2.1.3 General infrared spectroscopic assignments

Infrared absorption bands originate from excitation of transitions between vibrational (and rotational) states of a molecule (see Equation 2.5). Therefore different structural groups present in the molecule are bound to narrow and characteristic wavenumber regions in the spectrum due to their differences in the bond strengths and atomic masses. Consequently, different classes of molecules, such as i.e., aldehydes, alkynes, ketones or aromatics can be distinguished based on the appearance of characteristic infrared bands. Being mainly interested in the sorption and transport behaviour of light aliphatics and aromatic molecules ($C_6 - C_8$) only the individual regions attributed to C-H, C-C (single and multiple bonds), C-O and also O-H bond vibrations will be discussed (see Figure 2.11). The intensity of these bands varies significantly from very weak to very strong depending on the change in the corresponding transition dipole moment of the molecule upon vibration. Normally, the band positions are sufficiently separated from each other to be analyzed.
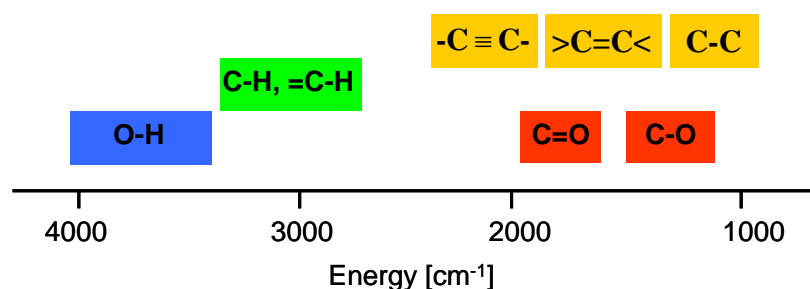
Figure 2.12   Empirical classification of IR band regions of interest.[25, 27]

Aluminosilicates: Typically, deformation and overtone vibrational bands of the Si-O-SI and Si-O-Al framework are observed between 1700 and 2150 cm^{-1} (see Figure 2.13) and are used for normalization of the IR spectra. The vibrational bands attributed to the O-H stretching of the hydroxyl groups of H-ZSM5 i.e., at 3745 (SiOH) and 3610 cm^{-1} (SiOHAl) are subsequently discussed in section 2.2.2.3.
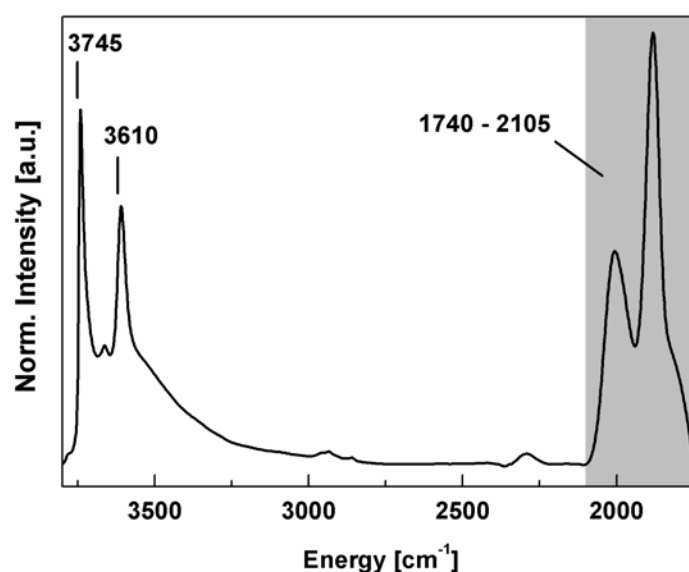

Figure 2.13   Infrared spectrum of activated zeolite H-ZSM5 at 403 K.

Aliphatic molecules: For these molecules, having only sp^3-configuration of the carbon atoms, the fundamental vibrational modes of the methylene and methyl fragments can be distinguished. For the -CH$_2$- fragment two stretching vibrations, a symmetric (v_s) and asymmetric one (v_{as}) are assigned to IR bands at 2850 and 2930 cm^{-1}, respectively. A symmetric bending deformation vibrational band δ_s appears at 1470 cm^{-1}.[27]
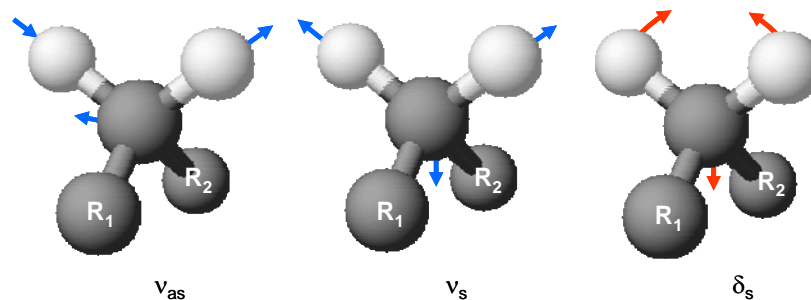
Figure 2.14   Stretching and bending vibrational modes of -CH$_2$- fragments.

The energies of the symmetric and asymmetric stretching vibrations of the -CH$_3$ fragment have similar values compared to those of the –CH$_2$– fragments. The bands are found at 2960 cm^{-1} and, depending on molecular symmetry two-fold degenerate, at 2870 cm^{-1}, respectively. The bending deformation vibrational bands of the methyl group appear at 1380 cm^{-1} (δ_s) and two-fold degenerate at 1470 cm^{-1} (δ_{as}), illustrated in Figure 2.14 and 2.15.
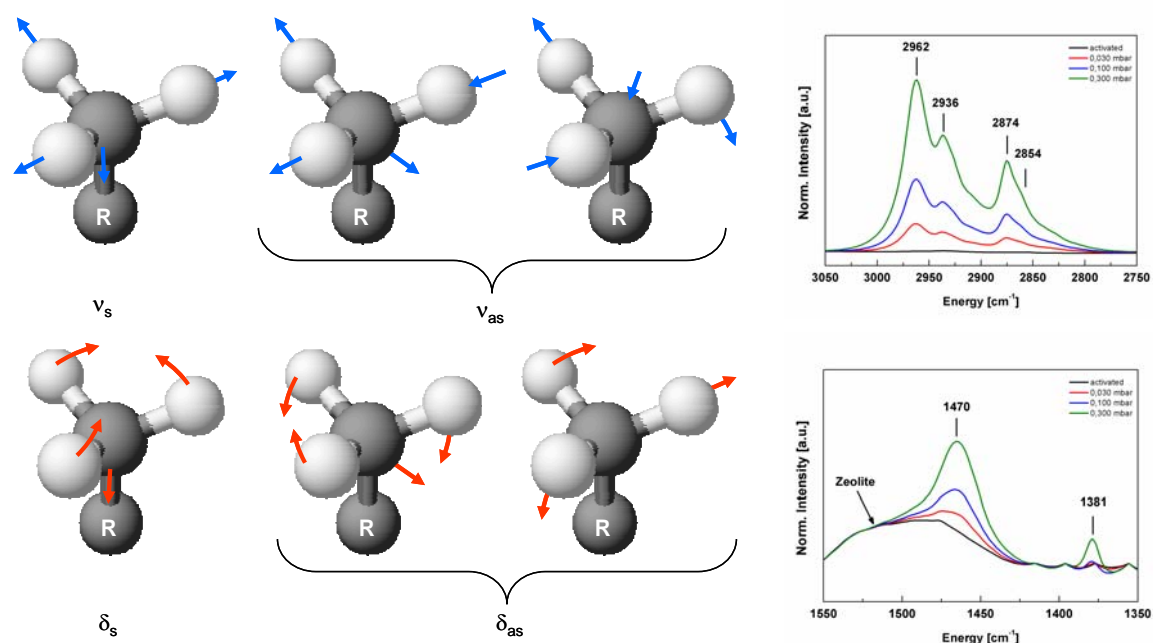

Figure 2.15   (top) Stretching vibrational and (bottom) bending deformation vibrational modes of -CH$_3$ fragments in hydrocarbons. The IR spectra correspond to butane at 323 K on unmodified HZSM-5.

For both fragments, additional types of deformation vibrational bands, i.e. due to rocking, twisting or wagging motions[26, 27] with energies below 1300 cm^{-1} are generally possible, but are not observed experimentally in our case. Using MFI-type zeolites, which show a strict cut-off (transmittance $\rightarrow$ 0) at low energies, the spectral

range is limited to wavenumbers above 1300 cm^{-1}. Note that for adsorbed or weakly bound hydrocarbons e.g., to a solid catalyst surface or active site, expected types of vibrational bands are in general preserved but characteristic shifts in the band position are induced in the spectra. Analyzing these shifts yields specific information about sorbate-sorbent interactions and corresponding changes within the polarization of the chemical bonds involved, which is essential for catalytic reactions.

Aromatic hydrocarbons: The vibrational modes are dominated by the sp^2-configuration of the aromatic carbon atoms. In contrast to aliphatic hydrocarbons, the C-H stretching vibrations (ν_s and ν_{as}) in the ring plane typically occur at energies above 3000 cm^{-1}. Characteristic deformation vibrations (δ_s) below 1300 cm^{-1} can not be observed as discussed above. Moreover, strong C-C stretching vibrational bands between 1500 and 1430 cm^{-1} and two weaker bands between 1585 and 1600 cm^{-1} can be assigned to the stretching vibrational motion of the aromatic ring itself. For the alkyl-substituted series of benzene molecules (herein toluene, *p*- and *o*-xylene) additional bands originating from the alkyl side-groups give rise to characteristic vibrational bands in analogy to the pure aliphatics introduced above.
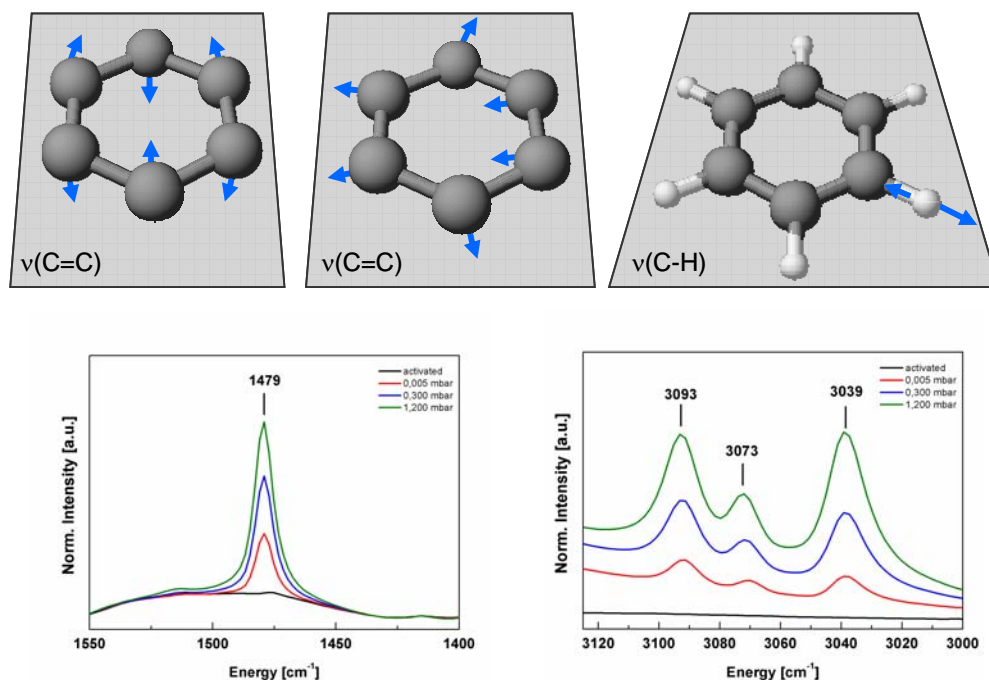

Figure 2.16 **(top) Three selected vibrational modes for the C=C (left, middle) and the C-H stretching vibrations (right) exemplified for benzene. (bottom) Exemplified shown are the vibrational bands for benzene on unmodified H-ZSM-5 at 373 K with varying partial pressure.**

2.2.2.2   Experimental design of the infrared spectrometer

2.2.2.2.1   General characteristics

Conventional absorption IR spectrometers, operating in mid-infrared (MIR) are composed of a light source, a sample chamber and a detector unit.[26, 32] In order to measure the transmittance of the sample with selection of a variable wavelength, formerly, dispersive spectrometer types made use of monochromator units. Nowadays these classical instruments have been totally replaced by Fourier-transformation (FT-) IR spectrometers using modern data recording and processing. The schematic principle[27] is shown in Figure 2.17.
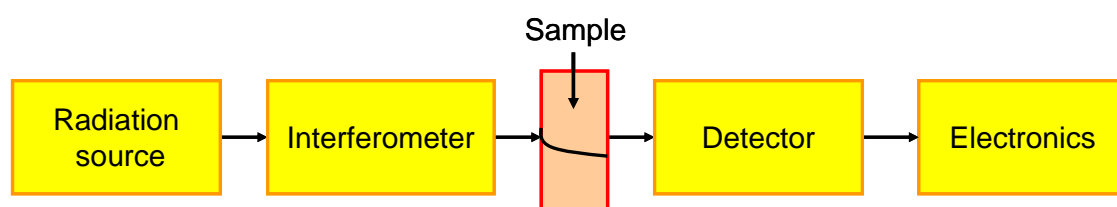

Figure 2.17   Schematic operating principle of an FTIR spectrometer.[27]

The interferometer, where a wavelength dependant modulation of the infrared radiation is achieved, represents the heart of the FTIR spectrometer.[26] This enables simultaneous detection of all frequencies of the IR spectrum without time-consuming single wavelength scanning via a monochromator unit. In most cases, classical Michelson interferometers are utilized, generating interferograms out of the polychromatic infrared radiation containing all the spectral information as function of time. The detected interferograms are subsequently converted from the time-domain into the energy domain via Fourier transformation, resulting in a single beam spectrum of the sample. For a detailed description the Michelson interferometer and of the Fourier transformation formalism, it is referred to the common literature.[20, 25, 26] Main advantages of FTIR spectroscopy are the reduction of measurement time, enhancement of time resolution, increased S/N-ratio and high wavelength precision.

2.2.2.2.2   Bruker IFS 66 v/S specifications

A Bruker IFS 66 v/S spectrometer, consisting of five subunits (optics module, electronics, water cooling, vacuum system and data station), depicted schematically in Figure 2.18 was used and will be roughly introduced in the following.[32] The optics

module is divided into three compartments (sample chamber, interferometer and detector compartment) which can be evacuated to below 1 mbar residual pressure. A Michelson high throughput interferometer with automated alignment is combined with a Ge-coated KBr beam splitter (1). A standard, water cooled SiC globar is utilized as radiation source generating the desired MIR radiation (2). The principally possible operating range of the instrument (7500 - 370 cm^{-1}) with maximum resolution of 0.5 cm^{-1} is practically limited by the use of different IR windows of the vacuum cell, beam splitters and IR sources. To detect the interferograms, the DTGS (Deutero-Triglycylsulfate) operating at room temperature or the liquid nitrogen cooled MCT (Mercury-Cadmium-Telluride) detector can be selected (3). Despite its limited operating time of approximately 8 h, for the measurements described herein, only the MCT detector was used because of its much higher sensitivity.
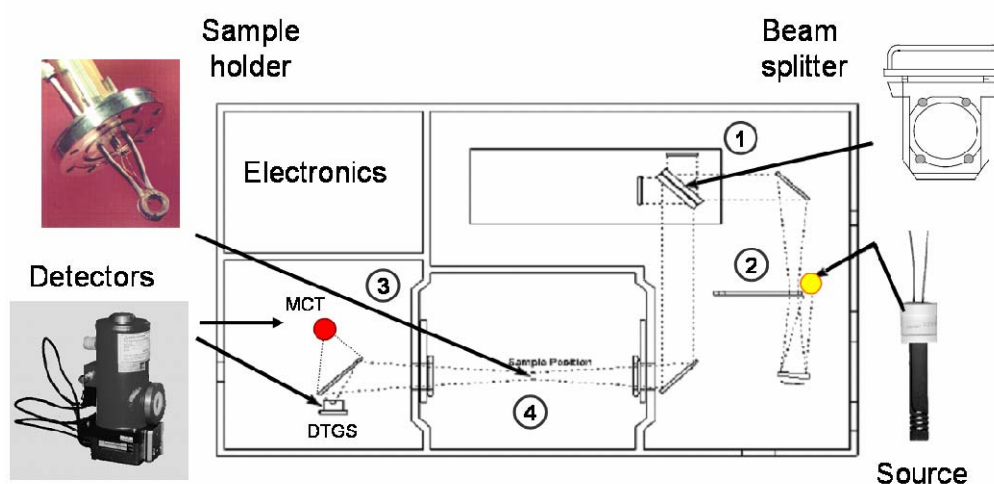

Figure 2.18   **Bruker IFS 66 c/S spectrometer with indicated optical path and compartments.**

For experiments in transmission mode, the solid samples are pressed into self supporting wafers and introduced into a home-built vacuum cell (4) with gold ring sample holder. The cell itself is penetrated by infrared radiation via two calcium fluoride (CaF_2) windows showing a strict cut-off at 1000 cm^{-1}. A Eurotherm 2640 temperature controller allows for incremental heating of the sample. The required vacuum system attached to the sample cell and equipped for periodic sample volume modulation is described in section 2.3. For initial data recording and processing, the software package OPUS 3.0 working on an OS/2 operated workstation is used.

2.2.2.3 Infrared spectroscopy on zeolites

2.2.2.3.1 General features of infrared spectra of MFI-type zeolites

The sorption and transport of hydrocarbons on zeolites was followed via the stretching vibrational bands ν_{OH} of the structural framework hydroxyl groups. These O-H bands appear in the MIR region between 3500 and 4000 cm^{-1} and represent an ideal probe to obtain specific information about the molecular interactions between the sorbing molecule and the zeolite framework. It is further possible to clearly separate in the infrared spectrum between the different characteristic hydroxyls of the zeolite (see Figure 2.13). These are e.g., for high silica zeolites such as H-ZSM5 silanol groups at the outer zeolite surface which terminate the periodic lattice (3747 cm^{-1}), bridging Brønsted acidic hydroxyls in the pore network (3610 cm^{-1}), silanol groups at defect sites or inside the channels (3725 cm^{-1}) or extra-lattice aluminium (EFAL, 3660 cm^{-1}), respectively.[3, 15, 33, 34] This allows precisely and quantitatively discriminating localized sorption processes, as the admission of basic sorbate molecules either leads to a distinct decrease in the intensity of the hydroxyl bands, via electron pair donor and acceptor interaction (EPD-EPA) with the sorbate.[31]

For the case, that the sorbate is not protonated upon adsorption, additional bands assigned to the resulting perturbed hydroxyls increase at distinctly lower wavenumber compared to the parent hydroxyl group. This difference $\Delta \bar{\nu}$ between the perturbed and unperturbed band is specific for the energetic and entropic environment of the sorbate at the active site.[34] The stronger the interaction, that means, the higher the basic properties of the sorbate molecules with respect to a given acid strength of the hydroxyl site, the larger the shift of the perturbed hydroxyl band to lower energies. This is commonly illustrated by the Bellamy-Hallam-Williams plot (BHW-plot), which correlates the wavenumber shift on terminal hydroxyls of amorphous silica $\Delta\nu_{SiOH}$ to those observed for zeolite acid sites $\Delta\nu_{SiOHAl}$ for a series of sorbates. The slope of this correlation is characteristic for the acid strength and the steric constraints of the sorbates within the confined spaces of the zeolite.[35, 36] For the case of protonation of the sorbate (e.g., for pyridine adsorption) the respective vibrational bands of the interacting hydroxyls completely disappear and new characteristic vibrational bands assigned to the protonated sorbate molecule arise.

In complementary to the O-H bands, stretching and deformation vibrations of the sorbate molecules themselves, interacting with the zeolite lattice are highly valuable and used to extract kinetic information about the overall sorption process. The characteristic C-H and C-C stretching vibrational bands of aromatic hydrocarbon molecules, as referred to in section 2.2.2.1.3 are thus analyzed.

2.2.2.3.2 Sample preparation and processing of infrared data

The zeolite samples in powder form (~ 15 mg) are pressed into self-supporting wafers to allow for high transmittance of infrared light. The wafer is placed in a gold ring sample holder and positioned inside the infrared cell inside the spectrometer. Prior to the measurements, samples have to be activated, as exemplified shown in Figure 2.19. The applied procedure specifically depends on the target material and is described in detail within the experimental chapter's four to six.
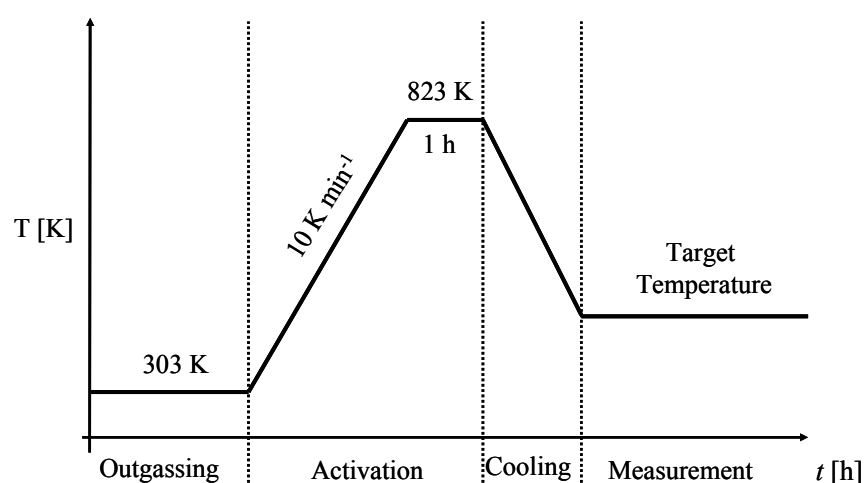

Figure 2.19   Typical sample preparation procedure for IR measurements

Single beam spectra were recorded using the spectrometer software OPUS3.0 and converted from signal intensity to IR absorbance A using Equation 2.5. Subsequently, baseline correction and all further data processing (i.e., integration, subtraction, normalization) was performed with the scientific software packages GramsAI® or Grams32 from Galactic Inc.. As in general, the real thickness of a pressed wafer and the volume irradiated by the infrared beam can not accurately be determined, spectral normalization is necessary to be able to compare and quantify experiments with different sample wafers. A series of infrared spectra during different

stages of the data processing are compiled within Figure 2.20. To account for differences in the wafer thickness, the integral intensity I of the lattice and overtone vibrational bands of the zeolite is used as normalization factor, yielding the normalized IR absorbance A_{norm}.[31]

$$A_{norm} = A_{measured} / I_{\left(2105-1740\,cm^{-1}\right)}$$ (2.16)

For H-ZSM5, the subject of interest the vibrational bands in the range of 2105 and 1740 cm^{-1} were used.[37] In order to clearly highlight the changes occurring in the positions and the intensities of the characteristic bands during the sorption and transport processes, the activated spectrum without sorbate molecules added is used as internal reference and subsequently subtracted from each spectrum during sorbate admission. From the resulting difference infrared spectra, precise information about the sorption processes at the active sites of the material (i.e., the coverage as function of the sorbate pressure = IR sorption isotherm) can be derived from integrating either the sorbate or the site specific vibrational bands. For the case of slightly overlapping bands the peak deconvolution formalism using the Curvefit.ab routine implemented in GramsAI$^{®}$ was applied. The corresponding integration ranges used for the sorbate molecules studied, are given within the respective chapters. For the terminal and bridging hydroxyl groups, the integration ranges of 3577 – 3640 cm^{-1} and 3700 – 3727 cm^{-1} were chosen, respectively.
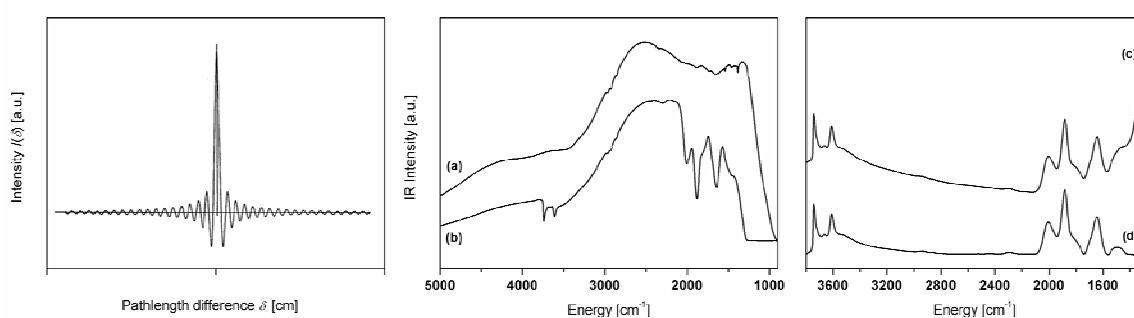

Figure 2.20 **(left) Typical interferograms detected on a Bruker IFS 66v/S spectrometer. (middle) Comparison of the background of the empty IR cell (a) and the single beam spectrum of activated ZSM5 (b). (right) Absorbance spectra of the activated H-ZSM5-p sample before (c) and after (c) the automated baseline correction.**

2.2.3   Theoretical description of sorption in equilibrium

2.2.3.1   Sorption isotherms in general

For every gas phase system containing sorbate molecules A and being exposed to a material surface with active sorption sites *, an equilibrium state between the adsorption and desorption is established for a given temperature and partial pressure of impinging molecules. Thermodynamically, the equilibrium values of the concentrations of adsorbed molecules (given as surface coverages θ) are defined by the thermodynamic sorption constant K_{eq}. Kinetically, this constant can be expressed by the quotient of the kinetic rate constants of the ad- and desorption steps.[19, 20, 38]

$$A \;+\; * \; \underset{k_{des}}{\overset{k_{ad}}{\rightleftarrows}} \; A-* \quad \textbf{with} \quad K_{eq} = \frac{k_{ad}}{k_{des}} \tag{2.17}$$
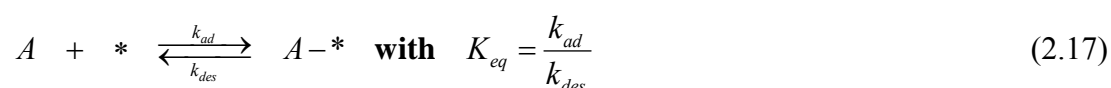
The course of the equilibrium surface coverage θ as function of the gas phase pressure p is usually referred to as the sorption isotherm of the sorbate (see Figure 2.10). Generally, sorption isotherms are experimentally accessible via a multitude of different techniques including the above described gravimetry and infrared spectroscopy. For the subsequent calculation of thermodynamic sorption parameters such as e.g., the sorption constant, the enthalpy or entropy of sorption, an accurate theoretical description of the experimentally measured course of data points is needed. Genuine models with different boundary conditions have been developed in the past to account for the existence of e.g., sorbate-sorbate interactions, variations in the enthalpy of adsorption with surface coverage or the heterogeneity of active sorption sites, which are present on realistic catalyst materials. For the case of aromatic hydrocarbons on H-ZSM5 in the low partial pressures range (< 10 mbar) and assuming equal, homogeneously distributed sorption sites and less than monolayer coverages, the Langmuir sorption model is most convenient and best matches the experimental data. For additional sorption models, i.e., the Freundlich, Langmuir-Freundlich or Tempkin model it is referred to the literature.[10, 19, 31, 39]

2.2.3.2   The Langmuir sorption model

Absence of sorbate interactions, monolayer coverages and constant enthalpy of sorption with coverage are the prerequisites for application of the Langmuir formalism.

This simplest form of Langmuir isotherm is given in Equation 2.18 with p^* denoting the dimensionless pressure of the sorbate, p_0 the standard reference pressure, q_{sat} the saturation coverage of the active sites and K_{eq} the corresponding equilibrium constant. Both parameters K_{eq} and q_{sat} are determined simultaneously from a least-square fit to the experimental data points.

$$q = q_{sat} \cdot \frac{K_{eq} \cdot p^*}{1 + K_{eq} \cdot p^*} \quad with \quad p^* = \frac{p}{p_0} \tag{2.18}$$

Unfortunately, when dealing with microporous materials, a distribution of heterogeneous sorption sites or also pores of different diameter is present. Drago et al.[39, 40] therefore proposed an extended form of the Langmuir isotherm (see Equation 2.19) to properly describe the experimental isotherm data including several independent sorption equilibria. For the simplest case of two different sorption sites or sorbate geometries during sorption, a dual-Langmuir approach (i = 2) is chosen.

$$q = \sum_i q_{sat}^i \cdot \frac{K_{eq}^i \cdot p}{1 + K_{eq}^i \cdot p} \quad with \quad q_{sat} = \sum_i q_{sat}^i \tag{2.19}$$

Theoretical fitting of the isotherm data enables a precise calculation of the expected coverage change within two given pressure limits (i.e., generated by a periodic volume modulation experiment) based on the experimental data gathered for each sorbate. Within chapter five, the theoretically obtained changes in the site coverage will be compared to the experimentally measured values to exclude experimental artefacts during the time-resolved measurements.

2.2.3.3 Isosteric heat of adsorption

Besides the above introduced (thermo-)gravimetric measurements, directly yielding the overall heat of adsorption from the heat signal, site-specific heats of adsorption for sorbates are determined from the IR sorption isotherms. Hereby, the temperature course of K_{eq} is analyzed via the Van't Hoff equation.[19, 20, 40] Moreover, by evaluating the changes in the sorbate partial pressure required to reach identical site coverages with varying temperature, isosteric heats of adsorption are calculated.

$$\left(\frac{d \ln p}{dT} \right)\Bigg|_{q=const} = -\frac{\Delta H_{iso}}{R \cdot T^2} \tag{2.20}$$

In analogy to the classical Clausius-Clapeyron relation between the vapour pressure and the vaporization enthalpy in classical thermodynamics, Equation 2.20 can be derived from the Langmuir isotherm. This formalism can easily be applied for, either terminal or bridging active sites of H-ZSM5, accounting for the local steric and energetic environment.

2.3 Investigation of hydrocarbon transport on zeolites

With regards to the optimization of the zeolite catalysts in terms of reactivity and selectivity, first of all, detailed information about the exact location of the sorbate molecules inside the catalyst pores and the respective coverages of the active sites, as defined by the thermodynamic equilibrium constants for given reaction conditions is necessary. Moreover, besides these thermodynamic parameters, the dynamics of all underlying steps during sorption and mass transport of the reactants from the bulk phase to the active sites inside the catalyst porosity is essential. A broad variety of microscopic or macroscopic, experimental methods with limited applicability of each, as indicated in the introductory section, are currently available to give further insight a molecular level. For the case of this thesis the experimental focus was set on the fast time-resolved infrared spectroscopy which allows differentiating between the kinetic processes occurring simultaneously at different active sites. In addition, the observed fundamental findings will be supported by independently performed, pressure frequency response measurements. An overview to both, including the experimental apparatus design, principle of data acquisition and interpretation is added as follows.

2.3.1 Time-resolved *in-situ* IR spectroscopy

2.3.1.1 General principle

The elementary kinetic steps during transport of light aliphatic and aromatic C_4 - C_8 hydrocarbons to the acid sites of a microporous catalyst typically occur in the time range of seconds to milliseconds. Unfortunately conventional single pressure-step uptake measurements using infrared spectroscopy require the co-addition of a large

number of interferograms in order to obtain acceptable signal-to-noise ratios. The practically achievable time resolution is thus limited to several seconds, depending on the specific sorbate. This disadvantage can be overcome by using time-resolved FTIR spectroscopy in rapid scan mode. It combines adequate time resolution in the range of milliseconds with good signal-to-noise ratio. In principle, the measurement is based on perfectly reversible and reproducible perturbations of a batch system in equilibrium state. Ad- and desorption kinetics of sorbate molecules are hence excited e.g., by periodic modulations of the system pressure, resulting in a characteristic system response in terms of sorbate concentration profiles (see Figure 2.20). Each modulation cycle is divided into short time slots of equal length in which a small number of interferograms is collected and subsequently co-added.
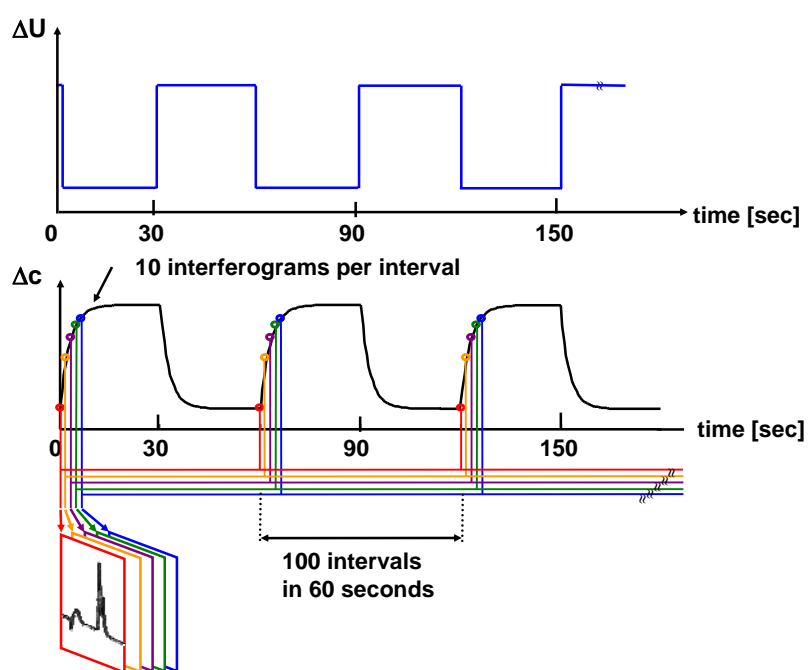
Figure 2.21   Data acquisition scheme for *in-situ* FTIR spectroscopy in rapid scan mode using a rectangular volume modulation (up). The full sorption experiment is divided into *n* cycles of 60 s, each composed of 100 time intervals (down).

The length of these slots corresponds to the time span required for recording the desired number of interferograms for a given spectral resolution and defines the achievable time resolution of the measurement. Because of the periodic repetition of the modulation up to several hundred times, a high number of interferograms needed for optimal S/N-ratio is easily obtained via co-addition of the cycles. It should be

mentioned hereby, that the reversibility of the kinetic processes under study and a perfect synchronisation of the modulation cycles and data recoding are mandatory. The schematic principle of the rapid scan method is illustrated for the case of a rectangular excitation function in Figure 2.21, but sinusoidal excitation functions are also possible.

2.3.1.2 Instrument design and experimental procedure

The experimental apparatus used consists of four principal parts which are depicted in Figure 2.22. A commercial Bruker IFS 66v/S spectrometer (1) equipped with transmission vacuum cell is connected to a home-built high vacuum system[41, 42] (2) enabling activation of solid samples and equilibration with the sorbate gases, which are added to the vacuum system via a separately pumped dosing system.
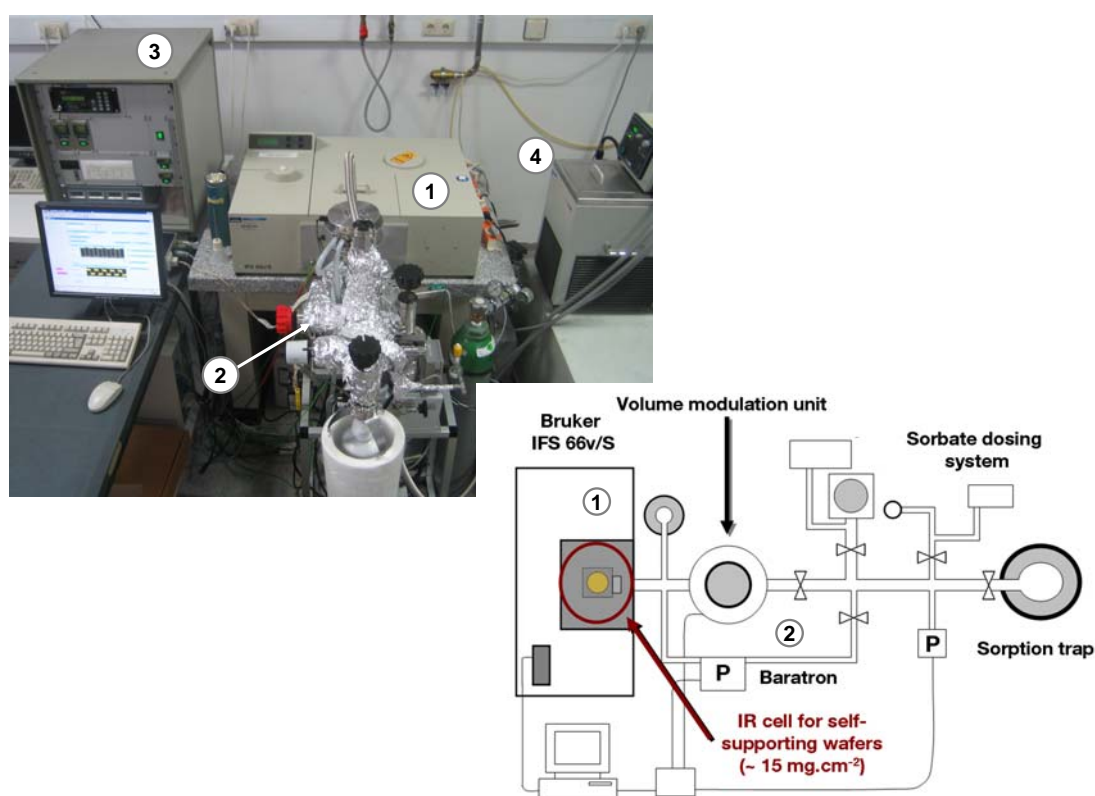
Figure 2.22   **Photograph (top) and scheme (bottom) of the combined *in-situ* FTIR and FR apparatus including a commercial infrared spectrometer (1), vacuum apparatus (2), electronic controlling unit (3) and water filled cryostat (4).**

A Pfeiffer UDV040 dosing valve is used to precisely adjust the pressure via an in-line pressure transducer (Baratron MKS 161 A11) operated at 333 K. The system is

pumped via a Pfeiffer TMU071 turbo molecular pump (70 l h^{-1}) and the sorbate dosing unit is attached to a GE Motors rotary vane pump type 7-5KCR. Further details concerning the instrument specifications are published elsewhere.[2, 3, 41, 42] Solid samples are introduced into the IR cell with a gold ring sample holder activated as described previously for the sorption experiments. Two Eurotherm® 2416 and 2460-type temperature controllers, embedded into a electronics unit (3) accurately control the temperature of the samples in a range of 298 to 873 K and of the vacuum system being held constant at 333 K. Excitation of the system volume is achieved via a magnetically driven modulation unit (see Figure 2.23), being composed of a pair of flexible UHV bellows separated by a metal separator plate, placed horizontally between two electromagnets. Periodic square wave perturbations of the system volume with adjustable frequency are realized by regularly switching the magnet polarization via a HP-Vee® based program. For *in-situ* IR experiments, a constant modulation frequency of 0.0167 Hz is utilized. As direct consequence, the volume modulation relates to perturbation of the pressure over the sample and results in reversible ad- and desorption of the sorbate. In order to suppress condensation of sorbate gases inside the vacuum bellows and to prevent over-heating of the magnets during time-consuming measurements, the volume modulation unit itself is hold at a constant temperature of 313 K by a water-filled cryostat (4).
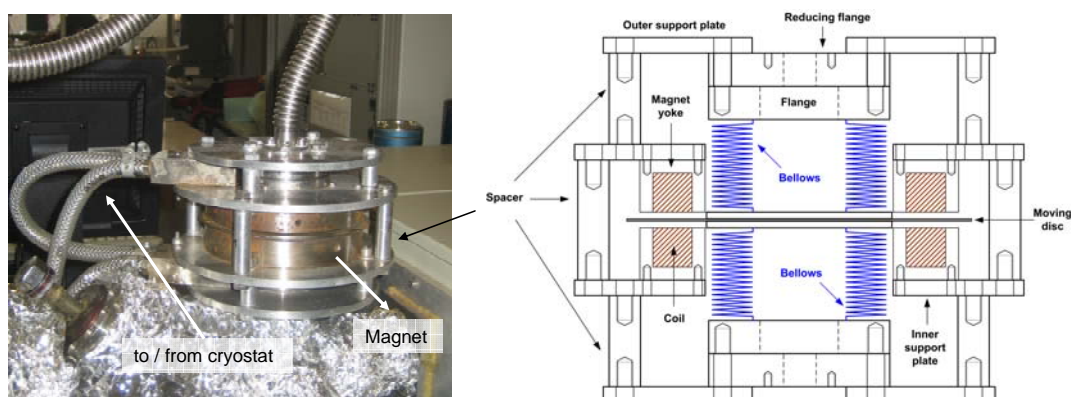

Figure 2.23   **Volume modulation unit (left) together with its cross section (right) adopted from H. Heydenrych, Master thesis, 2002.[41]**

To minimize adiabatic effects due to compression of the gas volume and to exclude local heat changes due to exothermic sorption processes, which would disturb

the underlying transport processes, the amplitude of the modulations is limited to $\Delta V = \pm 5$ %. For the combination of H-ZSM5 with aromatic hydrocarbons, a cycle time of 60 seconds and a total number of 400 cycles were found to be the most convenient set of experimental parameters[41, 42] and the sorption kinetics were followed with a time resolution of 600 ms. Prior to the IR measurements, the activated samples were equilibrated with the sorbate gas at a partial pressure of 0.06 mbar at 403 K and a series of 100 infrared spectra were recorded with OPUS 3.0, processed and normalized (see 2.2.2.2).

In order to clearly highlight the resulting changes in the surface and active site coverages, the first spectrum in the time series was subtracted from the subsequent ones, resulting in a series of 100 difference IR spectra. A typical example is illustrated for H-ZSM5 in Figure 2.24.
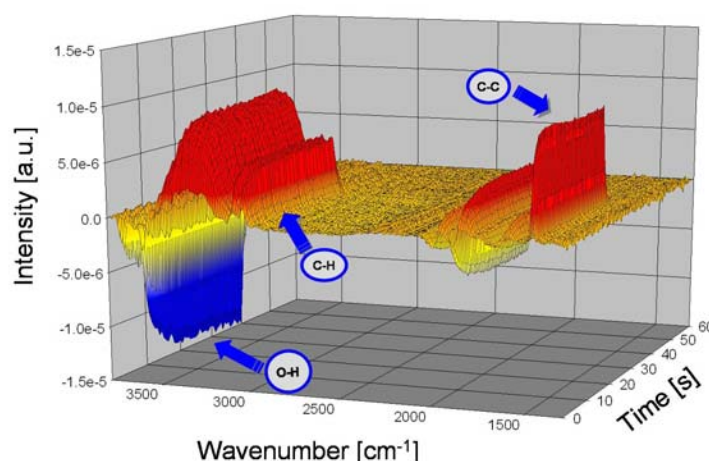
Figure 2.24   Series of 100 difference IR spectra during sorption of benzene on H-ZSM5 at 403 K with characteristic vibrational bands marked.

2.3.1.3   Analysis and evaluation of time-resolved IR spectroscopic data

The change in the sorbate concentrations on the hydroxyls (SiOH and SiOHAl) was calculated from the respective changes in the integral intensity of the corresponding O-H vibrational bands in analogy to the sorption experiments.[42, 43] It is assumed, as has been established previously, that one molecule is adsorbed per hydroxyl and the molar extinction coefficients are constant in the pressure range studied. Straight forward integration of the series of difference spectra results in

characteristic concentration profiles as illustrated in Figure 2.25. The concentration changes $\Delta c_{OH}(t)$ are mathematically described with a first order kinetic model[42, 44] in order to retrieve the individual kinetic parameters for the ad- and desorption branch.

Adsorption process $\qquad \Delta c_{\mathbf{OH}}\left(t\right) = \Delta c_{\mathbf{OH,eq}}\left(1 - e^{-t/\tau_{\mathbf{ad}}}\right) \quad \text{for} \quad 0 < t \le t_p/2$ $\qquad$ (2.21)

Desorption process $\qquad \Delta c_{\mathbf{OH}}\left(t\right) = \Delta c_{\mathbf{OH,eq}} e^{-\left[t-\left(t_{\mathbf{p}}/2\right)\right]/\tau_{\mathbf{de}}} \quad \text{for} \quad t_p/2 < t < t_p$ $\qquad$ (2.22)

Initial rate $\qquad r_{\text{ini,ad}} = \dfrac{d\left[\Delta c_{\text{OH}}(t)\right]}{dt} = \dfrac{1}{\tau_{\text{ad}}} \cdot \Delta c_{\text{OH,eq}} e^{-t/\tau_{\text{ad}}} \xrightarrow{t \ll t_p} r_{\text{ini,ad}} = \dfrac{\Delta c_{\text{OH,eq}}}{\tau_{\text{ad}}}$ $\qquad$ (2.23)

Herein $\Delta c_{OH,eq}$ denotes the difference in the sorbate concentration between the two sorption equilibrium states and τ_{ad}, τ_{de} are the kinetic time constants, which are equivalent to $1/k$ for first order processes. The corresponding initial sorption rates $r_{\text{ini,ad}}$ (i.e., dc/dt at $t \ll t_p$) following the immediate pressure steps are determined from the initial slopes of the concentration profiles according to Equation 2.23.[18]
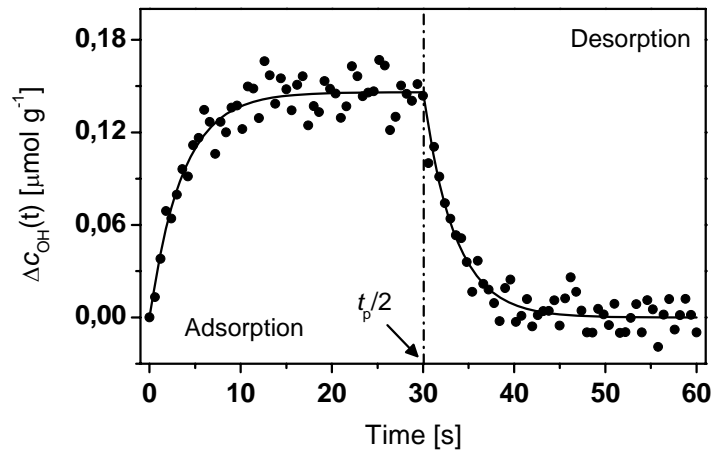
Figure 2.25 **Concentration profile on the terminal SiOH of H-ZSM5 subjected to a pressure modulation of $\Delta p = \pm 0.003$ mbar at 403 K.**

This quantification for a series of hydrocarbon molecules allows in the following chapters to differentiate between individual transport pathways within the overall transport network.[18] To be able to evidence the trends derived from the FTIR spectroscopic measurements, a second technique, the so called frequency response technique was applied in complementary.

2.3.2 Frequency response technique (FR)

2.3.2.1 General principle

The frequency response method is a macroscopic relaxation technique for batch absorbers subjected to a periodic i.e., sinusoidal or rectangular perturbation function of varying frequency and constant amplitude A_e (excitation function). This procedure transforms the inherent time-dependent transport information of the system from the time into the corresponding frequency domain. Phase lag φ and amplitude change A_r of the system response compared to the excitation are directly derived (sinusoidal case) or via Fourier transformation (rectangular excitation), as seen in Figure 2.26. From phase lags and amplitude changes, the characteristic functions of the frequency response in a batch system experiment are calculated.
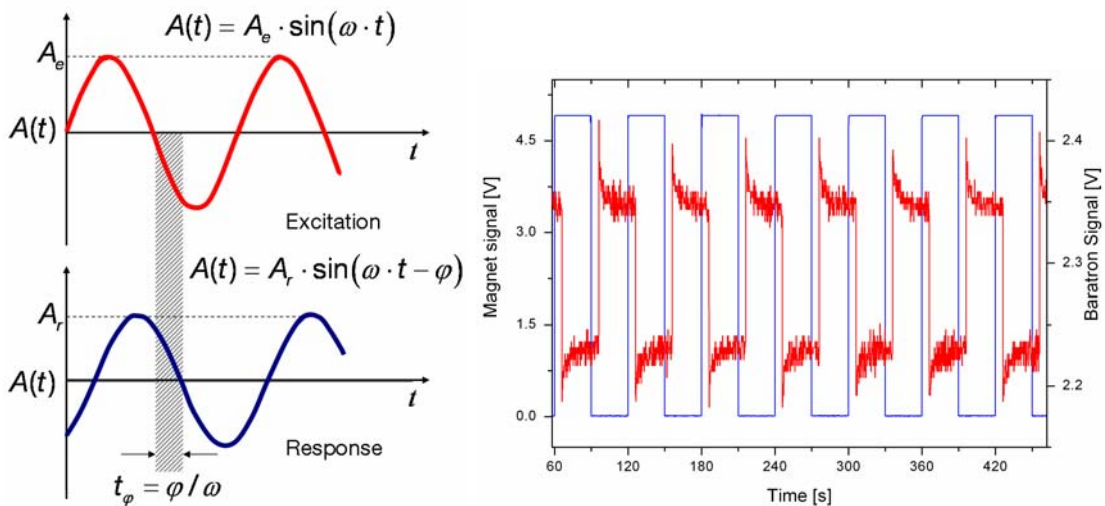
Figure 2.26 **(left) Comparison of system excitation and corresponding system response exemplified for a sinusoidal function. (right) Periodic rectangular magnet signal and resulting system pressure response exemplified for a frequency of 0.0167 Hz and benzene on H-ZSM5.**

The general methodology of the FR method for batch absorbers was developed by Naphtali and Polinski[45], subsequently adopted and extended to diffusive transport phenomena in molecular sieves by the group of Yasuda.[46] As simultaneously occurring processes such as e.g., diffusion or sorption behave additive in the frequency domain, they can in principle be easily distinguished from each other.
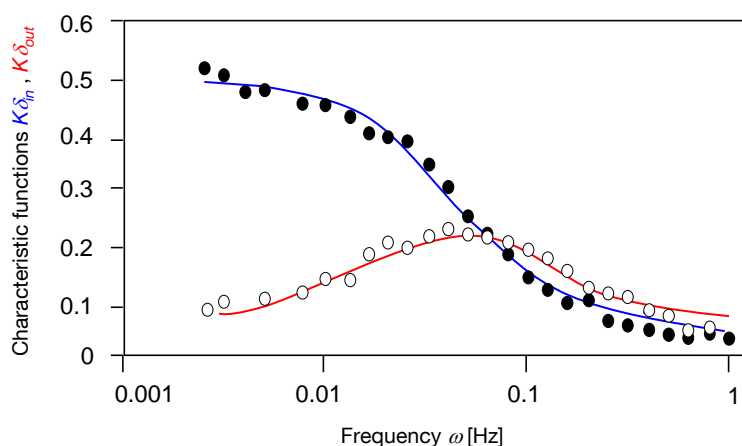
Figure 2.27   Exemplified characteristic in-phase (full) and out-phase (open) FR functions together with theoretical fit functions (lines).

In practice, the interpretation of experimentally measured frequency responses is complicated, especially due to ambiguities of multiple processes on similar time scales. Despite of that, only transport processes differing in time constants τ by at least one order of magnitude can be clearly separated within the experiment.[47] The shape of the frequency response is influenced by all steps involved during the transport of the gas phase molecules into the pores of the particles[42, 44], but also sensitive to heat or bed and particle size distribution effects. Using appropriate theoretical models to describe these effects, the characteristic transport time constants are accessible.

2.3.2.2   Applied experimental FR procedure

Within this thesis, FR experiments were performed on a vacuum system with volume modulation unit, already described for the *in-situ* infrared spectroscopy (see Figure 2.22 and 2.23). In contrast to the IR measurements with constant modulation frequency of 0.0167 Hz, in the typical FR experiment system responses were recorded for various frequencies in the range of 5 to 10^{-3} Hz. Higher frequencies than 5 Hz are excluded due to the apparatus design. The relative volume perturbation of $\Delta V = \pm 1$ % was chosen to eliminate heat effects originated from released heat of sorption. To increase in the signal-to-noise ratio, the zeolite samples (30 mg) were introduced in form of powder into a quartz tube, attached separately to the vacuum system instead of using the IR wafers. The samples were carefully dispersed on quartz wool at the bottom of the tube to avoid bed-depth effects and activated in accordance to the IR spectroscopic measurement to remove adsorbed water. For the FR measurements

described 0.3 mbar of sorbate were equilibrated with the samples between 333 and 423 K prior to starting the volume modulation. The pressure data was recorded with a high-sensitive Baratron MKS 161A11 pressure transducer. Amplitude and phase lag for each frequency were calculated from the frequency response data by Fourier transformation. The determination of the inherent transport information from the experimental data is addressed in the following section.

2.3.2.3 General aspects of frequency response data analysis

The FR of a closed volume system subjected to a periodic volume (~ pressure) modulation can be expressed by the characteristic in-phase δ_{in} and out-of-phase δ_{out} functions, which represent the solutions of the mass balance of the system and are given by Equation 2.24 and 2.25. Herein P denotes the pressure amplitude, φ the phase lag and the parameter K_j is directly coupled to the gradient of the corresponding sorption isotherm via the gas constant R, the temperature T and the total system volume V. Simultaneously occurring transport processes are additive in the FR and accounted for by summation over j within the characteristic functions. In order exclude non-ideal contributions of the apparatus itself to the frequency responses of interest, blank experiments under identical conditions are required. The corrected phase lag $\varphi_Z - \varphi_B$ and the amplitude ratio between zeolite sample and blank measurement P_Z / P_B are correspondingly utilized.

$$\frac{P_B}{P_Z}\cos(\varphi_Z - \varphi_B) \ -1 = \sum_{j=1}^{n} K_j \cdot \delta_{in}^{(j)} \quad \text{with} \quad K_j = RT/V \cdot (\partial q_j / \partial p) \tag{2.24}$$

$$\frac{P_B}{P_Z}\sin(\varphi_Z - \varphi_B) \ = \sum_{j=1}^{n} K_j \cdot \delta_{out}^{(j)} \tag{2.25}$$

From the resulting overall characteristic functions δ_{in} and δ_{out}, the desired transport parameters, i.e., the transport time constants τ of each process are obtained from fitting the experimental data points to the theoretical solutions of Fick's second law (= theoretical transport models). Nonlinear parameter fitting was herein performed using a CMA evolution strategy in Matlab®[48]. The root mean squared error normalized to the variance of the data (NRMS error) represents the objective function to be minimized during fitting.
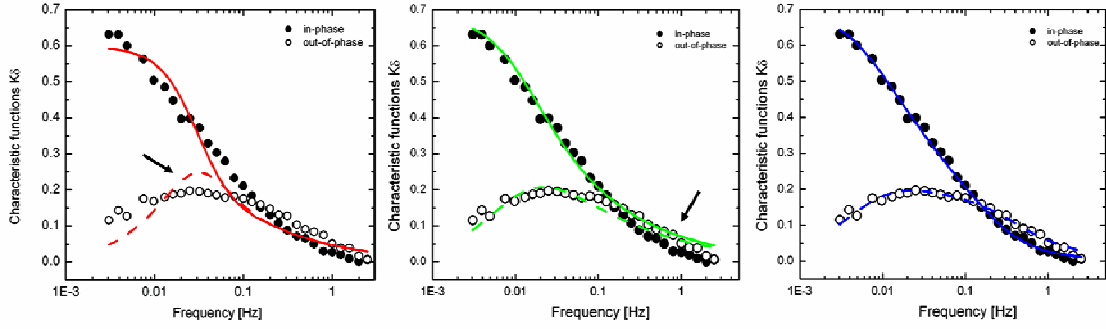
Figure 2.28 **Comparison of experimental characteristic functions for benzene on H-ZSM5 fitted with different theoretical models. The uniform single planar sheet model (left) was optimized via insertion of parameters related to a particle size distribution (middle) and surface barrier effects (right) to accurately reproduce the trends.**

To ensure that the only globally optimal sets of parameters are chosen, each optimization run was repeated three times with varying sets of starting parameters. Depending on the boundary conditions, i.e., target material, experimental conditions or time-scales of transport pathways, different theoretical models have been developed within literature in the past. For the purpose of this thesis, only the planar sheet diffusion model including surface barrier effects and a particle size distribution is discussed. The model best reproduces the experimental data measured (see Figure 2.27) and was thus solemnly chosen for further data evaluation and interpretation. The respective characteristic functions for the one dimensional planar sheet with thickness $2L$, including radial frequency ω and transport time constant τ are given in Equation 2.26 and 2.27.[46] For the case of pure intra-crystalline diffusion as single transport process present, the determined transport time constant equals L^2/D, resulting the transport diffusivity D. For alternative models, it is referred to a review of Yasuda.[46]

$$\delta_{in} = \delta_{1C} = \frac{1}{\eta}\left(\frac{\sinh\eta + \sin\eta}{\cosh\eta + \cos\eta}\right) \qquad \text{with} \quad \eta = \sqrt{2\omega\tau} \qquad (2.26)$$

$$\delta_{out} = \delta_{1S} = \frac{1}{\eta}\left(\frac{\sinh\eta - \sin\eta}{\cosh\eta + \cos\eta}\right) \qquad (2.27)$$

For the case of distinct adsorption processes on the material surface, so called surface barrier effects with a rate constant κ, the characteristic functions have to be

further adopted.[46] The normalized parameters a and c relate to the amount of sorbate located inside the pores c_C and on the external surface c_A. In many practical cases when dealing with zeolites $c \approx 1$ is valid and a can e neglected (see Equation 2.30).

$$\delta_{in} = \left(\frac{a\kappa}{\omega}\right)^2 \cdot \frac{a + c\delta_{1C}}{\phi} \qquad \text{with} \qquad \phi = \left(\frac{a\kappa}{\omega} + c\delta_{1S}\right)^2 + (a + c\delta_{1C})^2 \tag{2.27}$$

$$\delta_{out} = \left(\frac{a\kappa}{\omega}\right) \cdot \left[1 - \left(\frac{a\kappa}{\omega}\right) \cdot \frac{a\kappa/\omega + c\delta_{1C}}{\phi}\right] \tag{2.28}$$

$$a = \left(\frac{dc_A}{dp}\right) \bigg/ \left(\frac{d(c_A + c_C)}{dp}\right) \tag{2.29}$$

$$c = \left(\frac{dc_C}{dp}\right) \bigg/ \left(\frac{d(c_A + c_C)}{dp}\right) = 1 - a \tag{2.30}$$

Moreover, commercially available zeolite samples which are utilized in large scale industrial processes do not show clear, uniform and homogeneously distributed particle sizes and ideal shapes. This leads to distinct broadening of the experimental frequency responses. Therefore we had to introduce a normal distribution function with mean values of the characteristic function and of the crystal half thickness, $\bar{\delta}(\bar{L})$ and $\bar{L}$, respectively to modify the characteristic functions δ_i, in the following way[46]:

$$\bar{\delta}(\bar{L}) = \frac{1}{\sigma\sqrt{2\pi}} \int_0^\infty \delta \cdot \exp\left(-\frac{(L - \bar{L})^2}{2\sigma^2}\right) dL \tag{2.31}$$

Using the resulting modified equations 2.27 to 2.31, it was possible to adequately reproduce the experimental course of the data points (see Figure 2.27) for the molecules studied and to extract reasonable trends and transport time constants which were required to rationalize the results of the *in-situ* infrared measurements. A detailed differentiation and discussion of other transport models is be over the scope of this thesis, but for the interested reader it is referred to the prominent reviews of Yasuda[49, 50] and current publications.

2.4 References

[1]   A. Jentys, J. A. Lercher, in *Introduction to Zeolite Science and Practice* (Eds.: H. van Bekkum, E. M. Flanigen, P. A. Jacobs, J. C. Jansen), Elsevier, Amsterdam, **2001**, p. 345.

[2]   S. Zheng, PhD thesis, TU München (München), **2002**.

[3]   S. Zheng, H. R. Heydenrych, A. Jentys, J. A. Lercher, *J. Phys. Chem. B* **2002**, *106*, 9552.

[4]   S. Zheng, H. R. Heydenrych, H. P. Röger, A. Jentys, J. A. Lercher, *Top. Catal.* **2003**, *22*, 101.

[5]   L. Puppe, W. Büchner, *Naturwissenschaften* **1984**, *71*, 192.

[6]   J. H. de Boer, *Journal of Colloid and Interface Science* **1966.**, *21*, 404.

[7]   B. C. Lippens, J. H. de Boer, *J. Catal.* **1965**, *4*, 319.

[8]   S. Brunauer, P. H. Emmett, E. Teller, *J. Am. Chem. Soc.* **1938**, *60*, 309.

[9]   J. A. Lercher, in *Studies in Surface Science and Catalysis, Catalysis: An Integrated Approach, Vol. 123*, 2 ed. (Eds.: B. A. Averill, J. A. Moulijn, P. W. N. M. van Leeuwen, R. A. van Santen), Elsevier B.V., Amsterdam, **1997**, pp. 543.

[10]   C. H. Bartholomew, R. J. Farrauto, *Fundamentals of Industrial Catalytic Processes*, 2nd ed., John Wiley and Sons, Inc., Hoboken, New Jersey, **2006**.

[11]   M. Kruk, M. Jaroniec, J. Choma, *Carbon* **1998**, *36*, 1447.

[12]   S. J. Gregg, S. K. S. W., *Adsorption Surface Area and Porosity Vol. Gebundene Ausgabe (2nd)*, Gebundene Ausgabe (2nd) ed., Academic Press Inc.,U.S., London, **1982**

[13]   M. Jaroniec, M. Kruk, J. P. Olivier, *Langmuir* **1999**, *16*, 5410.

[14]   A. A. Isirikyan, A. V. Kiselev, *J. Chem. Phys.* **1961**, *65*, 601.

[15]   A. Jentys, in *South German Catalysis Institute, Ulm Course Lecture*, Garching, **2008**.

[16]   M. Kruk, M. Jaroniec, A. Sayari, *Langmuir* **1997**, *13*, 6267–6273.

[17]   E. P. Barrett, L. G. Joyner, P. P. Halenda, *J. Am. Chem. Soc.* **1951**, *73*, 373.

[18]   S. J. Reitmeier, O. C. Gobin, A. Jentys, J. A. Lercher, *Angew. Chem. Int. Ed.* **2009**, *48*, 533.

[19]   I. Chorkendorff, J. W. Niemantsverdriet, *Concepts of Modern Catalysis and Kinetics*, 2nd ed., Wiley VCH GmbH, Weinheim, **2007**.

[20]   P. Atkins, *Physical Chemistry*, 3 ed., Wiley-VCH Wiley, Weinheim, **2001**.

[21]   H. Pfeifer, D. Freude, J. Karger, *Z. Phys. Chem.* **1988**, *269*, 320.

[22]   D. Freude, M. Hunger, H. Pfeifer, **1987**, pp. 171.

[23]   M. Hunger, *Catal. Rev.-Sci. Eng.* **1997**, *39*, 345.

[24]   M. Hunger, D. Freude, T. Frohlich, H. Pfeifer, W. Schwieger, *Zeolites* **1987**, *7*, 108.

[25]   D. C. Harris, M. D. Bertolucci, *Symmetry and Spectroscopy*, 2 ed., Dover Publications, Inc., New York, **1989**.

[26]   M. Hesse, H. Meier, B. Zeeh, *Spektroskopische Methoden in der organischen Chemie*, 5 ed., Georg Thieme Verlag, Stuttgart, New York, **1995**.

[27]   H. Günzler, H.-U. Gremlich, *IR spectroscopy*, WILEY-CVCH Verlag Weinheim, **2002**.

[28]   L. Heinke, C. Chmelik, P. Kortunov, D. M. Ruthven, D. B. Shah, S. Vasenkov, J. Kärger, *Chem. Eng. Technol.* **2007**, *30*, 995.

[29]   L. Heinke, C. Chmelik, P. Kortunov, S. Vasenkov, D. M. Ruthven, D. B. Shah, J. Kärger, *Chemie Ingenieur Technik* **2007**, *79*, 1195.

[30]   W. Göpel, H. D. Wiemhöfer, *Statistische Thermodynamik*, 1 ed., Spektrum, Akademischer Verlag, Heidelberg, **2000**.

[31]   A. Jentys, J. A. Lercher, in *Studies in Surface Science and Catalysis: Introduction to Zeolite Molecular Sieves Vol. 168*, 3 ed. (Eds.: J. Cejka, H. van Bekkum, A. Corma, F. Schueth), Elsevier B.V., Amsterdam, **2007**, pp. 434.

[32]   Bruker Optik, *IFS 66v/S User Manual*, Bruker Optik GmbH, Karlsruhe, **1998**.

[33]   A. Jentys, R. R. Mukti, H. Tanaka, J. A. Lercher, *Microp. Mesop. Mat.* **2006**, *90*, 284.

[34]   R. R. Mukti, A. Jentys, J. A. Lercher, *J. Phys. Chem. C* **2007**, *111*, 3973.

[35]   L. J. Bellamy, H. E. Hallam, R. L. Williams, *Transactions of The Faraday Society* **1958**, *54*, 1120.

[36]   B. Onida, B. Bonelli, L. Borello, S. Fiorilli, F. Geobaldo, E. Garrone, *J. Phys. Chem. B* **2002**, *106*, 10518.

[37]   R. R. Mukti, PhD thesis, TU München (Garching), **2008**.

[38]   R. A. van Santen, J. W. Niemantsverdriet, *Chemical Kinetics and Catalysis*, Plenum Press, New York, **1995**.

[39]   W. Zhu, F. Kapteijn, J. A. Moulijn, *Phys. Chem. Chem. Phys.* **2000**, *2*, 1989.

[40]   R. S. Drago, C. E. Webster, J. M. McGilvray, *J. Am. Chem. Soc.* **1998**, *120*, 538.

[41]   H. R. Heydenrych, Master thesis, University of Cape Town (Cape Town, Munich), **2000**.

[42]   A. Jentys, H. Tanaka, J. A. Lercher, *J. Phys. Chem. B* **2005**, *109*, 2254.

[43]   T. Armaroli, M. Bevilacqua, M. Trombetta, A. G. Alejandre, J. Ramirez, G. Busca, *App. Catal. A-Gen.* **2001**, *220*, 181.

[44]   S. J. Reitmeier, R. R. Mukti, A. Jentys, J. A. Lercher, *J. Phys. Chem. C* **2008**, *112*, 2538.

[45]   L. M. Naphtali, L. M. Polinski, *J. Phys. Chem.* **1963**, *67*, 369.

[46]   Y. Yasuda, *Heterogen. Chem. Rev.* **1994**, *1*, 103.

[47]   L. Song, Z.-L. Sun, L. V. C. Rees, *Microp. Mesop. Mat.* **2002**, *55*, 31.

[48]   N. Hansen, in *Towards a new evolutionary computation. Advances on estimation of distribution algorithms* (Eds.: J. A. Lozano, P. Larranaga, I. Inza, E. Bengoetxea), Springer, **2006**, pp. 75.

[49]   Y. Yasuda, *Het. Chem. Rev.* **1994**, *1*, 103.

[50]   Y. Yasuda, in *Zeolites and Related Microporous Materials: State of the Art 1994, Vol. 84*, **1994**, pp. 1331.

Chapter 3

3. Theoretical methods – Statistical thermodynamics and collision theory

3.1   Fundamentals of statistical thermodynamics

3.1.1   General introduction

On one side, it is generally most convenient to treat complex systems with a minimal number of phenomenological parameters. In particular, the formalisms of thermodynamics[1] and classical mechanics are extensively used to describe the macroscopically relevant processes in equilibrium systems using experimentally accessible variables. Knowledge of the extensive and intensive state variables describing chemical systems i.e., temperature T, volume V, pressure p, particle numbers or molar number of the components) as well as of the underlying inter-relations are indispensably important for any technical application.

On the other side, modern natural sciences have benefited tremendously from the progress reached within understanding the behaviour of atoms, molecules, ions or electrons on an elementary basis. Quantum mechanics have allowed scientists to surpass the boundaries of classical mechanics to explain and even quantitatively calculate microscopically fundamental interactions of molecular species in gas, liquid or solid phases. Every chemical system has an intrinsic microscopic structure and the included particles populate its characteristic microstates. Statistical thermodynamics, being usually applied for equilibrium state systems, can quantitatively link the set of microscopically relevant wave functions of a many body system to macroscopically observable states with determining, phenomenological state variables. Classical mechanics hereby represent the limiting case of a complete quantum mechanical description (high energy approximation).

It can be further stated, that the statistical definition of the entropy of a system represents the key factor for understanding the populations of possible microscopic states and thus to quantifying the resulting state functions of the whole system. In order to be able to rationalize, emphasize or also to contradict to the experimental results obtained from spectroscopic and gravimetric measurements, as e.g., performed within this dissertation project, detailed theoretical approaches are highly necessary. Dealing with the molecular origin of transport phenomena at the interface between the gas phase and the surface of a solid, the fundamental aspects of kinetic gas theory and

statistical thermodynamics are most appropriate for this purpose. The changes observed within the molecular degrees of freedom of a system, expressed by molecular partition functions, can be translated into the variations of the fundamental state functions of interest: entropy S, enthalpy H or Gibbs free enthalpy G of the system. Evaluation of these state functions for a given reaction, sorption process or transport step allows shedding more light on complex network of molecular interactions or a transport mechanisms. Herein only a brief introduction into the main aspects of statistical thermodynamics will be given, as far as it is needed for the interpretation of the spectroscopically gathered data within the following chapters. For a more detailed description of the subject, it is referred to P. W. Atkins[2] and to W. Göpel and H.-D. Wiemhöfer.[3]

3.1.2 Fundamental definitions and Boltzmann distribution function

Consider an ensemble of particles i.e., molecules, atoms or ions with total energy E_{tot} which is composed of a set of n_{tot} energetic subsystems, so called microstates i with population numbers n_i and corresponding energy E_i,of each. Assuming a large number of such subsystems, a huge variety of different possibilities to distribute the total energy in small portions on these microstates exist. Large numbers are necessary in order to be able to statistically derive meaningful ensemble parameters.

Statistical thermodynamics are particularly interested in analyzing the respective energy distributions and possibilities to populate a certain energetic microstate with respect to maximizing the respective system entropy. Every set of population numbers $[n_0,\ n_1\ \ldots\ n_i]$ for the energetic microstates consequently characterizes a possible macroscopic state of the whole ensemble which occurs with a characteristic probability Pi. As boundary conditions when driving Pi, the two following equations have to be further fulfilled.

Energy conservation: $\sum_i n_i \cdot E_i = E_{tot} = const$ (3.1)

Constant number of subsystems: $\sum_i n_i = n_{tot} = const$ (3.2)

Applying a generalized multi-nominal distribution formalism, Stirling's approximation and the mechanism of Lagrange[3], the mathematical description of the microstate energy distribution function, being in the heart of statistical thermodynamics, can be obtained. The so called Boltzmann distribution function denotes the probability P_i that a certain microstate with energy E_i (see Equation 3.3), is populated at a given temperature T. Analyzing the population distributions of the system with varying temperature leads to macroscopic measures of the whole system, such as the inner energy U or entropy S.

$$P_i = \frac{n_i}{n_{tot}} = \frac{\exp\left(-\dfrac{E_i}{k_B T}\right)}{\sum_i \exp\left(-\dfrac{E_i}{k_B T}\right)} \tag{3.3}$$

3.1.3 Partition functions of atoms and molecules

The summation over all possible microstate energies ("Zustandssumme" in German spelling) E_i, included within the denominator of equation 3.3 is necessary to ensure that the summation over the calculated probabilities is normalized to unity. This summation represents the key factor for every equilibrium state statistical thermodynamics calculation and is conventionally[3] denoted as partition function q (Q) of a single particle (or system), defined in Equation 3.4.

$$\text{Partition function: } q = \sum_i \exp\left(-\frac{E_i}{k_B T}\right) \tag{3.4}$$

In principle, the single particle partition function q phenomenologically describes the number of electronic states of the system, which are thermally available (that means, can be populated) at a given temperature. As it is calculated by summarizing over all energy levels E_i, partition functions intrinsically contain all thermodynamic properties of the whole system.[2] Note, that for the case of a system composed of N non-interacting and non-distinguishable particles, the total partition function Q has to be taken into consideration when aiming to derive macroscopic

quantities. Q is given as product of all individual partition functions q reduced by the amount of equivalent configurations of the system as shown in equation 3.5. Notably, every thermodynamic property and (state) function of the system, including the average energy U, the Gibbs free energy G or the heat capacity C, can be straightforward and directly calculated from the corresponding partition functions. Furthermore, this approach allows determining a statically based value of the molecular entropy.

$$\text{Total partition function } Q = \frac{1}{N!}q^N = \frac{1}{N!}\left[\sum_i \exp\left(-\frac{E_i}{k_B T}\right)\right]^N \tag{3.5}$$

Relevant physical parameters expressed in terms of Q are exemplified given below.

$$S = k_B\left[\left(\frac{\partial \ln Q}{\partial \ln T}\right)\bigg|_{V,N} + \ln Q\right] \tag{3.6}$$

$$E = k_B T^2 \cdot \left(\frac{\partial \ln Q}{\partial T}\right)\bigg|_{V,N} \tag{3.7}$$

$$G = -k_B T\left[\ln Q - \left(\frac{\partial \ln Q}{\partial \ln V}\right)\bigg|_{T,N}\right] \tag{3.8}$$

For the above mentioned system of N non-interacting particles (i.e., an ideal gas) with independent degrees of freedom (DGFs), the total energy E_{tot} of the system can be split into the sum of all single particle energies E_j. These energies are in a second step separated additively into their internal (vibration, rotation, electronic and nuclear state energies) and external (translational energy) contributions, which will be shortly discussed in the following sections. With increasing molecular size and system temperature, the internal DGFs represent a more and more strongly increasing part of the average energy of the molecules.

$$E_{j,tot} = E_{j,trans} + E_{j,el} + E_{j,vib} + E_{j,rot} + E_{j,nuc} \tag{3.9}$$

The additivity of the individual energies is directly related (according to equation 3.7) to a multiplicatory combination of the corresponding partition functions of the system (see Equation 3.10). Breaking down the whole system into its independent contributions by means of translational, vibrational or rotational motion, general macroscopic phenomena e.g., observed within spectroscopic studies can be easily addressed on a molecular level. As introduced above, quantitative knowledge of the partition functions enables quantification of thermodynamically relevant parameters and state functions of interest for a given ensemble of particles.

$$q_{tot} = q_{trans} \cdot q_{el} \cdot q_{vib} \cdot q_{rot} \cdot q_{nuc} \cdot q_{zero}$$ (3.10)

For the case of simplicity, instead of the total partition function Q, which is accessible via Equation 3.6, the respective ingle particle partition functions q for all possible degrees of freedom (DGFs) will be discussed in the following sections in detail. The number of total degrees of freedom depends on the number of atoms within the subjected molecule. For a non-linear molecule of three atoms, i.e., $3 \times 3 = 9$ degrees of freedom (three translational, two rotational and four vibrational DGFs) have to be evaluated. For this dissertation thesis, dealing with *in-situ* infrared spectroscopy, transport measurements and the investigation of the corresponding sorption and transport phenomenon, a statistical thermodynamics focus will be set on the translational, rotational and vibrational contributions to the partition functions and thus the entropic effects governing the transport processes will be unravelled.

3.1.4 Translational motion and its contribution to the partition function

Every freely moving particle of mass *m*, possesses three degrees of translational freedom and can be characterized in the phase space by its momenta $p_{x,y,z}$ and kinetic energies $E_{kin,x,y,z}$ along the three Cartesian coordinates *x*, *y* and *z*. For each coordinate, the following contribution (Equation 3.12) to the translational single particle partition function is obtained:

$$q_{trans} = \prod_{j=x,y,z} q_{trans,j} = \prod_{j=x,y,z} l_j \cdot \frac{(2\pi \cdot m \cdot k_B \cdot T)^{\frac{1}{2}}}{h}$$ (3.11)

$$q_{trans}^{2D} = A \cdot \frac{\left(2\pi \cdot m \cdot k_B \cdot T\right)}{h^2} \tag{3.12}$$

$$q_{trans}^{3D} = V \cdot \frac{\left(2\pi \cdot m \cdot k_B \cdot T\right)^{\frac{3}{2}}}{h^3} = \frac{V}{\Lambda^3} \tag{3.13}$$

The equation obtained for the one-dimensional case exactly reproduces the quantum mechanical result for a particle in a box. For the two- and three-dimensional case, *A* and *V* represent the area or the volume fraction, the particle is freely moving in. It can be concluded, that the translational partition function crucially depends on the mass and the temperature, as well as on the dimensionality of the space it is moving in. Conveniently, translational partition functions can be written as function of the thermal wavelength Λ of the particle (see Equation 3.13), allowing to respectively estimating the validity of the Boltzmann distribution conditions via i.e., for three dimensions $V / \Lambda^3 \gg 1$.

3.1.5 Vibrational motion and contributions to the partition function

Using the approximation of the harmonic oscillator, the vibrational motion of a particle located in a parabolic potential defined by the force constant *k* and vibrating with a characteristic frequency of ν_j around its equilibrium position, can be mathematically described.[2-5]

$$\nu_j = \frac{\omega_j}{2\pi} = \frac{1}{2\pi} \cdot \sqrt{\frac{k_j}{\mu_j}} \tag{3.14}$$

In contrast to classical mechanics applied to macroscopic particles, quantum mechanics result in a distinct quantization of the vibrational energies with respect to a characteristic quantum number *i*. For non-linear molecules consisting of *N* atoms, in total *j* = 3*N*-6 vibrational degrees of freedom can be distinguished (*j* = 3*N*-5 for linear ones) and the characteristic, non-degenerate energy levels for each vibrational DGF are given by
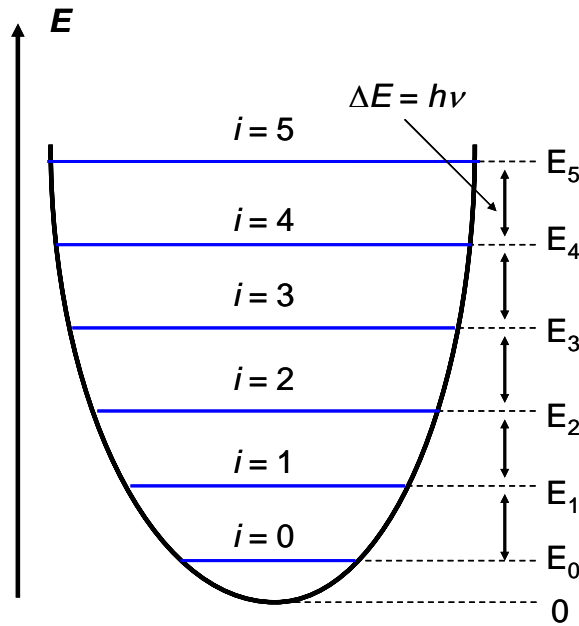
Figure 3.1   **Energy scheme for a vibrating system according to the harmonic oscillator approximation with quantum number *i*.**

$$E_i^{\text{harmonic oscillator}} = \left(i + \frac{1}{2}\right) \cdot h \cdot v_j = \left(i + \frac{1}{2}\right) \cdot h \cdot c \cdot \bar{v}_j \tag{3.15}$$

It should be noted that, using the harmonic oscillator approximation, the lowest occupied state does not equal zero energy, but constant value of ½ hv_j. For the evaluation of the vibrational partition functions, this fact is taken into account by shifting the zero energy upward to the energetic ground state. The resulting partition function with respect to this downshift thus becomes:

$$q_{vib}^j = \sum_{i=0}^{\infty} \exp\left(-\frac{E_i^j}{k_B T}\right) = \sum_{i=0}^{\infty} \exp\left(-\frac{i \cdot h \cdot v_j}{k_B T}\right) = \left[1 - \exp\left(-\frac{h \cdot v_j}{k_B T}\right)\right]^{-1} \tag{3.16}$$

$$q_{vib} = \prod_{j=1}^{3N-6(5)} \left[1 - \exp\left(-\frac{h \cdot v_j}{k_B T}\right)\right]^{-1} = \prod_{j=1}^{3N-6(5)} \left[1 - \exp\left(-\frac{\Theta_{vib,j}}{T}\right)\right]^{-1} \tag{3.17}$$

The commonly occurring factor hv_j/k_B within the exponential, having the unit of a temperature, is called the characteristic vibrational temperature $\Theta_{vib,j}$ of the vibrational

mode, which can be determined experimentally from the vibrational spectrum of the molecule. Normally at ambient temperature, the vibrational partition function is close to unity, but for the case of low frequency vibrations and high temperatures with T >> Θ_{vib}, a limiting partition function can be calculated.

$$q_{vib} = \prod_{j=1}^{3N-6(5)} \left[1 - \exp\left(-\frac{\Theta_{vib,j}}{T} \right) \right]^{-1} \overset{T \gg \Theta_{vib,j}}{\approx} \prod_{j=1}^{3N-6(5)} \frac{T}{\Theta_{vib,j}} \qquad (3.18)$$

According to the translational motion, the contributions of the vibrational motion to the thermodynamic parameters can be calculated analogously.

3.1.6 Rotational motion and rotational partition function

In addition to the vibrational motion, rotations of molecule around its principal axes represent source of internal degrees of freedom, contributing to the total system energy. In contrast to vibrations which normally have high characteristic vibrational temperatures under standard conditions, rotations are already strongly excited at ambient temperature. The model of a rigid rotor can be adopted from classical mechanics and utilized to define the rotational partition functions. Classically, the overall rotational motion (gyration) of a rigid molecule can be separated into the independent rotations around the principal axes of the molecule, which are commonly chosen. These are exemplified shown for a methyl chloride molecule in Figure 3.2. Note, that for high temperatures, the dimension of a gas phase molecule is apparently given by its radius of gyration.

The total rotational energy of a polyatomic molecule is given by the sum of the three energetic terms calculated from the principal moments of inertia I_x, I_y and I_z and corresponding radial frequencies ω_x, ω_y and ω_z.

$$E_{rot} = \frac{1}{2} I_x \cdot \omega_x^2 + \frac{1}{2} I_y \cdot \omega_y^2 + \frac{1}{2} I_z \cdot \omega_z^2 \quad \text{with} \quad I = \sum_i \mu_i \cdot r_i^2 \qquad (3.19)$$

Applying the principles of quantum mechanics and using the solutions of the Schrödinger Equation for the classical model of the rigid rotor leads, in contrast to

classical mechanics, to quantization of the molecular rotational energy levels with corresponding quantum number J ($J = 0,1,2…$). The rotational energy is straight foreword expressed as function of the corresponding quantum state of the angular momentum L with $L = I \cdot \omega$. Furthermore, contrary to vibrational energy levels, each rotational energy level except the ground state is degenerate with a degeneracy factor of $g_J = 2J + 1$. For the case of a linear molecule, the rotational energy is defined as follows in Equation 2.20 with all parameters and constants summarized within the characteristic rotation constant B_i (see Equation 2.20). For the case of more complex spherical and symmetric molecular rotors, it is referred to literature.[2, 3]
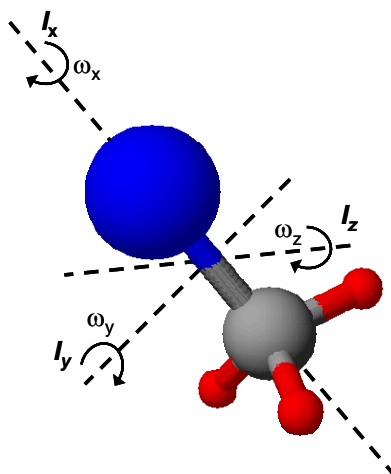
Figure 3.2   **Principal axes with corresponding moments inertia for a methyl chloride molecule (adapted from ref. [3]).**

$$E_{rot} = \sum_{i=x,y,z} J_i(J_i+1)\frac{\hbar^2}{2I_i} = \sum_{i=x,y,z} J_i(J_i+1)\frac{h^2}{8\pi^2 I_i} = \sum_{i=x,y,z} J_i(J_i+1)B_i \qquad (3.20)$$

The insertion of Equation 2.20 into the definition of the partition function (see Equation 3.4) together with the degeneracy of the rotational levels g_J yields, for the simplest case, the rotational partition function of a linear diatomic molecule with two equal moments of inertia $I = I_x = I_y$. For symmetric molecules such as O_2 or N_2, a molecular symmetry number σ has to be included in order to account for quantum mechanically indistinguishable atom positions. This symmetry number, according to general group theory[2], represents the number of possibilities to generate an

indistinguishable orientation of the molecule with respect to the rotation around its principal axes. Some symmetry numbers for a series of molecules are exemplified give within Table 3.1.

$$q_{rot}^{2DGF} = \frac{1}{\sigma} \cdot \sum_{J=1}^{\infty} g_{rot} \cdot \exp\left(-\frac{E_{rot}}{k_B T}\right) =$$
$$= \frac{1}{\sigma} \cdot \sum_{J=1}^{\infty} (2J+1) \cdot \exp\left(-\frac{J(J+1) \cdot B}{k_B T}\right)$$

(3.21)

Table 3.1   Examples for values of the symmetry number σ

Molecule	H_2, H_2O	Toluene	o-Xylene	NH_3	p-Xylene	CH_4	Benzene
Symmetry σ	2	2	2	3	4	12	12

The formula for the rotational partition function can be modified by introducing in analogy to the vibrational motion the characteristic rotational temperature Θ_{rot} of the rotation. In the high temperature limit, the summation over all populated states can then be approximated by the integration over all states J, yielding a simplified expression of q_{rot} being only function of the system temperature. It is noted, that for most molecules, the characteristic rotation temperatures are very low with values below 20 K and thus the integral approximation is valid even at ambient temperature. For the exact calculation of q_{rot} even below T < 10 Θ_{rot} being over the scope of this thesis it is referred to the common literature.

$$\Theta_{rot,i} = \frac{B_i}{k_B} = \frac{h^2}{8\pi \cdot I_i \cdot k_B}$$

(3.22)

$$q_{rot}^{2DGF} = \frac{1}{\sigma} \cdot \sum_{J=1}^{\infty} (2J+1) \cdot \exp\left(-\frac{J(J+1) \cdot \Theta_{rot}}{T}\right)$$
$$\approx \frac{1}{\sigma} \cdot \int_{J=0}^{\infty} (2J+1) \cdot \exp\left(-\frac{J(J+1) \cdot \Theta_{rot}}{T}\right) dJ = \frac{1}{\sigma}\left(\frac{T}{\Theta_{rot}}\right)$$

(3.23)

The expression derived for the simplest case can easily be extended to larger, non-linear and even complex, polyatomic molecules in the gas phase, having three

rotational DGFs with different moment of inertia along all three principal axes. Instead of the overall symmetry number σ, here the product of the individual symmetry numbers along these axes has to be introduced with $\sigma_{tot} = \sigma_x \cdot \sigma_y \cdot \sigma_z$.

$$q_{rot}^{3DGF} = \pi^{\frac{1}{2}} \cdot \prod_{i=x,y,z} \frac{1}{\sigma_i} \left(\frac{T}{\Theta_{rot,i}} \right)^{\frac{1}{2}} = \frac{\pi^{\frac{1}{2}}}{\sigma_{total}} \cdot \left(\frac{8\pi^2 k_B T}{h^2} \right)^{\frac{3}{2}} \cdot \left(I_x \cdot I_y \cdot I_z \right)^{\frac{1}{2}} \text{ for } T \gg \Theta_{rot,i} \quad (3.24)$$

If the rotational motion of the poly-atomic molecule is severely hindered, e.g., by steric constraints in confined spaces, the rotational partition function has accordingly to be modified. For the case of adsorption processes, where the molecule is strongly bound to an active site, it is assumed herein, that q_{tot} is reduced to unity and that all formerly free rotational DGFs will be lost. For the aromatic molecules studied in this work, small characteristic rotation temperatures occur and thus the classical high temperature limit is satisfactorily fulfilled. It should be noted, that for rationalizing the observed sorption and transport phenomena, estimations of the changes within the molecular entropy of the sorbate on the basis of the molecular rotational partition functions are sufficient and the inter-conversions of rotational and vibrational DGFs as well as deviations from the generalized rigid rotor model were neglected for simplicity.

$$S_{rot}^{3DGF} = R \cdot \ln \left[\frac{\pi^{\frac{1}{2}}}{\sigma_{total}} \cdot \left(\frac{T^3 \cdot e^3}{\Theta_{rot,x} \cdot \Theta_{rot,y} \cdot \Theta_{rot,z}} \right)^{\frac{1}{2}} \right] \text{ for } T \gg \Theta_{rot,i} \quad (3.25)$$

Using the obtained expression for the rotational partition function in 3D, the amount of molar entropy conserved within the rotational DGFs at every given temperature can be calculated from Equation 3.25. The higher the rotational partition function i.e., the lower the characteristic rotational temperature, and the higher the molecular symmetry, the lower the amount of molecular entropy preserved within rotational DGFs.

3.2   Hard sphere collision theory and sticking probability

With regards to molecular transport processes at the interface of gas phase and the surfaces of porous solids, the hard sphere collision theory represents a powerful tool which, combined with statistical thermodynamics, provides a profound theoretical basis to explain the observed transport phenomena. The probability for a molecule to stick to a catalyst surface in a surface element A and to be subsequently distributed to the active sites is proportional to the total number of collisions with the surface, the strength of the sorbate-sorbent interaction and to the accommodation of the released collision energy. A gas molecule, described as hard sphere, at a certain distance from the surface is able to hit the surface element A in a time interval Δt when it has the appropriate velocity u. This velocity is accessible from the Maxwell-Boltzmann velocity distribution in one dimension being reported in literature.[2-5]
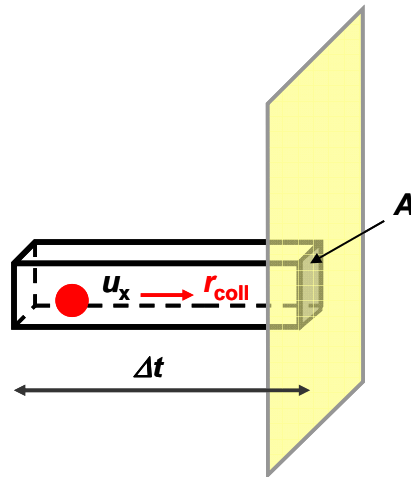
Figure 3.3   **Scheme illustrating molecules having a velocity u_x, colliding with a surface element A in the incremental time Δt adopted from ref. [6].**

$$F(u_x) = \left(\frac{m}{2\pi k_B T}\right)^{\frac{1}{2}} \cdot \exp\left(\frac{-m \cdot u_x^2}{2k_B T}\right)$$

(3.26)

The corresponding collision rate of the gas phase molecules with the surface, normalized to the surface area A, is concludingly derived as a function of the molecule density N/V and the mean gas velocity $\bar{u}$.

$$r_{coll} = \frac{N}{V} \cdot \left(\frac{m}{2\pi k_B T} \right)^{\frac{1}{2}} \cdot \int\limits_{u_x=0}^{\infty} u_x \cdot \exp\left(\frac{-m \cdot u_x^2}{2 k_B T} \right) \cdot du_x$$

$$= \frac{N}{V} \cdot \left(\frac{k_B T}{2\pi m} \right)^{\frac{1}{2}} = \frac{1}{4} \cdot \frac{N}{V} \cdot \overline{u} \overset{ideal\ gas}{=} \frac{p}{\left(2\pi \cdot m \cdot k_B \cdot T \right)^{\frac{1}{2}}}$$

(3.27)

For every heterogeneously catalyzed reaction, only the molecules that have successfully adsorbed on the surface can subsequently undergo desired chemical reactions at the active sites of the catalyst. Therefore, the total number of surface collisions has to be reduced by those, leading to immediate redirection of the molecule to the gas phase. Consequently, the adsorption rate is defined by the collision rate multiplied by a proportionality constant, which is denoted the theoretical sticking probability α of the molecule (Equation 3.28). Thus, the sticking probability can be determined from the quotient of the adsorption and the collision rate of the sorbate molecules according to Equation 3.29.

$$r_{ad} = \alpha \cdot r_{coll} = \alpha \cdot \frac{1}{4} \cdot \frac{N}{V} \cdot \overline{u}$$

(3.28)

$$\alpha = \frac{r_{ad}}{r_{coll}}$$

(3.29)

A straightforward way to experimentally measure the sticking probabilities on a sorbent surface is to follow the uptake kinetics of gas sorbate molecules on the surface as function of the sorbate partial pressure. Spectroscopic methods, such as the photo electron spectroscopy (XPS) or the time-resolved infrared spectroscopy (IR), being highly sensitive to the surface or to the specific active sites, are most appropriate for this purpose. While for small molecules on metal surfaces, such as e.g., CO, CO_2 or CH_4 on platinum metal surfaces or metal clusters, the sticking probabilities have been already extensively investigated with accepted values close to one, less knowledge exists about sticking for larger hydrocarbons on the metal oxide surfaces (silica, alumina) and in particular on the surfaces of porous molecular sieves. In the past, several research groups have challenged this phenomenon but have come up with strongly different values for the sticking coefficient ranging from below 10^{-7} up to

almost unity, which led to a controversy debate. Obviously, finding in addition an independent experimental way to determine sticking probabilities of hydrocarbon molecules on zeolites and post-synthetically modified materials represents an interesting and demanding task. A very promising approach, as indicated by previous investigations of Jentys et al.[7] and R. Mukti[8], based on time-resolved infrared spectroscopy will therefore be experimentally addressed in detail within chapter four of this thesis using H-ZSM5 zeolites of Si/Al-ratio of 45.

3.3 References

[1]   I. M. Klotz, R. M. Rosenberg, *Chemical Thermodynamics*, 5 ed., John Wiley & Sons, Inc., New York, **1994**.

[2]   P. Atkins, *Physical Chemistry*, 3 ed., Wiley-VCH Wiley, Weinheim, **2001**.

[3]   W. Göpel, H. D. Wiemhöfer, *Statistische Thermodynamik*, 1 ed., Spektrum, Akademischer Verlag, Heidelberg, **2000**.

[4]   D. C. Harris, M. D. Bertolucci, *Symmetry and Spectroscopy*, 2 ed., Dover Publications, Inc., New York, **1989**.

[5]   M. Hesse, H. Meier, B. Zeeh, *Spektroskopische Methoden in der organischen Chemie*, 5 ed., Georg Thieme Verlag, Stuttgart, New York, **1995**.

[6]   I. Chorkendorff, J. W. Niemantsverdriet, *Concepts of Modern Catalysis and Kinetics*, 2nd ed., Wiley VCH GmbH, Weinheim, **2007**.

[7]   A. Jentys, R. R. Mukti, J. A. Lercher, *J. Phys. Chem. B* **2006**, *110*, 17691.

[8]   R. R. Mukti, PhD thesis, TU München (München), **2007**.

Chapter 4

4. Experimental and theoretical investigation of the sticking probability of aromatic hydrocarbons on H-ZSM5 and SiO$_2$

4.1 Introduction

In order to tailor the shape selective properties of catalytically active materials and sorbents e.g., by post-synthetic modifications[1, 2], a detailed understanding of sorption and transport processes of hydrocarbon reactants on microporous materials, including adsorption on the outer material surface, pore entering and intra-crystalline diffusion to the active sites inside the pore network is essential. In the past, various experimental[2-20] as well as theoretical[21-28] methods have been applied to investigate diffusion phenomena involving aromatic hydrocarbon molecules in molecular sieves (see also chapter one)[29], but the appearance of surface barrier effects influencing the transport diffusion are still controversially discussed.[9, 30, 31] The elementary transport steps prior to the intra-crystalline diffusion as well as the energetic and entropic contributions controlling sorption in the pores of MFI zeolites were recently addressed for aromatic hydrocarbons by Jentys et al.[23, 24, 32, 33] and Mukti et al.[34]. It was indicated, that the transport processes on the external zeolite surface govern the pore entrance of the reactants, subsequent diffusion steps and sorption to intra-pore sites. Direct pore entrance from the gas phase into the zeolite micropores was excluded for the aromatic molecules studied[35, 36] due to their minimum kinetic diameter similar to the pore apertures of H-ZSM5. Molecular dynamics studies of Skoulidas and Sholl[37] presented in detail in chapter six further support this assumption..

For the case of benzene, toluene, *p*- and *o*-xylene on H-ZSM5, the kinetic processes at the active sites occur on the time scale of seconds to milliseconds and involve only very small fractions of reactant molecules, as shown previously.[33, 35] Therefore, a fast spectroscopic technique providing a high time-resolution in the range of milliseconds and at the same time an appropriate signal-to-noise ratio is absolutely mandatory. In this context, *in-situ* time-resolved infrared spectroscopy in rapid scan mode represents a promising tool. Recently, the complex network of transport steps occurring during the sorption of aromatic molecules on H-ZSM5 could be unraveled using this technique.[33] The overall sorption process was dissected into a series of consecutive and parallel transport pathways including the initial collision of the molecules with the surface, sorption into a physisorbed surface state, transport to the terminal silanol groups as well as pore entering followed by sorption to the intra-pore bridging hydroxyl sites.[33] With regards to investigating the effects of external surface

modifications on the overall transport properties, primarily, the sticking of reactants on the unmodified zeolite surface has to be understood in detail. Therefore, in this chapter the experimental focus is set on the first step in the transport network, the capturing of gas phase molecules on the particle surface after collision, which can be described by the sticking probability of the sorbate.[38] From the uptake rates of the rigid aromatic molecules, the sticking probabilities on micropore-free amorphous silica and on zeolite H-ZSM5 were roughly estimated in a first approach[23, 33] to be in the order of 10^{-7}. In contrast, significantly different sticking probabilities close to unity were derived for *n*-butane on aluminum-free zeolite ZSM5 (Silicalite-1) by Simon et al.[39] from PFG-NMR studies and theoretical simulations.[35] In this context, external mass transport limitations of the sorbate molecules in the inter-crystalline void spaces were suggested to account for the low experimental values.

Statistical thermodynamics calculations strongly indicated that such low values of the sticking probability in the order of 10^{-7} were reasonable for sorbate molecules losing large amounts of rotational entropy during the sorption step on the surface.[23] If the free motion of the molecules in the gas phase is severely hindered, successful sticking becomes less favorable and resulting in a low sticking probability observed. This interpretation led to a re-estimation of the sticking probability of benzene on Silicalite-1 by Kärger et al.[40], also resulting in a small value of 10^{-4}. Further confirmation of the low order of magnitude of the sticking probabilities for the aromatic hydrocarbons was presented in a theoretical study by A. Schüring[41], who reported a correlation between the diffusion coefficient and the probability for a molecule to enter into circular pores (entering probability). Although this study was carried out for ethane in LTA zeolites, an extrapolation based on the diffusion coefficients for benzene in MFI-type zeolites led to a sticking probability in the order of 10^{-6} to 10^{-7}. For the case of aliphatic hydrocarbons such as e.g., ethane in zeolite NaX or *iso*-butane in Silicalite-1, contrarily, much higher values in the order of 10^{-2} were reported.[31, 40] Moreover, using interference microscopy, Heinke et al. recently provided experimental evidence that the sticking probability of hydrocarbon molecules on microporous materials can cover values, ranging from very small to close to one.[31] The difference between the aliphatic and aromatic molecules is explained by a higher conformational flexibility and thus different gas phase geometry[35] of the aliphatic

molecules compared to the rigid aromatic compounds. Accordingly more molecular entropy can be preserved during the sorption and pore entering step of the aliphatic molecule and a higher sticking coefficient is obtained.[42]

Within this chapter the mass transport processes of aromatic molecules benzene, toluene, *o*- and *p*-xylene from the gas phase to the bridging hydroxyl groups inside the pore network of zeolite H-ZSM5 is explored by studying the impact of different substitutions on the benzene ring on the sticking probability. In addition, amorphous SiO_2 was investigated to compare the sticking probabilities with those on a non-porous silica material. The obtained results should allow a better understanding of the transport properties of different aromatic molecules during sorption on zeolite surfaces on a molecular level and set the basis for systematically addressing transport on surface modified materials. Experimentally this is addressed by combining periodic pressure modulation experiments and *in-situ* IR spectroscopy to follow the kinetic processes at the active hydroxyl groups of the materials.

4.2 Experimental

4.2.1 Materials

Zeolite H-ZSM5 (Süd-Chemie AG, denoted H-ZSM5-p) with a Si/Al ratio of 45 was used to study the sticking probabilities of the aromatic hydrocarbons molecules. An average particle size of the zeolite crystals of 0.5 µm was determined by SEM (see chapter two, section 2.1.4). ^{27}Al/MAS-MNR analysis performed by Zheng et al.[1] indicated the absence of octahedral Al in the zeolite sample. The concentrations of terminal silanol (SiOH) and bridging hydroxyl groups (SiOHAl groups, Brønsted acid sites) of the zeolite sample were 0.27 and 0.21 mmol g^{-1}, respectively, determined by ^{1}H/MAS-NMR spectroscopy, described in chapter two, section 2.1.6.

Amorphous, micropore free SiO_2 (Aerosil 200) was utilized to compare the sorption processes on the H-ZSM5-p sample with a material that does not have the additional transport limitations in the micropores. The specific surface area and the concentration of OH groups of the amorphous SiO_2 were 200 $m^2 g^{-1}$ and 0.54 mmol g^{-1}, respectively. As aromatic hydrocarbon sorbate molecules, benzene, toluene *p*- and *o*-

xylene obtained from Sigma-Aldrich (Fluka) in spectroscopic grade (> 99.8 %) were used without further purification.

4.2.2 Methods

4.2.2.1 *In-situ* time-resolved infrared spectroscopy

The general measurement principle[33], the instrument setup and also the signal-to-noise ratio requirements of *in-situ* fast time-resolved IR spectroscopy in rapid scan mode were presented in detail within chapter two. The sample materials were pressed to self-supporting wafers and subsequently inserted in a vacuum cell with geometry optimized for transmission IR spectroscopic measurements. Series of infrared spectra to follow hydrocarbon transport and sorption on the material were recorded with a resolution of 8 cm^{-1}. The samples were activated under vacuum below 10^{-7} mbar, heated with a rate of 10 K min^{-1} to 823 K and kept there for 1 h. The IR experiments were subsequently carried out at 403 K. The samples were equilibrated with the sorbate gases and the system volume was periodically modulated ($\Delta V \pm 5\%$) by a magnetically driven pair of vacuum bellows using a square-wave modulation function of 0.0167 Hz, synchronized with the recording of the IR spectra[33] (see also chapter two, section 2.3.1 for further details). The partial pressure of the sorbates for following the transport processes was chosen to 0.06 mbar, which fell into the nearly linear region of the isotherm to be able to observe the maximum change in the coverage during the pressure modulations. Normalization of all infrared spectra as described in chapter two, section 2.2.2 allows to quantitatively compare the surface coverages of the adsorbed hydrocarbons. The concentration changes at the bridging SiOHAl and terminal SiOH groups were calculated from the corresponding integral intensities of the IR stretching vibrational bands (see Figure 4.2). Hereby, it was assumed that the molar extinction coefficients for these vibrational bands are independent form the site coverage in the sorbate partial pressure range studied.

4.2.2.2 Frequency response technique to study hydrocarbon transport

The transport diffusivities for the aromatic hydrocarbons of interest, benzene, toluene and *p*-xylene were determined from additional transport measurements using

the frequency response method.[2, 10, 43] An overview to this technique can be found in chapter two, section 2.3.2. The zeolite samples either in the form of dispersed powder or pressed as a self-supporting wafer and subsequently broken into small pieces were placed on glass wool at the bottom of a quartz tube which was connected to a vacuum system. Activation was performed in analogy to the time-resolved IR spectroscopic measurements in rapid scan mode. The hydrocarbon sorbates were added to the activated sample with a partial pressure of 0.20 mbar and equilibrated for at least 1 h at 403 K. Subsequently, the system volume was periodically modulated ($\Delta V = \pm 1$ %) with a square-wave modulation function of varying frequency in the frequency range between 0.001 and 1 Hz. An in-line Baratron pressure transducer of type MKS 161A11 was used to precisely record the resulting frequency response of the system pressure following the periodic volume perturbation.

Using Fourier transformation (for details see Appendix B) the phase lag and amplitude change of the frequency response with respect to the applied periodic modulation function were calculated for each frequency. From these values characteristic in-phase and out-of-phase functions $\delta_{in}, \delta_{out}$ of the frequency response experiment (Equation 4.1 and 4.2) were obtained. Herein P_B and P_Z are the respective amplitudes of the pressure during the volume change in the presence (Z) or the absence of the zeolite sample (blank, B) and φ_{Z-B} is the difference between the phases of the measured pressure responses. Blank measurements under identical conditions are required to exclude non-ideal contributions of the apparatus itself. The constant K is related to the gradient of the sorption isotherm around the equilibrium partial pressure and contains information about the amount of molecules adsorbed in the sample.

In phase function: $\qquad (P_B / P_Z) \cos \varphi_{Z-B} - 1 = K \cdot \delta_{in}$ $\qquad\qquad$ (4.1)

Out-of-phase function: $\qquad (P_B / P_Z) \sin \varphi_{Z-B} = K \cdot \delta_{out}$ $\qquad\qquad$ (4.2)

By fitting theoretical solutions of Fick's second law to the experimental characteristic functions according to chapter two, section 2.3.2, the desired transport diffusivities D of the aromatic sorbates could be determined. Herein, a simplified theoretical model (planar sheet model) assuming diffusion of only a single molecular

species in a solid slab being subjected to a periodic pressure modulation was applied for data evaluation.[43] For the corresponding definitions of the theoretical in-phase and out-of-phase functions see Equations 2.26 and 2.27 in chapter two.

4.3 Results

4.3.1 Transport properties of aromatic hydrocarbons determined by *in-situ* infrared spectroscopy

Upon sorption of an aromatic molecule in H-ZSM5-p, the interaction with the hydroxyl sites leads to a characteristic decrease in the intensity of the vibrational bands of the bridging SiOHAl and terminal SiOH groups. At the same time, the formation of two new bands assigned to perturbed bridging hydroxyl groups and one band assigned to perturbed silanol groups is observed (see chapter two, section 2.2.2.3).[4, 44] The changes in the time-resolved infrared spectra during the pressure modulation of benzene at 403 K over H-ZSM5-p are shown in Figure 4.1, where the first spectrum of the time-resolved series was subtracted from the subsequent ones.
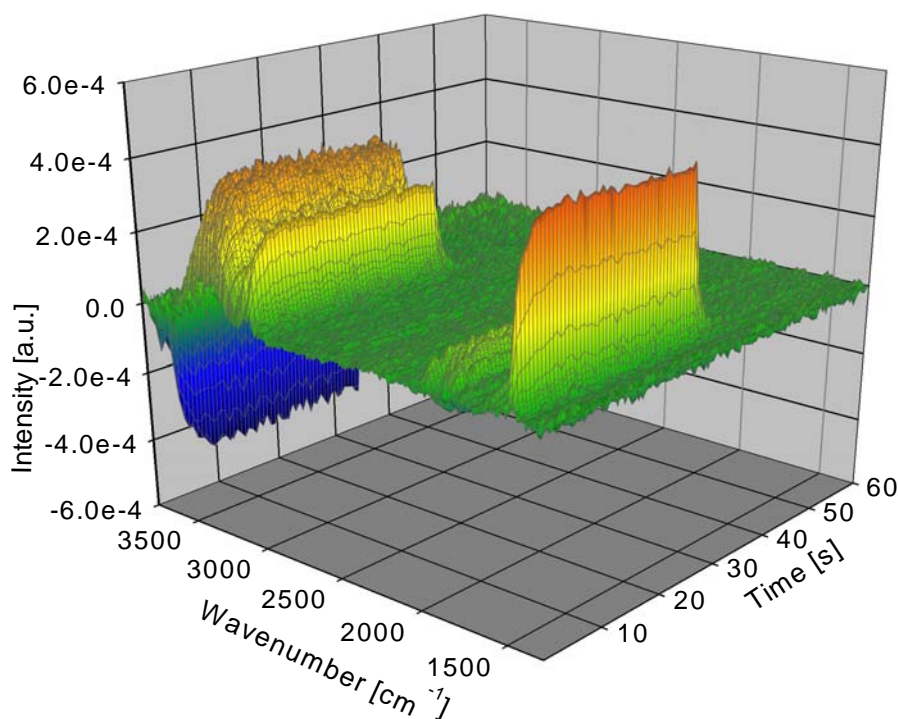
Figure 4.1   **Time-resolved IR spectra of benzene adsorbed on H-ZSM5-p during a pressure modulation of 0.003 mbar at an equilibrium partial pressure of 0.06 mbar at 403 K.**
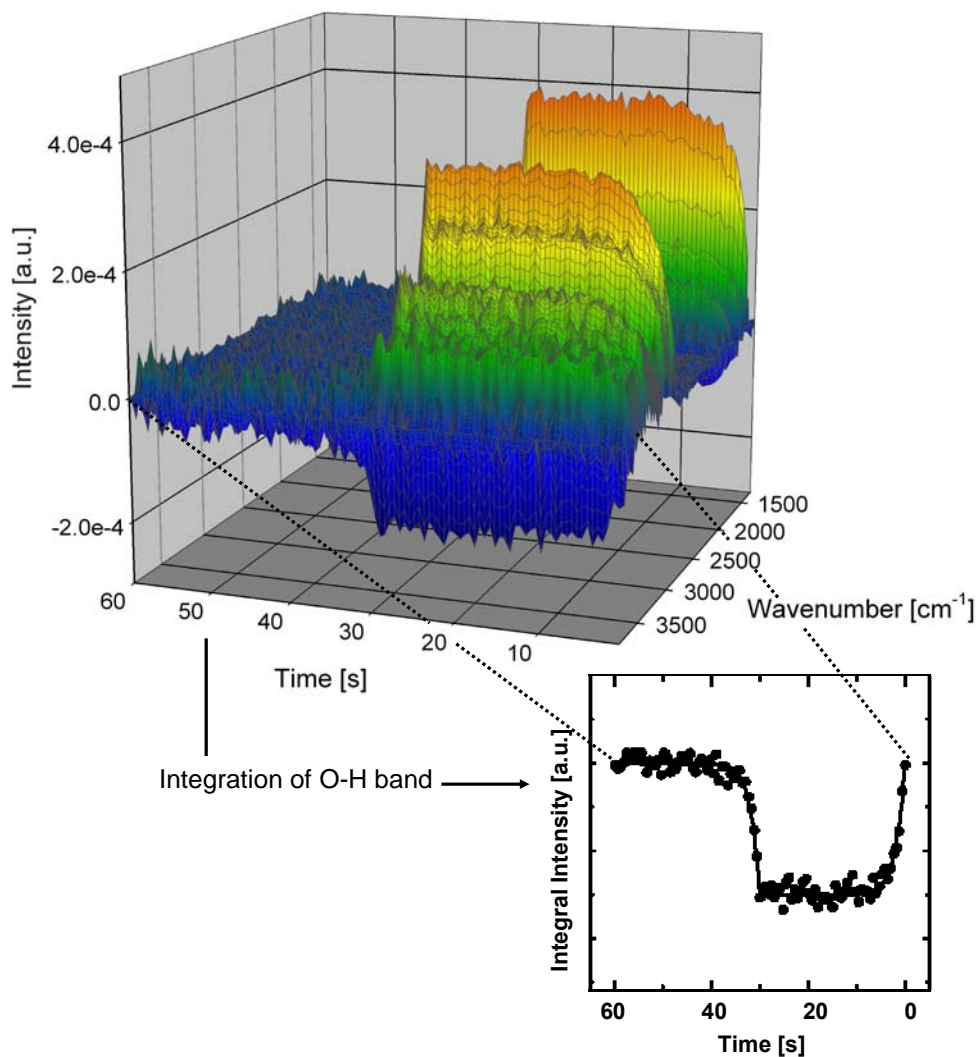
Figure 4.2   Time-resolved IR spectra of toluene adsorbed on H-ZSM5-p during a pressure modulation of 0.003 mbar at an equilibrium partial pressure of 0.06 mbar at 403 K. The insert shows the integrated intensity of the stretching vibrational band of the SiOHAl group.

Those bands increasing in intensity are positive and point upwards, whereas bands decreasing in intensity are negative and point downwards. The characteristic OH stretching vibrational bands were integrated and the integrated intensities [cm^{-1}] were used to calculate the coverage of the hydroxyl groups [mmol g^{-1}]. The corresponding coverage changes of the SiOH and SiOHAl groups of H-ZSM5 and the SiOH groups of Aerosil200 with benzene resulting from the ad- and desorption of benzene during the pressure modulation, determined from the intensities of the bands at 3745 and 3610 cm^{-1}, respectively, are shown in Figure 4.3. Note, that the bridging SiOHAl groups are located inside the pores at the channel intersections while the SiOH groups exclusively terminate the crystals on the outer zeolite surface.

Table 4.1 **Characteristic time and rate constants for the sorption of aromatic molecules on the bridging SiOHAl groups of H-ZSM5.**

SiOHAl	Sorbate	τ_{ad} [s]	τ_{de} [s]	τ [s]	k [s^{-1}]
	Benzene	2.01	2.02	2.02	0.50
	Toluene	1.84	1.86	1.85	0.54
H-ZSM5-p	*p*-Xylene	1.36	1.46	1.41	0.71
	o-Xylene	6.01	5.98	6.00	0.17

The time dependency of the coverage changes of the hydroxyl groups $\Delta c_{OH}(t)$ after the stepwise change of the sorbate partial pressure Δp during the modulation experiment was fitted with exponential functions according to Equations 2.21 and 2.22 given in chapter two. This approach yielded the characteristic time constants of the transport process during the adsorption and desorption step given by τ_{ad} and τ_{de}, respectively. Assuming first order kinetics, small time constants correspond to fast sorption processes. From the time constants and the equilibrium coverage changes $\Delta c_{OH,eq}$ the initial sorption rates at each site were determined from the adsorption branch of the concentration profiles (see Equation 2.23 in chapter two).

Table 4.2 **Characteristic time and rate constants for the sorption of aromatic molecules on the terminal SiOH groups of H-ZSM5 and of micropore-free amorphous silica SiO$_2$.**

SiOH	Sorbate	τ_{ad} [s]	τ_{de} [s]	τ [s]	k [s^{-1}]
	Benzene	3.61	3.50	3.56	0.28
	Toluene	2.39	2.54	2.52	0.39
H-ZSM5-p	*p*-Xylene	2.05	2.10	2.07	0.49
	o-Xylene	0.94	0.96	0.95	1.05
	Benzene	3.21	3.22	3.21	0.31
SiO$_2$	Toluene	2.49	2.54	2.52	0.40
(Aerosil 200)	*p*-Xylene[45]	0.99	1.07	1.03	0.98
	o-Xylene	0.95	0.93	0.94	1.06

The time and rate constants on H-ZSM5-p and amorphous SiO_2 are compiled in Table 4.1 for the SiOHAl groups and in Table 4.2 for the SiOH groups, respectively. The slight differences for the tabulated values to the numbers previously published by Jentys et al.[33] result from a change in the integration ranges of the IR bands used for determination of the surface coverages.[45] For those molecules being able to enter easily into the zeolite pores, the sorption rates on the SiOHAl groups were faster compared to the terminal SiOH groups, where the sorption rates showed a distinct increase with sorbate size.
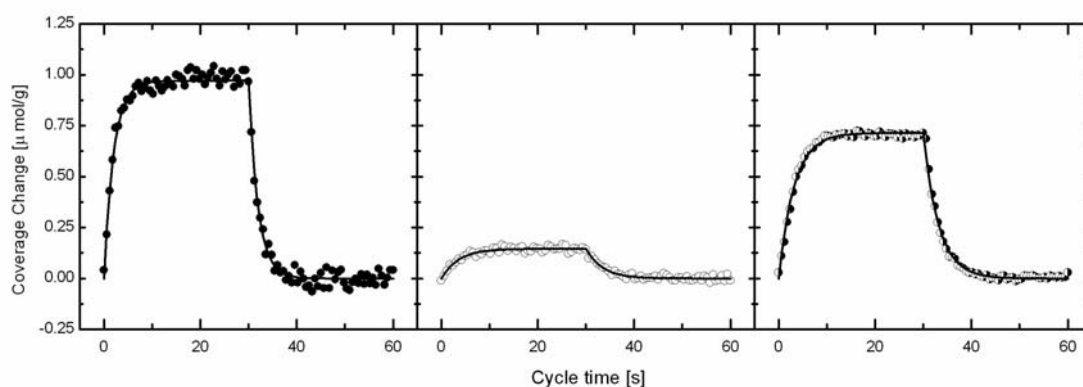
Figure 4.3   **Changes in the coverage of the SiOHAl (left), SiOH groups (middle) of H-ZSM5-p and SiOH groups of SiO₂ (right) for the sorption of benzene during pressure modulation of 0.003 mbar at equilibrium partial pressure of 0.06 mbar at 403 K.**
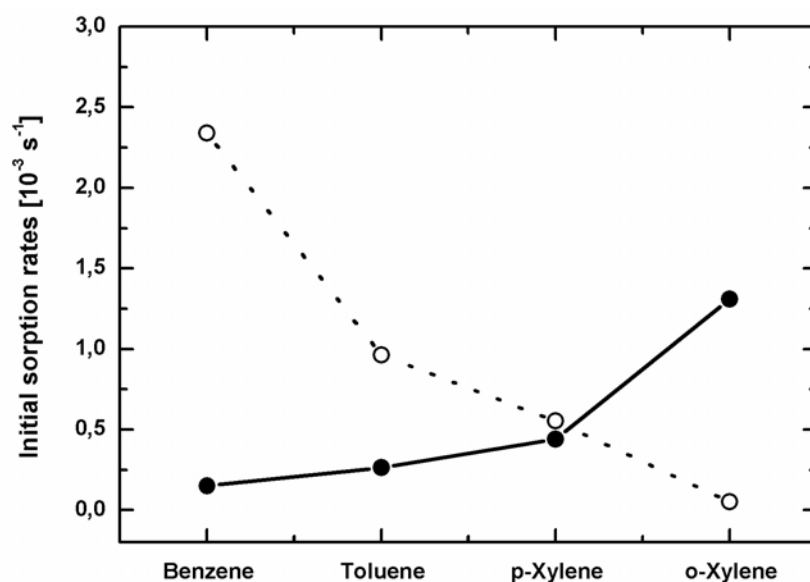
Figure 4.4   **Initial sorption rates (TOF) of aromatic molecules on the SiOH (●) groups and SiOHAl groups (○) of H-ZSM5-p at 403 K.**

Note also, that the rate of equilibration of the sorbates with the SiOH groups on the zeolite surface was distinctly lower than the rate of equilibration with the SiOH groups of amorphous SiO_2. In contrast, for *o*-xylene, which is hardly reaching the SiOHAl groups on the time scale of 60 s for the infrared spectroscopic experiment, the time constants for the sorption on the SiOH groups on H-ZSM5-p and amorphous SiO_2 were similar. For the SiOHAl groups the time constant for the sorption of *o*-xylene was significantly lower than for the other sorbates.

4.3.2 Experimental determination of the sticking probabilities of aromatic hydrocarbons on zeolite H-ZSM5

Following a hard sphere collision theory approach[38, 46], the rate of adsorption r_{ad} for gas phase molecules impinging on the surface of a solid can be expressed by Equation 4.3 in which α denotes the sticking probability, T the temperature, p the gas pressure, N the total number of molecules, V the system volume and M the molecular mass of the sorbate. R and N_A are natural constants denoting the general gas constant and Avogadro's number, respectively. The sticking probability represents the probability for a gas phase molecule to continue its trajectory on the surface and in the pores after having encountered the external zeolite surface. A detailed derivation of Equation 4.3 was presented within chapter three, section 3.2.

$$r_{ad} = \alpha \cdot \frac{1}{4} \sqrt{\frac{8 \cdot R \cdot T}{\pi \cdot M}} \cdot \frac{N}{V} = \alpha \cdot \frac{1}{4} \langle u \rangle \cdot \frac{p \cdot N_A}{R \cdot T} \qquad (4.3)$$

Consequently, α for a given sorbate and temperature can be determined from the sorption rate change within the pressure limits p_1 and p_2 before and after the volume modulation given as follows in Equation 4.4:

$$\Delta r_{ad} = r_{ad}(p_2) - r_{ad}(p_1) = \alpha \cdot \frac{\langle u \rangle}{4} \cdot N_A \cdot \left(\frac{p_2}{R \cdot T} - \frac{p_1}{R \cdot T} \right) \qquad (4.4)$$

$$\alpha = \Delta r_{ad} \cdot \frac{4}{\langle u \rangle} \cdot \frac{RT}{N_A} \cdot (p_2 - p_1)^{-1} \qquad (4.5)$$

Using time-resolved infrared spectroscopic measurements, the respective change in the sorption rate Δr_{ad} is experimentally accessible, according to chapter two,

section 2.3.1, via the initial slope of the corresponding concentration profiles (see Figure 4.3) at the hydroxyl groups after the stepwise pressure increase (Equation 4.6). Hereby it is assumed, that during the time-resolved infrared experiments in rapid scan mode, each modulation cycle is fully reversible in the adsorption and desorption step and that the overall position of the sorption equilibrium established before the pressure modulations is not changed.

$$\Delta r_{ad} = \frac{\Delta c_{OH,eq}}{\tau_{ad}} e^{-t/\tau_{ad}} \overset{t \ll t_p}{\approx} \frac{\Delta c_{OH,eq}}{\tau_{ad}} \tag{4.6}$$

Insertion of the sorption rate change Δr_{ad} into Equation 4.5 directly yields the experimental sticking probability α as function of the equilibrium coverage change at the hydroxyl sites $\Delta c_{OH,eq}$ and of the characteristic sorption time constant τ_{ad}.

$$\alpha = \frac{\Delta c_{OH,eq}}{\tau_{ad}} \cdot \frac{4}{\langle u \rangle} \cdot \frac{RT}{N_A} \cdot \left(p_2 - p_1 \right)^{-1} = \frac{4 \cdot RT \cdot \Delta c_{OH,eq}}{\langle u \rangle \cdot \left(p_2 - p_1 \right) \cdot N_A \cdot \tau_{ad}} \tag{4.7}$$

Alternatively, by substituting $\Delta c_{OH,eq}$ using Equation 2.22, the experimental sticking probability can be expressed as function of the coverage of the hydroxyl groups $\Delta c_{OH}(t)$.[35]

$$\alpha = \frac{4 \cdot RT \cdot \Delta c_{OH}(t)}{\langle u \rangle \cdot N_A \cdot \left(p_2 - p_1 \right) \cdot \tau_{ad} \cdot \left(1 - e^{-t/\tau_{ad}} \right)} \tag{4.8}$$

As the SiOH groups are the only sorption sites on amorphous SiO_2 therefore, the sticking probability can be directly calculated from the sorption rate of the molecules on the terminal silanol groups.[47] According to the previously postulated transport model for aromatic hydrocarbons on MFI-type zeolites[33], a weakly bound physisorbed surface state of the sorbate on the outer zeolite surface precedes the transport to either the surface sites or pore entering and sorption to the internal bridging SiOHAl groups. Due to this fact, the sum of the uptake rates measured on both, the terminal SiOH and bridging SiOHAl groups of H-ZSM5-p was used for the calculation of the experimental sticking probability on the zeolite sample.

The resulting experimental sticking probabilities for the series of aromatic hydrocarbons on H-ZSM5-p and amorphous SiO_2, compiled in Table 4.3 are in the range of 10^{-7}. The highest sticking probabilities were observed for *p*-xylene, followed by benzene, *o*-xylene and by toluene. Despite small differences in the absolute values in the series of the four aromatic molecules studied, the same trend was observed on either the H-ZSM5-p or the amorphous SiO_2 sample.

Table 4.3 **Theoretical and experimental sticking probability of aromatic molecules on H-ZSM5-p and amorphous silica (Aerosil200), rotational partition function at 403 K and symmetry numbers of the sorbates. The theoretical values $\alpha^{\#}$ were calculated by statistical thermodynamics assuming the total loss of rotational degrees of freedom upon sorption and neglecting vibrational contributions.**

Sorbate Molecule	q_{rot}^{3DGF} (*)	$\alpha^{\#}$ (Theory)	α (Aerosil 200)	α (H-ZSM5-p)
Benzene	1.17×10^{4}	8.69×10^{-5}	1.57×10^{-7}	2.04×10^{-7}
Toluene	1.35×10^{5}	7.40×10^{-6}	1.50×10^{-7}	1.69×10^{-7}
p-Xylene	1.10×10^{5}	9.11×10^{-6}	1.96×10^{-7}	2.18×10^{-7}
o-Xylene	2.21×10^{5}	4.52×10^{-6}	1.67×10^{-7}	2.00×10^{-7}

(*) For details concerning the calculation of the rotational partition functions of the sorbate molecules in the gas phase it is referred to chapter three.

4.3.3 Transport processes of aromatic hydrocarbon molecules followed by pressure frequency response

In addition to the infrared spectroscopic measurements, the transport processes of the aromatic molecules were studied in H-ZSM5-p prepared as a self-supporting wafer (pressure of $5.2 \cdot 10^{6}$ Pa) and in the form of dispersed powder using the frequency response technique, described in section 4.2.2.2. This allows, in perfect agreement to previous experiments[2, 35], to exclude potential influences of the sample preparation method on the observed transport kinetics and thus the experimental sticking probabilities. The experimental characteristic in- and out-of-phase functions (δ_{in} and δ_{out}) together with the theoretical fits are shown in Figure 4.5 for the diffusion

of benzene molecules in H-ZSM5-p samples prepared by the aforementioned methods. In analogy, for toluene and *p*-xylene, also similar characteristic functions indicating similar diffusion processes for both sample preparation methods were observed.[35]
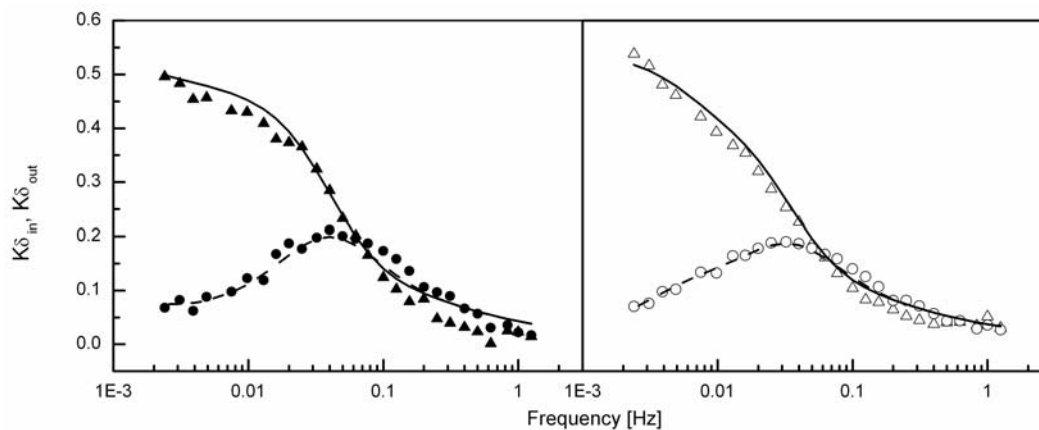
Figure 4.5   **Frequency response data for the diffusion of benzene in H-ZSM5-p measured in form of pressed pellet (left; ●,▲) or dispersed powder sample (right; ○, △) at 403 K. The in-phase functions are marked with the solid line and the out-of-phase functions are dashed.**

Furthermore, the inter-particle space between individual zeolite crystals, estimated from scanning electron microscopy (SEM) micrographs was identical for the samples in powder and pellet form. These findings are in agreement to the previous measurements of Jentys et al.[23] and R. Mukti[35] based on H-ZSM5 samples with a Si/Al-ratio of 82.

4.4 Discussion

As previously postulated by Jentys et al.[33] and already discussed in section 4.1, transport of hydrocarbons from the gas phase to the active sites of zeolite materials proceeds via a weakly bound physisorbed state on the external zeolite surface, characterized by high two-dimensional mobility of the sorbates. Subsequently sorption to the terminal hydroxyls or entering into the zeolite micropore network prior to sorption on the intra-pore bridging hydroxyls groups occurs. According to Mukti et al.[34, 35], the sorption enthalpy of the alkyl-substituted aromatic molecules on MFI zeolites increases monotonously with increasing molar mass (20 kJ mol^{-1} per additional methyl group[34]). This additional contribution to the heat of adsorption and

the differences in the size of the molecules leads to the observed course of the rate constants on the SiOHAl groups for the molecules having a minimum kinetic diameter below the zeolite pore diameter. As the heat of adsorption of the molecules on MFI-type materials is mainly influenced by the non-specific interaction of the sorbate with the pore walls, while only a minor energetic contribution is due to the directed interaction of the aromatic electron donor function with the SiOHAl groups, similar values on Silicalite-1 and H-ZSM5 are found.[34] In contrast, for the sorption of linear *n*-alkane molecules the heat of adsorption is directly proportional to the chain length, while the interaction with the SiOHAl groups adds only a constant energetic contribution to this interaction.[48] The comparison clearly shows the differences in sorption enthalpies as function of the size and possible orientations of the molecules. This strongly influences the trapping of the molecules from the gas phase into a physisorbed state after a collision with the surface, as the efficient distribution (accommodation) of the enthalpy is favored with increasing heat of sorption (or increasing size of the molecule).
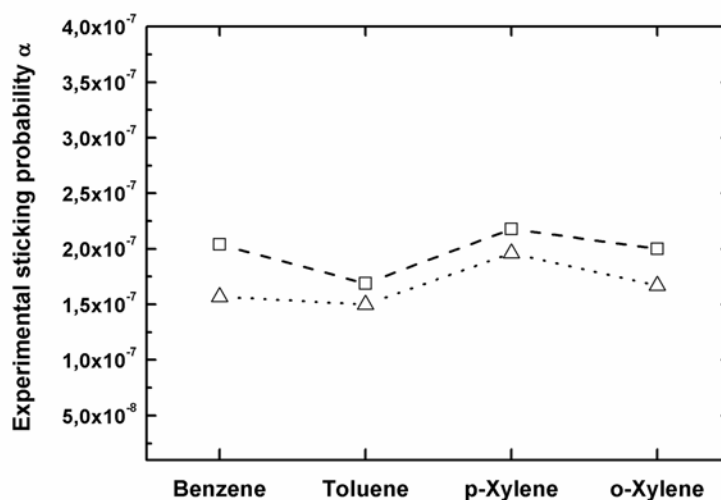
Figure 4.6   **Experimental sticking probabilities for benzene, toluene, *p*- and *o*-xylene on H-ZSM5 (Si/Al = 45, □) and amorphous SiO$_2$ (△) determined at 403 K from in-situ infrared spectroscopy.**

For the alkyl-substituted benzene molecules adsorbed on the oxide surface of H-ZSM5-p and amorphous SiO$_2$ the values of the experimental sticking probabilities α are in the order of ~ 10^{-7} and thus about six orders of magnitude lower compared to typical sticking probabilities of nitrogen[49], carbon monoxide[50] or ethylene which are

between 10^{-2} and 1 on metal oxide and pure metal surfaces.[38, 46] Molecular dynamics simulations theoretically predicted sticking probabilities close to 1 for the small aliphatic molecules on Silicalite-1.[39, 51] Despite the fact, that sorption of a aliphatic molecule behaves geometrically and also energetically entirely different to the sorption of rigid aromatic molecules due to the higher flexibility of the aliphatic sorbate[24, 34, 42] such a huge difference in the sticking probabilities would not have been expected at first sight when assuming only heat effects.

Before discussing in detail the course of the experimental sticking probabilities, clear evidence for the absence of external mass transfer limitations generated by pressing the samples into self-supporting wafers and suggested by Simon at al.[39] to account for the low sticking probabilities (see section 4.1) has to be given. Therefore, additional frequency response measurements with the H-ZSM5-p sample as powder or pressed wafer were performed. In general, the frequency response method as a powerful tool can in principle separate between simultaneously occurring diffusion processes in a system, when the respective diffusion coefficients of these processes differ sufficiently by at least half an order of magnitude.[43] This difference would i.e., be expected for diffusion inside a micropore network or in the void spaces between the crystallites. Thus, transport limitations generated by a second diffusion process within the inter-particle void spaces of zeolites should give rise, for the samples in pressed wafer form, to a second maximum in the experimentally determined out-of-phase FR characteristic function δ_{out}. As can be exemplified for benzene seen in Figure 4.5, both preparation methods resulted in identical diffusion processes for the aromatic hydrocarbons studied. This finding satisfactorily confirms that the method of sample preparation, typically applied for transmission IR spectroscopy, does not induce additional transport resistances which interfere with the transport processes of interest. Note, that the corresponding diffusion coefficients obtained for the three sorbates (in the order of 10^{-15} m^2 s^{-1}) were also in agreement to previous studies.[38, 46, 52, 53] Further experimental support for the absence of experimental artifacts is given by the identical concentration changes observed during the time-resolved kinetic measurements for the hydroxyl sites and the thermodynamically estimated values based on the concentration changes calculated from the equilibrium sorption isotherms of the sorbates on the H-ZSM5-p samples (see also Appendix C for further information).

Having satisfactorily confirmed the absence of external mass transport limitations, a statistical thermodynamics approach was chosen in order to explain differences between the alkyl-substituted molecules and to rationalize the low sticking probabilities observed experimentally. In general, the sticking of a molecule on the surface of a zeolite can be regarded as the collision of a gas phase molecule, having all 3N degrees of rotational, vibrational and translational freedom, with the external surface. Herein N denotes the number of atoms the molecule consists of, eg., 12 for benzene. The collision event is either followed by deflection of the molecule back to the gas phase or successful trapping into a weakly bound surface state, comparable to a two-dimensional gas with hindered rotational and translational degrees of freedom. For this mechanism, four interconnected factors influencing the absolute value of the experimental sticking coefficient α can be distinguished: (1) the degrees of (translational and rotational) freedom lost, (2) the initial entropy of the gas phase molecule (expressed by the total symmetry number σ of the molecule considering similar moments of inertia along the principal axes), (3) the compensation of the heat of sorption ΔH_{ads} (proportional to the differences in the molar mass, i.e. benzene < toluene < xylene) and (4) the geometrical dimensions of the molecule determining the space occupied on the external surface.

$$\alpha = \chi \cdot \alpha^{\#} \tag{4.8}$$

The experimentally observed (apparent) sticking probability of a sorbate molecule can according to van Santen and Niemantsverdriet et al.[46] be expressed by the product of a theoretical sticking coefficient $\alpha^{\#}$ (determined by the first two contributions) and a trapping coefficient χ (determined by the latter two contributions). If both factors are large, a high experimental sticking probability is expected and fewer collisions with the surface are necessary, before the molecule is successfully adsorbed on the surface and bound in the physisorbed surface state. If both factors are small, the observed sticking coefficient will decrease significantly.

Using a statistical thermodynamics approach, it is further possible to define the theoretical sticking probability $\alpha^{\#}$ via the loss of molecular degrees of freedom during the sorption process on the zeolite surface. Therefore, the changes within the molecular partition functions (see chapter three) before and during sorption have to be evaluated.

$$\alpha^{\#} = \frac{q_{rot}^{\#} \cdot q_{vib}^{\#}}{q_{rot}^{gas} \cdot q_{vib}^{gas}} \qquad\qquad (4.9)$$

Herein q_{rot}^{gas} and q_{vib}^{gas} correspond to the rotational and vibrational contribution to the total partition function of the sorbate molecule with free molecular motion in the gas phase. The corresponding statistical thermodynamics definition of the vibrational and rotational partition functions have already been presented in chapter three, section 3.1.3. Within the numerator of Equation 4.9 $q_{rot}^{\#}$ and $q_{vib}^{\#}$ account for the contributions to the partition functions of the sorbates in the physisorbed state especially with reduced or hindered rotational motion. A complete derivation of this Equation following van Santen and Niemantsverdriet can be found in the references.[38, 46] Note, that this expression already accounts for the reduction of the translational degrees of freedom (from three to two) upon sorption, assuming that the gas phase molecules will loose one degree of translational freedom, when being adsorbed into a weakly bound surface state after collision with the zeolite surface.
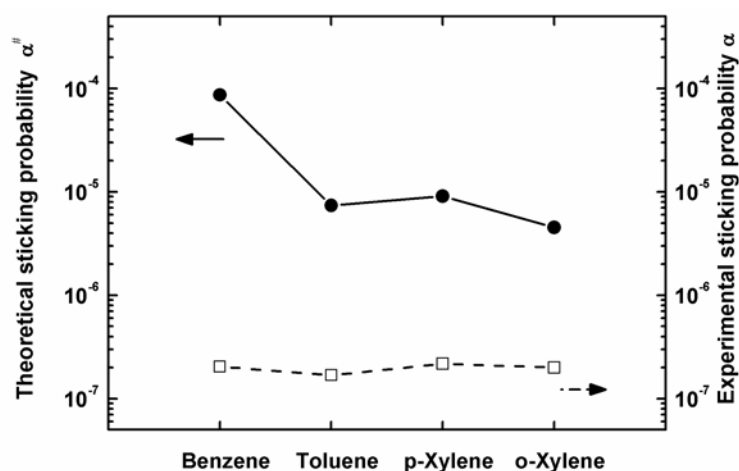
Figure 4.7   Theoretical (●) and experimental sticking probabilities at 403 K
             for a series of aromatic hydrocarbons on H-ZSM5 (Si/Al = 45, □).

Furthermore, it is assumed that the free gas phase rotations of the molecule around its principal axes are significantly hindered when the molecule is physisorbed in the weakly bound state. A detailed statistical thermodynamics approach taking into account all possible internal and external contributions to the molecular partition functions for the sorbate molecules in the physisorbed state would be beyond the scope of this thesis. The changes in the vibrational contributions and also the interchange of

external degrees of freedom to low-frequency vibrations will be neglected for the case of simplicity in our estimations and $q_{vib}^{\#} = q_{vib}^{gas}$ is used in the following calculations. Herein, it is mainly intended to give a theoretical rational for the low order of magnitude of the experimental sticking probabilities measured. Therefore, the theoretical sticking probabilities $\alpha^{\#}$ were calculated for the aromatic hydrocarbons benzene, toluene, *p*-xylene and *o*-xylene for $q_{rot}^{\#} = 1$, assuming the total loss of all gas phase rotational degrees of freedom upon sorption into the physisorbed state.
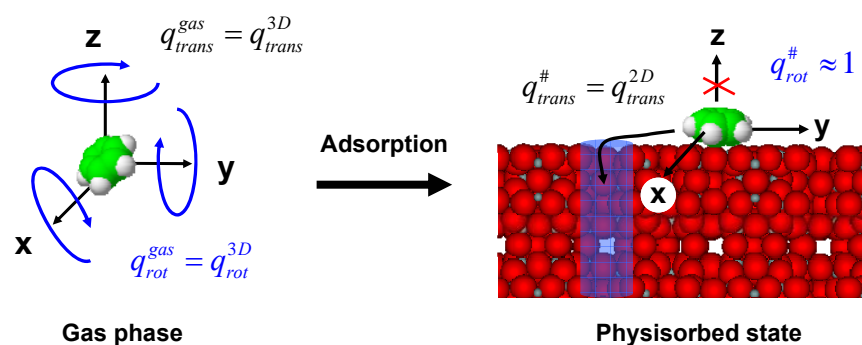
Figure 4.8   Changes in the degrees of freedom upon sorption on H-ZSM5.

The resulting values are compared in Figure 4.7 together with the experimentally determined sticking probabilities on both samples. The rotational partition functions and calculated sticking probabilities for the aromatic hydrocarbon molecules on H-ZSM5 and amorphous SiO_2 are compiled in Table 4.3. As the partition function of a system is directly connected to the thermodynamic state functions i.e., the rotational entropy S_{rot} via Equation 3.16 and 3.25 within chapter three, correspondingly a decreasing $\alpha^{\#}$ directly relates to a decrease of the molecular rotational entropy in the physisorbed state. It can be further seen that the symmetry number of the molecule is of crucial importance for the theoretical sticking probability. The higher the symmetry of the sorbate, the lower the loss of entropy upon sorption is and consequently the higher the theoretical sticking coefficient.

The experimental and theoretical sticking probabilities differ by approximately one order of magnitude. This can be explained by the fact, that the measured sticking probability is the product of the theoretical sticking probability and of the trapping coefficient χ of the sorbent (see Equation 4.8). The absolute magnitude of the trapping coefficient accounts for the accommodation of energy released upon trapping into the

physisorbed state during an exothermic collision with the surface[46] and for the space the sorbate molecule occupies on the surface. With increasing heat of sorption and larger size dimensions i.e., higher number of atoms of the sorbate molecule, the trapping coefficient strongly increases. For the case of strongly bound molecules as e.g., carbon monoxide on metal surfaces, trapping coefficients close to one are observed. In contrast, for weakly bound surface species, much smaller values are predicted. Herein the trapping coefficients were estimated using the experimentally measured and theoretically determined sticking probabilities (see Table 4.4).

Table 4.4   Trapping coefficient of aromatic molecules on H-ZSM5 and amorphous silica (Aerosil200). Values calculated assuming total loss of rotational degrees of freedom upon sorption.

Sorbate Molecule	Symmetry σ	χ (Aerosil 200)	χ (H-ZSM5)
Benzene	12 (= 6*2)	1.81×10^{-3}	2.34×10^{-3}
Toluene	2	2.03×10^{-2}	2.28×10^{-2}
p-Xylene	4 (= 2*2)	2.15×10^{-2}	2.39×10^{-2}
o-Xylene	2	3.69×10^{-2}	4.42×10^{-2}

Summarizing, the experimental values of the sticking probabilities on amorphous, non-porous and porous materials for the different aromatic molecules benzene, toluene and xylene, are similar. This shows that the properties of the external zeolite surface seem to be comparable to that of the non-porous amorphous SiO_2 with respect to the sorption processes studied. The subtle differences observed between the aromatic molecules with increasing degree of substitution result from their differences in the geometry (symmetry) and the heat of adsorption. For toluene and *o*-xylene, the molecules with the lower symmetry numbers σ in the gas phase, lower sticking probabilities on H-ZSM5-p were obtained. In contrast, for benzene, the molecule with the highest symmetry number ($\sigma = 12$) in the gas phase, the high theoretical sticking coefficient is compensated by a low trapping coefficient due to the lower molar mass and the lower heat of sorption. For *p*-xylene, with a symmetry number of four, large geometrical dimensions and the highest heat of sorption, the high trapping coefficient compensates for a lower theoretical sticking coefficient and, therefore, the highest experimental sticking probability is observed. In perfect agreement to this model, the

experiments result in the lowest sticking probability for toluene among the four molecules investigated, as it has a low symmetry number corresponding to high entropy in the gas phase that has to be reduced upon adsorption, an intermediate heat of sorption and molecular dimension. Generally, high sticking and therefore large trapping coefficients relate to a long residence time of the sorbate on the external surface in the physisorbed state, which allows accommodating the heat of adsorption.

4.5 Conclusions

Fast time-resolved infrared spectroscopy in rapid scan mode was used to study the surface transport processes of benzene, toluene, *p*- and *o*-xylene and to experimentally derive the sticking probabilities of these sorbates. The determined sticking probabilities on H-ZSM5 and amorphous SiO_2 were comparable in the order of 10^{-7}. The highest sticking probability was observed for *p*-xylene, followed by benzene, *o*-xylene and toluene. The course of the sticking probabilities was found to be mainly governed by three factors: (1) the symmetry of the sorbate molecule, (2) the sorption enthalpy of the sorbate, which increases with the molar mass and (3) the space the sorbate molecule occupies on the surface. According to statistical thermodynamics the low sticking probabilities observed were related to the total loss of all external rotational degrees of freedom of the gas phase molecule upon sorption. The trapping coefficient, as the second contribution to the sorption process, can be directly related to the heat of sorption and the dimensions of the sorbate molecules, respectively. The series of alkyl-substituted aromatic molecules showed the same trend in the sticking probability on H-ZSM5-p and amorphous SiO_2. This supports the previously proposed existence of the weakly bound physisorbed state being the first step in the sorption process on the oxide surfaces of both materials. A detailed comparison between H-ZSM5 in the form of powder or pressed pellet clearly confirmed the absence of possible mass transfer limitations resulting from the pressing of the zeolite samples.

4.6 Acknowledgments

4.7   References

[1]   S. R. Zheng, H. R. Heydenrych, A. Jentys, J. A. Lercher, *J. Phys. Chem. B* **2002**, *106*, 9552.

[2]   S. R. Zheng, H. Tanaka, A. Jentys, J. A. Lercher, *J. Phys. Chem. B* **2004**, *108*, 1337.

[3]   A. de Mallmann, D. Barthomeuf, *J. Phys. Chem.* **1989**, *93*, 5636.

[4]   A. Jentys, J. A. Lercher, *Stud. Surf. Sci. Catal.* **1989**, *46*, 585.

[5]   J. Kärger, J. Caro, *J. Chem. Soc. Faraday Trans.* **1977**, *73*, 1363.

[6]   J. Kärger, H. Pfeifer, T. Wutscherk, S. Ernst, J. Weitkamp, J. Fraissard, *J. Phys. Chem.* **1992**, *96*, 5059.

[7]   D. H. Olson, G. T. Kokotailo, S. L. Lawton, W. M. Meier, *J. Phys. Chem.* **1981**, *85*, 2238.

[8]   A. Pampel, F. Engelke, P. Galvosas, C. Krause, F. Stallmach, D. Michel, J. Kärger, *Microp. Mesop. Mat.* **2006**, *90*, 271.

[9]   D. M. Ruthven, B. K. Kaul, *Ind. Eng. Chem. Res.* **1993**, *32*, 2047.

[10]   L. J. Song, Z. L. Sun, H. Y. Ban, M. Dai, L. V. C. Rees, *Phys. Chem. Chem. Phys.* **2004**, *6*, 4722.

[11]   B. L. Su, D. Barthomeuf, *J. Catal.* **1993**, *139*, 81.

[12]   B. L. Su, D. Barthomeuf, *App. Catal. A-Gen.* **1995**, *124*, 81.

[13]   B. L. Su, D. Barthomeuf, *Zeolites* **1995**, *15*, 470.

[14]   B. L. Su, J. M. Manoli, C. Potvin, D. Barthomeuf, *J. Chem. Soc. Faraday Trans.* **1993**, *89*, 857.

[15]   R. Cartarius, H. Vogel, J. Dembowski, *Phys. Chem. Chem. Phys.* **1997**, *101*, 193.

[16]   H. Jobic, A. N. Fitch, J. Combet, *J. Phys. Chem. B* **2000**, *104*, 8491.

[17]   L. V. C. Rees, D. M. Shen, in *Characterization of Porous Solids III, Vol. 87*, **1994**, pp. 563.

[18]   D. M. Ruthven, *Adsorption* **2007**, *13*, 225.

[19]   D. M. Ruthven, in *Studies in Surface Science and Catalysis, Zeolites: A Refined Tool for Designing Catalytic Sites, Vol. 97* (Eds.: L. Bonneviot, S. Kaliaguine), Elsevier B.V., Amsterdam, **1995**, pp. 223.

[20]   D. M. Ruthven, M. Eic, *Abstr. Paper Am. Chem. Soc.* **1988**, *195*, 201.

[21]   S. Chempath, R. Q. Snurr, J. F. M. Denayer, G. V. Baron, *Stud. Surf. Sci. Catal.* **2004**, *154*, 1983.

[22]   S. Chempath, R. Q. Snurr, J. J. Low, *Aiche Journal* **2004**, *50*, 463.

[23]   A. Jentys, R. R. Mukti, J. A. Lercher, *J. Phys. Chem. B* **2006**, *110*, 17691.

[24]   A. Jentys, R. R. Mukti, H. Tanaka, J. A. Lercher, *Microp. Mesop. Mat.* **2006**, *90*, 284.

[25]   S. Mohanty, H. T. Davis, A. V. McCormick, *Chem. Eng. Sci.* **2000**, *55*, 2779.

[26]   S. Mohanty, H. T. Davis, A. V. McCormick, *Aiche Journal* **2000**, *46*, 1662.

[27]   R. Q. Snurr, A. T. Bell, D. N. Theodorou, *J. Phys. Chem.* **1993**, *97*, 13742.

[28]   R. Q. Snurr, A. T. Bell, D. N. Theodorou, *J. Phys. Chem.* **1994**, *98*, 11948.

[29]   S. Brandani, Z. Xu, D. Ruthven, *Microporous Mater.* **1996**, *7*, 323.

[30]   J. Kärger, M. Bullow, B. R. Millward, J. H. Thomas, *Zeolites* **1986**, *6*, 146.

[31]   L. Heinke, P. Kortunov, D. Tzoulaki, J. Karger, *Phys. Rev. Lett.* **2007**, *99*.

[32]   A. Jentys, H. Tanaka, J. A. Lercher, *Stud. Surf. Sci. Catal.* **2004**, *154*, 2041.

[33]   A. Jentys, H. Tanaka, J. A. Lercher, *J. Phys. Chem. B* **2005**, *109*, 2254.

[34]   R. R. Mukti, A. Jentys, J. A. Lercher, *J. Phys. Chem. C* **2007**, *111*, 3973.

[35]   R. R. Mukti, PhD thesis, TU München (München), **2007**.

[36]   J. Kärger, D. M. Ruthven, in *Handbook of Porous Solids, Vol. 4*, **2002**, p. 2089.

[37]   A. I. Skoulidas, D. S. Sholl, *J. Chem. Phys.* **2000**, *113*, 4379.

[38]   I. Chorkendorff, J. W. Niemantsverdriet, *Concepts of Modern Catalysis and Kinetics*, 2nd ed., Wiley VCH GmbH, Weinheim, **2007**.

[39]   J.-M. Simon, J.-P. Bellat, S. Vasenkov, J. Kärger, *J. Phys. Chem. B* **2005**, *109*, 13523.

[40]   J. Kärger, S. Vasenkov, *J. Phys. Chem. B* **2006**, *110*, 17694.

[41]   A. Schüring, *J. Phys. Chem. C* **2007**, *111*, 11285.

[42]   J. A. Z. Pieterse, S. Veefkind-Reyes, K. Seshan, J. A. Lercher, *J. Phys. Chem. B* **2000**, *104*, 5715.

[43]   Y. Yasuda, *Het. Chem. Rev.* **1994**, *1*, 103.

[44]   T. Armaroli, M. Bevilacqua, M. Trombetta, A. G. Alejandre, J. Ramirez, G. Busca, *App. Catal. A-Gen.* **2001**, *220*, 181.

[45]   S. J. Reitmeier, R. R. Mukti, A. Jentys, J. A. Lercher, *J. Phys. Chem. C* **2009**, *113*, 1640.

[46]   R. A. van Santen, J. W. Niemantsverdriet, *Chemical Kinetics and Catalysis*, Plenum Press, New York, **1995**.

[47]   *Compendium of Chemical Terminology IUPAC Research Triangle Park NC*, **1997**.

[48]   F. Eder, M. Stockenhuber, J. A. Lercher, *J. Phys. Chem. B* **1997**, *101*, 5414.

[49]   A. Hellman, B. Razaznejad, B. I. Lundqvist, *Phys. Rev. B* **2005**, *71*.

[50]   M. Hirsimaki, M. Valden, *J. Chem. Phys.* **2001**, *114*, 2345.

[51]   M.-H. Tsai, *Comput. Phys. Commun.* **2002**, *147*, 130.

[52]   W. Niessen, H. G. Karge, *Microporous Mater.* **1993**, *1*, 1.

[53]   H. G. Karge, *Cr. Chim.* **2005**, *8*, 303.

Chapter 5

5. Enhancement of sorption processes in zeolite HZSM5 by post-synthetic surface modification

5.1   Introduction

Medium pore size zeolites such as H-ZSM5[1] are key catalyst components in many petrochemical and refining applications.[2-5] These molecular sieves are not only used in catalytic processes such as the toluene alkylation[6-9], disproportionation and xylene isomerization[5, 10-13], but also for the hydrocarbon separation[14]. Shape selective sorption and transport[10,15,16] of (substituted) aromatic molecules are the key properties of the zeolites for these applications. Surface modification by chemical liquid (CLD) and chemical vapour deposition (CVD), or modifying the outer surface and the pore apertures by pre-coking have been applied to fine tune these properties.[10, 16] Recently, we experimentally differentiated the elementary steps during sorption of rigid molecules such as alkyl benzenes into MFI pores. Using fast time-resolved infrared spectroscopy to monitor these transport and diffusion processes[14, 17], a complex, interconnected network of sequential transport steps has been established, as schematically depicted for benzene in Fig. 5.1.[14] The derived model is able to coherently explain several unconnected theoretical[18-22] and experimental[23-29] studies focusing on sorption and diffusion[28, 29] of aromatic molecules.

Overall, the macroscopic sorption process consists of five consecutive steps. These include collisions of gas phase molecules with the external zeolite surface (Fig. 5.1, (b)), the sorption into a physisorbed surface state, characterized by a high two-dimensional mobility (Fig. 5.1, (c)), the parallel adsorption on terminal hydroxyls (Fig. 5.1, (c),(d)), and the diffusion into the pores followed by the sorption at intra-pore sites (Fig. 5.1, (f)).[10] Direct experimental evidence showed, that the sticking probabilities for aromatic molecules on H-ZSM5 are unexpectedly small in the order of 10^{-7}, such low values being a consequence of the difference between the gas phase and surface degrees of freedom in rigid molecules.[30] Primarily, the sticking of the aromatic molecules is governed by the sorbate mass and the decrease of entropy in the sorption process. The latter contribution is critically influenced by factors such as the geometrical sorbate dimensions, the symmetry of the sorbate molecule and the space occupied on the surface, as well as the external surface morphology.[31] The observed order of the experimental sticking probabilities on unmodified zeolite H-ZSM5, i.e., *p*-xylene > benzene > *o*-xylene> toluene, agrees perfectly with the estimates by statistical

thermodynamics, suggesting that overall the sticking probabilities are strongly entropically controlled for the case of H-ZSM5 zeolites.[30, 32]
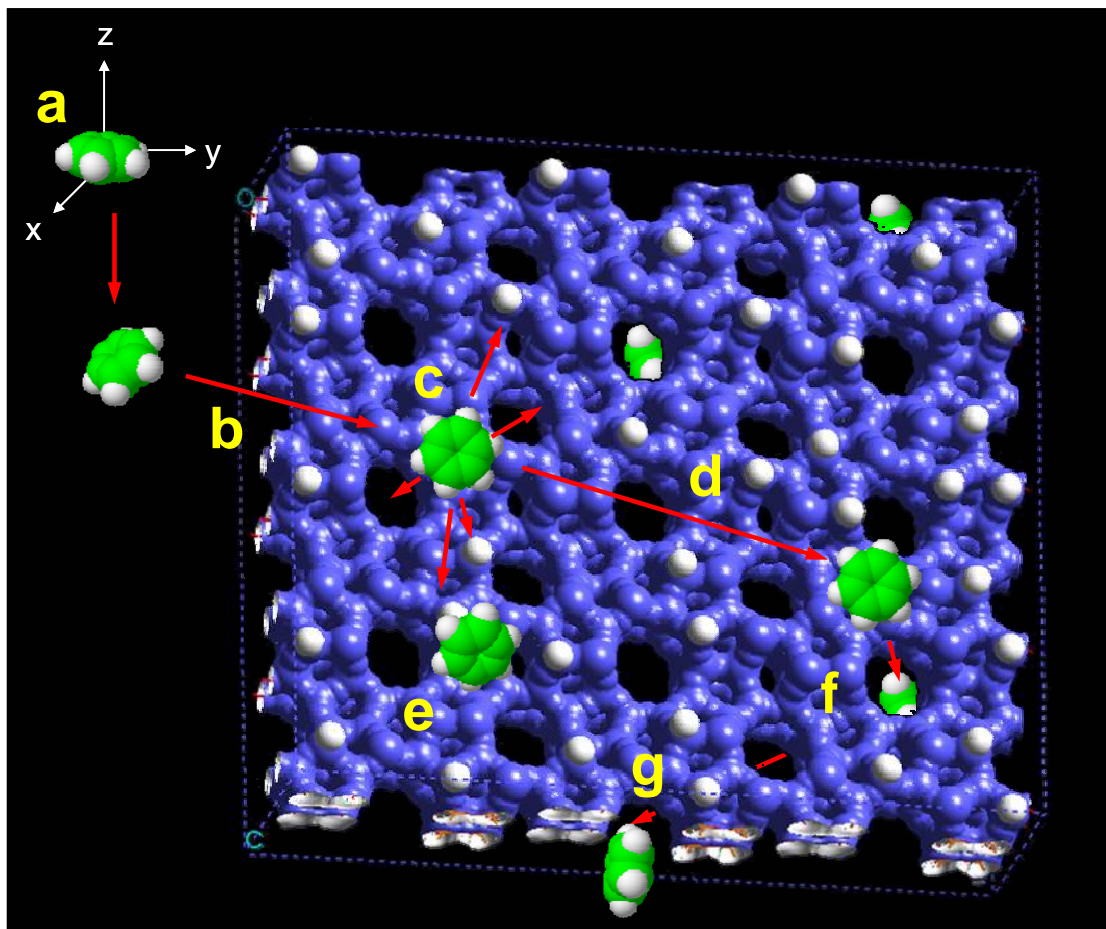
Figure 5.1   **Schematic model describing the elementary transport steps from the gas phase with free molecular motion (a) to the active sites of H-ZSM5 during benzene sorption (adapted from A. Jentys et al.[14]). A typical sketch of an H-ZSM5 crystal is shown with zeolite lattice highlighted in blue and the hydrogen atoms in white. Preliminary collision with the zeolites surface (b), trapping from in a weakly-bound surface state (c), high surface mobility (d), parallel transport to the active sites (e), in the pores (f) and finally intra-crystalline diffusion (g).**

Sorption of the relatively rigid aromatic molecules studied shows a high sensitivity of the sticking probability on the number of statistically favourable orientations[31] of the gas phase molecules during the collision with the external surface. Enhancing the total number of advantageous orientations of the molecules on

the surface would lead to an enhanced trapping of the molecules after the collision, and as a direct consequence to markedly increased sticking probabilities. Using these results, it has been predicted that the increased relative surface roughness i.e., a three dimensionally structured surface induced by post-synthetic surface modification enhances the number of advantageous orientations of symmetric molecules such as benzene in the sorption process as it would allow retaining a higher flexibility in their degrees of freedom when adsorbing from the gas phase.

5.2   Experimental

5.2.1   Materials

With this in mind, a series of surface modified H-ZSM5 zeolites was prepared as prototypes of a new series of zeolites that show enhanced sorption properties compared to conventional materials. Commercial zeolite H-ZSM5 provided by Süd-Chemie AG with a silicon to aluminium ratio of 45 measured by AAS and an average crystal size of 0.5 μm evidenced by SEM was used for the experiments. Concentrations of terminal and bridging hydroxyl groups were determined to be 0.27 and 0.21 mmol g^{-1} by ^{1}H/MAS-NMR spectroscopy (see Figure 5.2). Additional ^{27}Al/MAS-NMR spectroscopy excluded changes in the concentration framework aluminium during the modification procedure.[35]

Silica overlayers were prepared on the parent H-ZSM5 sample by post-synthetic reaction of the zeolite sample with tetraethyl-orthosilicate (TEOS) and subsequent hydrolysis and calcinations steps according to Zheng et al.[35, 36] The unmodified sample is denoted H-ZSM5-p, the resulting two TEOS modified samples, H-ZSM5-1m and H-ZSM5-3m, denoting one or three cycles of modification and calcinations, respectively. The modified zeolites showed concentrations of terminal hydroxyl groups of 0.18 and 0.12 mmol g^{-1} as well as for the bridging hydroxyl groups of 0.18 and 0.16 mmol g^{-1}, respectively, determined by ^{1}H/MAS-NMR. The corresponding NMR spectra for H-ZSM5-p and H-ZSM5-3m are exemplified compiled in Figure 5.2.
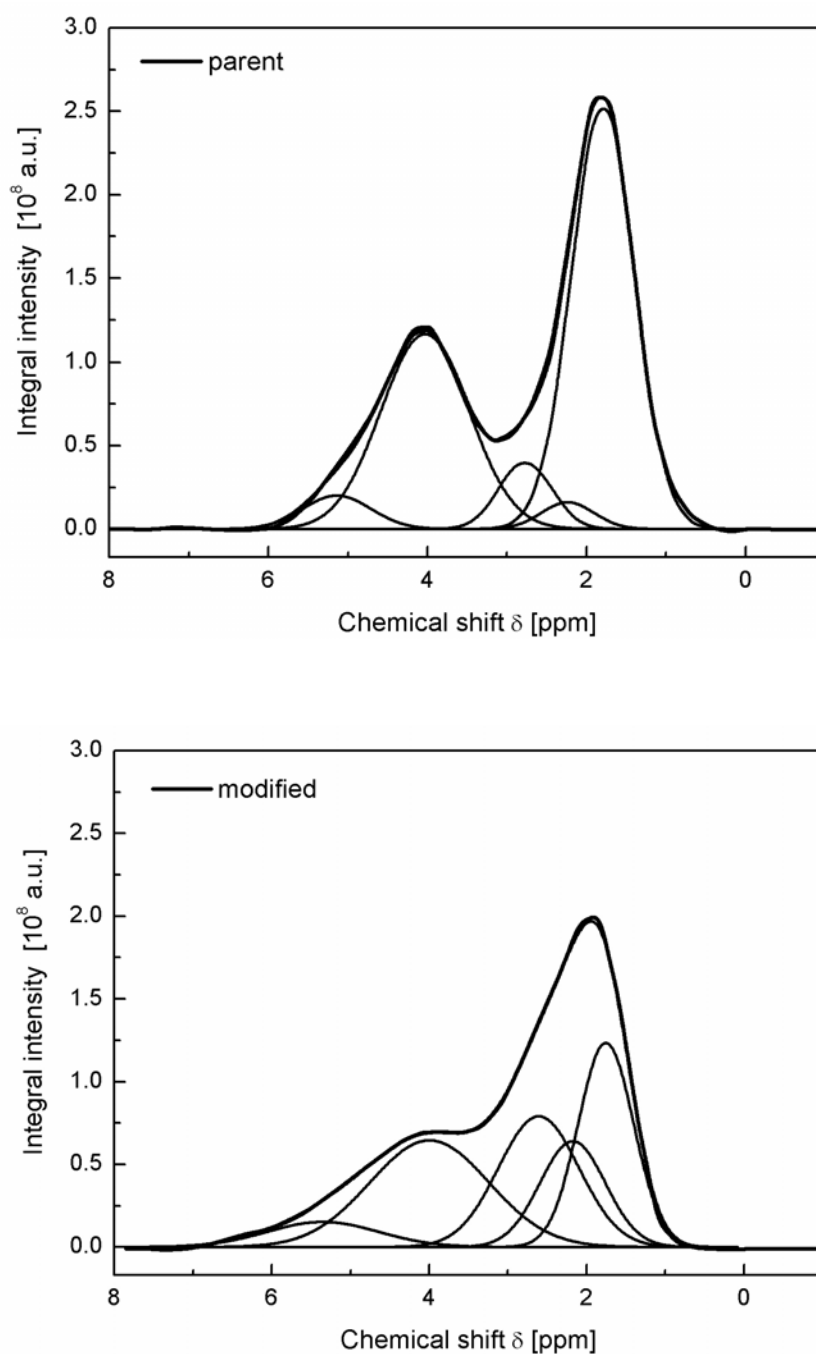
Figure 5.2 **^{1}H/MAS-NMR spectra of (up) H-ZSM5-p and (down) modified H-ZSM5-3m (12 wt-% SiO_2 deposited). The peaks shown resulted from the peak deconvolution of the original spectra using Gaussian peak shape. For both samples, peaks with the chemical shift of 2.0 ppm for terminal SiOH, 2.3 ppm for defect site SiOH, 2.8 ppm for non-framework AlOH, 4.1 ppm for bridging SiOHAl and 5.2 ppm for perturbed SiOHAl sites were chosen according to chapter 2.**
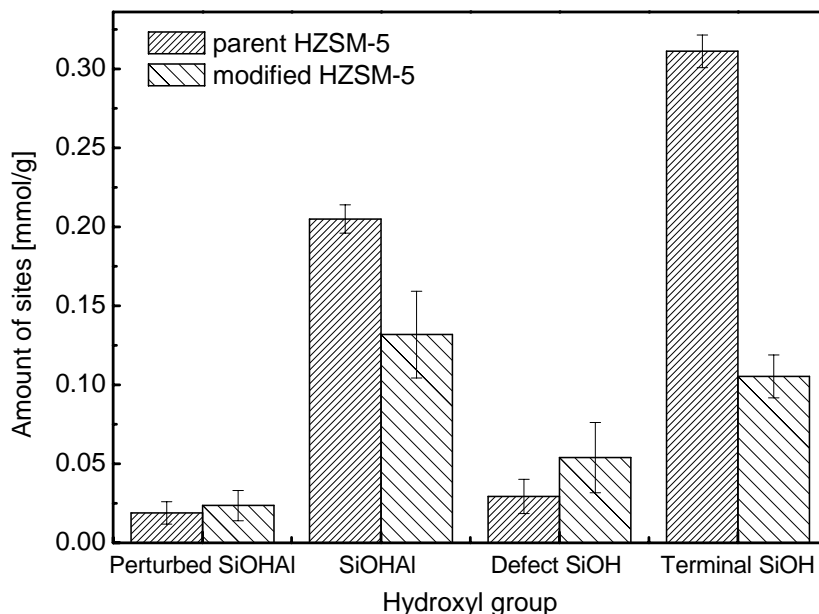
Figure 5.3 **Changes in the concentration of the hydroxyl groups on parent (dense striped) and modified (sparse striped) H-ZSM5, determined from the integrated peak areas by deconvolution of the ^{1}H/MAS-NMR spectra using adamantane as external standard.**

The solid state ^{1}H/MAS-NMR spectra of H-ZSM5-p and H-ZSM5-3m shown in Figure 5.2 were measured on a Bruker Avance AMX-500 NMR-spectrometer with magnetic field strength of 11.75 T. The samples were evacuated below 10^{-2} mbar and activated as described in chapter two, section 2.1.6. As external reference material, adamantane $C_{10}H_{16}$ was used. Processing of the NMR spectra was performed with GramsAI$^®$. For deconvolution Gaussian peak definitions and fixed peak positions according to common literature were chosen. For further details, see chapter two.

5.2.2 Electron microscopy

All transmission electron micrographs (TEM) presented were measured on a JEOL-2011 electron microscope operating at 200 kV. The TEM micrographs of H-ZSM5-p show a clean well defined surface terminating the crystalline zeolite, suggesting a surface structure similar to the one depicted in Figure 5.4. In contrast, the crystalline core of the modified material was (partially) surrounded by a thin and un-textured region attributed to an amorphous SiO_2 layer (see insert in Fig. 5.4). TEM micrographs further reveal the average thickness for the deposited layers to be 2.5 to 3.0 nm. Theoretical estimates based on the average crystallite size obtained by

scanning electron microscopy and the amount of TEOS added during the synthesis suggest an average thickness of approximately 3.0 nm, which agrees perfectly. The statistically and randomly distributed deposits of SiO_2 on the zeolite generated by TEOS chemisorption, hydrolysis, and calcinations led to a roughened external surface consisting of a porous amorphous overlayer. As a secondary effect, a minor fraction of the zeolite pores may be blocked or narrowed.
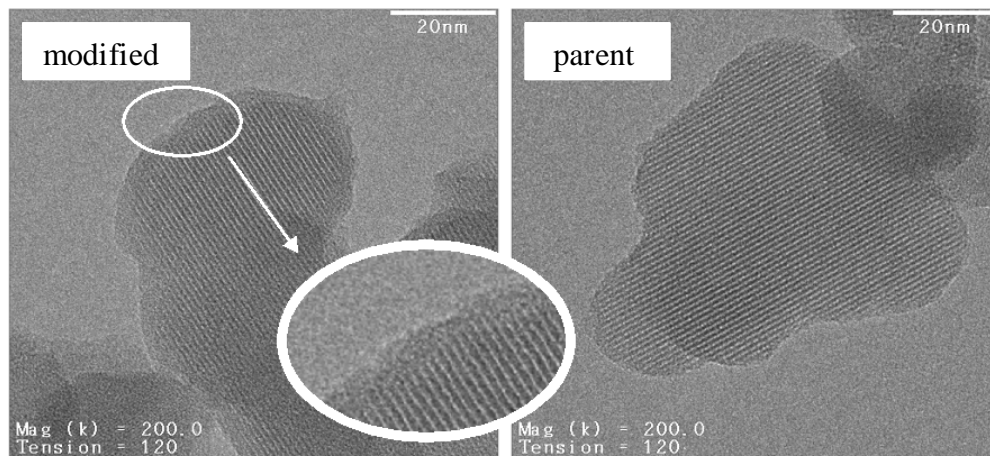
Figure 5.4 **Transmission electron micrographs of a typical parent H-ZSM5-p and modified H-ZSM5-3m crystal. The insert emphasizes the amorphous SiO_2 fragments and overlayers with an average thickness of 2.5 to 3.0 nm deposited on the zeolite surface. From nitrogen physisorption measurements large overlayer micropores of about 1.5 nm were evidenced.**

5.2.3 Nitrogen physisorption measurements

Nitrogen physisorption was used to distinctly characterize the properties and the porosity of this amorphous layer. Nitrogen physisorption isotherms, shown in Figure 5.5 for H-ZSM5-p and H-ZSM5-3m were measured with a PMI Automated sorptometer operating at liquid nitrogen temperature (77 K), after outgassing under vacuum at 473 K for at least 6 h. The apparent surface area was calculated by applying the Brunauer–Emmett–Teller (BET) equation to the adsorption isotherms over a relative pressure range from 0.03 to 0.15 (see Table 5.1). The pore volumes were evaluated using the α_s comparative plot[39] with nonporous, hydroxylated silica[40] as the reference adsorbent, compared in Figure 5.6. Pore size distributions were obtained by applying the Barrett–Joyner–Halena (BJH) method[41] on the adsorption branch.

During the modification, TEOS is hydrolyzed in the first step and condensed during the subsequent calcinations steps forming free hydroxyl groups at the surface and in the pore mouth region, as described by Zheng et al..[34] A layer of SiO_2 consisting of large micropores e.g., small mesopores is formed with an average porosity of approximately 30 % calculated from the total amount of deposited SiO_2 combined with the N_2 physisorption. Especially, the increase in mesopore volume (+ 1.4×10^{-2} cm^3 g^{-1}) of H-ZSM5-3m should be noted. Together all characterization methods suggest that the H-ZSM5 crystals are partially covered by SiO_2 with an average thickness of 2.5 – 3.0 nm, which partially narrows the pore openings, and forms large microporous channels with aperture of about 1.5 nm.

Table 5.1 **Selected structural properties of zeolite H-ZSM5-p and H-ZSM5-3m determined from nitrogen physisorption measurements.**

Sample	S_{BET} [m^2 g^{-1}]	V_{micro} [cm^3 g^{-1}]	V_{meso} [$cm^3 g^{-1}$]	V_{total} [$cm^3 g^{-1}$]
H-ZSM5-p	423	0.121	0.017	0.364
H-ZSM5-3m	383	0.113	0.031	0.322
Induced change	- 40	- 0.008	+ 0.014	- 0.041
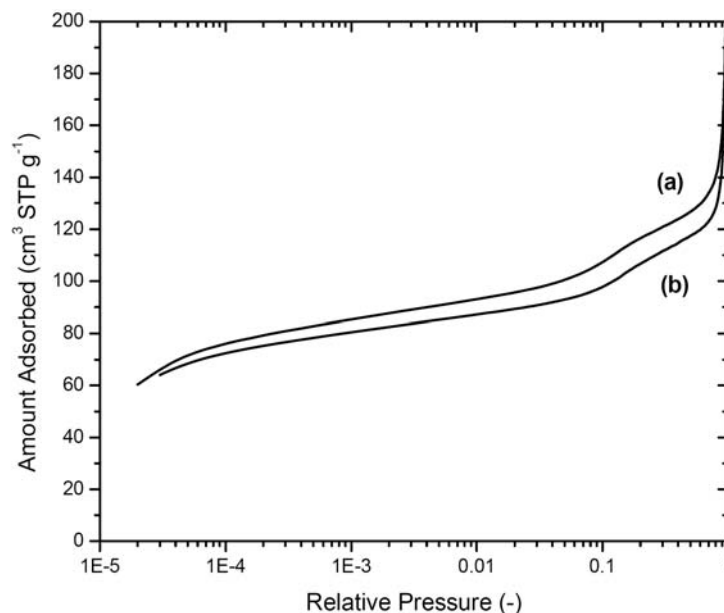
Figure 5.5 **Nitrogen adsorption isotherms of (a) the parent H-ZSM5-p sample and (b) of the sample after surface modification H-ZSM5-3m.**
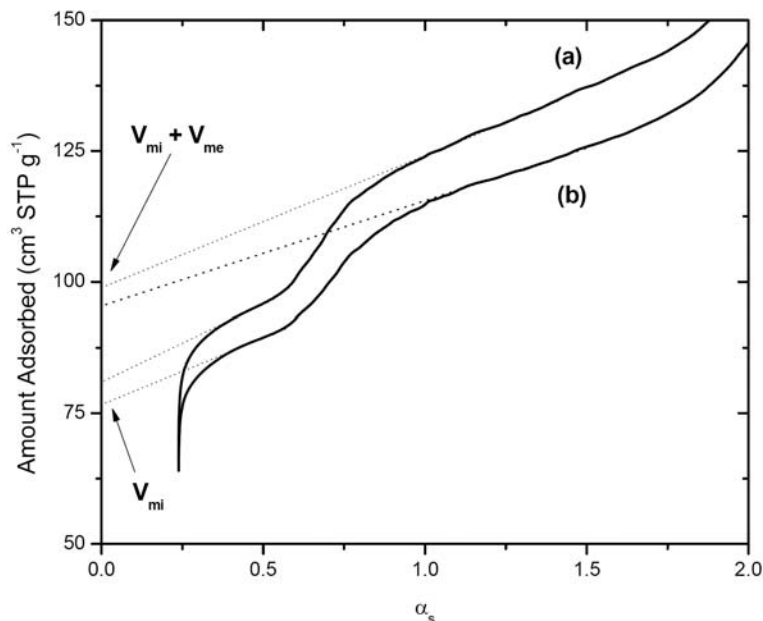
Figure 5.6 α_s **plots of (a) the parent H-ZSM5 sample and (b) the sample after surface modification H-ZSM5-3m. Two linear regions are identified: a low pressure linear region at $\alpha_s = 0.5$ and a linear region at $\alpha_s = 1.2$ corresponding to the micropore volume and the sum of the micro- and mesopore volume, respectively.**

5.2.4 Fast time-resolved rapid scan infrared spectroscopy

A detailed description of the measurement principle, the instrument setup and the requirements for the signal-to-noise ratio of fast time-resolved rapid scan IR spectroscopy is indicated in chapter two, section 2.3.1 and can furthermore be found in ref. [17]. As sorbate, benzene in spectroscopic grade (GC standard > 99.96 %, Sigma-Aldrich) was used without further purification. The zeolite samples were prepared as self-supporting wafers with approximately 25 mg cm^{-2} and were inserted in a vacuum cell with a geometry optimized for transmission infrared spectroscopy. The samples were activated under vacuum below < 10^{-7} mbar at 823 K (heating increment 10 K min^{-1}) for 1 h. All subsequent infrared spectra were recorded at 403 K with a spectral resolution of 8 cm^{-1}. After the sorption equilibrium was established at a desired partial pressure, the volume of the system was modulated periodically ($\Delta V = \pm$ 5%) by a magnetically driven pair of vacuum bellows, synchronized with the recording of the infrared spectra.[17] The partial pressure of the sorbate for following the transport processes was 0.06 mbar, which fell into the nearly linear region of the corresponding

sorption isotherm. This allows observing the maximum change in the site coverage during the pressure modulations for the terminal SiOH and the bridging SiOHAl groups at the same time.

In order to directly compare the surface coverage of the adsorbed species, all spectra were normalized using the overtone and lattice vibrations of the zeolite framework in the spectrum of the activated zeolites between 2105 and 1740 cm^{-1}. The coverage changes of the SiOHAl and SiOH groups were converted to concentrations (in mmol g^{-1}) from the variations in the integral intensity of the corresponding infrared vibrational bands. Therefore, it is assumed that the molar extinction coefficients for the stretching vibrations of the corresponding hydroxyl group are independent form the coverage.

5.3   Results

5.3.1   Kinetics of benzene sorption on surface modified H-ZSM5 samples

The individual sorption rates on the functional hydroxyl groups at the outer surface and inside the pores of the H-ZSM5 zeolite were studied by time resolved rapid scan infrared spectroscopy as described above. The coverage of the sorption sites was directly determined form the intensity changes of the bands. For H-ZSM5 the stretching vibrational bands located at 3745 cm^{-1} and 3610 cm^{-1}, assigned to the terminal and the bridging hydroxyl groups, were used to follow the uptake kinetics of the benzene molecules. The molar extinction coefficients were determined from the concentration of these groups studied by ^{1}H/MAS NMR, as shown in Figure 5.3. The observed characteristic concentration changes during the rapid scan experiment were fitted with two exponential functions as described in chapter two, section 2.3.1 in order to calculate the initial sorption rates r_{ini} given in Equation 5.1.

$$r_{ini} = k_{ad} \cdot \Delta c_{OH,eq} e^{-t/\tau_{ad}} \overset{t \ll \tau_{ad}}{\approx} k_{ad} \cdot \Delta c_{OH,eq} = \frac{\Delta c_{OH,eq}}{\tau_{ad}} \tag{5.1}$$

The characteristic time profiles at the SiOH and SiOHAl groups are compiled in Figure 5.7, the initial sorption rates are compared in Table 5.2 and 5.3 for both materials investigated.

Table 5.2   **Equilibrium coverage changes, characteristic time constants and initial sorption rates on the terminal hydroxyl groups at 403 K for benzene on a series of surface modified H-ZSM5 zeolites.**

	Terminal SiOH groups		
Sample	Δc_{eq} [μmol g^{-1}]	τ [s]	r_{in} [μmol g^{-1} s^{-1}]
H-ZSM5-p	0.145	3.5	0.042
H-ZSM5-1m	0.096	3.7	0.026
H-ZSM5-3m	0.060	3.6	0.017

Table 5.3   **Equilibrium coverage changes, characteristic time constants and initial sorption rates on the bridging hydroxyl groups at 403 K for benzene on the series of surface modified H-ZSM5 zeolites.**

	Bridging SiOHAl groups		
Sample	Δc_{eq} [μmol g^{-1}]	τ [s]	r_{ini} [μmol g^{-1} s^{-1}]
H-ZSM5-p	0.978	2.0	0.477
H-ZSM5-1m	0.907	1.2	0.741
H-ZSM5-3m	0.722	0.7	1.044
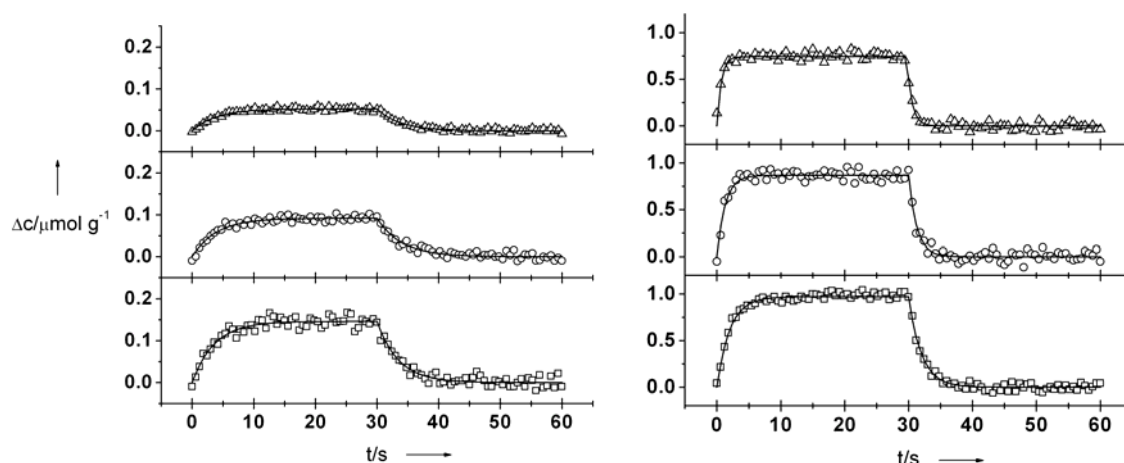
Figure 5.7   **Coverage changes Δc of terminal (left) and bridging hydroxyls (right) at 403 K on the materials H-ZSM5-p ($\square$), H-ZSM5-1m ($\circ$) and H-ZSM5-3m ($\triangle$) during a periodic volume perturbation around the equilibrium partial pressure of 0.06 mbar.**

It can be seen, that identical time constants were observed for the terminal hydroxyls, while the equilibrium coverage decreased after the modification. This is paralleled by the reduced concentration of the free SiOH groups (3747 cm^{-1}) in the sequence H-ZSM5-p > H-ZSM5-1m > H-ZSM5-3m as deduced from the infrared spectra of the activated zeolites. In the case of bridging hydroxyl groups, the time constants τ decreased continuously from 2.0 s to 0.70 s with the surface modification, indicating an increasing sorption rate with an increasing amount of SiO_2 deposited during modification. Thus, the sorption rates for the two possible sorption pathways doubles for the three-fold modified sample compared to the parent one under identical experimental conditions. This increase appears to be related to the greater sticking probabilities, which also increased by the same factor (see Table 5.4).

Table 5.4 **Sticking probabilities calculated for benzene on a series of surface modified zeolite samples at 403 K.**

Zeolite sample	Sticking probability α [-]
H-ZSM5-p	2.10×10^{-7}
H-ZSM5-1m	2.48×10^{-7}
H-ZSM5-3m	2.96×10^{-7}

Hence, the present data show for the first time that it is possible to increase the rate of sorption of benzene by corrugating the external surface of the particle by modification. For the nearly rigid and highly symmetric benzene molecule the roughened surface and the open pore structure allows more entropically favourable orientations of the molecules during their collision with the surface, which is increasing the probability for being successfully trapped. Benzene colliding with the modified surface appears to be pre-directed to the pore openings. Statistically unfavorable gas phase orientations of benzene, e.g., orientations with the benzene ring plane oriented distinctly tilted with respect to the surface are gradually adjusted during the transport through the overlayer, leading to successful trapping and direction of the molecules into the weakly bound physisorbed state. As the mesopores formed have diameters about two times larger than the kinetic diameter of benzene (0.58 nm), additional transport limitations are not generated. However, this effect would not account for sterically more demanding molecules such as *p*-xylene (length 0.98 nm)

with typical dimensions in the same order as the large micropores in the SiO_2 layer. Preliminary experiments with such molecules show indeed a retardation of the sorption rate by surface modification for *p*-xylene. Tailored surface modification thus selectively increases the sorption rate of molecules that have a drastically lower kinetic diameter than the micropore size generated in the overlayer.

Additional support for this conclusion is given by single pressure-step variations ($0 \rightarrow 0.10$ mbar) of benzene at low coverage. The changes of the coverage of the bridging hydroxyl groups with benzene, calculated from the infrared intensities, are shown in Fig. 5.8. The initial slopes of the uptake curves directly represent the initial sorption rates and follow the same sequence H-ZSM5-p < H-ZSM5-1m < H-ZSM5-3m as previously described for the time-resolved experiments with repeated modulation of the pressure in a small interval.
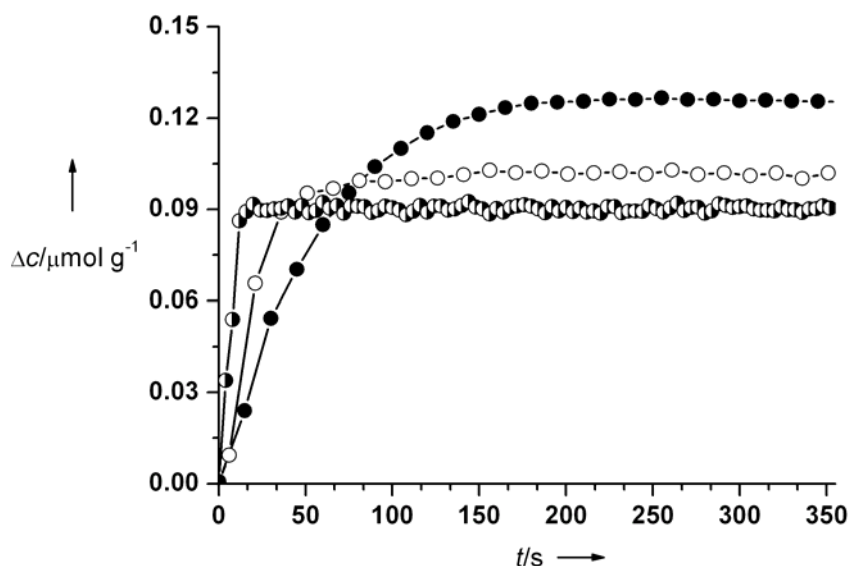
Figure 5.8   Time-resolved sorption profiles for benzene on SiOHAl sites of H-ZSM5-p (●) H-ZSM5-1m (○) and H-ZSM5-3m (◐) following an initial pressure step from 0 to 0.11 mbar at a temperature of 403 K.

The ratios of the SiOHAl sorption rates were 1.8 for H-ZSM5-1m /H-ZSM5-p and 2.6 for zeolite H-ZSM5-3m/H-ZSM5-p. These ratios are in perfect agreement with the values determined from the uptake rates (summarized in Tables 5.2 and 5.3). Thus, it is well established that the rates of benzene sorption on the hydroxyl sites inside the pores are strongly enhanced after surface modification with a porous silica overlayer.

5.3.2 Confirmation of the absence of mass transfer limitations

To ensure that the enhancement of the intra-pore sorption rates does not result from experimental artefacts or from a severe blocking of a fraction of the pore volume after the modification or mass transfer limitations, the sorption isotherms for benzene on the three H-ZSM5 samples were measured by infrared spectroscopy. The identical uptake $\Delta c_{eq,RS}$ of benzene on the SiOHAl groups at the typical pressure difference Δp of the time-resolved rapid scan experiment and the uptake Δc_{iso} calculated from the sorption isotherm at these pressures clearly confirmed that all hydroxyl groups inside the zeolite pores were accessible for the sorbate molecules (see Figure 5.9).
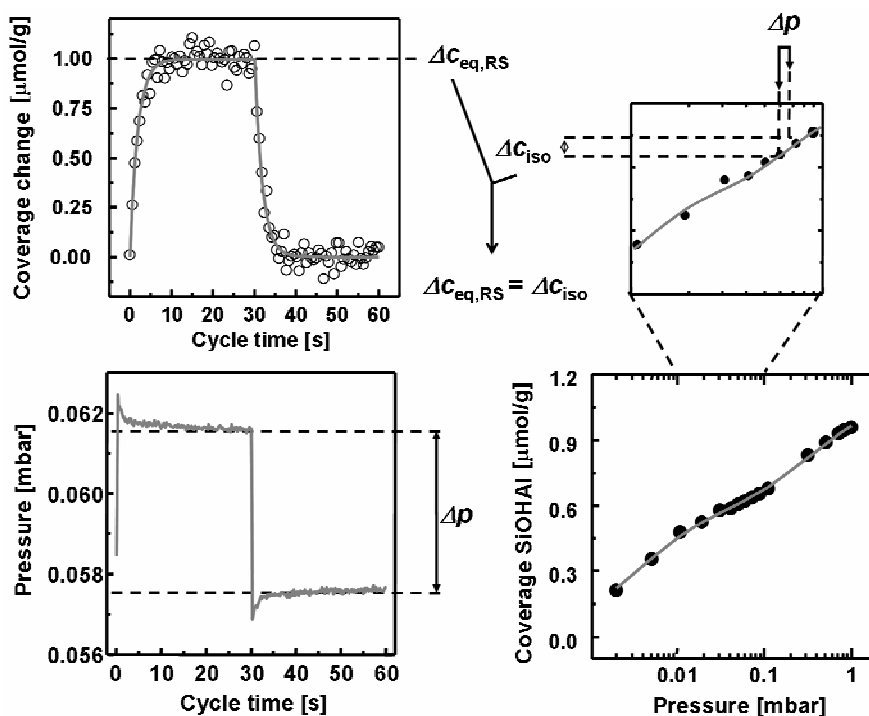
Figure 5.9   **Comparison of the dynamic time-resolved infrared measurements in rapid scan mode (left, top) and the equilibrium sorption isotherms for benzene (right) on the bridging hydroxyl groups of unmodified H-ZSM5-p at 403 K. From the pressure signal recorded simultaneously to the infrared recording the equilibrium pressure change is calculated as illustrated (left, bottom)**

To calculate the corresponding equilibrium coverage change Δc_{iso} within the given pressure limits, the experimental sorption isotherms were fitted using a dual-site Langmuir sorption model (see Equation 2.19 in chapter two). For further details and a

correlation between the experimental and theoretical values for all aromatic molecules studied on unmodified H-ZSM5 it is referred to Appendix C.

5.4 Discussion

5.4.1 Transport diffusivities of benzene in modified HZSM-5

In order to establish that the higher uptake rates observed can also be practically implemented industrially e.g., for separation processes, transport diffusivities were determined using pressure frequency response measurements. The characteristic functions of the frequency response experiment in a temperature range of 343 K to 423 K are shown in Figure 5.10 and the values for the transport diffusivities D_0 are summarized in Table 5.5. In agreement with the rapid scan infrared spectroscopic measurements, the transport diffusivities increased upon modification revealing a faster transport process for the modified material. The apparent activation energies of diffusion for parent and modified sample were 23 and 24 kJ mol^{-1}, respectively and are in the range expected from previous studies.[22, 33]

Table 5.5 **Diffusion time constants L^2/D, transport diffusivities D_0, and frequency response parameters K for equilibrium uptake at varying temperature for parent and three-fold modified H-ZSM5.**

	H-ZSM5-p			H-ZSM5-3m		
T	L^2/D_0	D_0	K	L^2/D_0	D_0	K
[K]	[s]	[m^2 s^{-1}]	[-]	[s]	[m^2 s^{-1}]	[-]
343	27.7	9.0×10^{-15}	0.75	9.7	2.6×10^{-14}	0.70
373	14.2	1.8×10^{-14}	0.47	4.7	5.4×10^{-14}	0.46
403	8.9	2.9×10^{-14}	0.30	2.5	1.0×10^{-13}	0.32

The corresponding pre-exponential factors increase significantly from a value of 3.0×10^{-11} to 8.0×10^{-11} m^2 s^{-1} by modification. The equal energies of activation indicate that the surface modification does not increase the energy required for benzene to diffuse into the zeolite. Such an enthalpic barrier leading to higher observed

energies of activations for adsorption would have been expected for markedly narrowed pores. In turn, the higher sticking coefficient can be understood by analyzing the elementary steps of the adsorption process.
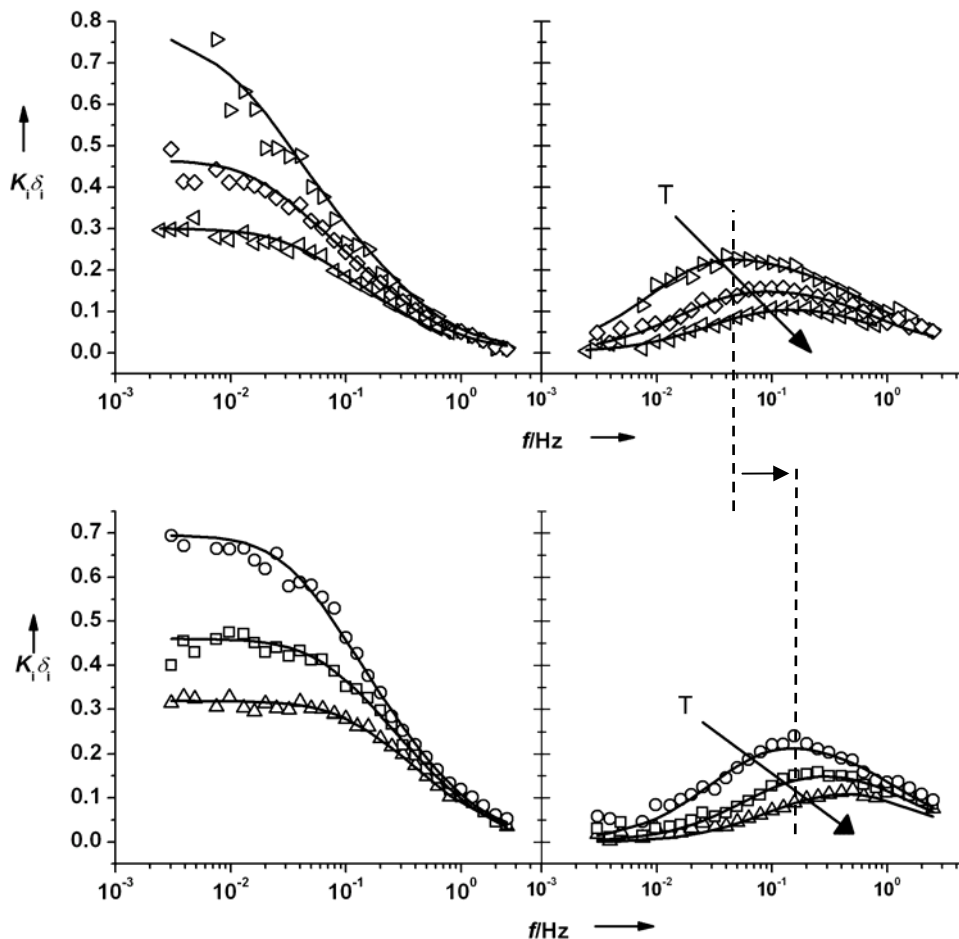
Figure 5.10 **Characteristic in-phase (left) and out-of-phase (right) pressure frequency response functions $K_i \delta_i$ for benzene on H-ZSM5-p (top) and H-ZSM5-3m (bottom) at 373 K, 403 K and 423 K**

It has been theoretically shown, that the probability to enter a pore, increases dramatically as the pore size increases.[34] The amorphous surface layer containing meso- and large micropores pores will, therefore, allow a larger fraction of molecules to directly adsorb into mesopores enhancing so the sticking coefficient. In more general terms, the higher pre-exponential factor is interpreted as being due to a retention of a higher portion of the entropy compared to adsorption on the surface of the parent zeolite (see Figure 5.1), which has only the pore openings of micropores at the outer surface. Note that on the relatively flat surface of the parent zeolite the

molecules adsorb into a state of a two-dimensional gas, while in the mesoporous surface a three-dimensional component in the movement of the adsorbed particles is retained.

5.4.2 Schematic model for hierarchic materials with surface overlayers
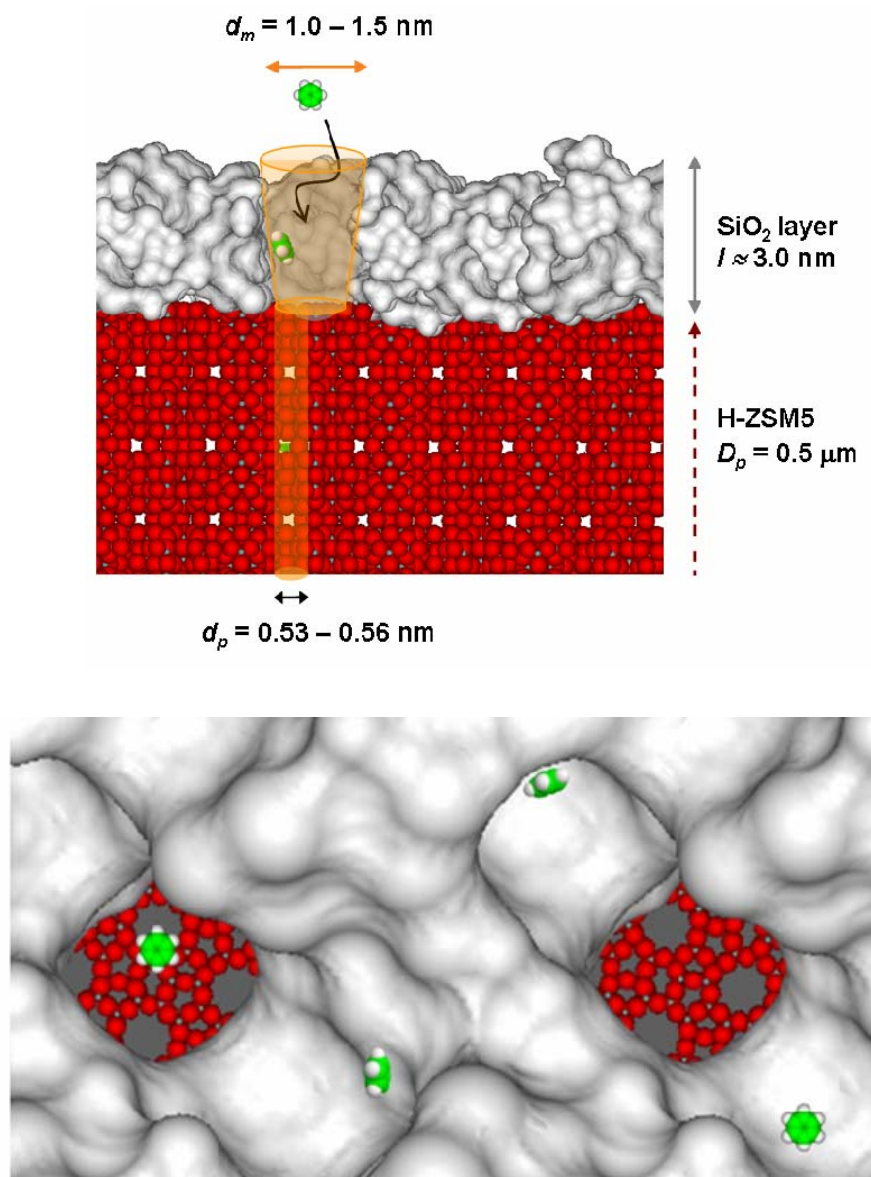
Figure 5.11 **Scheme of H-ZSM5 zeolite crystals shown in cross section (top) and top view (right) with average particle diameter of $D_p = 0.5$ μm and silica overlayer on the surface of $l = 2.0$ to 3.0 nm thickness. The overlayer, containing large micropores with an average diameter d_m around 1.5 nm functions as a funnel directing the sorbing benzene molecules in the gas phase into the micropores of the zeolite with pore aperture d_p.**

The silica overlayer functions for the sorbing molecules as funnel to direct them into the micropores and provides a gradual loss of the entropy instead of the step change found in the parent material, as seen in Figure 5.11. As a direct consequence the pore diameter of the overlayer is crucial for the successful synthesis of materials with improved sorption properties. The larger the pores will be the higher the enhancement should be. In return, we expect seeing a gradual reversion of this positive effect as the free rotation of the adsorbed molecules in the pores of the overlayer will be hindered with increasing diameter of the adsorbed aromatic molecules.

5.5 Conclusions

We have shown that new surfaces can be tailored by a hierarchically structure of pores over a microporous material. Such surface modification can be realized by a silica overlayer, reducing also the concentration of terminal free hydroxyl groups on the external surface and of non-selective bridging hydroxyls in the pore mouth region. It is remarkable that the coverage does not lead to enhanced blockage of a larger portion of the channels and that all acid sites in the zeolite remained accessible after the modification. The enhanced sorption rate to sites inside the pores results primarily from the increase in the sticking probability through the gradual loss of the entropy at the collision with the corrugated surface and the mesoporous overlayer, without creating barriers that have to be overcome by energy. This is, however, aided by the effect of the meso- and large micropores in the overlayer, which lead to a larger concentration of molecules in these pores and as consequence to larger transport rate to the zeolite micropores. The size of the mesopores needs to be sufficiently large to allow free rotation about the longest axis of the molecule.

If this is not possible, preliminary experiments indicate that the advantage of the overlayer design turns into a disadvantage, leading to a retardation of the sorption of molecules with identical minimum, but different maximum diameter. While being unlikely, it cannot be fully excluded, however, that the lower concentration of hydroxyl groups at the outer surface also aids the higher uptake rate. The enhancement of the sorption rate into zeolites by chemically modifying the outer surface as reported here highlights a new strategy to enhance separation without an overall retardation of

the sorption rates to the internal sites. By tailoring the overlayer pores and maximizing the roughness of the outer surface it should be possible to synthesize surface modified materials that enhance the sorption rate of small molecules and retard at the same time the sorption rate for slightly larger ones, even for identical minimum kinetic diameter of the molecules.

5.6 Acknowledgments

5.7 References

[1]   G. Kokotailo, S. Lawton, D. Olson, W. Meier, *Nature* **1978**, *272*, 437

[2]   A. Corma, *Chem. Rev.* **1995**, *95*, 559

[3]   J. Weitkamp, *Solid State Ionics* **2000**, *131*, 175.

[4]   P. R. Pujado, J. A. Rabo, G. J. Antos, S. A. Gembicki, *Catal. Today* **1992**, *13*, 113.

[5]   P. B. Weisz, *Pure Appl. Chem.* **1980**, *58*, 841

[6]   Ivanova, II, A. Corma, in *Zeolites: A Refined Tool For Designing Catalytic Sites, Vol. 97*, **1995**, pp. 27.

[7]   X. D. Sun, Q. X. Wang, L. Y. Xu, S. L. Liu, *Catal. Lett.* **2004**, *94*, 75.

[8]   T.-C. Tsai, S.-B. Liu, I. Wang, *App. Catal. A-Gen.* **1999**, *181*, 355.

[9]   G. Mirth, J. A. Lercher, *J. Catal.* **1994**, *147*, 199.

[10]   S. M. Csicsery, *Pure Appl. Chem.* **1986**, *58*, 841

[11]   E. Klemm, G. Emig, *Chem. Eng. Sci.* **1997**, *52*, 4329.

[12]   E. Klemm, J. G. Wang, G. Emig, *Chem. Eng. Sci.* **1997**, *52*, 3173.

[13]   J. Weitkamp, A. Raichle, Y. Traa, M. Rupp, F. Fuder, *Chem. Comm.* **2000**, 1133.

[14]   A. Jentys, H. Tanaka, J. A. Lercher, *J. Phys. Chem. B* **2005**, *109*, 2254.

[15]   P. B. Weisz, V. Frilette, *J. Phys. Chem.* **1960**, *64*.

[16]   B. Smit, T. L. M. Maesen, *Nature* **2008**, *451*, 671.

[17]   A. Jentys, H. Tanaka, J. A. Lercher, in *Stud. Surf. Sci. Catal., Vol. 154*, **2004**, pp. 2041.

[18]   F. R. Ribeiro, F. Alvarez, C. Henriques, F. Lemos, J. M. Lopes, M. F. Ribeiro, *J. Mol. Catal. A - Chemical* **1995**, *96*, 245.

[19]   G. Sastre, N. Raj, C. R. A. Catlow, R. Roque-Malherbe, A. Corma, *J. Phys. Chem. B* **1998**, *102*, 3198.

[20]   U. Schemmert, J. Kärger, J. Weitkamp, *Microp. Mesop. Mat.* **1999**, *32*, 101.

[21]   R. Q. Snurr, A. T. Bell, D. N. Theodorou, *J. Phys. Chem.* **1993**, *97*, 13742.

[22]   L. Song, Z.-L. Sun, L. V. C. Rees, *Microp. Mesop. Mat.* **2002**, *55*, 31.

[23]   S. Brandani, M. Jama, D. M. Ruthven, *Ind. Eng. Chem. Res.* **2000**, *39*, 821.

[24]   L. V. C. Rees, D. M. Shen, in *Characterization of Porous Solids III, Vol. 87*, **1994**, pp. 563.

[25]   S. I. Reshetnikov, S. B. Ilyin, A. A. Ivanov, A. S. Kharitonov, *Reac. Kin. Catal. L.* **2004**, *83*, 157.

[26]   H. G. Karge, *Abstracts of Papers of The American Chemical Society* **1993**, *205*, 143.

[27]   J. Kärger, *Adsorption* **2003**, *9*, 29.

[28]   C. Forste, A. Germanus, J. Karger, H. Pfeifer, J. Caro, W. Pilz, A. Zikanova, *J. Am. Chem. Soc. Faraday T. I* **1987**, *83*, 2301.

[29]   Y. Fu, F. Ye, W. G. Sanders, M. M. Collinson, D. A. Higgins, *J. Phys. Chem. B* **2006**, *110*, 9164.

[30]   S. J. Reitmeier, R. R. Mukti, A. Jentys, J. A. Lercher, *J. Phys. Chem. C* **2008**, *112*, 2538.

[31]   Y. S. Bhat, J. Das, K. V. Rao, A. B. Halgeri, *J. Catal.* **1996**, *159*, 368

[32]   M. Schenk, S. Calero, T. M. L. Maesen, T. J. H. Vlugt, L. L. van Benthem, B. Schnell, B. Smit, *J. Catal.* **2003**, *214*, 88

[33]   L. J. Song, L. V. C. Rees, *Microp. Mesop. Mat.* **2000**, *35-6*, 301.

[34]   A. I. Skoulidas, D. S. Sholl, *J. Chem. Phys.* **2000**, *113*, 4379.

[35]   S. Zheng, H. R. Heydenrych, A. Jentys, J. A. Lercher, *J. Phys. Chem. B* **2002**, *106*, 9552.

[36]   S. R. Zheng, H. Tanaka, A. Jentys, J. A. Lercher, *J. Phys. Chem. B* **2004**, *108*, 1337.

[37]   Y. Yasuda, *Het. Chem. Rev.* **1994**, *1*, 103.

[38]   Y. Yasuda, in *Zeolites and Related Microporous Materials: State of the Art 1994, Vol. 84*, **1994**, pp. 1331.

[39]   M. Kruk, M. Jaroniec, J. Choma, *Carbon* **1998**, *36*, 1447.

[40]   S. J. Gregg, S. K. S. W., *Adsorption Surface Area and Porosity* 2nd ed., Academic Press Inc.,U.S., **1982**

[41]   S. Brunauer, P. H. Emmett, E. Teller, *J. Am. Chem. Soc.* **1938**, *60*, 309.

Chapter 6

6. Influences of surface modification on shape selective transport of aromatics in H-ZSM5

6.1 Introduction

Within the past decades, a large variety of micro- and mesoporous solids (e.g., zeolites) have reached indispensable technical importance as catalyst and sorbent in the fields of modern petrochemical and refining industry.[1-7] ZSM5 as medium pore size zeolite is widely used for large scale applications[8-10] such as alkylation[11] and isomerization[9, 12-14] of aromatic and aliphatic hydrocarbons as well for hydrocarbon separation. It generates very narrow products distributions[15] based on the kinetic diameter of the reactant/sorbate molecules.[16] The three-dimensional structure of ZSM5 is characterized by two types of intersecting ten-membered ring channels forming a regular pore network with cages of 0.9 nm in diameter. The straight and sinusoidal channels have elliptical pore openings of 0.54×0.58 nm and 0.54×0.56 nm, respectively.[17] The high preference to *para*-selectivity of ZSM5 is crucial for the production of desired alkyl-substituted aromatic products.[6, 7, 18] The shape selective sorption and transport properties of ZSM5[19, 20] are directly linked to its structural features[21] and to the similarity of pore apertures and the kinetic diameter of the sorbates.

Activity and shape selectivity of catalysts with a given chemical composition and structure are known to critically depend on the crystallite size, the ratio between external and internal pore volume, the pore apertures and, as a key factor, on the distribution of catalytically active sites[22-25]. Consequently a large amount of sites at the pore entrances will decrease the shape selective behavior.[19, 26] Well-tailored blockage of unselective sites can minimize this disadvantage, and exact control and adjustment of pore apertures by post-treatment have been addressed extensively in the past. Attempting to develop novel generations of catalysts with hierarchical pore structure[19, 27-29] and selective sorption and transport properties for separation purposes, a profound and comprehensive understanding of all involved transport steps on a molecular level is mandatory.

According to theoretical simulations of Skoulidas and Scholl[30] as well as Ford and Glandt[30, 31], direct pore entering from the gas phase can be excluded for rigid reactant molecules with minimum kinetic diameter similar to the pore aperture (see

Figure 6.1). Consequently, sorption into zeolite pores involves the collisions of the sorbates/reactants from the gas phase with the external catalyst surface. The successful individual sorption event is described by the sticking probability α of the sorbate. For rigid aromatic hydrocarbon molecules on H-ZSM5 the sticking probability is directly related to the sorption enthalpy and the decrease in entropy of the sorbate on the zeolite surface[32]. A smaller loss of entropy, i.e., of molecular degrees of freedom during the sorption step strongly enhances the sticking probability[32], while a retarded accommodation of the sorption enthalpy on the unmodified zeolite surface significantly decreases the sticking probability. Sticking on the surface is followed by a series of subsequent surface and intra-pore transfer processes, [33-35] which in the past have been subject of several theoretical[36-40], experimental[41-48] and molecular dynamics simulation studies.[37, 49-51]

$$d_p = 0.53 - 0.56 \text{ nm}$$
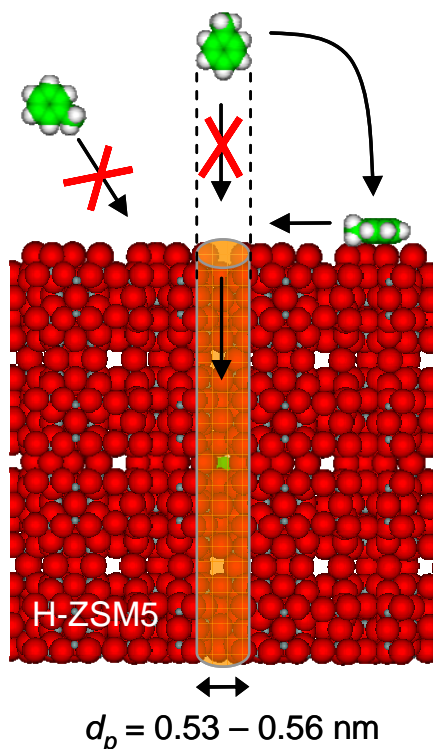
Figure 6.1 **A typical crystal of zeolite H-ZSM5-p with toluene molecules is shown in cross section. Toluene molecules enter the pore network (straight channel highlighted in orange) via a weakly-bound physisorbed surface state. Due to its minimum critical diameter of 0.58 nm no direct pore entering is possible from the gas phase.**

Using time-resolved infrared spectroscopy we have recently described the sequence of interconnected transport steps on unmodified H-ZSM5 for alkyl

substituted aromatic molecules.[52, 53] After impinging on the external surface a physisorbed surface state with high two dimensional mobility of the sorbate molecules is populated. Two parallel pathways leading to sorption on terminal hydroxyls and into the micropores exist and their probability depends primarily upon the relative abundance of the two options. Diffusion inside the two channel types of H-ZSM5 precedes sorption to the bridging hydroxyl groups.[53] The detailed kinetic analysis of this network indicated that none of the sorption rates is clearly rate determining. Therefore, the observed overall rate must be a result of the subtle interplay between these steps with a schematic overview being given in Figure 5.1 within chapter five. Inside the channels of the zeolite intra-crystalline diffusion in the sub-micron length scale is supposed to be rather fast compared to the pore entering process. Consequently, the sorption rates observed at the internal sites are dominated by the external surface properties and the pore entering probability, rather than by the differences between the transport processes in the sinusoidal or straight channels. In contrast, for large zeolite crystals that exhibit longer intra-pore transport pathways, diffusion within the channels becomes rate limiting.[54]

Based on the transport model reported, we could furthermore show that the presence of a systematically corrugated (roughened) zeolite surfaces with hierarchical pore structure strongly enhances the sorption rates of benzene. This was attributed to the increased sticking probability and an entropically favourable "funnelling effect" of the overlayer in a recent note.[54, 55] In this contribution a series of gradually surface silylated H-ZSM5 samples was investigated upon sorption of aromatic hydrocarbons by *in-situ* time-resolved infrared spectroscopy. The role of the molecular size dimensions and the aspect ratio of the adsorbed aromatic molecules on the sorption rates will be investigated and described with a theoretical model.

6.2 Experimental

6.2.1 Materials

Zeolite H-ZSM5 provided by the Süd-Chemie AG (denoted H-ZSM5-p), with a Si/Al ratio of 45 (confirmed by AAS) was used for the experiments. Concentrations of terminal silanol (SiOH) and bridging hydroxyls (SiOHAl) were determined by

^{1}H/MAS-NMR spectroscopy to 0.27 mmol g^{-1} and 0.21 mmol g^{-1}, respectively as presented in Figure 5.3 within chapter five. The gradual post-synthetic modification of the external zeolite surface by chemical liquid deposition (CLD) of tetraethyl orthosilicate (TEOS) is described by Zheng et al. [48, 56]. Modified samples are referred to H-ZSM5-1m and H-ZSM5-3m, corresponding to one, respectively three modification cycles with 4 wt-% of SiO_2 deposited within each cycle. The resulting concentrations of SiOH groups were 0.18 and 0.12 mmol g^{-1} and of SiOHAl groups 0.18 and 0.16 mmol g^{-1} for H-ZSM5-1m and H-ZSM5-3m.[56]. Benzene, toluene and *p*-xylene were used in spectroscopic grade (GC standard, > 99.6 % from Fluka). Prior to first use, all sorbates were transferred to the dosing system under argon and further degassed using the pump-and-freeze method three to five times. Scanning electron microscopy (SEM) was performed on a REM JEOL 5900 LV microscope operated at 25 kV with resolution of 5.0 nm and magnification of 3.0 x 10^{6}. For transmission electron microscopy (TEM), the powdered samples were suspended in ethanol solution and dried on a copper-carbon-grid. All micrographs shown were measured on a JEOL-2011 electron microscope operating at 200 kV.

6.2.2 Infrared spectroscopy

Experimental Setup: A high vacuum system equipped with a unit for periodic volume modulations was combined with a vacuum cell for infrared measurements in transmission mode. The IR spectra were measured with a Bruker IFS 66 v/S infrared spectrometer in rapid scan mode using a periodic volume modulation with an amplitude of $\Delta V = \pm 5\%$.[53] Such small variations of the system volume were necessary to exclude adiabatic effects due to local exothermicity otherwise interfering with the transport kinetics of the sorbate. A detailed description of the full instrumental setup and the principle of time-resolved infrared spectroscopy are found in refs.[48, 53].

Sample preparation and activation: The powdered samples were pressed into self-supporting wafers (~ 20 mg cm^{-2}) and subsequently inserted into a gold ring sample holder in the IR cell. Preliminary evacuation at 403 K was followed by activation under vacuum < 10^{-7} mbar at 823 K for 1 h using 10 K min^{-1} heating rate. The activated samples were equilibrated with 0.06 mbar of sorbate gas and the IR

spectra were recorded at 403 K with a resolution of 4.0 cm^{-1} for sorption and 8.0 cm^{-1} for transport experiments. For a direct comparison of the concentrations of the adsorbed species all spectra were baseline corrected and normalized to the integral of the overtone lattice bands between 2105 and 1740 cm^{-1}. The infrared spectra of the activated H-ZSM5 samples are shown in Figure 6.2.
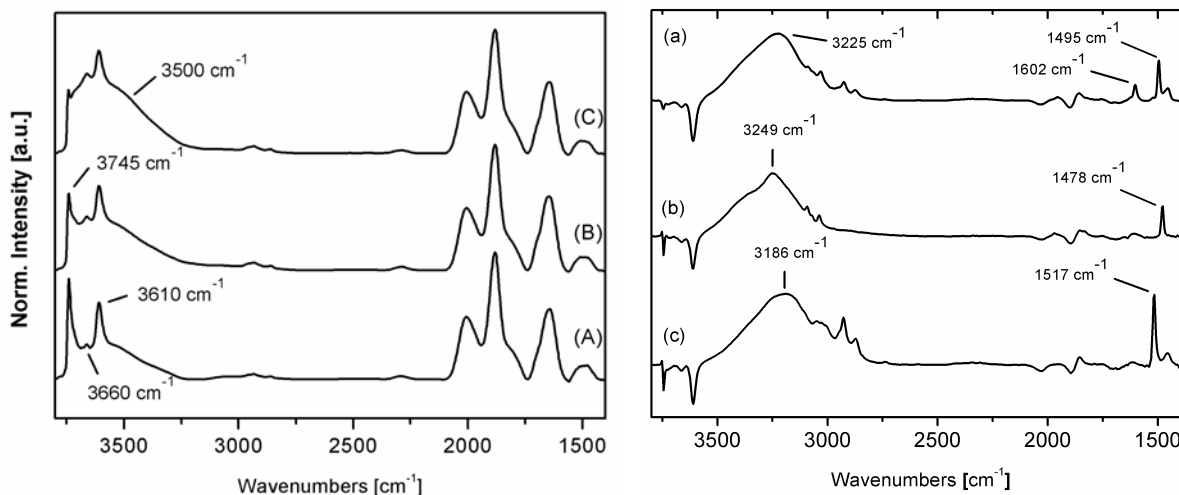
Figure 6.2 **(left) IR spectra of activated (A) H-ZSM5-p and modified samples (B) H-ZSM5-1m and (C) H-ZSM5-3m under vacuum (below 10^{-7} mbar) at 403 K. The spectra are normalized to the integral of the lattice and overtone vibrations bands of ZSM-5 between 2105 and 1740 cm^{-1}. (right) Difference IR spectra of H-ZSM5-1m after adsorption of (a) toluene, (b) benzene and (c) *p*-xylene measured with partial pressure of 0.06 mbar at 403 K.**

Fast time-resolved IR spectroscopy: To follow sorption kinetics in micro- and small mesopores on a timescale of milliseconds, high time resolution combined with an excellent signal-to-noise ratio is required. IR spectra were collected by the infrared spectroscopy in rapid scan mode. A rectangular modulation function with time period of t_p = 60 s separated into 100 segments was used and 400 adsorption-desorption cycles followed, yielding in total 4000 co-added interferograms for each spectrum with a time resolution of 600 ms. The magnet signal and the system pressure were recorded in parallel to the co-addition to follow the stability and accuracy of the modulation function. Within the series of IR spectra, the last spectrum was subtracted to emphasize the changes within the vibrational bands. A typical series of difference spectra obtained for benzene on H-ZSM5 can be seen in Figure 2.24 in chapter two.

The coverage of the terminal and bridging hydroxyl groups was calculated directly from the intensity of the O-H stretching bands via integration in the ranges of 3727 to 3770 cm^{-1} and 3577 to 3640 cm^{-1}, respectively. Assuming a constant molar extinction coefficient the integral intensities were transferred into sorbate concentration profiles. In order to obtain the individual sorption kinetics of the sorbate molecules at the hydroxyl groups, the corresponding concentration time profiles were fitted with two independent exponential functions (see Equations 2.21 and 2.22 within chapter 2 section 2.3.1.3). The initial sorption rates r_{ini} of the sorbate molecules can analogously be derived from the initial slopes of the concentration profiles according to Equation 6.1 from the change of the sorbate concentration when reaching the equilibrium $\Delta c_{OH,eq}$ after the volume perturbation and the time constant of the adsorption process τ_{ad}.

Initial rate: $$r_{ini} = \frac{d\left(\Delta c_{OH}(t)\right)}{dt} = \frac{1}{\tau_{ad}} \cdot \Delta c_{OH,eq} e^{-t/\tau_{ad}} \text{ for } t \ll \tau_{ad} \quad r_{ini} \approx \frac{\Delta c_{OH,eq}}{\tau_{ad}} \quad (6.1)$$

Note hereby, that the stoicheometry of the sorbate molecules did not depend on the coverage in the pressure range studied[53]; therefore the variations in the hydroxyl bands Δc_{OH} were directly related to respective sorbate concentrations.

6.2.3 Transport studied by the frequency response method

The temperature dependency of the transport rates of benzene, toluene and *p*-xylene was additionally determined for H-ZSM5-p and H-ZSM5-3m using the (pressure modulation) frequency response method. 30 mg of powdered sample were dispersed on quartz wool at the bottom of a quartz tube to avoid influences of bed-depth effects and subsequently activated under vacuum below 10^{-7} mbar for 1 h at 823 K with a ramp of 10 K min^{-1}. The sorbate was equilibrated with a partial pressure of 0.30 mbar at temperatures of 343, 373 and 423 K and the system volume was modulated periodically with $\pm$ 1 % amplitude at frequencies in the range of 0.001 to 5 Hz. The pressure response of the system was recorded with an in-line pressure transducer (MKS 616A11 Baratron). From the amplitude and the phase lag of the frequency response, the characteristic frequency response functions were determined.

A planar-sheet theoretical transport model taking into account particle size distribution effects and surface resistance parameters, was chosen for data analysis.[57, 58] Fitting of the theoretical functions representing analytical solutions of the 2nd Fickian law, to the experimental frequency response was performed using the CMA evolution strategy in Matlab[59]. From the resulting transport parameters as function of temperature, the Arrhenius energies of activation and corresponding pre-exponential factors were estimated.

6.3   Results

6.3.1   Characterization of target materials

Scanning electron microscopy (SEM) reveals an average size of the crystallites of 0.5 μm and the presence of a small amount of larger agglomerates for all three samples. The XRD patterns of H-ZSM5-p and H-ZSM5-3m are shown in Figure 2.5 within chapter two. Besides the typical reflection peaks for the MFI-structure of ZSM5 zeolites, the distinctly increased baseline in the XRD pattern of H-ZSM5-3m confirms the presence of a small fraction of amorphous contributions compared to H-ZSM5-p.
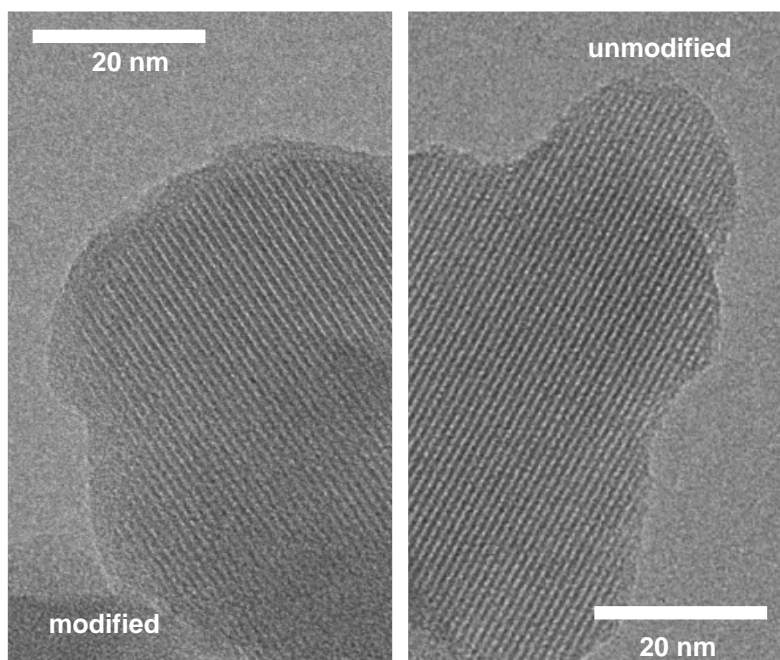
Figure 6.3   **Transmission electron micrographs of a (right) the unmodified zeolite H-ZSM5-p and (left) three-fold modified H-ZSM5-3m sample. The surface layer consisting of amorphous SiO$_2$ covering the crystalline core is clearly seen (left).**

Differences in the surface morphology between H-ZSM5-p and the series of TEOS modified samples were monitored by TEM. The crystal lattices of the zeolite framework are clearly seen on all micrographs shown in Figure 6.3. In contrast to the unmodified zeolite, the crystalline core of the TEOS modified zeolite reveals a thin, untextured region covering the outer surface. This non-crystalline region was attributed to amorphous SiO_2 overlayers with an average thickness of 3.0 nm estimated from the TEM micrographs and from the amount of TEOS added (4 wt-% of SiO_2) in each modification cycle. An average porosity of 30 % and the presence of large micropores in the overlayers having an average diameter of around 1.5 nm were derived from nitrogen physisorption.[32]

6.3.2 Time-resolved in-situ infrared spectroscopy

Activated zeolites: The infrared spectra of activated H-ZSM5-p, H-ZSM5-1m and H-ZSM5-3m, as compiled in Figure 6.2, clearly show the characteristic bands at 3610 cm^{-1} and 3745 cm^{-1} assigned to the SiOHAl and SiOH groups, respectively. The weaker bands at 3726 cm^{-1} and 3660 cm^{-1} originate from internal SiOH groups and OH groups located on extra-framework alumina (EFAl)[56]. Moreover, a broad band around 3500 cm^{-1} resulted from the presence of perturbed hydroxyl groups in the modified samples. Surface silylation mainly affected the external SiOH groups, while the bridging SiOHAl groups decreased to a lesser extent, because the TEOS molecules with a kinetic diameter of 1 nm can only react with surface and pore mouth near hydroxyls. The observed spectral changes are in perfect agreement with ^{1}H/MAS-NMR spectra[32, 56], pyridine and DTB*Py* sorption measurements performed by Zheng et al..[56]

Sorption of aromatic hydrocarbons: Upon sorption, the interaction of the aromatic molecules benzene, toluene and *p*-xylene with H-ZSM5 led to a distinct decrease in the intensity of the O-H stretching bands[60] (see Figure 6.2). In addition, due to the hydrogen bonding interaction between the electron pair donor function of the aromatic molecules and the hydroxyl groups of the zeolite, the formation of perturbed hydroxyls observed at lower wave numbers (3200 – 3500 cm^{-1}).[60] A more detailed description is given within section 2.2.2.3 of chapter two.
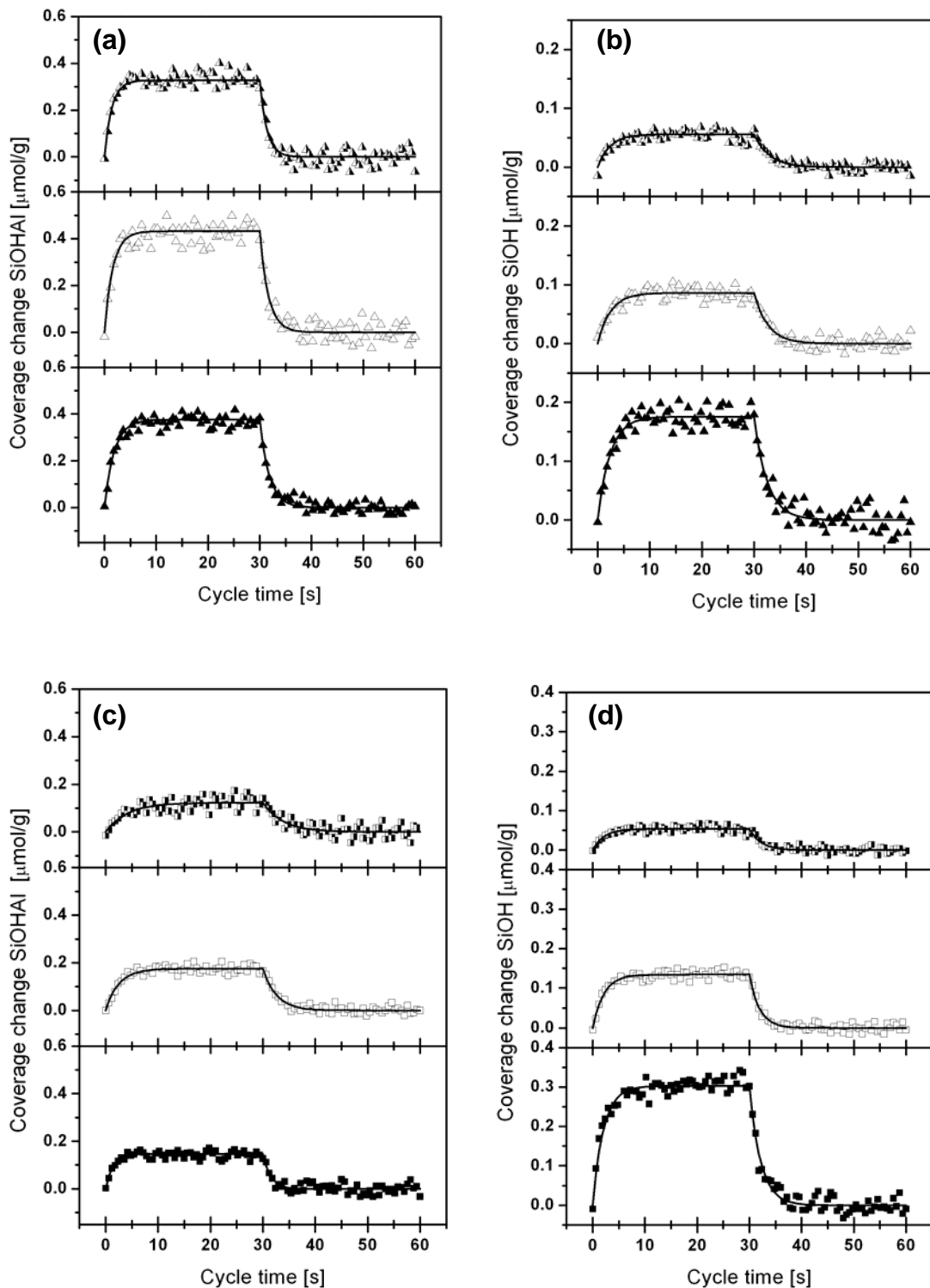
Figure 6.4   **Concentration time profiles measured at 403 K following the sorption of toluene (top) and p-xylene (bottom) on (right) the terminal SiOH and (left) the SiOHAl groups of (▲, ■) H-ZSM5-p, (△, □) H-ZSM5-1m and (▲, ◨) H-ZSM5-3m. A volume perturbation of ±5 % around the equilibrium pressure of 0.06 mbar was applied. (For benzene see chapter five)**

Besides the O-H vibrations, strong bands between 2800 and 3200 cm^{-1} as well as 1400 and 1600 cm^{-1}, assigned to the C-H stretching and C-C deformation vibrations of the sorbates, respectively, were observed.[53, 60, 61] In order to analyze the individual transport kinetics of the sorption process during the pressure modulation, the changes in the coverage of the hydroxyl groups after modification were determined. The typical concentration time profile for toluene and *p*-xylene sorption on the terminal SiOH and bridging SiOHAl groups of three samples is shown in Figure 6.4, for the profiles of benzene, it is referred to Figure 5.7 in chapter five. The time constants τ_{ad} for adsorption and τ_{de} desorption steps were identical for each sorbate, indicating that the sorption processes studied are microscopically reversible. Therefore, the initial sorption rates, compiled in Table 6.1, were calculated from the average values of τ_{ad} and τ_{de}.

Table 6.1   **Initial sorption rates of benzene, toluene and *p*-xylene on terminal SiOH and internal SiOHAl groups at 403 K for a series of post-treated H-ZSM5 calculated using Equation 6.1.**

r_{ini} [10^{-3} s^{-1}]	H-ZSM5-p		H-ZSM5-1m		H-ZSM5-3m	
	SiOH	SiOHAl	SiOH	SiOHAl	SiOH	SiOHAl
Benzene	0.15	2.34	0.16	4.04	0.16	6.37
Toluene	0.26	0.96	0.23	1.30	0.25	1.68
p-Xylene	0.44	0.55	0.42	0.41	0.41	0.24

p-Xylene, the largest molecule within the series of aromatic molecules studied showed the highest sorption rate to the terminal SiOH groups. For toluene, and benzene a monotonous decrease in the rates was observed in the sequence benzene < toluene < *p*-xylene. This monotonous decrease was preserved after surface modification on the three modified samples.

The trends in the sorption rates to the internal bridging SiOHAl groups are in contrast more complex. From the rates given in Table 6.1 it is clearly seen that the initial sorption rates on the unmodified H-ZSM5-p as well as on the modified materials H-ZSM5-1m and H-ZSM5-3m decrease monotonously with the sorbate size (benzene > toluene > *p*-xylene), inverse to the trend observed on the terminal hydroxyls. The

highest rate on the bridging SiOHAl groups among all samples studied (see Figure 6.5) was observed for benzene on H-ZSM5-3m. This relates to the different abilities of the alkyl-substituted molecules to enter the zeolite micropores. Having an identical (minimum) kinetic diameter d_{min}, the sorption rates of the aromatic molecules follow the maximum diameter d_{max} defined by the radius of gyration of the sorbate. The corresponding size dimensions are summarized in Table 6.2.
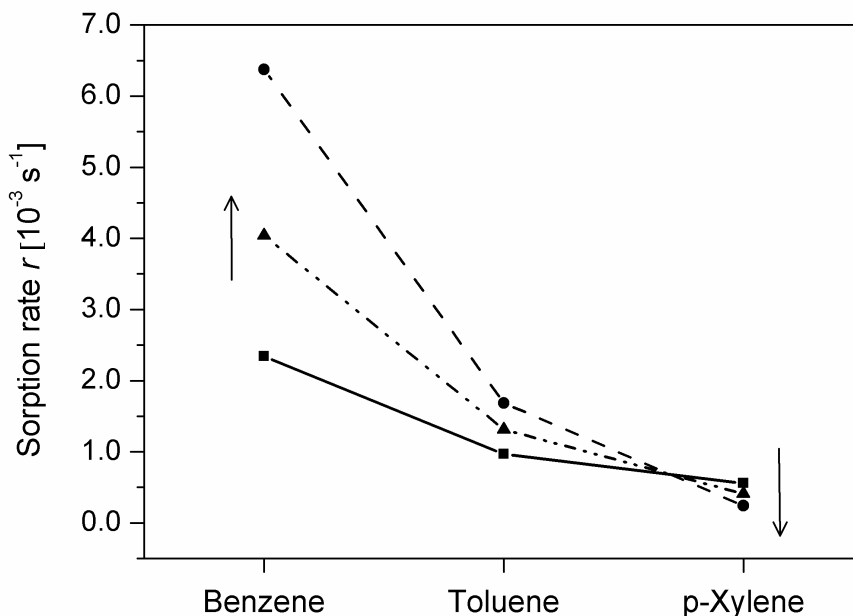
Figure 6.5 **Course of the initial sorption rates for the aromatic molecules benzene, toluene, *p*-xylene on the bridging SiOHAl groups of unmodified H-ZSM5-p (■) and on the modified materials H-ZSM5-1m (▲) and H-ZSM5-3m (●). Trends are indicated with arrows.**

Table 6.2 **Minimum kinetic diameter (d_{min}) and maximum dimension, e.g., length (d_{max}) of the aromatic hydrocarbon molecules and tetraethyl orthosilicate. The values are in agreement to those reported by Choudhary et al.[62, 63] and Zheng et al.[20, 56, 64]**

Molecule	Benzene	Toluene	*p*-Xylene	TEOS
d_{min}	0.58	0.58	0.58	1.05
d_{max}	0.67	0.84	0.98	1.05

While surface modification resulted in strongly increased rates for benzene[32], this trend does not hold for the other aromatic sorbate molecules. Slightly increased

rates were observed for toluene, and at the same time, those of *p*-xylene strongly decreased in the sequence H-ZSM5-p > H-ZSM5-1m >> H-ZSM5-3m (see Table 6.1). The ratio between the sorption rates of benzene and *p*-xylene on the unmodified H-ZSM5 was 4.3, which is in agreement with the shape selective behavior of H-ZSM5 zeolites.[14, 15] After the modification the ratio of the sorption rates increased to a factor of 27. To further elucidate the origin of this enhancement, the sticking probabilities α for the sorbate molecules on all three samples were investigated.[32]

Table 6.3 **Sticking probabilities α for alkyl-substituted aromatic molecules on the series of the surface modified H-ZSM5 samples.**

$10^{-7} \times \alpha$ [-]	H-ZSM5-p	H-ZSM5-1m	H-ZSM5-3m
Benzene	2.10	2.48	2.96
Toluene	1.69	1.70	1.72
p-Xylene	2.18	1.05	0.64

The trends in the sticking probabilities α (summarized in Table 6.3) with respect to the surface modification are in line with the trend seen for the initial sorption rates. Whereas on unmodified H-ZSM5 surfaces, the variations in the sticking probabilities are related to the symmetry, the sorbate size and to the accommodation of the enthalpy of adsorption[32], on H-ZSM5-3m a decrease from benzene to *p*-xylene with a factor of 4.7 was observed. For benzene the initial sorption rates at the SiOHAl groups and α strongly increased after the modification. For toluene only a slight increase, while for *p*-xylene both the initial sorption rates and α decreased markedly after modification.

6.4 Discussion

Surface silylation of the H-ZSM5 zeolites generated an amorphous silica overlayer with micropores in the range of 1.5 nm on the zeolite surface, which critically influences the sorption and transport of alkyl-substituted aromatic molecules. The observed initial sorption rates on the terminal SiOH groups for unmodified and

modified samples followed the order of sorption enthalpy[60] i.e., benzene < toluene < *p*-xylene. For benzene, due to its lowest sorption enthalpy and its smallest aspect ratio, the pore entering and sorption on the intra-pore bridging hydroxyls is preferred, which is reflected in the lowest rates to the terminal sites. These findings are in line with the previously established transport network model on unmodified H-ZSM5 consisting of two parallel transport pathways (see Figure 6.1) [52, 53] to the SiOH and SiOHAl groups. As both pathways are kinetically coupled, blocking of one pathway enhances the rate in the other. However, in the present case changes in the populations of the parallel pathways cannot account for the large differences observed for the transport rates to the SiOHAl groups (i.e., an 200 % increase for benzene) after modification only.
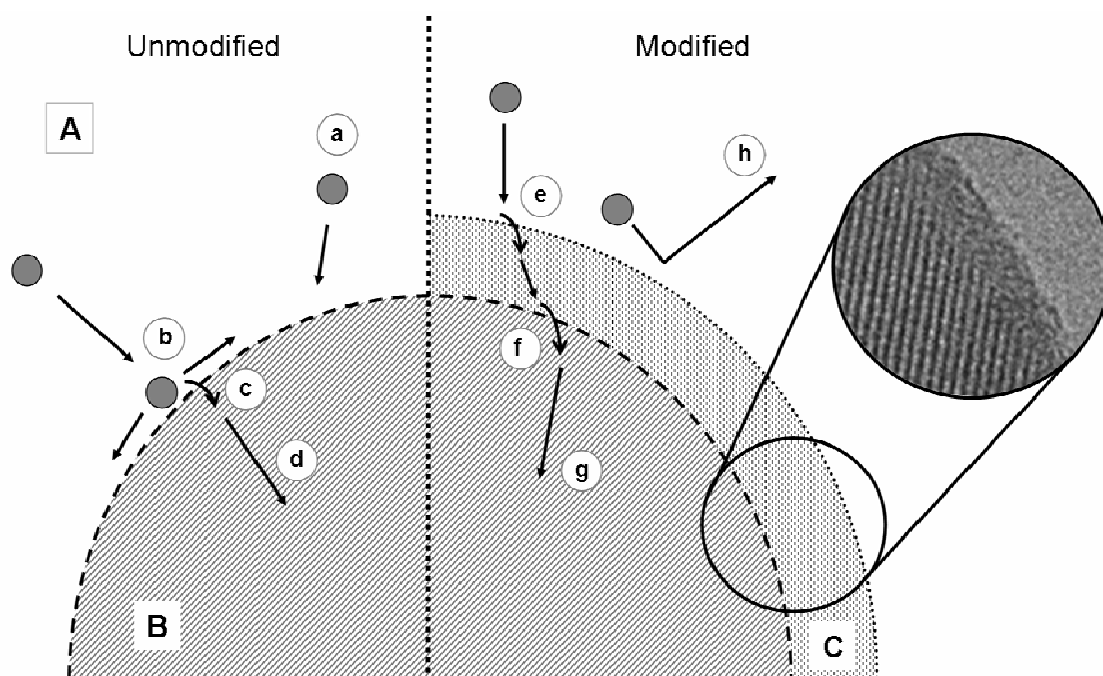
Figure 6.6   **Scheme illustrating the interconnected sorption and transport pathways on unmodified (left) compared to surface modified (right) zeolites. For the unmodified one, molecules originated from (A) the gas phase collide (a) with the zeolites (B) surface and a physisorbed state is populated followed by pore entering (c) and intracrystalline diffusion (d). On modified zeolites they primarily impinge with the silica surface overlayer (C) and with a certain probability, they can directly enter (e) the overlayer porosity. A subsequent step (f) is necessary here to access the crystalline zeolite core hidden below this overlayer, shown in the TEM inset. Those molecules, having trajectories distinctly tilted from the perpendicular plane of the pore opening are instantaneously rejected to the gas phase (h).**

We therefore assume that the properties of the hierarchical overlayer structure also influence the sorption rates of alkyl-substituted aromatic molecules. On unmodified zeolite surfaces, the gas phase molecules have to be primarily trapped on the external surface in a two-dimensional gas like state, because the direct entering into the micropores can be (statistically) excluded due to the sorbate size.[30, 31] In contrast the large pores in the overlayer of the modified samples allow a direct transfer of the molecules from the gas phase to the surface and into the pores at the interface between the amorphous layer and the zeolite surface. This effect is strongly enhanced with decreasing sorbate dimensions.

Consequently, we can dissect the overall transport process to the sorption sites inside the pores into two coupled regimes. The first being the transport of sorbate molecules through the interface between the gas phase and the amorphous overlayer, the second, the transport from the amorphous overlayer into the micropore openings (see Figure 6.6). Applying this subdivision, the total mass flux of the sorbate molecules to the sites inside the pores can be seen to is influenced by the ratio between the overlayer pore dimensions and the gyration radius of the sorbate (controlling the probability of the molecules for entering into the overlayer pores) and the ratio between the diameter of the zeolite micropores and the kinetic diameter of the sorbate.

The surface silylated samples H-ZSM5-1m and H-ZSM5-3m exhibit distinctly different trends for the sticking probabilities compared to H-ZSM5-p (see Table 6.3). On unmodified H-ZSM5 the sticking probability hardly varied[32], while on the modified zeolites the sticking probability monotonously decreased from benzene to *p*-xylene with a factor of almost five. On H-ZSM5-1m and H-ZSM5-3m the sticking probability is controlled by the probability for the molecule to be directly captured by the overlayer pores, which allows an entropically more advantageous route compared to the sorption on a flat surface. The smaller the radius of gyration the easier direct pore entering and the higher the resulting sorption rates on the internal sites. This argumentation based on the ability of the sorbate to preserve molecular entropy during the sorption into the overlayer is supported by the temperature dependency of the transport processes. The rate constants of adsorption τ^{-1} [s^{-1}], obtained by pressure modulation frequency response methods for benzene and toluene on H-ZSM5-p and

H-ZSM5-3m increased significantly with modification, while for *p*-xylene a decrease was observed (see Figure 6.7).
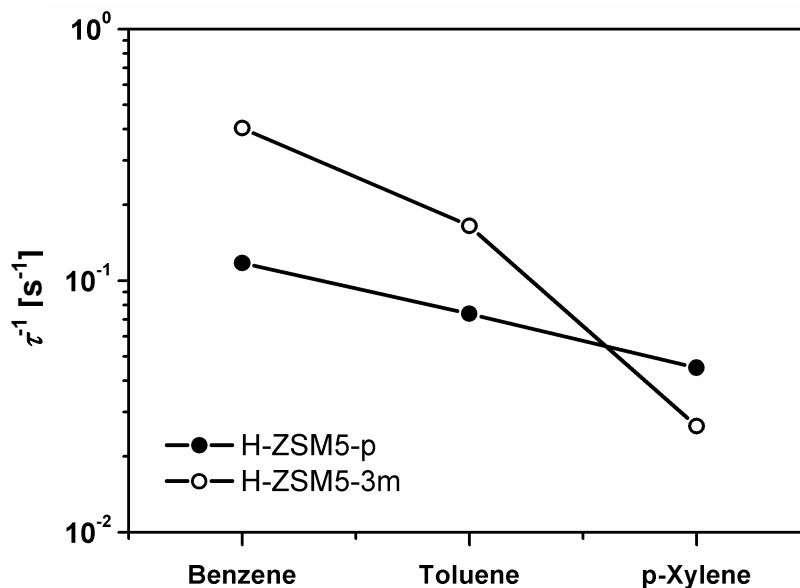
Figure 6.7   **Inverse transport time constants measured by pressure frequency response with 0.30 mbar sorbate partial pressure for benzene, toluene and *p*-xylene at 403 K on the zeolites H-ZSM5-p and H-ZSM5-3m. Values were determined assuming a single planar-sheet diffusion model with particle size distribution and surface resistance effects included.**

In order to exclude the generation of external energy barriers that hinder the accessibility of the zeolite pores during the modification the Arrhenius energies of activation E_A and the corresponding pre-exponential factors k_0 [s^{-1}]were determined from the frequency response data (see Table 6.4).

Table 6.4   **Arrhenius activation energies E_A and pre-exponential factors k_0 derived from the temperature course of the frequency response measurements with benzene, toluene and *p*-xylene in H-ZSM5-p and H-ZSM5-3m in the temperature range of 343 to 423 K.**

Molecule	H-ZSM5-p		H-ZSM5-3m	
	E_A [kJ mol^{-1}]	k_0 [s^{-1}]	E_A [kJ mol^{-1}]	k_0 [s^{-1}]
Benzene	23	1.2×10^2	24	4.5×10^2
Toluene	25	1.6×10^2	25	2.4×10^2
p-Xylene	33	6.1×10^2	31	2.7×10^2

The energies of activation showed a marked increase in the series of aromatic molecules from benzene (23 kJ mol^{-1}) to *p*-xylene (33 kJ mol^{-1}). The almost identical values for each sorbate on H-ZSM5-3m and H-ZSM5-p indicated that the surface modification did not dramatically increase the energy required for transport into the zeolite pore network. Assuming severely narrowed or even blocked pores, considerably higher barriers and energies of activation would be expected on the modified sample. Contrarily, significant changes in the pre-exponential factors were found (see Table 6.4). For toluene the pre-exponential factor increased only slightly, for *p*-xylene a decrease by a factor of two was observed, while for benzene the pre-exponential factor increased markedly after modification. The higher pre-exponential factors on modified samples result from the smaller reduction of sorption entropy compared to the adsorption process on the outer surface of unmodified HZSM-5. On the unmodified zeolite the molecules adsorb on the surface in a state of a two-dimensional gas [32], while in the porous overlayer the entropy of the molecules is more gradually lost after the collision with the pore walls and can also be partially retained in the adsorbed state. In the contrary, a lower pre-exponential factor indicates that pore entry requires more reorientations for the alignment of the sorbate in the overlayer pores, as schematically depicted for *p*-xylene in Figure 6.9. This sorption mode is more entropically demanding compared to the unmodified sample.

Molecular dynamics studies performed by Skoulidas and Scholl[30] based on hard sphere collision theory and preliminary work of Ford and Glandt[65] underline this model. Mass transport of hard sphere molecules entering into rigid pores with circular pore openings is controlled by the ratio between the diameters of the pores and of the sorbate [31, 65]. The probability for direct pore entering decreases sharply for molecules impinging with a collision angle distinctly tilted from the normal incident. Mathematically, the resulting effective mass transfer coefficient $k(D)$ as function of the pore aperture D can be calculated according to Equation 6.2 (assuming spherical particles and rigid pores)[31, 65] neglecting the flexibility of the pore openings and the internal degrees of freedom of the sorbate. [30] Within the temperature range of 343 to 423 K and for sorbate partial pressures between 0.01 and 1.00 mbar, the rotational degrees of freedom of the sorbates in the gas phase are highly excited, excluding pre-

oriented collisions of the molecules with the surface, which allows treating the molecules as rigid spheres characterized by their radius of gyration.

$$k = \frac{\pi \cdot (D*-1)^2}{4 \cdot (L*)^2} \left[\frac{a + (D*-1)^{3/4}}{b + (D*-1)^{3/4}} \right] \qquad (6.2)$$

$$\frac{n_1}{n_2} = \frac{p_1}{p_2} \cdot \sqrt{\frac{M_2}{M_1}} \cdot \frac{k_1(D)}{k_2(D)} \qquad (6.3)$$

Herein, $D*$ denotes the pore diameter divided by the (spherical) molecular diameter, $L*$ the normalized unit cell length, and a, b are two empirical parameters.[30] For a given pore diameter and collision rate with the surface the direct mass transfer into the pores strongly decreases with increasing radius of gyration of the molecule.
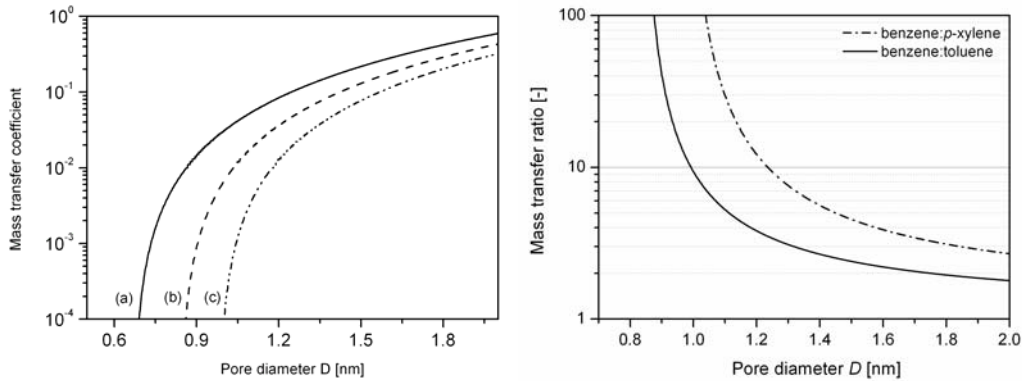
Figure 6.8 **(left) Mass transfer coefficient *k(D)* for adsorption of rigid spheres into circular pores as a function of the pore diameter *D* for benzene (a), toluene (b) and *p*-xylene (c). (right) Mass transfer ratios for successful direct circular pore entering depending on the pore aperture *D*. The solid line indicates the ratio between benzene and toluene and the dash-dotted line the corresponding ratio between benzene and *p*-xylene.**

This size dependency of transport into the overlayer pores can be more clearly seen from the mass transfer ratios $\dot{m}_1 / \dot{m}_2$ between two molecules [30] entering the pores as function of the overlayer pore aperture D (see Figure 6.8). For benzene versus *p*-xylene and benzene versus toluene, a factor of about five and two, respectively, in

the mass transfer ratios is expected, assuming 1.5 nm overlayer pores. This agrees well with the course of the experimental sticking probabilities on the modified material discussed above (see Table 6.3). Further support for our finding is given by the fact that sticking probability and mass transfer coefficient are directly correlated (see Figure 6.9).
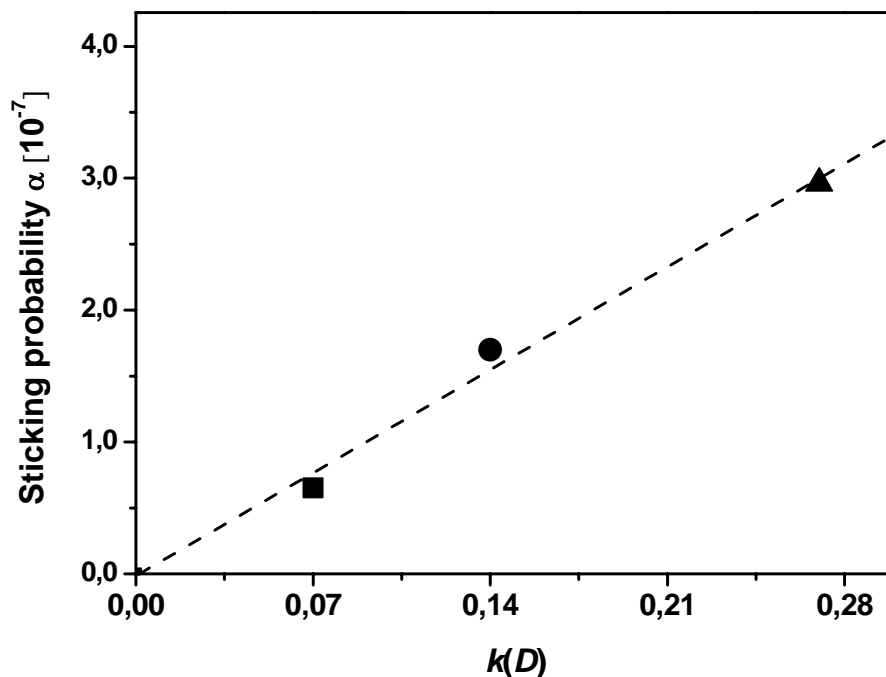
Figure 6.9   **Correlation of the experimental sticking probability α and the theoretical mass transfer coefficient $k(D)$ calculated for an overlayer pore diameter of 1.5nm for the aromatic molecules benzene ($\blacktriangle$), toluene ($\bullet$) and p-xylene ($\blacksquare$) on H-ZSM5-3m.**

Hard sphere collision theory provides a first rational for the course of sorption rates and sticking probabilities, but the differences in the mass transfer ratios are not sufficient to describe the trends quantitatively. Therefore, the transport processes at the interface between overlayer and zeolite core have to be taken into account. For molecules with a given kinetic diameter, the radius of gyration significantly influences the number of statistically favorable orientations with respect to the micropore openings (see Figure 6.11). For molecules with a larger radius of gyration less favorable orientations of the molecule exist, therefore, the reorientation processes aligning the molecule at the pore contributes to a higher loss of molecular entropy. Benzene, with a small radius of gyration of 0.67 nm a reorientation at the pore

openings is not required, while for the larger molecules an additional reorientation becomes necessary as schematically presented in Figure 6.10 for *p*-xylene molecules.
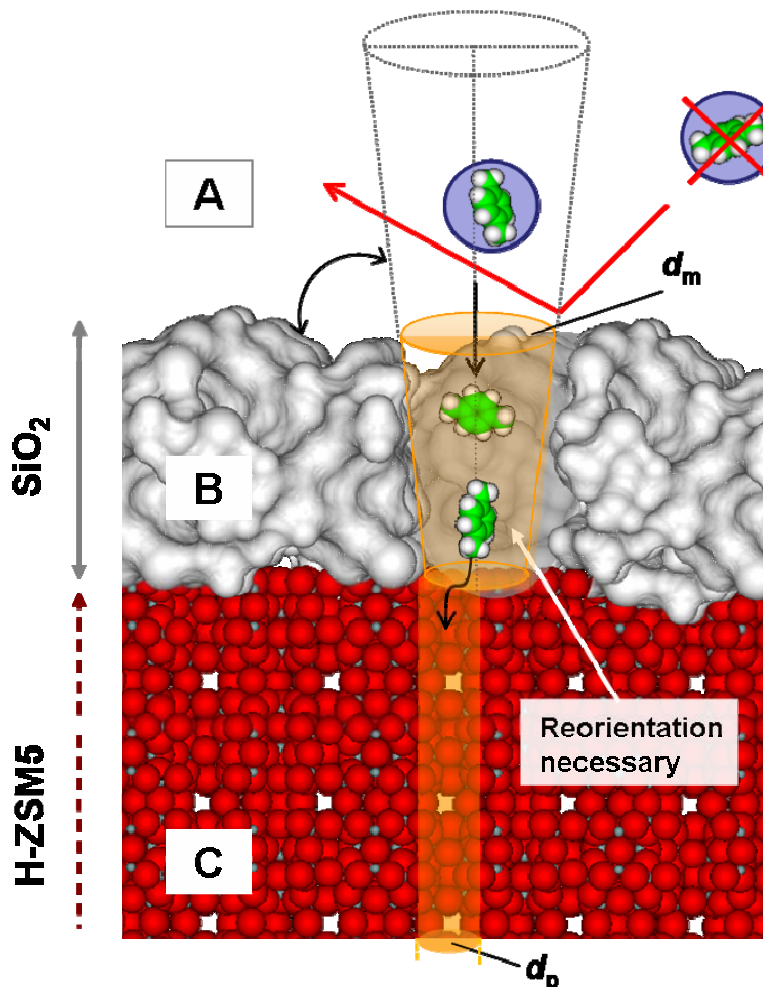
Figure 6.10   **Scheme of a typical H-ZSM5-3m crystal in cross section with silica surface overlayers with average thickness of 3.0 nm. These overlayers contain large micropores with average pore diameter d_m in the range of 1.5 nm, directing the sorbing molecules with appropriate radius of gyration into the micropores of the zeolite. The *p*-xylene molecules, exemplified shown can directly enter the overlayer pores but have subsequently to reorient and align in order to access the zeolite micropores.**

Combining the effects in both interfaces we have theoretically described the transport kinetics with a simplified transport model. In this context, we had to assume that the intra-crystalline and intra-overlayer transport steps are distinctly faster than the pore entering steps. In first approximation we simplified the highly complex transport network of transport steps by using a in steady state kinetic system with two

consecutive steps (see Equation 6.4).[66, 67] The experimental concentration profiles at the bridging hydroxyls for the adsorption step were fitted to these theoretical solutions with the rate constants k_A and k_B describing the process of sticking and entering into the mesopores and the entering into the zeolite micropores, respectively.

$$\text{Gas phase} \xrightarrow{k_A} \text{Overlayer Mesopores} \xrightarrow{k_B} \text{Intracrystalline pore network} \qquad (6.4)$$
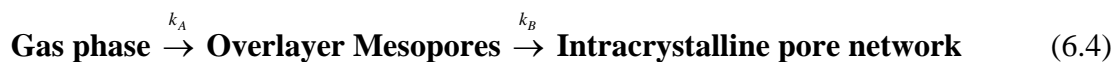
As boundary conditions for the fit both, the already determined mass transfer ratios resulting from the overlayer and the size exclusion factor of unmodified H-ZSM5 were used. The experimental concentration profiles and the sorption rates at bridging hydroxyls of H-ZSM5-p and H-ZSM5-3m could be accordingly reproduced within ± 15 %. The initial rates obtained from this fit yielded an overall rate ratio between benzene and p-xylene of 26, which agrees well with the experimentally expected separation factor of 27. For comparison, the experimental and fitted rates together with the relative deviation are compiled in Table 6.5.
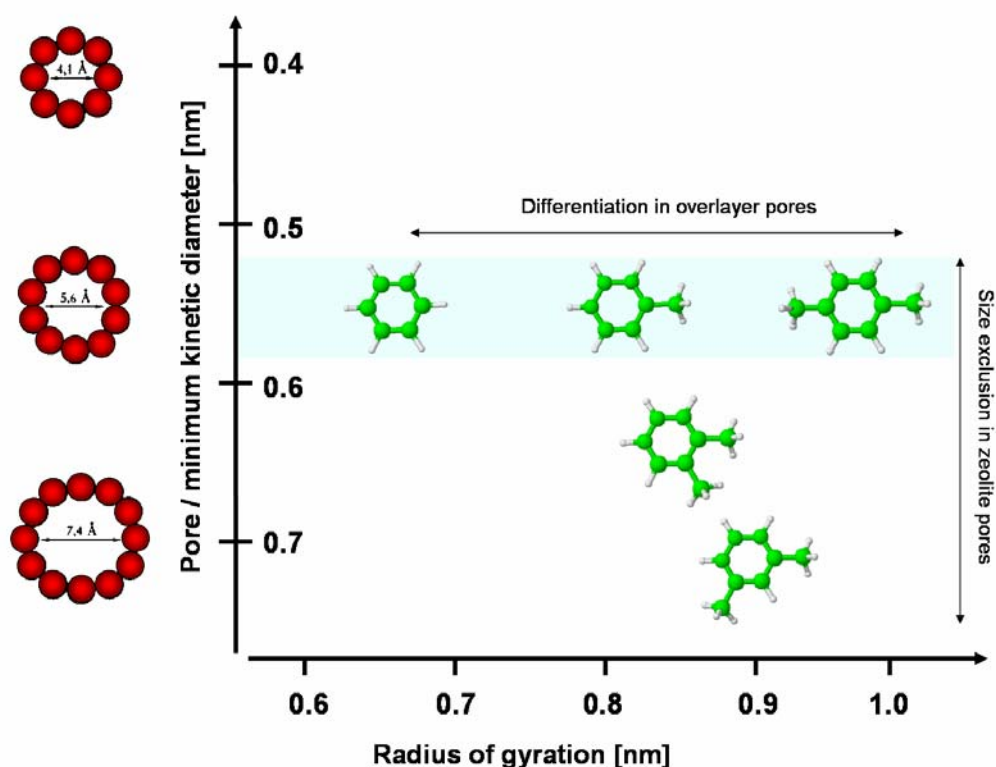
Figure 6.11   Comparison of radius of gyration and minimum kinetic diameter for a series of alkyl-substituted benzene molecules

Table 6.5 **Comparison of the initial rates r_{ini} (RS) at the internal SiOHAl groups calculated from the time-resolved measurements according to Equation 6.1 with those vales obtained from fitting the experimental data to the simplified transport model consisting of two consecutive steps r_{ini} (Model).**

Material	Sorbate	r_{ini} (RS) $[10^{-3}\ s^{-1}]$	r_{ini} (Model) $[10^{-3}\ s^{-1}]$	Deviation [%]
	Benzene	2.34	2.40	3.0
H-ZSM5-p	Toluene	0.96	0.88	8.0
	p-Xylene	0.55	0.58	5.6
	Benzene	6.37	6.63	4.2
H-ZSM5-3m	Toluene	1.68	1.60	5.0
	p-Xylene	0.24	0.27	12.5

Using this simplified model, we propose that the combination between the corrugated surface morphology and the intrinsic size exclusion properties of the zeolite pore structure controls the transport rates from the gas phase to the intra-pore sorption sites and leads to the significantly enhanced separation factor between benzene and *p*-xylene from 4.3 to 27.
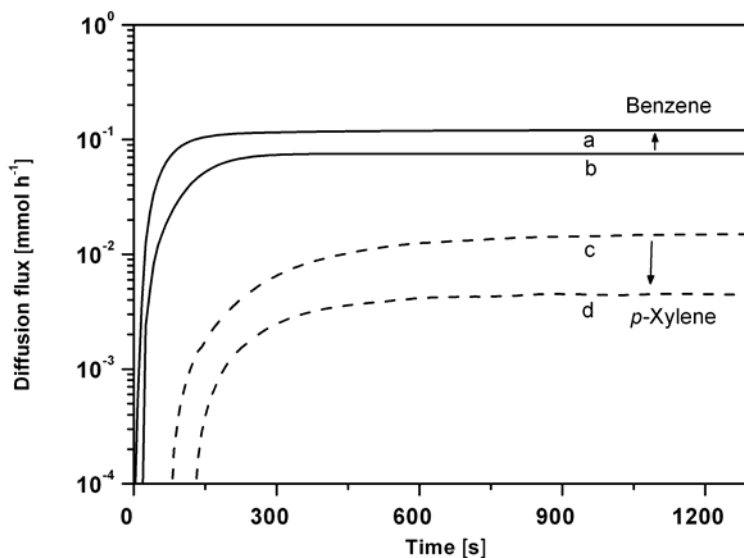
Figure 6.12 **Continuous separation of a 1:1 mixture of benzene and *p*-xylene. Either H-ZSM5-p (b,c) or H-ZSM5-3m (a,d) was subjected to the mixture in a modified Wicke-Kallenbach experiment at 403 K. The equilibrium diffusion flux of benzene (solid lines) and *p*-xylene (dashed lines) gives rise to a distinctly increased separation factor.**

Finally, this increase in the separation factor as deduced from the sorption rate ratios of the aromatic hydrocarbons could be perfectly reproduced experimentally for the continuous separation of a mixture of benzene and *p*-xylene on H-ZSM5-3m as presented in Figure 6.12. The separation measurements were carried out on a modified Wicke-Kallenbach[68, 69] experimental setup, described in detail in Appendix A. Comparison of the detected diffusion flux of benzene and *p*-xylene (mmol h^{-1}), as shown in Figure 6.12, give rise to a distinct separation factor of 27.4 ± 1.8 between both on H-ZSM5-3m. For the unmodified material, a separation factor of 4.7 ± 0.3 was obtained, which is in good agreement to the value of 4.3, estimated from the sorption rate ratios within in-situ time-resolved infrared spectroscopy. The obtained results indicate, hence, the possibility to design porous materials by a combination of pores that accelerate sorption of molecules having a radius of gyration that is below a threshold and at the same time decelerate selectively the sorption of molecules with a larger radius. A well-tailored adjustment of the overlayer porosity should in principle allow to fine tune the sorption rate ratios with regard to enhanced kinetic separation.

6.5 Conclusions

The sorption and transport properties for alkyl-substituted benzene molecules on surface modified H-ZSM5 are primarily controlled by the secondary pore structure with lager pores deposited on the zeolite surface. On modified zeolites the sorption rates to hydroxyl groups inside the pores are strongly entropically controlled. The overall transport process has two contributions the sorption from the gas phase into the porous overlayer and diffusion from the overlayer into zeolite micropores. For the first step, ratio between the pore diameter of the overlayer and the radius of gyration is decisive, while for the seconds step the minimum kinetic diameter and the aspect ratio of the sorbate are the discriminating factors. The radius of gyration affects the total number of reorientations necessary to achieve an entropically advantageous alignment of the sorbate during the sorption process within the surface overlayer, which determines the sticking probability. In combination, both factors can satisfactorily explain the differences in the sorptive properties of alkyl-substituted benzene molecules with respect to the enlarged differences in the transport rates after modification. Consequently, chemically modifying the outer zeolite surfaces opens

novel strategies to improve current industrially relevant separation processes. In contrast to the well-known concept of pore aperture adjustment to enforce shape selectivity by overall retardation of transport processes, well-defined hierarchical overlayer architectures and porosities could be used as a very powerful method for tailoring the separation factors between target molecules with identical minimum kinetic diameter and varying radius of gyration.

6.6 Acknowledgments

6.7 References

[1]   J. Perez-Ramirez, C. H. Christensen, K. Egeblad, C. H. Christensen, J. C. Groen, *Chem. Soc. Rev.* **2008**, *37*, 2530.

[2]   P. R. Pujado, J. A. Rabo, G. J. Antos, S. A. Gembicki, *Catal. Today* **1992**, *13*, 113.

[3]   A. Corma, *Chem. Rev.* **1997**, *97*, 2373.

[4]   J. Weitkamp, *Solid State Ionics* **2000**, *131*, 175.

[5]   M. E. Davis, *Nature* **2002**, *417*, 813.

[6]   J. Dwyer, *Nature* **1989**, *339*, 174.

[7]   B. Smit, T. L. M. Maesen, *Nature* **2008**, *451*, 671.

[8]   A. Corma, *J. Catal.* **2003**, *216*, 298.

[9]   S. M. Csicsery, *Pure Appl. Chem.* **1986**, *58*, 841

[10]   J. Weitkamp, A. Raichle, Y. Traa, M. Rupp, F. Fuder, *Chem. Comm.* **2000**, 1133.

[11]   X. D. Sun, Q. X. Wang, L. Y. Xu, S. L. Liu, *Catal. Lett.* **2004**, *94*, 75.

[12]   S. M. Csicsery, *Zeolites* **1984**, *4*, 202.

[13]   E. Klemm, H. Scheidat, G. Emig, *Chem. Eng. Sci.* **1997**, *52*, 2757.

[14]   P. B. Weisz, *Pure Appl. Chem.* **1980**, *58*, 841

[15]   M. W. Anderson, J. Klinowski, *Nature* **1989**, *339*, 200.

[16]   A. van Miltenburg, W. Zhu, F. Kapteijn, J. A. Moulijn, in *Studies in Surface Science and Catalysis, Vol. 158*, **2005**, pp. 979.

[17]   W. M. Meier, D. H. Olson, *Atlas of Zeolite Structure Types*, Butterworth-Heineman, Boston, MA, **1992**.

[18]   T. Armaroli, M. Bevilacqua, M. Trombetta, F. Milella, A. G. Alejandre, J. Ramirez, B. Notari, R. J. Willey, G. Busca, *App. Catal. A-Gen.* **2001**, *216*, 59.

[19]   J. H. Kim, A. Ishida, M. Okajima, M. Niwa, *J. Catal.* **1996**, *161*, 387.

[20]   S. Zheng, H. R. Heydenrych, H. P. Röger, A. Jentys, J. A. Lercher, *Top. Catal.* **2003**, *22*, 101.

[21]   G. Kokotailo, S. Lawton, D. Olson, W. Meier, *Nature* **1978**, *272*, 437

[22]   F. Eder, J. A. Lercher, *J. Phys. Chem. B* **1997**, *101*, 1273.

[23]   D. Barthomeuf, *Mater Chem Phys* **1987**, *17*, 49.

[24]   R. A. Vansanten, G. J. Kramer, *Chem. Rev.* **1995**, *95*, 637.

[25]   T. Armaroli, L. J. Simon, M. Digne, T. Montanari, M. Bevilacqua, V. Valtchev, J. Patarin, G. Busca, *App. Catal. A-Gen.* **2006**, *306*, 78.

[26]   J. H. Kim, M. Okajima, M. Niwa, *Progress in Zeolite and Microporous Materials* **1997**, *105*, 1965.

[27]   Y. S. Bhat, J. Das, K. V. Rao, A. B. Halgeri, *J. Catal.* **1996**, *159*, 368

[28]   R. W. Weber, K. P. Moller, C. T. O'Connor, *Microp. Mesop. Mat.* **2000**, *35-6*, 533.

[29]   J. Liu, Q. Yang, X. S. Zhao, L. Zhang, *Microp. Mesop. Mat.* **2007**, *106*, 62.

[30]   A. I. Skoulidas, D. S. Scholl, *J. Chem. Phys.* **2000**, *113*, 4379.

[31]   D. M. Ford, E. D. Glandt, *J. Membrane Sci.* **1995**, *107*, 47.

[32]   S. J. Reitmeier, R. R. Mukti, A. Jentys, J. A. Lercher, *J. Phys. Chem. C* **2008**, *112*, 2538.

[33]   J. Kärger, H. Pfeifer, T. Wutscherk, S. Ernst, J. Weitkamp, J. Fraissard, *J. Phys. Chem.* **1992**, *96*, 5059.

[34]   J. Kärger, D. M. Ruthven, *Handbook of Porous Solids* **2002**, *4*, 2089.

[35]   E. Klemm, G. Emig, *Chem. Eng. Sci.* **1997**, *52*, 4329.

[36]   F. R. Ribeiro, F. Alvarez, C. Henriques, F. Lemos, J. M. Lopes, M. F. Ribeiro, *J. Mol. Catal. A - Chemical* **1995**, *96*, 245.

[37]   G. Sastre, N. Raj, C. R. A. Catlow, R. Roque-Malherbe, A. Corma, *J. Phys. Chem. B* **1998**, *102*, 3198.

[38]   U. Schemmert, J. Kärger, J. Weitkamp, *Microp. Mesop. Mat.* **1999**, *32*, 101.

[39]   R. Q. Snurr, A. T. Bell, D. N. Theodorou, *J. Phys. Chem.* **1993**, *97*, 13742.

[40]   L. Song, Z.-L. Sun, L. V. C. Rees, *Microp. Mesop. Mat.* **2002**, *55*, 31.

[41]   S. Brandani, M. Jama, D. M. Ruthven, *Ind. Eng. Chem. Res.* **2000**, *39*, 821.

[42]   L. V. C. Rees, D. M. Shen, in *Studies in Surface Science and Catalysis; Characterization of Porous Solids III, Vol. 87* (Eds.: E. J. P. Feijen, J. A. Martens, P. A. Jacobs), Elsevier B.V., Amsterdam, **1994**, pp. 563.

[43]   S. I. Reshetnikov, S. B. Ilyin, A. A. Ivanov, A. S. Kharitonov, *Reac. Kin. Catal. L.* **2004**, *83*, 157.

[44]   J. Kärger, *Adsorption* **2003**, *9*, 29.

[45]   C. Forste, A. Germanus, J. Karger, H. Pfeifer, J. Caro, W. Pilz, A. Zikanova, *J. Am. Chem. Soc. Faraday T. I* **1987**, *83*, 2301.

[46]   Y. Fu, F. Ye, W. G. Sanders, M. M. Collinson, D. A. Higgins, *J. Phys. Chem. B* **2006**, *110*, 9164.

[47]   H. Tanaka, S. Zheng, A. Jentys, J. A. Lercher, in *Studies in Surface Science and Catalysis; Impact of Zeolites and Other Porous Materials on the New Technologies at the Beginning of the New Millennium, Vol. 142* (Eds.: R. Aiello, F. Testa, G. Giordano), Elsevier B.V., Amsterdam, **2002**, pp. 1619.

[48]   S. R. Zheng, H. Tanaka, A. Jentys, J. A. Lercher, *J. Phys. Chem. B* **2004**, *108*, 1337.

[49]   L. M. Bull, N. J. Henson, A. K. Cheetham, J. M. Newsam, S. J. Heyes, *J. Phys. Chem.* **1993**, *97*, 11776.

[50]   F. Jousse, S. M. Auerbach, D. P. Vercauteren, *J. Phys. Chem. B* **2000**, *104*, 2360.

[51]   M. Schwartz, D. Duan, R. J. Berry, *J. Phys. Chem. A* **2005**, *109*, 8637.

[52]   A. Jentys, H. Tanaka, J. A. Lercher, in *Stud. Surf. Sci. Catal., Vol. 154*, **2004**, pp. 2041.

[53]   A. Jentys, H. Tanaka, J. A. Lercher, *J. Phys. Chem. B* **2005**, *109*, 2254.

[54]   S. J. Reitmeier, O. C. Gobin, A. Jentys, J. A. Lercher, *Angew. Chem. Int. Ed.* **2009**, *48*, 533.

[55]   S. L. Reitmeier, O. C. Gobin, A. Jentys, J. A. Lercher, *Angewandte Chemie-International Edition* **2009**, *(submitted)*.

[56]   S. Zheng, H. R. Heydenrych, A. Jentys, J. A. Lercher, *J. Phys. Chem. B* **2002**, *106*, 9552.

[57]   Y. Yasuda, *Het. Chem. Rev.* **1994**, *1*, 103.

[58]   Y. Yasuda, in *Studies in Surface Science and catalysis; Zeolites and Related Microporous Materials: State of the Art 1994, Vol. 84* (Eds.: E. J. P. Feijen, J. A. Martens, P. A. Jacobs), Elsevier B.V., Amsterdam, **1994**, pp. 1331.

[59]   N. Hansen, in *Towards a new evolutionary computation. Advances on estimation of distribution algorithms* (Eds.: J. A. Lozano, P. Larranaga, I. Inza, E. Bengoetxea), Springer, **2006**, pp. 75.

[60]   R. R. Mukti, A. Jentys, J. A. Lercher, *J. Phys. Chem. C* **2007**, *111*, 3973.

[61]   A. Jentys, R. R. Mukti, H. Tanaka, J. A. Lercher, *Microp. Mesop. Mat.* **2006**, *90*, 284.

[62]   V. R. Choudhary, T. V. Choudhary, *Chem. Eng. Sci.* **1997**, *52*, 3543.

[63]   V. R. Choudhary, V. S. Nayak, T. V. Choudhary, *Ind. Eng. Chem. Res.* **1997**, *36*, 1812.

[64]   S. Zheng, *PhD. Thesis* **2002**.

[65]   D. M. Ford, E. D. Glandt, *J. Phys. Chem.* **1995**, *99*, 11543.

[66]   I. Chorkendorff, J. W. Niemantsverdriet, *Concepts of Modern Catalysis and Kinetics*, 2nd ed., Wiley VCH GmbH, Weinheim, **2007**.

[67]   R. A. van Santen, J. W. Niemantsverdriet, *Chemical Kinetics and Catalysis*, Plenum Press, New York, **1995**.

[68]   W. Kast, C. R. Hohenthanner, *Int. J. Heat Mass Trans.* **2000**, *43*, 807.

[69]   E. Wicke, R. Kallenbach, *Kolloid-Z* **1941**, *97*, 135.

Chapter 7

7. Research outlook

7. Research Outlook

Sorption and transport phenomena of aromatic hydrocarbon reactants have been described in detail in this thesis. The interplay of a variety of transport steps has been identified. In a systematic approach, modification of the external surface of the zeolite, resulting in novel composite materials with hierarchic pore architectures were described as promising tool to tailor hydrocarbon transport properties in a well-defined way . From the single component measurements performed a conceptual new way to separate aromatic hydrocarbon molecules was derived.

Using a modified Wicke-Kallenbach experiment, this concept was confirmed experimentally by separating a binary mixture of *p*-xylene and benzene over surface modified H-ZSM5. These experiments presented in the last part of this thesis can be seen as basis for future design of high performance materials for industrial large-scale applications. Concerning the next possible steps to achieve this goal, two research directions are suggested and shortly mentioned in the following sections: (1) transfer of the deduced separation concepts from aromatic to aliphatic hydrocarbons and (2) investigation of the sorbate-sorbate and sorbate-sorbent interactions in hydrocarbon mixtures over zeolite materials.

7.1   Sorption and transport of aliphatic hydrocarbons

Besides the rigid, aromatic hydrocarbon molecules studied in this thesis, aliphatic hydrocarbons being flexible and able to change their conformational state upon sorption or reaction are of high petrochemical interest with respect to aliphatic separation, alkylation or isomerization reactions. Testing the applicability of the transport network and transfer of the concept from the aromatic reactants to aliphatic becomes thus necessary. Microporous materials with regular pore and modified surface properties and deposited pore architectures will provide an ideal target for a systematic experimental approach. In analogy to the aromatic hydrocarbons, the influences of sorbate type, size and zeolite material on the transport steps have to be explored primarily. Despite the well known fact, that sorption processes in the confined spaces of zeolite pore networks depend crucially on the length dimensions of the sorbates,

these phenomena are still hardly understood on a molecular level, especially for flexible chain-like sorbate molecules.

Experimental differentiation between the energetic and entropic contributions will represent a challenging task for future research projects. Therefore, systematic series of transport measurements with hydrocarbons of either (1) increasing chain length, such as in the C_3 to C_6 series of propane, n-butane, n-pentane and n-hexane or (2) of increasing degree of substitution, such as for the series of n-hexane isomers appear to be a promising starting point. The proposed experiments could not only be beneficial for the optimization of selected large-scale industrial processes but also enlarge the fundamental physicochemical knowledge about transport under reaction conditions. In the next step, the sorbate-sorbate interactions between different hydrocarbons in hydrocarbon mixtures and the tailoring of separation factors should be explored.

7.2   Investigation of realistic hydrocarbon mixtures

Having already indicated that post-treatment of microporous materials might be industrially exploited to enhance separation factors within kinetic separation according to the molecular radius of gyration. Nevertheless, additional experiments are mandatory to further develop and establish high performance sorbents. In a first step, new generation of hierarchic composite materials, e.g., zeolites or zeolite-related materials with adjusted surface overlayer architectures and gradually decreasing pore diameter seem to be a promising target. It should be noted, that for flexible chain-like molecules with increasing length, the calculation of the corresponding radii of gyration is challenging. Furthermore, the complexity in realistic reactant mixtures increases strongly non-linear with the total number of components, thus a step-wise approach to realistic conditions is most convenient. Based on the knowledge derived from single component measurements with aromatic compounds, simple binary hydrocarbon mixtures, either aliphatic/aromatic or aromatic/aromatic are currently subject of research. Exemplified, some most recent infrared spectroscopic results for a n-butane/benzene mixture are given as final outlook.

7.3   FTIR of benzene/*n*-butane mixtures on H-ZSM5 - a first step

Dealing with *in-situ* infrared spectroscopic studies, successful derivation of kinetic information will crucially depend on the choice of the reactants within the binary mixture. On one hand, transport of both hydrocarbons should be observable on the time-scale of the volume modulation experiment. On the other hand, both components adsorbed to the hydroxyl sites of the zeolite have to be distinguished simultaneously via clearly separated bands in the infrared spectra.
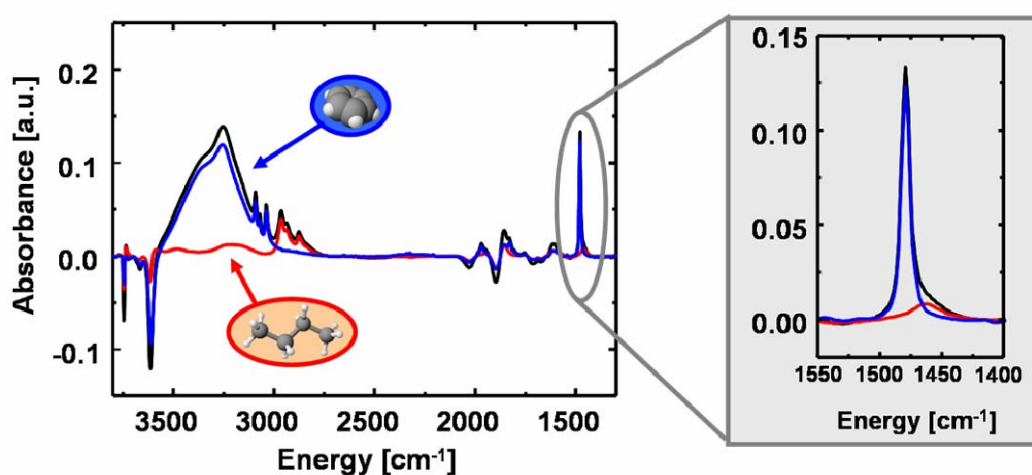
Figure 7.1   **IR spectrum of a *n*-butane/benzene mixture (with 0.1 mbar each) adsorbed on H-ZSM5 at 373K. The insert shows the overlapping C-C vibrational bands of benzene and *n*-butane.**

Note that particularly the partial pressures have to be chosen in an appropriate range to follow both uptake processes at the same time. Binary mixtures of *n*-butane and benzene of varying composition on H-ZSM5 have been chosen as first test system. Both sorbates can be sufficiently differentiated by infrared spectroscopy either via the characteristic C-H stretching or C-C stretching / deformation vibrational bands for quantification. Depending on the pressure range, overlapping of the vibrational bands occurs but can be treated by peak deconvolution methods. A typical infrared spectrum of the investigated mixture at 373 K together with the single component infrared spectra at the corresponding sorbate partial pressures of 0.1 mbar are given in Figure

7.1. This example underlines the complexity of experimental approaches and data evaluation when trying to follow the transport of several species within hydrocarbon mixture instead of a single component. As a first result, a significant reduction of the transport rates of benzene (the bulkier hydrocarbon component) was found in the 1:1 mixture compared to pure benzene at identical conditions, while transport of butane was hardly changed (see Figure 7.2). Such a marked competition effect in the mixture on the bulkier component would not be expected at first sight and needs to be further investigated on a molecular level..
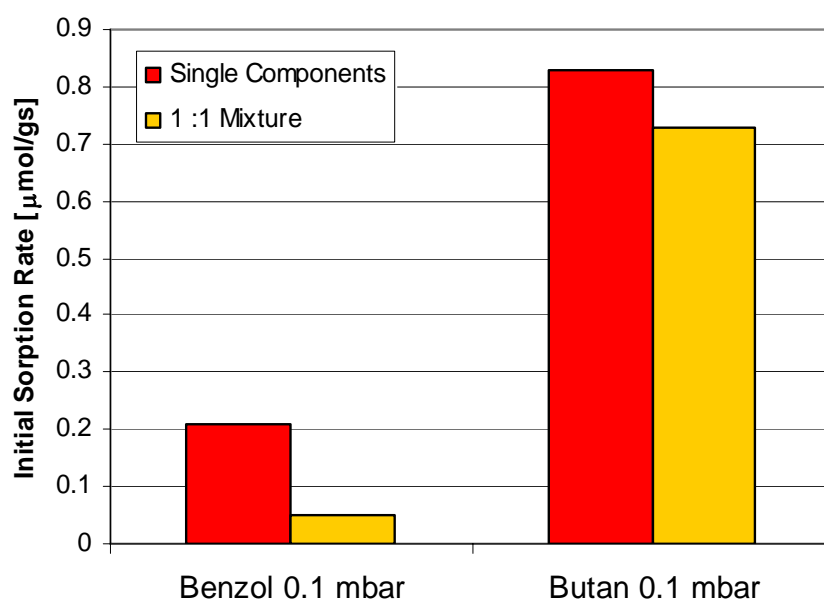
Figure 7.2   **Comparison of the initial sorption rates for benzene and n-butane either as pure component or binary mixture at 373 K.**

In order to give a concise explanation for this effect, further experimental efforts will have to be performed with different compositions of the mixture, different aliphatic hydrocarbon molecules (C_3 to C_6) at varying temperatures and partial pressures. Several topics are thus imaginable for future research projects extending the presented transport studies towards multi-component systems. Desirably, a profound understanding of hydrocarbon transport under reaction conditions might finally enable the *a-priori* design of sorbents and catalysts with pre-defined properties for a given industrial purpose without empirical material development.

Chapter 8

8. Summary

8.1   Concluding summary

Molecular sieves and porous solid acids in general represent key components as catalyst material, catalyst support or sorbent material for a huge variety of industrial applications. A detailed understanding of sorption and shape selective transport of hydrocarbon reactant molecules is thus crucial to their further usage in heterogeneous catalysis or sorptive separation. The present dissertation thesis is scientifically situated at the interface of physical chemistry, technical chemistry and chemical engineering, covering the investigation of the fundamental phenomena of hydrocarbon transport, sorption as well as diffusion in zeolite materials. Combining infrared spectroscopy, statistical thermodynamics and general knowledge about heterogeneous catalysis, the first part of the thesis provides deeper insight into the molecular basis of the interconnected transport steps and the underlying kinetic mechanisms. The second part subsequently deals with the optimization of the zeolite properties by surface modification, a promising new tool to generate highly selective sorbents and catalysts with significantly improved properties.

For this thesis, the experimental focus was set on the class of MFI-type zeolites because of their unique structural properties with a three-dimensional, intersecting channel system. The size of the pores is furthermore similar to the dimensions of industrially relevant aliphatic and aromatic hydrocarbon molecules, i.e., benzene or *p*-xylene. In particular, zeolite HZSM-5, one of the frequently used industrial zeolites at present was selected and subjected to a series of alkyl-substituted benzene molecules. On one side, H-ZSM5 is already commonly used as highly selective catalyst for the production of *para*-substituted aromatic products with respect to the otherwise thermodynamically limited distributions of product isomers. This is achieved by applying the principles of classical shape selectivity and molecular traffic control: The reactants with size similar to the pore dimensions are hereby differentiated during the reaction inside the pore network according to their minimum kinetic dimensions. In order to fine-tune the shape selective properties of a given reaction, post-synthetic treatment, such as modification of the external catalyst surface, the surface morphology and porosity by chemical deposition techniques using tetraethyl orthosilicate, or advanced pre-coking methods have increasingly emerged. It can be

stated, that there exist huge industrial demand for high performance solid acids catalysts and sorbents having the potential to replace currently utilized, expensive or toxic large scale processes. Despite enormous experimental efforts sorption and diffusion phenomena and their interplay in zeolites are still not understood at a molecular level due to the large heterogeneity of the materials synthesized which vary strongly in literature. In order to achieve the increasing requirements for novel materials within modern material science and design, a complete description of the either energetically or entropically driven interactions of the reacting hydrocarbons with the catalyst, including all possible sorption, transport and subsequent intra-pore transfer pathways are unambiguously important. However, this knowledge represents a fundamental prerequisite in order to synthesize new molecular sieves with improved transport properties.

Therefore in the first part of this thesis, the elementary steps of how aromatic molecules adsorb on H-ZSM5 surfaces and how they are being transported from the gas phase through the sub-nanometer wide pores to the active sites were systematically addressed. The relatively rigid alkyl-substituted aromatic molecules - benzene, toluene, *o*- and *p*-xylene - were specifically chosen to simplify the kinetic problem and aiming to obtain a generalized and unified transport model for MFI-type zeolites. A combination of *in-situ* infrared spectroscopy, providing an excellent signal-to-noise ratio and high time resolution with the pressure frequency response method to study intra-crystalline transport, have been chosen as major experimental tools. The micro-kinetic steps occurring at the hydroxyl sites of the zeolite, either located at the surface or inside the pores were monitored with a resolution of milliseconds and the whole transport network was unraveled. The overall transport process is subdivided into five e.g., consecutive or parallel elementary steps, including (1) population of a highly mobile, physisorbed surface state, (2) surface and (3) intra-pore transport pathways and also (4, 5) sorption at the hydroxyl sites. The collision of the reactants with and the trapping of the aromatic sorbates on the external surface of unmodified H-ZSM5 crystals represent the preliminary transport step. Based on the *in-situ* infrared spectroscopic measurements, an experimental measure, the so called sticking probability of the sorbates was derived. In analogy to the surface of non-porous amorphous silica, which was investigated in comparison, very low values in the order

of 10^{-7} were obtained for the aromatic molecules studied. The characteristic non-linear trend, with *p*-xylene showing the highest and toluene the lowest sticking probability, was explained by the subtle interplay of three intrinsic factors: (1) the symmetry of the sorbate, (2) the molecular size dimensions of the sorbate, which defines the corresponding space occupied on the zeolite surface and also (3) the possibility for the impinging molecules to accommodate their enthalpy of adsorption on the surface, are of crucial importance. Possible artifacts arising from the sample preparation as self-supporting wafers were excluded by comparing the transport behavior of the sorbates either on pressed or powdered samples using the frequency response. Theoretical support and rationalization for the low experimental values was given by a statistical thermodynamics approach. Detailed evaluation of the elementary contributions to the molecular partition functions of the sorbates during the sorption process gave rise to a theoretical measure of the sticking probability. The loss of rotational degrees of freedom and thus rotational entropy of the molecules upon sorption was found to govern the sticking process. A higher amount of entropy conserved leads to more favorable sorption and thus a higher sticking probability. These explanations are perfectly in line with the existence of a weakly bound surface state which precedes sorption to the surface or intra-pore hydroxyls.

Based on the knowledge obtained for the complex transport network, the influences of specific *de-novo* modifications of the external material surface by chemical liquid deposition of tetraethyl orthosilicate on the interplay of the individual transport steps was subject of interest of the second part of the thesis. For the transport measurements described, a series of hierarchically structured composite materials based on H-ZSM5 was utilized. Transmission electron microscopy indicated that those composites combine distinct silica overlayers having pores in the range of 1.5 nm (evidenced by nitrogen physisorption), with the inherent micropore structures of zeolite H-ZSM5. The silica deposition significantly altered the surface morphology but, what is remarkable, did not block larger portions of the channels by reducing their accessibility. While conventional surface silanization leads to passivation of pore-near unselective sites and to exclusion of bulky reactants from the pore network with respect to their minimum kinetic dimensions to increase catalytic selectivities (e.g., in toluene disproportionation), herein a radically different approach was followed. For the

first time a highly selective increase in the uptake rates of an individual molecular species (i.e., by 200 % for benzene) at the intra-pore active sites of the molecular sieve was found, contrary to an overall retardation of the transport processes. Frequency response measurements further underlined this finding. The reported enhancement effect was directly linked to the increase in the sticking probability on the modified samples and explained through a more gradual loss of rotational entropy within the overlayer porosity compared to sorption on a flat zeolite surface. Sorbates are somewhat favorably captured at the interface between solid surface (i.e., silica overlayer) and gas phase by the funnel structure of the silica overlayer. This leads to the expectation that separation of aromatic hydrocarbons could benefit from the novel composite materials. As main prerequisite in this context, the effective size of the molecule (radius of gyration, given by the longest molecular dimension) needs to be sufficiently smaller than the overlayer pores. From the conceptual point of view, a gradual increase in the size of the gas phase molecule should at some point inverse the advantageous funnel effect of the overlayer pores.

To further elucidate this phenomenon within the last part of this thesis, toluene and *p*-xylene were subjected to the hierarchical material. The expected inversion of the enhancement could be perfectly evidenced by experimentally: benzene sorption had strongly benefited (rate increase by 200 %) from the overlayer pores, toluene (by 70%) in reduced strength, whereas for *p*-xylene even strong retardation (by 60 %) of the transport process was found either by in-situ infrared spectroscopy or frequency response. Consequently the rate differences observed at the internal hydroxyl sites and thus the kinetic separation factors between the aromatic molecules were dramatically enlarged despite the identical minimum dimensions of the sorbates. The relation of the radius of gyration of the sorbate to the overlayer pore diameter determined the transport into the overlayer pores. The observed mass transfer directly correlated with the sticking probability, which is governed by the entropically advantageous alignment of the molecules during sorption within the silica overlayer. The more formerly free gas phase rotations are hindered, the stronger the mass transfer into the overlayer declines. Further differentiation of the molecules that had entered the overlayer pores occurred at the zeolite micropores with respect to the aspect ratio of the sorbate. Having identical minimum dimension but increasing aspect ratio, entrance to the

microporous zeolite is further retarded in this step. The observed trends in the sorbate uptake rates within the series of alkyl-substituted benzene molecules showed a significant increase in the rate ratio between benzene and *p*-xylene and thus the kinetic separation factor from four to twenty seven. This finding opens totally novel strategies to improve industrially relevant separation processes by well-adjusted surface modification procedures.

Summarizing, the practical applicability of this concept, deduced from single component sorption rates, for aromatic hydrocarbon separations in general was successfully indicated by the continuous separation of binary aromatic hydrocarbon mixtures following a modified Wicke-Kallenbach approach. The fact, that for benzene and *p*-xylene mixtures subjected to the modified zeolite samples, a separation factor of around twenty seven was found, which is in perfect agreement to the sorption rate ratios, strongly emphasized the importance of the findings. The post-synthetically surface modified H-ZSM5 zeolites presented herein can be seen among the first examples of novel composite materials with hierarchical overlayer architectures and porosities to be utilized in hydrocarbon separation processes. These materials give a primary hint to the potential of well-defined overlayer architectures, possibly enlarging the existing "tool box" of material science and in the future enabling to fine-tune separation factors for any given purpose.

Nevertheless, additional investigations are needed to understand the complex behaviour of multi-component sorption and transport in zeolite catalysts and to further expand the reported concepts e.g., to aliphatic hydrocarbon separation. These efforts have already been initiated by the described Wicke-Kallenbach experiments and by *in-situ* infrared spectroscopic measurements with binary aliphatic-aromatic hydrocarbon mixtures on H-ZSM5. Summarizing all findings, it can be stated, that the identified molecular network of transport steps, the differentiation of hydrocarbon transport by distinct post-synthetically generated overlayer architectures and their utilization for hydrocarbon separation, represent the fundamental basis or promising starting point for future material design.

8.2   Abschließende Zusammenfassung

Poröse Festkörperkatalysatoren, Zeolithe und Molekularsiebe stellen Schlüssel-Komponenten für eine Vielzahl industrieller Anwendungen im Bereich der heterogenen Katalyse und Stofftrennung dar. Folglich ist ein detailliertes Verständnis der Sorption und des Transports von aliphatischen und aromatischen Kohlenwasserstoffmolekülen von entscheidender Bedeutung für eine spätere, erfolgreiche technische Anwendung dieser Materialien. Die vorliegende Arbeit ist daher an der Schnittstelle von physikalischer und technischer Chemie, sowie chemischer Verfahrenstechnik angesiedelt und umfasst die Untersuchung der Phänomene des Oberflächentransports, der Sorption sowie der Diffusion von Kohlenwasserstoffen. Als Hauptzielsetzung soll im ersten Teil der Arbeit durch die Kombination moderner Infrarotspektroskopie, grundlegender Kenntnisse der heterogenen Katalyse sowie statistischer Thermodynamik ein tieferer Einblick in die elementaren Transportschritte auf molekularer Ebene erreicht werden. Der zweite Teil der Arbeit befasst sich mit der gezielten Optimierung der verwendeten Zeolithmaterialien durch post-synthetische Oberflächenmodifikation. Diese stellt ein vielversprechendes, neues Werkzeug im Bereich der Materialwissenschaften dar, um hochselektive Katalysatore und Sorbentien mit verbesserten Eigenschaften gezielt herzustellen.

Der experimentelle Fokus dieser Arbeit liegt auf Zeolithen des MFI-Strukturtyps. Diese zeichnen sich vor allem durch ihre strukturellen Eigenschaften mit einem dreidimensionalen Kanalsystem mit sich kreuzenden Kanälen und Porendurchmessern im Bereich der Größenordnung aromatischer Kohlenwasserstoffe aus. Zeolith HZSM-5, einer der großtechnisch vielfältig genutzten Zeolithe wurde im Speziellen ausgewählt und hinsichtlich des Transportverhaltens einer Reihe alkyl-substituierter aromatischer Moleküle näher untersucht. Einerseits wird H-ZSM5 als hochselektiver Katalysator für die Erzeugung *para*-substituierter aromatischer Produkte ausgehend von deren thermodynamisch limitierten Verteilung verwendet. Die Präferenz für *para*-Produkte lässt sich dabei durch die klassischen Prinzipien der Formselektivität erklären. Produktmoleküle, werden dabei während der Reaktion innerhalb des Porensystems gemäß ihren minimalen, kinetischen Durchmessern

differenziert. Diese Eigenschaft führte in der Folge zur Entwicklung zahlreicher Verfahren zur post-synthetischen Modifizierung der äußeren Katalysatoroberfläche sowie der effektiven Porendurchmesser um die Eigenschaften der Materialien weiter zu optimieren. Dazu zählen z.B. die Gasphasen- oder Flüssigphasenabscheidung von SiO_2 ausgehend von Tetraethylorthosilikat (TEOS).

Auf der anderen Seite steigt die industrielle Nachfrage nach alternativen Konzepten und neuen Hochleistungsmaterialien für die effektive Trennung von Kohlenwasserstoffgemischen stetig mit dem Ziel an, oftmals teure und giftige Prozesse zunehmend zu ersetzen. Trotz enormer experimenteller Anstrengungen ist das Zusammenspiel von Sorption und Transport bisher auf molekularer Ebene nicht vollständig verstanden. Um jedoch die zunehmenden Anforderungen, die Materialwissenschaften an moderne Katalysatormaterialien und Sorbentien stellen, erfüllen zu können ist ein vollständiges Verständnis der energetischen und entropischen Wechselwirkungen der Reaktanden mit dem Katalysator unabdingbar. Dies schließt die genaue Kenntnis aller möglichen Sorptions- und Transportpfade an der Oberfläche und innerhalb des Porensystems und an der Oberfläche mit ein. Dies liegt vor allem an der großen Heterogenität der, in der Literatur beschriebenen Katalysatormaterialien. Ein detailliertes Verständnis der Elementarschritte stellt die grundlegende Vorraussetzung dar, um neue Molekularsiebe mit verbesserten Transporteigenschaften zu realisieren.

Die Reihe der aromatischen Moleküle, Benzol, Toluol, *p*- und *o*-Xylol, wurde ausgewählt um im ersten Teil der Arbeit das Transportnetzwerk systematisch zu untersuchen. Die Auswahl der verhältnismäßig starren Moleküle erlaubte es, unter Vernachlässigung möglicher Konformationsänderungen der Moleküle während der Sorption, ein vereinfachtes, vereinheitlichtes Transportmodell für H-ZSM5 zu entwickeln. Die Kombination von *in-situ* Infrarotspektroskopie mit hoher Zeitauflösung und exzellentem Signal-zu-Rausch Verhältnis und der Frequenz-Antwort-Methode bietet die experimentelle Möglichkeit simultan mikrokinetische Transportschritte an den Hydroxylgruppen sowohl der Oberfläche als auch in den Poren zu verfolgen. Der gesamte Transportprozess von der Gasphase zu den aktiven Zentren lässt auf mikroskopischer Ebene in fünf konsekutive bzw. parallele Elementarschritte, darunter (1) der Transport an der Oberfläche und (2) innerhalb der

Poren, (3) die Population eines mobilen, physisorbierten Oberflächenzustands sowie (4,5) die Sorption an den aktiven Zentren unterteilen. Für unmodifizierten H-ZSM5 (Si/Al = 45) konnte das Haften der starren, aromatischen Moleküle nach dem Stoß mit der äußeren Oberfläche als primärer Transportschritt identifiziert werden. Die zugehörige Haftwahrscheinlichkeit der Moleküle wurde mittels *in-situ* IR-spektroskopischen Messungen experimentell bestimmt. Mögliche Artefakte die durch das, der Messung vorausgehende Pressen der Materialien hervorgerufen werden und die erhaltenen Ergebnisse beeinflussen könnte, wurden durch Vergleichsmessungen an pulverförmigen und gepressten Proben mittels der Frequenzantwort-Methode ausgeschlossen.

Sowohl für H-ZSM5 als auch für amorphes Siliziumdioxid, welches als nichtporöses Vergleichsmaterial fungierte, wurden sehr kleine Werte für die Haftwahrscheinlichkeiten im Bereich von 10^{-7} berechnet. Der beobachtete Trend innerhalb der Reihe der aromatischen Moleküle, mit dem höchsten Wert für *p*-Xylol und dem niedrigsten Wert für Toluol beruht auf dem Zusammenspiel dreier Einflussfaktoren: Neben (1) der Symmetrie sind (2) die Ausmaße der Moleküle, welche den Platzbedarf an der Oberfläche definieren und zuletzt (3) die Fähigkeit der Moleküle die bei Stoß und Sorption freiwerdende Energie zeitnah auf innere Freiheitsgrade zu verteilen von entscheidender Bedeutung. Unter Verwendung statistisch-thermodynamischer Überlegungen wurden die niedrigen experimentellen Haftwahrscheinlichkeiten zusätzlich theoretisch untermauert. Die detaillierte Auswertung individueller Beiträge zur molekularen Rotationszustandssumme vor und nach der Sorption lieferte ein theoretisches Maß für die Haftwahrscheinlichkeit des Moleküls. Der Verlust von molekularen Rotationsfreiheitsgraden und damit von Rotationsentropie während der Sorption bestimmt den Sorptionsprozess. In direkter Konsequenz führt ein geringerer Entropieverlust zu einer deutlich erhöhten Haftwahrscheinlichkeit des Moleküls. Diese, aus der statistischen Thermodynamik abgeleitete Erklärung steht in Einklang mit der Existenz des zuvor postulierten, physisorbierten Zustands der Sorbatmoleküle. Dieser geht der Sorption an den terminalen Hydroxylgruppen des Zeoliths und dem Poreneintritt der Sorbatmoleküle voraus und ist mit stark eingeschränkten (gehinderten) Rotationsfreiheitsgraden verbunden.

Basierend auf der genauen Kenntnis des kompletten Netzwerks individueller Transportschritte, befasst sich der weitere Teil der Arbeit mit der Erforschung des Einflusses von post-synthetischen Modifikationen der externen Katalysatoroberfläche auf das Zusammenspiel der einzelnen Transportschritte. Für die spektroskopischen Messungen wurde dazu eine Serie hierarchisch strukturierter H-ZSM5 Materialien verwendet. Durch elektronenmikroskopische Messungen (TEM) konnte das Vorhandensein einer amorphen aber porösen Siliziumdioxid-Schicht auf der äußeren Katalysatoroberfläche der modifizierten H-ZSM5 Kristallite eindeutig nachgewiesen werden. Eine Charakterisierung mittels Stickstoff-Physisorption ergab einen effektiven Porendurchmesser von ca. 1.5 nm für die Poren der Siliziumdioxidschicht. Die Modifikation führt somit zwar zu einer signifikanten Veränderung der Oberflächenmorphologie der H-ZSM5 Kristallite, aber nicht zu einer vollständigen Blockierung großer Teile der Porenöffnungen des darunter liegenden Kanalsystems von H-ZSM5.

Konventionelle Verfahren zur Oberflächenmodifikation setzen zur Steigerung von katalytischen Selektivitäten auf die Passivierung unselektiver, aktiver Zentren nahe der Porenöffnungen sowie den Ausschluss sterisch anspruchsvoller Reaktanden vom Porengefüge, in Abhängigkeit von deren minimalen kinetischen Durchmessern (klassische Formselektivität, z.B. bei der Disproportionierung von Toluol). Im Gegensatz dazu wurde im Rahmen dieser Arbeit ein vollkommen anderer Ansatz verfolgt, die Differenzierung von Sorbatmolekülen mittels oberflächenmodifizierter Materialien basierend auf dem Gyrationsradius anstelle des minimalen kinetischen Durchmessers. Zum ersten Mal überhaupt wurde eine selektive Erhöhung der Sorptionsraten einer individuellen molekularen Spezies, mit fast 200 % für Benzol, an den internen Zentren eines Molekularsiebs gefunden. Diese experimentellen Befunde konnten zusätzlich zur zeitaufgelösten Infrarotspektroskopie auch über weitere Transportmessungen mittels der Frequenzantwort-Methode gestützt werden.

Die beobachtete Erhöhung der Sorptionsraten hängt direkt mit dem Anstieg der Haftwahrscheinlichkeiten der Moleküle an oberflächenmodifiziertem H-ZSM5 zusammen. Dieser resultiert aus einem deutlich geringeren und zugleich schrittweisen Verlust der Rotationsentropie der Gashasenmoleküle innerhalb der Poren der Siliziumdioxid-Schicht verglichen mit dem unmodifizierten Zeolith. Sorbatmoleküle

werden durch die Schicht sozusagen direkt an der Grenzfläche von Gasphase und Festkörperoberfläche eingefangen und zu den darunter liegenden Mikroporen des Zeoliths geleitet. Dies legt den Schluss nahe, hierarchisch-strukturierte Materialien zur Trennung aromatischer Kohlenwasserstoffe ausnutzen zu können. Als wichtigste Vorrausetzungen muss dazu die effektive Größe der Moleküle, definiert durch die maximale Längendimension in der Gasphase, deutlich kleiner sein als der Durchmesser der Poren. Konzeptionell bedeutet dies jedoch, dass durch schrittweise Vergrößerung der Sorbatmoleküle z.B. durch zusätzliche Seitengruppen, der positive Effekt der Poren der Siliziumdioxidschicht, vergleichbar mit dem Einfangen der Moleküle der Gasphase wie in einem Trichter, kontinuierlich verringert werden sollte. Um dieses Phänomen experimentell zu bestätigen, wurden abschließend Toluol und *p*-Xylol in gleicher Weise hinsichtlich ihres Transportverhaltens an modifiziertem H-ZSM5 untersucht. Der erwartete Effekt konnte experimentell eindeutig belegt werden: Während Benzol wie beschrieben noch signifikant von der amorphen Schicht profitiert hatte (Steigerung der Sorptionsrate um 200 %), beobachtet man dies nur noch in viel geringerem Maße für Toluol (70 %). Im Falle des *p*-Xylols wurde sogar eine deutliche Verlangsamung des Transportprozesses gefunden (um 60 %). In Kombination bewirkt dies eine starke Zunahme des Verhältnisses der individuellen Sorptionsraten für Benzol zu *p*-Xylol an den internen Hydroxylgruppen von vier auf siebenundzwanzig. Trotz gleicher minimaler kinetischer Durchmesser der Moleküle wurden die kinetischen Trennfaktoren an oberflächenmodifiziertem H-ZSM5 deutlich gesteigert.

Es zeigte sich, dass das Verhältnis von Gyrationsradius des Moleküls (definiert durch die maximale Länge) zum Porendurchmesser in der Oberflächenschicht entscheidend für den direkten Transport aus der Gasphase in die Zeolithporen ist. Der beobachtete Massentransport lässt sich direkt mit der Haftwahrscheinlichkeit am modifizierten Material korrelieren, welche in charakteristischer Weise von der entropisch günstigen Ausrichtung der Sorbatmoleküle innerhalb der Schicht abhängt. Je mehr die zuvor freien Gasphasenrotationen des Moleküls bei der Sorption in den Poren der Schicht behindert werden, umso geringer ist der direkte Stofftransport und der dem Eintritt der Moleküle in das Gefüge der Zeolithporen. Eine weitere Differenzierung der Sorbatmoleküle in Abhängigkeit ihres Längenverhältnisses erfolgt in Analogie zum unmodifizierten Material über die Mikroporen des Zeoliths. Im Falle

identischer minimaler Durchmesser und zunehmender Moleküllänge führt dies zu einer weiteren Verlangsamung des Transports zu den aktiven Zentren. Die beschriebenen Trends und Sorptionsraten innerhalb der Reihe der alkyl-substituierten Aromaten eröffnen neue experimentelle Wege um industriell relevante Trennprozese gezielt durch Oberflächenmodifikation der Materialien zu optimieren. Eine praktische Anwendbarkeit für die selektive Trennung aromatischer Kohlenwasserstoffe konnte durch erste Messungen mit einem modifizierten Wicke-Kallenbach Aufbau und Kohlenwasserstoffmischungen gestützt werden. Für den Fall einer binären Benzol/*p*-Xylol-Mischung wurde für oberflächenmodifizierten H-ZSM5 ein Trennfaktor von siebenundzwanzig bestimmt. Dies steht in sehr guter Übereinstimmung mit dem über die Verhältnisse der Sorptionsraten der Einzelkomponenten erwarteten Wert.

Zusammenfassend sei herausgestellt, dass die Möglichkeit der Steigerung von Trennfaktoren zwischen Molekülen gleichen minimalen Durchmessers ein vollkommen neues Konzept darstellt. Bisher bekannte Methoden der Anpassung von effektiven Porendurchmessern zur Erhöhung der formselektiven Eigenschaften der Materialien führten im Ergebnis immer zu einer generellen Verlangsamung des Transports aller beteiligten Reaktanden. Die im Rahmen dieser Arbeit vorgestellten, hierarchisch-strukturierte Materialien liefern einen ersten Hinweis auf das große Potential das ein gezieltes Maßschneidern der Trenneigenschaften von Zeolithen durch das Aufbringen poröser Oberflächenschichten besitzen könnte. Um dies zu praktisch zu realisieren und um die generellen Konzeptideen auf industriell gefragte Trennprozesse unter Beteiligung aliphatischer Kohlenwasserstoffe zu übertragen, ist jedoch eine weitere Erforschung der Sorptions- und Transportphänomene in komplexen Kohlenwasserstoffmischungen notwendig. Als Ausgangspunkt könnten dabei die beschriebenen Wicke-Kallenbach-Experimente und erste zeitaufgelöste infrarotspektroskopische Messungen mit einem *n*-Butan/Benzol-Gemisch an H-ZSM5 gesehen werden. Abschließend ist festzuhalten, dass die Aufklärung des molekularen Transportnetzwerks für H-ZSM5, die Beschreibung der Steigerung von Sorptionsprozessen und die damit verbundene Möglichkeit zur Differenzierung von Kohlenwasserstoffen mittels definierter Oberflächenschichten auf mikroporösen Materialien die grundlegende Basis für ein zukünftiges *a-priori* Design von Katalysatormaterialien darstellen wird.

Appendices

Appendix A

A. Wicke-Kallenbach Method

A.1 Wicke-Kallenbach setup – Apparatus design

Intending to give a first proof of principle for the concepts and implications of the hierarchic overlayer architectures derived in chapter 7, the continuous separation between hydrocarbons in a binary mixture over the surface modified H-ZSM5 materials was studied. Therefore, a modified Wicke-Kallenbach approach was applied.

A.1.1 General background

In general, the Wicke-Kallenbach method has first been invented by Wicke and Kallenbach et al.[1] to experimentally determine effective diffusion D_{eff} coefficients of reactants in porous materials with tortuous and intersecting pore networks. The experimental setup utilized, denoted classical Wicke-Kallenbach setup in the following, consist of a gas cell composed of two connected compartments, which are separated by the sample material in form of a pressed pellet or membrane. The Wicke-Kallenbach cell design is illustrated schematically in Figure A1.
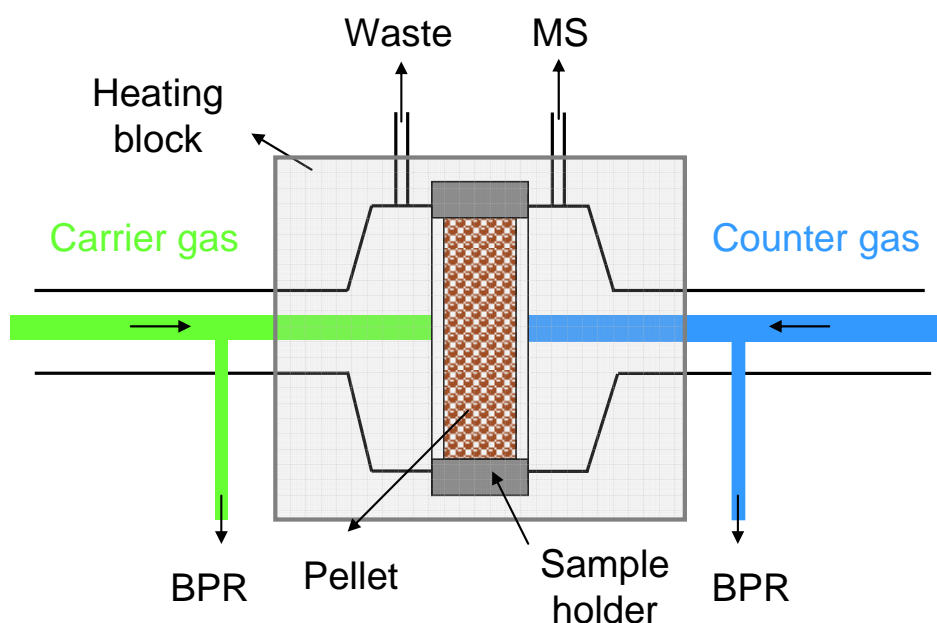
Figure A.1   **Scheme of the classical Wicke-Kallenbach cell design.**

Having two separate gas flows on both sides of the sample allows injecting a target reactant with well-defined concentration into one of the flows (carrier gas) and

detection of the uptake of the reactant in the second gas flow (counter gas) as function of time. The uptake profiles observed are characteristic for the transport properties of the pore network of the sample and allow deriving the desired effective diffusion coefficients. Therefore, detailed knowledge about the sample porosity, precise thickness and diameter are mandatory. Analogously, by injecting a mixture of reactants with known composition into the carrier gas flow and following the respective uptake profiles for each reactant in the counter gas flow with time, the separation factor of the material is accessible via the simultaneously detected equilibrium diffusion flows.

A.1.2 Experimental setup

A home-built experimental setup representing a modified version of a classical Wicke-Kallenbach design[1] is schematically shown in Figure A.2 and was used for the separation experiments within this thesis.
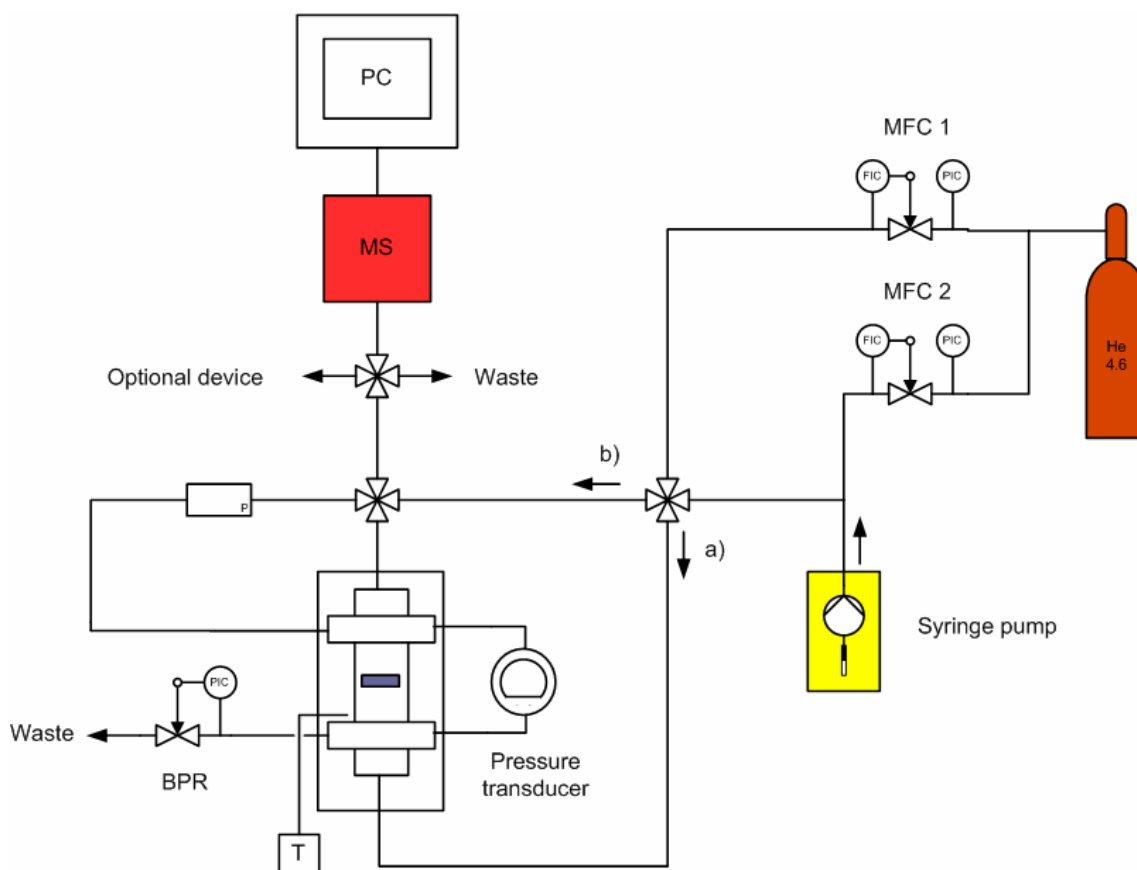
Figure A.2   Experimental Wicke-Kallenbach experimental setup

The Wicke-Kallenbach cell with sample holder is located in a heating block to adjust the temperature in a temperature range of 300 – 443 K via a Eurotherm® 2640 controller. The temperature range achievable herein was limited by the main sealing used to ensure completely independent cell compartments. Helium (Air-Liquide, He 4.6) was used as carrier gas. Two independent gas flows pass the sample pellet at both sides, which can be either directed to a mass spectrometer (MS, Pfeiffer Prisma QMS100) to be analyzed or to the waste for optional bypass measurements. The gas flow rates in the range of 5 - 100 ml min^{-1} were controlled with two calibrated Bronckhorst mass flow controller (MFC 1, 2) via a FlowView V1.09 communication. To ensure that the pressure on both sides of the cell was equal and to exclude additional convectional mass transport, a pressure transducer and a back pressure regulator (BPR) were used. In order to inject small amounts of liquid mixtures (e.g., aromatic hydrocarbons) into the carrier gas flow, the system was equipped with a syringe pump (adjusted for 100 μl syringe). The online monitoring of the actual composition of the counter gas flow was performed with the mass spectrometer.

A.2 Wicke-Kallenbach separation measurements – Experimental

Separation measurements with benzene, toluene and *p*-xylene at 403 K were performed on a modified, home-build Wicke-Kallenbach experimental setup described above. As carrier and counter gas flows, helium (He 4.6 from Air Liquide) with constant flow rate of 50 ml min^{-1} was used. The pressure on both sides of the sample cell was atmospheric and identical. A detailed description of the Wicke-Kallenbach method and underlying theoretical principles can be found elsewhere in great detail.[1-3] The H-ZSM5 samples under study (approximately 20 mg) were pressed into a stainless steel sample holder of 13 mm diameter and placed inside the Wicke-Kallenbach cell. Benzene, toluene and *p*-xylene as obtained from Sigma-Aldrich/Fluka in spectroscopic grade with purity > 99.6 % was used without further purification. The 1:1 molar mixtures of benzene and *p*-xylene, or benzene and toluene were injected into the carrier gas flow using a syringe pump system with a constant flow rate of 30 μl h^{-1}. The relation between flow rate of the carrier gas flow and the syringe pump injection rate was optimized prior to the separation measurements within calibration experiments with the single components.

Detection and quantification of the individual diffusion flux of benzene, toluene and *p*-xylene in the counter gas flow were carried out with a Pfeiffer QMS100 mass spectrometer, based on the respective ion intensities of the fragments at m/z 78 and 91, respectively. Calibration measurements with the individual components were performed using the identical helium flow of 50 ml min^{-1} and varying injection flow rates of the syringe pump in the range of 10 to 30 µl h^{-1}. A blank measurement without zeolite sample was further used to eliminate possible experimental artifacts originated from the syringe pump system and the Wicke-Kallenbach apparatus itself.

Comparison of the detected diffusion flux of benzene and *p*-xylene (mmol h^{-1}), in the counter gas flow, as shown in Figure 6.12, give rise to a distinct separation factor of 27.4 ± 1.8 between both sorbates on modified H-ZSM-5. For the unmodified material, a separation factor of 4.7 ± 0.3 was obtained, which is in good agreement to the value of 4.3, estimated from the sorption rate ratios within *in-situ* time-resolved infrared spectroscopic measurements. For benzene and toluene, separation factors of 2.3 ± 0.2 for the unmodified and 3.1 ± 0.3 for the modified material were determined. These values also agree well to the sorption rate ratios.
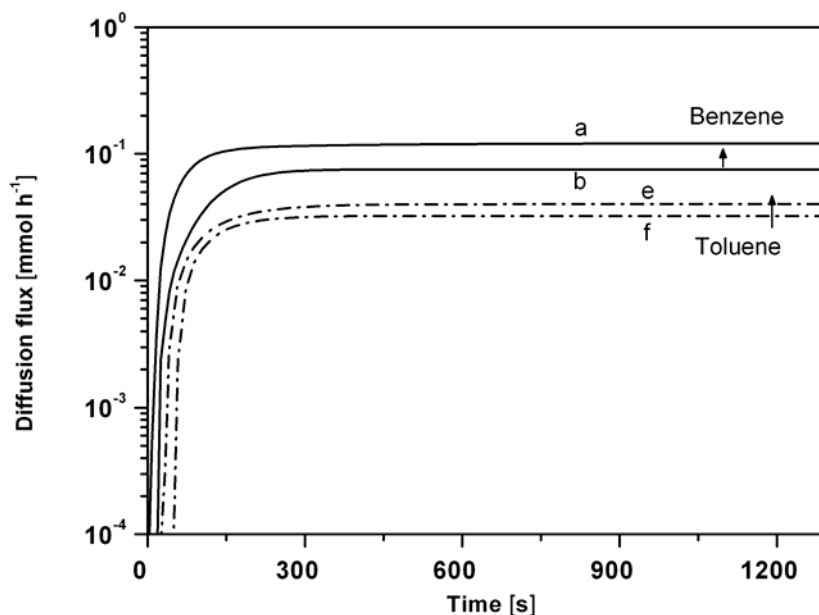
Figure A.3   **Continuous separation of a 1:1 mixture of benzene and toluene. Either unmodified (b,f) or modified (a,e) H-ZSM-5 was subjected to the mixture in a modified Wicke-Kallenbach experiment at 403 K. The equilibrium diffusion flux of benzene (solid lines) and toluene *(*dashed lines) give rise to a slightly increased separation factor.**

A.3 References

[1]   E. Wicke, R. Kallenbach, *Kolloid-Zeitschrift* **1941**, *97*, 135.

[2]   K. Soukup, P. Schneider, O. Solcova, *Chem. Eng. Sci.* **2008**, *63*, 4490.

[3]   K. Soukup, P. Schneider, O. Solcova, *Chem. Eng. Sci.* **2008**, *63*, 1003.

Appendix B

B. **Determination of phase lag and amplitude of periodic functions**

B.1 General Fourier Transformation

The Fourier transformation formalism is essential for every modern spectroscopic application i.e., the infrared spectroscopy.[1, 2] The fundamental expression in mathematics which relates the time and the frequency information of a system is the Fourier transform.[3]

$$f(\omega) = \int_{-\infty}^{\infty} f(t) \cdot e^{i\omega t} dt \tag{B.1}$$

Herein $f(t)$ represents the time domain data and $f(\omega)$ is the required frequency spectrum. It is noted, that this Equation, being an integral of complex numbers, for practical cases needs to be evaluated using efficient numerical algorithms.

B.2 Determination of frequency response parameters

Periodic functions in the time domain t can mathematically be expressed as the series of harmonic sinusoidal terms using the angular frequency ω and the order of the harmonic term k (harmonic order). For the case of a frequency response experiment, the system volume is e.g., excited periodically with a rectangular excitation function resulting in a periodic response of the system.[4-6] The excitation function can be described as a Fourier series $E(t)$ of the following form:

$$E(t) = \frac{4}{\pi} \cdot \sum_{k=1,3,5}^{\infty} \frac{1}{k} \cdot \sin(k\omega t) \tag{B.2}$$

Accordingly, the response of the system pressure $R(t)$ can be written as function of the frequency response parameters phase lag φ_k and the pressure amplitude P_k of the kth harmonic term, which can be subsequently derived via Fourier transformation.

$$R(t) = \sum_{k=1,3,5}^{\infty} P_k \cdot \sin(k\omega t + \varphi_k) \tag{B.3}$$

Therefore $R(t)$ is rearranged using trigonometric addition theorems, resulting in:

$$R(t) = \sum_{k=1,3,5}^{\infty} P_k \cdot \cos(\varphi_k) \cdot \sin(k\omega t) + \sum_{k=1,3,5}^{\infty} P_k \cdot \sin(\varphi_k) \cdot \cos(k\omega t) \tag{B.4}$$

By comparing Equation B.4 with the general definition of the Fourier expansion of $R(t)$, the characteristic Fourier coefficients a_k and b_k can be directly related to the frequency response parameters of interest.

$$a_k = P_k \sin(\varphi_k) \tag{B.5}$$

$$b_k = P_k \cos(\varphi_k) \tag{B.6}$$

Further rearrangements and substitution of Equation B.5 into B.6 yield the phase lag φ_k and amplitude P_k in the following form.

$$P_k = \sqrt{a_k^2 + b_k^2} \tag{B.7}$$

$$\varphi_k = \arctan\left(\frac{a_k}{b_k}\right) \tag{B.8}$$

The respective Fourier coefficients, needed for the calculation can be mathematically determined from the pressure response $R(t)$ via Fourier transformation.

$$a_k = \frac{\omega}{\pi} \cdot \int_{-\pi/\omega}^{\pi/\omega} R(t) \cdot \cos(k\omega t) dt \tag{B.9}$$

$$b_k = \frac{\omega}{\pi} \cdot \int_{-\pi/\omega}^{\pi/\omega} R(t) \cdot \sin(k\omega t) dt \tag{B.10}$$

For the purpose of this thesis, only the first harmonic term was evaluated within the frequency response measurements yielding the first order characteristic functions δ_{1C} and δ_{1S}, respectively. The higher harmonics (k = 1, 3, 5, ... ∞) of the pressure response were neglected, as the signal-to-noise ratio of the pressure recording did not allow a more detailed analysis.[4]

B.3 References

[1]   M. Hesse, H. Meier, B. Zeeh, *Spektroskopische Methoden in der organischen Chemie*, 5 ed., Georg Thieme Verlag, Stuttgart, New York, **1995**.

[2]   H. Günzler, H.-U. Gremlich, *IR spectroscopy*, WILEY-CVCH Verlag Weinheim, **2002**.

[3]   F. Reif, *Fundamentals of Statistical and Thermal Physics*, 20 ed., McGraw-Hill Book Company, Singapore, **1988**.

[4]   H. R. Heydenrych, University of Cape Town (Cape Town, Munich), **2000**.

[5]   Y. Yasuda, *Heterogeneous Chemistry Reviews* **1994**, *1*, 103.

[6]   Y. Yasuda, in *Zeolites and Related Microporous Materials: State of the Art 1994, Vol. 84*, **1994**, pp. 1331.

B.3 References

Appendix C

C. Analysis of mass transfer limitations during FTIR measurements

C.1   Analysis of external mass transfer limitations

It is intended to emphasize at this point, that the experimental rapid scan results given within chapter four to six were to the best of our knowledge free of experimental artifacts as well as mass transfer limitations generated e.g., by a complete blockage of a whole fraction of the zeolite pore network due to the silica overlayer architectures. Using conventional post-synthesis modification techniques, a partial blockage of pore openings would be expected.[1] To ensure the accessibility of the full zeolite micropore volume and thus of all potentially available SiOHAl groups after the modification, the uptake changes $\Delta c_{eq,\text{OH}}$ (according to the typical pressure difference of the rapid scan experiment) and the theoretically expected uptake Δc_{OH} were compared. The latter were calculated from the corresponding infrared sorption isotherms within these pressure limits of the time-resolved infrared spectroscopic measurements (see Figure 5.6). The results of the calculations are compared within Figures C.1 and C.2 for either the terminal SiOH as well as bridging SiOHAl sites of H-ZSM5. It is clearly illustrated, that the experimental and theoretical values are in very good agreement.
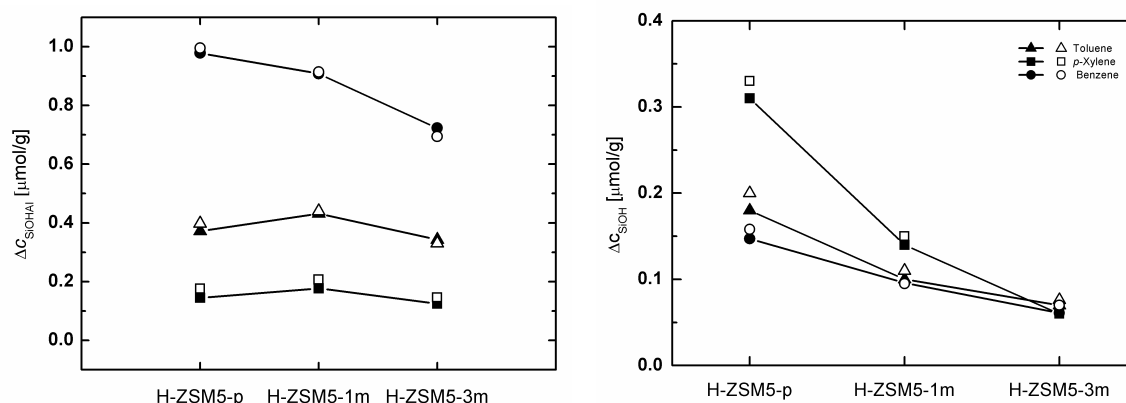
Figure C.1   **Comparison of the equilibrium coverage changes $\Delta c_{\text{eq,OH}}$ (full symbol) on the SiOHAl groups (left) and SiOH groups (right) for benzene ($\bullet$, $\bigcirc$), toluene ($\blacktriangle$, $\triangle$), and *p*-xylene ($\blacksquare$, $\square$) during a time-resolved measurement. The system pressure was modulated around 0.06 mbar. Open symbols represent theoretical coverage changes estimated from the corresponding sorption isotherm data at 403 K.**

The below mentioned correlation of the thermodynamically expected and the experimentally measured coverage changes for all sorption processes, samples, sorbate molecules and active sites resulted in a straight line with a slope of 1.04, presented in

Figure C.2. It can be stated, that the trends found in the initial sorption rates to the internal hydroxyls of the H-ZSM5 samples were not generated by a lower total concentration of accessible sites or blocked pore openings. The deviations of the data points represented by the error bars given within Figure C.2 were calculated using the RMS-errors obtained from fitting the concentration change profiles or the isotherms.
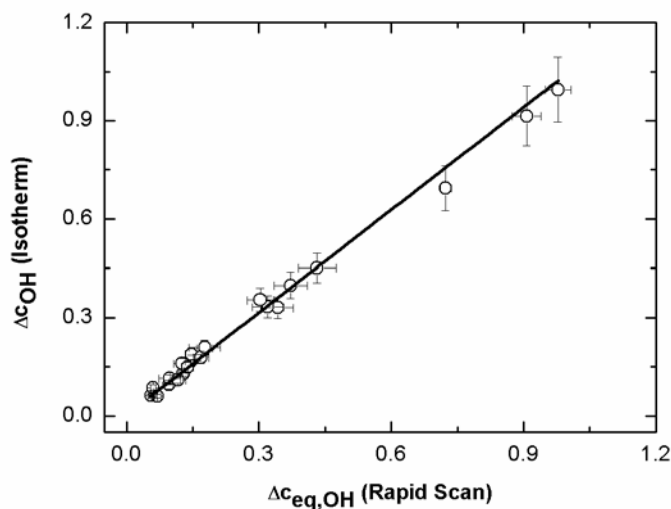
Figure C.2 **Correlation of experimental ($\Delta c_{eq,OH}$) and thermodynamic coverage changes (Δc_{OH}) for the series of aromatic sorbate molecules on H-ZSM5-p, -1m and -3m at 403K. The least-square fit of the data (RMS-error minimized) resulted in a straight line with a slope of 1.04, confirming that the data gathered by equilibrium thermo-dynamics is in perfect agreement to the dynamic experiments.**

Additional evidence for the absence of external limitations has already been given within chapter four by comparing the transport processes of the aromatic sorbates benzene, toluene and *p*-xylene in zeolite H-ZSM5 using the frequency response and the samples in powder or pressed IR wafer form.[2, 3]

C.2 References

[1] S. R. Zheng, H. Tanaka, A. Jentys, J. A. Lercher, *J. Phys. Chem. B* **2004**, *108*, 1337.

[2] S. J. Reitmeier, R. R. Mukti, A. Jentys, J. A. Lercher, *J. Phys. Chem. C* **2008**, *112*, 2538.

[3] S. J. Reitmeier, R. R. Mukti, A. Jentys, J. A. Lercher, *J. Phys. Chem. C* **2009**, *113*, 1640.

List of figures

Chapter 3

Chapter 6

Appendices

Appendix A

Appendix C

List of tables

Chapter 5

Chapter 6

Short Curriculum Vitae – Stephan J. Reitmeier

Stephan J. Reitmeier was born in Ingolstadt a. D., Germany, on June 24th 1980. After accomplishing his high school education at the Apian Gymnasium Ingolstadt in June 2000, he received a student scholarship for studies in natural sciences by the Studienstiftung des Deutschen Volkes. In October 2000, he started his studies in Chemistry at the Technische Universität München and graduated as chemist in 2005 (Diplom, Dipl.Chem. Univ.) with excellent grades. For his diploma thesis in 2005 he joined the research group of Prof. Martin K. Beyer at the Chair of Physical Chemistry 2 at the Technische Universität München, dealing with the topic of gas phase transition metal and water cluster reactions followed by mass spectrometry. His thesis is entitled "Reactivity and thermochemsitry of transient species in water clusters" and was awarded with the Jürgen-Manchot-Studienpreis given by the Jürgen-Manchot Foundation and the Technische Universität München. In September 2005 he joined the research group of komm. Prof. Olav Schiemann for one year and worked at the interface between Physical Chemistry, Biophysical Chemistry and Biophysics at the Johann-Wolfgang-Goethe Universität Frankfurt and the Technische Universität München. The project was entitled "Investigation of the structure-dynamic-function relationships in DNA-based nanomagnets and RNR-type enzymes using electron paramagnetic resonance spectroscopy".

In 2006 he received a PhD scholarship by the Studienstiftung des Deutschen Volkes and started his PhD thesis supervised by Prof. Johannes A. Lercher at the Chair of Technical Chemistry 2 at the Technische Universität München, which he currently finishes. Between October 2007 and April 2008 he attended the South German Catalysis Institute in Ulm with certificate. His research comprises the investigation of the fundamental elementary processes of sorption and transport of hydrocarbon molecules on molecular sieves. He focussed his research on zeolite H-ZSM5 as target catalyst and precisely investigates the influences of external surface modifications by post-synthesis methods on the catalytic performance using advanced *in-situ* infrared spectroscopy and the frequency response technique. Besides his academic research, Stephan J. Reitmeier has acquired profound experiences in academic education as lecture assistant for several practical as well as theoretical courses in Physical and Technical Chemistry.

Publications

2006   Stephan J. Reitmeier, O. Petru Balaj, Vladimir E. Bondybey and Martin K. Beyer *"Reactions of hydrated electrons $(H_2O)_n^-$ with formic acid"*, *Int. J. Mass Spect.* **2006**, *249-250*, 106-111

2007   Chi-Kit Siu, Stephan J. Reitmeier, Iulia Balteanu, Vladimir E. Bondybey, and Martin K. Beyer *"Substrate Poisoning in the Catalytic Conversion of CO and N_2O to CO_2 and N_2 on Pt_4^- in the Gas Phase"*, *Eur. Phys. J. D*, **2007**, 43, 189

2007   Stephan J. Reitmeier, Rino R. Mukti, Andreas Jentys and Johannes A. Lercher *"Surface transport processes and sticking probability of aromatic molecules in HZSM-5"*, *J. Phys. Chem. C,* **2008***, 112, 2538 – 2544*

2008   Stephan J. Reitmeier, Andreas Jentys and Johannes A. Lercher, *"Experimental and theoretical investigation of the sticking probability of benzene, toluene and o-/p-xylene on amorphous SiO_2 and HZSM-5"*, Zeolites and related materials – trends, targets and challenges in *Studies in Surface Science and Catalysis* **2008**, Vol. 174 A, p. 585 – 590, Proceedings of the 4th European FEZA Conference

2009   **(a)** Stephan J. Reitmeier, Oliver C. Gobin, Andreas Jentys and Johannes A. Lercher *"On the enhancement of sorption processes on HZSM-5 by post synthetic surface modification"*, *"Angew. Chem. Int. Ed.,* **2009***, 48*, 533 – 538,

          (b) Stephan J. Reitmeier, Oliver C. Gobin, Andreas Jentys and Johannes A. Lercher *"On the enhancement of sorption processes on HZSM-5 by post synthetic surface modification"*, *"Angew. Chem.,* **2009***, 121*, 541 - 546

2009   O. Petru Balaj, Christian B Berg, Stephan J Reitmeier, Vladimir E Bondybey and Martin K. Beyer *"A Novel Design of a Temperature Controlled FT-ICR Cell for Low-Temperature Black-Body Infrared Radiative Dissociation (BIRD) Studies of Hydrated Ions"*, *Int. J. Mass Spec.,* **2009***, 279, 5 - 9*

2009   Oliver C. Gobin, Stephan J. Reitmeier, Andreas Jentys and Johannes A. Lercher *"Diffusion pathways of benzene, toluene and p-xylene in MFI"*, *Microp. Mesop. Mat.,* **2009**, *125*, 3-10 (**Invited article**)

2009   Stephan J. Reitmeier, Andreas Jentys and Johannes A. Lercher *"Understanding transport in MFI-type zeolites on a molecular basis to enhance well-defined tailoring of shape selectivity"*, Book-Title: *"Ideas in Chemistry and Molecular Sciences, Advances in Nanotechnology, Materials and Devices (Vol.3)",* Editor: Prof. B. Pignataro, Wiley-VCH Verlag, Weinheim (**Invited book chapter**)

2009   Stephan J. Reitmeier, Oliver C. Gobin, Andreas Jentys and Johannes A. Lercher *"Influence of post-synthetic modification on transport processes of aromatic molecules in HZSM-5"*, *J. Phys. Chem. C* (**in press**)

2009   Stephan J. Reitmeier, Oliver C. Gobin, Andreas Jentys and Johannes A. Lercher *"Hierarchically structured microporous materials separate aromatic molecules based on their radius of gyration"*, *Angew. Chem.,* (**submitted**)

2009   Oliver C. Gobin, Stephan J. Reitmeier, Andreas Jentys and Johannes A. Lercher *"Comparison of the transport of aromatic compounds in small and large MFI particles"*, *J. Phys. Chem. C,* 2009, (**submitted***)

Conference Contributions I – Posters

1. <u>S. J. Reitmeier</u>, O. P. Balaj, M. Gruber, V. E. Bondybey, and M. K. Beyer, *Temperature-resolved black-body radiation induced reactivity of hydrated vanadium cations $V(H_2O)_n^{+}$*, CNF-Symposium, 2005, Bad Herrenalb, Deutschland

2   O. P. Balaj, I. Balteanu, <u>S. J. Reitmeier</u>, G. Kummerlöwe, Z. Sun, T. J. Roßteuscher, V. E. Bondybey, and M. K. Beyer, *Adsorption and catalytic conversion of CO to CO_2 on gas phase platinum clusters,* CNF-Symposium, 2005, Bad Herrenalb, Deutschland

3. <u>S. J. Reitmeier</u>, G. Clever, T. Carell, O. Schiemann, „*Investigation of magnetic coupling between Cu^{2+} centers in DNA using EPR spectroscopy*", Instituts-Symposium TU München 2006, Garching, Deutschland

4. R. R. Mukti, <u>S. J. Reitmeier</u>, A. Jentys and J. Lercher, *Transport and sticking probability of aromatic molecules in medium-pore zeolites*, 19. Deutsche Zeolithtagung, 2007, Leipzig, Deutschland

5. R. R. Mukti, <u>S. J. Reitmeier</u>, A. Jentys and J. Lercher, *Sorption and orientation of alkyl-substituted aromatic molecules in the pores of MFI zeolites"* 19. Deutsche Zeolithtagung, 2007, Leipzig, Deutschland

6. <u>S. J. Reitmeier</u>, G. Clever, T. Carell, O. Schiemann, „*Investigation of the magnetic coupling J between Cu^{2+} centers in novel synthesized artificial DNA using EPR spectroscopy*", GDCh Wissenschaftsforum 2007, Ulm, Deutschland

7. <u>S. J. Reitmeier</u>, R. R. Mukti, A. Jentys and J. A. Lercher, *"Transport of aromatics in medium-pore zeolites",* GDCh Wissenschaftsforum 2007, Ulm, Deutschland

8. <u>S. J. Reitmeier</u>, R.R. Mukti, A. Jentys and J. A. Lercher, *"Sticking probability of aromatic molecules on HZSM-5 and SiO_2 – an experimental and theoretical approach",* 20. Deutsche Katalysetagung 2008, Weimar, Deutschland

9. <u>S. J. Reitmeier</u>, A. Jentys and J. A. Lercher, *"Effects of post synthetic surface modification on the sorption processes of aromatic molecules in HZSM-5",* 20. Deutsche Zeolithtagung, 2008, Halle a.d. Saale, Deutschland **(Poster-Award)**

10. <u>S. J. Reitmeier</u>, O. C. Gobin, A. Jentys and J. A. Lercher, *"Influences of surface modification by CLD of TEOS on the intracrystalline diffusion of aromatic molecules in HZSM-5",* 20. Deutsche Zeolithtagung, 2008, Halle a.d. Saale, Deutschland

11. <u>O. C. Gobin</u>, S. J. Reitmeier, A. Jentys and J. A. Lercher, *"Measuring diffusion in zeolites by pressure frequency response",* 20. Deutsche Zeolithtagung, 2008, Halle a.d. Saale, Deutschland

12. <u>S. J. Reitmeier</u>, R. R. Mukti, A. Jentys and J. A. Lercher, *"Experimental and theoretical investigation of the sticking probability of benzene, toluene and o-/p-xylene on amorphous SiO_2 and HZSM-5",* 4th FEZA Conference, 2008, Paris, Frankreich

13. S. J. Reitmeier, O. C. Gobin, A. Jentys and J. A. Lercher, *"On the transport processes in nanopores", NanoCat meeting,* 2008, München, Deutschland

14. S. J. Reitmeier, O. C. Gobin, A. Jentys and J. A. Lercher, *"Influences of surface modification on shape selective properties of HZSM-5 studied by transport processes of aromatic molecules",* 4th FEZA Conference, 2008, Paris, Frankreich

15. S. J. Reitmeier, R.R. Mukti, A. Jentys and J. A. Lercher, *"On the influences of external surface modification on sorption of aromatic molecules in the pores of HZSM-5",* 2nd EUCHEMS Chemistry Congress, 2008, Turin, Italien (**Award: Invited book article**)

16. S. J. Reitmeier, G. Clever, T. Carell, O. Schiemann, „*Towards bio-inspired nanomagnets – EPR spectroscopic study of the magnetic coupling between Cu^{2+} centers in artificial DNA*" Chemical Nanotechnology Talks IX, Bio meets Nano 2008, Frankfurt a. M., Deutschland

17. S. J. Reitmeier, O. C. Gobin, A. Jentys, J. A. Lercher, „*Enhancement of intra-crystalline transport by surface modification as novel concept in separation technology*" 21. Deutsche Zeolithtagung, 2009 Kiel, Deutschland

18. S. J. Reitmeier, M. Zeilinger, A. Jentys, J. A. Lercher, „Transport behaviour of light aliphatics C3 to C6 studied on H-ZSM5 studied by time-resolved infrared spectroscopy" 21. Deutsche Zeolithtagung 2009, Kiel, Deutschland

19. S. J. Reitmeier, M. Zeilinger, A. Jentys and J. A. Lercher, *"Sorption and transport in binary butane-benzene mixtures on HZSM-5 studied by time-resolved infrared spectroscopy", 21.* Deutsche Katalysetagung 2009, Weimar, Deutschland

20. S. J. Reitmeier, O. C. Gobin, A. Jentys and J. A. Lercher, *"Enhancement of intra-crystalline transport processes by post-synthetic modification – benefit for separation technology", 21.* Deutsche Katalysetagung 2009, Weimar, Deutschland

21. O. C. Gobin, S. J. Reitmeier, A. Jentys and J. A. Lercher, *"Sorption and transport processes of hexane isomers in H-ZSM-5 with surface modification", 21.* Deutsche Katalysetagung 2009, Weimar, Deutschland

22. O. P. Balaj, C. B. Berg, S. J. Reitmeier, V. E. Bondybey, M. K. Beyer, *"Design and performance of a temperature controlled FT-ICR cell for low temperature BIRD studies of water clusters"* 108. Bunsentagung 2009, Köln, Deutschland

23. S. J. Reitmeier, O. C. Gobin, M. Hölzel, T. Fuess, W. W. Schmahl, A. Jentys and J. A. Lercher, *"Construction of a novel sample environment for the activation of catalyst samples for neutron powder diffraction experiments",,* FRM-2 User-Meeting 2009, Garching, Deutschland

24. S. J. Reitmeier, O. C. Gobin, A. Jentys and J. A. Lercher, *"Surface modification of zeolites as novel approach to enhance separation of hydrocarbons",* GDCh Wissenschaftsforum 2009, Frankfurt, Deutschland

25. S. J. Reitmeier, O. C. Gobin, A. Jentys and J. A. Lercher, *"Sorption and transport in binary butane-benzene mixtures on HZSM-5 studied by infrared spectroscopy",* GDCh Wissenschaftsforum 2009, Frankfurt, Deutschland

Conference Contributions II – Talks

1. <u>S. J. Reitmeier,</u> V. E. Bondybey and M. K. Beyer, „*Temperature-resolved BIRD reactivity of hydrated vanadium cations*" Cluster-Treffen, CNF-Symposium, 2005, Bad Herrenalb, Germany

2. <u>S. J. Reitmeier,</u> A. Jentys and J. Lercher, "*Surface processes and sticking probability of aromatic molecules on HZSM-5*", project meeting, DFG-Research group, Zeolitic Diffusion, 2007, Leipzig, Germany

3. <u>S. J. Reitmeier,</u> O. C. Gobin, A. Jentys and J. A. Lercher, *"Shape selective properties of surface modified H-ZSM5 – Influences on the transport processes", 20.* Deutsche Katalysetagung, 2008, Weimar, Germany

4. <u>S. J. Reitmeier,</u> A. Jentys and J. A. Lercher, *"Theoretical and experimental approach to determine the sticking probability of aromatics on HZSM-5 and amorphous SiO$_2$", 20.* Deutsche Zeolithtagung, 2008, Halle, Germany

5. S. J. Reitmeier, O. C. Gobin, <u>A. Jentys</u> and J. A. Lercher, *"On the role of transport processes on the shape selective properties of HZSM-5", 14th International Congress on Catalysis,* 2008, Seoul, South-Korea

6. <u>S. J. Reitmeier,</u> G. Clever, T. Carell, O. Schiemann, „*Two copper(II) ions incorporated in artificial DNA - Investigation of the magnetic coupling using EPR spectroscopy*", 2nd EUCHEMS Chemistry Congress, 2008, Turin, Italy

7. <u>S. J. Reitmeier,</u> R.R. Mukti, A. Jentys and J. A. Lercher, *"Surface processes on medium-pore zeolites – Investigation of the sticking probability of aromatic molecules",* 2nd EUCHEMS Chemistry Congress, 2008, Turin, Italy

8. <u>S. J. Reitmeier,</u> O. C. Gobin, A. Jentys, J. A. Lercher, *"Influences of post-synthetic treatment of MFI-zeolites on the sorption and transport properties"* 21. Deutsche Zeolithtagung, 2009, Kiel, Germany (**Invited talk**)

9. <u>O. C. Gobin,</u> S. J. Reitmeier, A. Jentys, J. A. Lercher, „*Diffusion of aromatics in MFI-type zeolite*s" 21. Deutsche Zeolithtagung 2009, Kiel, Germany

10. <u>S. J. Reitmeier,</u> O. C. Gobin, A. Jentys and J. A. Lercher, *"Hydrocarbon transport on surface modified microporous solids – an in-situ infrared spectroscopic study."* 58. Bunsentagung 2009, Köln, Germany

11. <u>S. J. Reitmeier</u> *"Surface modification of zeolites enhancing hydrocarbon transport - a promising concept for catalyst design"* 2nd DSM Science and Technlogy Awards South, 2009, Vitznau, Switzerland (**Invited Talk**)

12. <u>S. J. Reitmeier</u> *"Highlights of current research in the NanoCat center of excellence"* 59th Nobel Laureate Meeting, Lindau, Germany

13. S. J. Reitmeier, O. C. Gobin, A. Jentys and <u>J. A. Lercher,</u> *"Silica layers on zeolites to enhance catalytic performance in hydrocarbon separation"* 9th EUROPACAT Conference, 2009, Salamanca, Spain